Turbulence Structure and Bank Erosion Processes in Dredged Channels

A Thesis Submitted

In partial fulfilment of the requirement for the degree of

Doctor of Philosophy

Submitted by

Sukhjeet Arora

(206104020)

Under the Supervision of

Prof. Bimlesh Kumar

Department of Civil Engineering

Indian Institute of Technology Guwahati

Guwahati – 781039, India

October 2024

Dedicated to the Almighty and my loving Family

Declaration

I, Sukhjeet Arora, declare that this thesis titled, "Turbulence Structure and Bank Erosion Processes in Dredged Channels", is part of my research for the Doctor of Philosophy degree. All the work presented in this thesis is my own, and the results generated are of the original research.

I confirm that

• The work contained in this thesis is original and was done wholly or mainly while in candidature for the research degree at this institute under the guidance of my supervisor.

• The work reported herein has not been submitted to any other Institute for any degree or diploma.

• Wherever I reported material from other sources, I have duly cited and acknowledged their respective authors and sources.

• I also affirm that no part of the thesis is plagiarised to the best of my knowledge.

• I take complete responsibility for the results and inferences reported in the thesis

Place: IIT Guwahati, India

Sukhjeet

Date: 06/01/2025 Sukhjeet Arora

Dr. Bimlesh Kumar

Professor

bimk@iitg.ac.in

0361-258 2420

CERTIFICATE

This is to certify that the thesis entitled "Turbulence Structure and Bank Erosion Processes in Dredged Channels", submitted by Sukhjeet Arora (206104020), in partial fulfilment of the requirements for the award of the degree of Doctor of Philosophy to the Indian Institute of Technology Guwahati, is a record of bonafide research work under my supervision. I certify that this thesis is worthy of consideration for the award of the degree of Doctor of Philosophy of the Institute. To the best of my knowledge, no part of the work reported in this thesis has been presented for the award of any degree at any other institution.

Date: 06/01/2025

Place: IIT Guwahati

(Prof. Bimlesh Kumar)

Journal Publications:

- Arora, S., & Kumar, B. (2024). Effect of emergent vegetation on riverbank erosion with sediment mining. Scientific Reports, 14(1), 11193. https://doi.org/10.1038/s41598-024-61315-9.
- Arora, S., & Kumar, B. (2024). The riverbank vegetation for mitigating the adverse effects of sediment dredging. Ecohydrology, e2656. http://doi.org/10.1002/eco.2656.
- Arora, S., Patel, H. K., Srinivasulu, G., & Kumar, B. (2024). Turbulent characteristics at interface of partly vegetated alluvial channel. International Journal of Civil Engineering, 22(1), 75-85, https://doi.org/10.1007/s40999-023-00890-w.
- Arora, S., Lade, A. D., & Kumar, B. (2023). Higher-order turbulence statistics and multiscale characterization of morphodynamics in a riverbank section with an upstream mining pit. Physics of Fluids, 35(6). # https://doi.org/10.1063/5.0159014.
- Arora, S., Patel, H. K., Lade, A. D., & Kumar, B. (2023). Turbulence structure and bank erosion process in a dredged channel. River Research and Applications, 39(4), 613-628, https://doi.org/10.1002/rra.4100.
- Arora, S., & Kumar, B. (2025). Effects of Proximity of Sediment Mining Pit on Riverbank Stability. (Under Review)

[#] A Scilight magazine article highlighted our work as "Examining downstream impacts of riverbed dredging. Scilight, 2023(26)"

Conferences:

- North-East Research Conclave (NERC 2022) [20th – 22nd May 2022]

  Conference Publication (Book Chapter) and Oral Presentation on "Flow Characteristics of a Compound Channel Due to Vegetation" https://doi.org/10.1007/978-

981-97-5870-8_14 by Sukhjeet Arora, Harish K Patel, Shovit Kumar, and Bimlesh Kumar.

- Research and Industrial Conclave (RIC 2023) [14th – 16th May 2023]

  Poster presentation on "Shear Stresses in a Dredged Channel with Riverbank" by Sukhjeet Arora, Harish K Patel, Abhijit D Lade, and Bimlesh Kumar.

- International Symposium of River Sedimentation (ISRS 2023) [5th-8th September 2023], held in Florence, Italy. Oral presentation on "Turbulent Characteristics of Flow in Wide and Narrow Alluvial Channels". Abstract book https://www.isrs2022.it/wp-content/uploads/2023/09/Abstract_book.pdf by Sukhjeet Arora, Harish K Patel, Abhijit D Lade, and Bimlesh Kumar.
- EGU General Assembly 2024, [15th – 18th April 2024] Conference Publication and Online Poster Presentation: "Secondary Flow and Turbulent Kinetic Energy in a Dredged Channel with Riverbank " https://doi.org/10.5194/egusphere-egu24-14030 by Sukhjeet Arora, Harish K Patel, Abhijit D Lade, and Bimlesh Kumar.
- International School of Hydraulics (ISH) 2025, [20th – 23rd May 2025] Abstract accepted on “Effects of Sediment Mining Volume on Riverbank Stability.” by Sukhjeet Arora and Bimlesh Kumar.

ACKNOWLEDGEMENT

The journey of my Doctoral degree has been a wonderful experience, with lots of things to learn. It would have been impossible without the support and guidance of several people. First of all, I am highly indebted to my supervisor, Prof. Bimlesh Kumar, for his guidance and supervision in completing my research work and finding the next phase of life. During my PhD, he gave me the freedom to work and engaged me in new ideas. His unconditional support and motivation gave me strength and lifted my spirit whenever I got stuck. I would also like to thank members of my doctoral committee, Dr Anil Kumar Mishra (Chairman), Prof. Ajay S Kalamdhad (member), and Prof. Sisir K Nayak (member) for their insightful comments, encouragement, and valuable time throughout the research. I would like to acknowledge the Department of Civil Engineering at IIT Guwahati for providing me with the required resources.

I would like to express my sincere gratitude to Dr Mahesh K Patel, Dr Abhijit D Lade, Dr Jyotirmoy Barman, and Dr Jyotismita Taye for their valuable input on various complex topics. I will always cherish the time I spent in the laboratory with Harish K Patel and Waseem Ghani during my PhD days. I would also like to thank Shovit, Chandramauli, Joychen, and Mrinal. I sincerely thank Bazal Da (Bazal Hoque), who generously gave his time to help me in my experiments, even during the Covid period.

A special thanks to Harish K Patel for his consistent motivation, support, and guidance throughout my PhD journey. I sincerely thank him for being there for me every end of the way.

I owe a debt of gratitude to my mother, my father, and my sister for the love and support that made this journey possible. I want to give special thanks to my dear friends Ravi, Angana Bhattacharya, and Chandra Bhan for their unwavering support and love during my PhD. I also want to thank Prof Gagan Kumar for his guidance in personal and academic matters.

Finally, I humbly bow my head in deepest gratitude to the Supreme Lord and seek his blessings.

Abstract

Riverbank erosion has significant geomorphological and anthropogenic consequences. The geomorphological impacts include form changes such as lateral channel migration, meanders, channel expansion, etc. The anthropogenic effects include the threat to floodplain human habitation, agricultural land, and stability of instream hydraulic structures and buried pipelines. Channel dredging for the extraction of sand and gravel has seen a multi-fold rise in the last few decades. Pit excavation directly impacts the fluvial erosion characteristics of the riverbank. Pit action increases the Reynolds shear stress fields in the near-bank flow, which causes progressive fluvial erosion of the berm at the bank toe. The erosivity of the main channel flow in the riverbank also leads to channel degradation, which increases the exposed height of the bank slope. Pit dredging leads to the generation of stronger ejection bursts which provide a mechanism for berm sediment mobility and erosion. The study reveals that instream mining has notable effects on the inherent nature of higher-order turbulence statistics, especially near the bank slope and toe, as well as the multiscale morphological structures.

Wholly vegetated sections exhibited a highly fluctuating transverse flux, indicating a larger intermixing rather than a unidirectional movement. Based on the findings, it is recommended to opt for a wholly vegetated cover instead of a partly vegetated cover in riverbanks or near structures such as bridge piers and river training structures affected by a lateral or laterally accelerating flow.

This experimental study uses sparsely dense, flexible, and bladed vegetation to study the annulment effects of vegetation against the existing mining pit. Near-bed turbulence and sediment transport have increased in the test section in the presence of a mining pit. The increase in near-bed streamwise and transverse Reynolds shear stresses helped us understand the increased sediment movement in streamwise and lateral directions. The morphology of the test section showed increased riverbed erosion at the beginning of the test segment. The entire

cross-section was levelled at the end of the test section, and aggradation was downstream of the test segment. In contrast, in the vegetated riverbank case, the initial profile of the bank was almost unchanged for the same discharge of flow and upstream sand pit. The sparse vegetation overperformed the intended negation effects. This study establishes that sparse vegetation would perform better in maintaining the channel morphology, which otherwise in dense vegetation would have faced a high erosion rate in the main channel while giving the same protection to the riverbanks.

The abrupt variation in Reynolds Shear Stress (RSS) and transverse RSS at the location of the berm induces instability and erodes the berm present at the toe of the riverbank. The combination of the vegetation and sandpit led to increased turbulent kinetic energy (TKE) of the flow at the near-bed and berm locations. The morphological analysis showed complete riverbank erosion in both cases of the unvegetated riverbank, i.e., without or with an upstream pit. The installed stems of rigid vegetation on the riverbank helped decrease the fluvial erosion of the riverbank, and its profile observed minimal changes over the length of the test segment. However, the main channel erosion was amplified due to the vegetation (in no-pit case) at the beginning of the test segment, which eroded the bed of the main channel by about 67% of the bed thickness. Also, in the vegetated riverbank cases, the upstream pit caused an increase in erosion by 7.66% at the center of the main channel.

Contents

List of Figures

List of Tables

Notations

Q	Flow discharge
B	The top surface width of the flow
$\bar{u}$	mean velocity in the streamwise direction
u'	fluctuation of turbulent velocity in the streamwise direction
k	Turbulent Kinetic Energy
ε	rate of dissipation of turbulent kinetic energy
ρ	density of water
G	Specific gravity
σ	standard deviations
S	Channel bed slope
L	Width of the notch
H	Flow Depth
C_d	Coefficient of discharge
D_{50}	Median grain diameter
τ_c	critical bed shear stress
u_*c	critical shear velocity
g	acceleration due to gravity
u,v,w	Instantaneous velocities in streamwise (X), transverse (Y), and vertical (Z) directions.
u',v',w'	Instantaneous velocity fluctuations in streamwise (X), transverse (Y), and vertical (Z) directions.
$\sqrt{u'u'}$	Turbulence intensity in the streamwise direction
$\sqrt{v'v'}$	Turbulence intensity in the transverse direction
$\sqrt{w'w'}$	Turbulence intensity in the transverse direction
$-\rho u'w'$	Reynolds shear stress in the streamwise direction

$-\rho u'v'$	Reynolds shear stress in the transverse direction
R_e	Reynolds number
F_r	Froude number
U	Average velocity in the channel
ν	Kinematic viscosity
z	Vertical distance from the bed surface
ADV	Acoustic Doppler Velocimeter
URS	Ultrasonic Ranging System
TKE	Turbulent kinetic energy
RSS	Reynolds Shear Stress
TI	Turbulence Intensity

1. Introduction

1.1 Background

Rivers and waterways play a fundamental role in the Earth's natural environment, providing critical habitats for ecosystems and serving as essential conduits for transportation and commerce. However, human activities such as dredging can significantly disrupt the delicate equilibrium of these systems, leading to both short- and long-term environmental impacts (Knighton, 1998). One of the most profound effects of dredging is its influence on the turbulence structure within river channels, which directly affects erosion processes, particularly along riverbanks. The interplay between turbulence and bank erosion is a critical area of research for effective river management and sustainable infrastructure development.

Dredging, which involves the removal of sediments from the riverbed to ensure navigability or extract resources, alters the natural flow dynamics and sediment transport patterns (Aberle & Smart, 2003). These modifications often result in changes to the characteristics of turbulence, including intensity, length scales, and spatial distribution, all of which play a significant role in the erosion of riverbanks. Bank erosion, a process where the natural forces of flowing water gradually wear away the banks, is often exacerbated in dredged channels, where altered turbulence amplifies erosion rates (Simon & Collison, 2002). Thus, understanding the mechanisms by which turbulence affects bank erosion is essential for predicting erosion patterns, implementing effective erosion control measures, and mitigating the negative consequences of dredging on both ecosystems and infrastructure.

Several dynamic factors influence the complex process of riverbank erosion. Hydrological variables such as flow velocity and water level fluctuations—often caused by floods or dam operations—can increase shear stress on riverbanks, destabilizing them (Batalla & Vericat, 2009). Sediment load, consisting of both coarser materials that exert abrasive forces and finer

particles that are easily transported, plays a crucial role in this process. Geotechnical factors, including the composition and moisture content of the soil, determine the bank's susceptibility to erosion. Loose, unconsolidated materials are particularly vulnerable, while saturated soils are prone to mass wasting (Lawler et al., 1997). Vegetation, with its root systems and protective cover, significantly stabilizes riverbanks. However, human activities such as deforestation, agriculture, and urban development disrupt natural flow patterns, increasing runoff and contributing to erosion. Climatic factors like heavy rainfall, which leads to increased surface runoff, or droughts, which weaken soil cohesion, also influence erosion rates (Knighton, 1998). Geological aspects, such as the type and structure of bank materials and the slope's steepness, further affect erosion susceptibility, particularly in meandering rivers and those with steep gradients. Moreover, wave action generated by boats or wind in wider river sections plays a critical role in accelerating erosion.

A thorough understanding of these interconnected factors is essential for managing and mitigating riverbank erosion. Rivers, enclosed by beds and banks but open to the atmosphere, transport water from sources such as glaciers, other rivers, or aquifers, to their endpoints, which may be another river or an ocean. Gaining insight into the interaction between river water and suspended or bed sediment loads is crucial for understanding how water and sediment traverse the river's course (Knighton, 1998). It is important to understand that a river can typically be classified into two kinds i.e., a wide (shallow) or a narrow (deep) river. This classification is based on the top width-to-depth ratio (Nezu et al., 1993). Deep rivers are often found in mountainous regions, while wide, shallow rivers are typically located in plains. This distinction can be attributed to the steep slopes and rocky riverbed materials commonly found in mountains, as opposed to the gentle slopes found in plains.

Riverbeds are composed of various-sized materials depending on geographical location and proximity to upstream mountains. Fluvial processes transport sediment from mountainous

regions, with sediment size typically decreasing downstream. The geological characteristics of the source mountains play a significant role in determining sediment load. For example, older, more stable mountains typically experience less erosion and thus have rivers with clearer water and lower suspended sediment loads. In contrast, rivers originating from younger mountain ranges, such as the Himalayas, carry larger suspended loads due to the ease of rock abrasion. This results in higher turbidity and increased sediment transport in Himalayan rivers. While these factors add complexity to river systems, focusing on individual components such as, sediment transport due to fluvial action—enables a more detailed understanding of river dynamics (Knighton, 1998). Figure 1.1A shows an image of a riverbed of a tributary to Dawki River in Meghalaya, India. Figure 1.1(B and C) shows an ideal sediment particle (spherical) along with the streamwise velocity distribution along the depth (Lee & Balachandar, 2017). The location of the sediment particle was described using h_{BL}, δ, and L, which illustrates height of base level from rough boundary, gap between particle and base level, and total distance from bottom. Figure 1.1D shows the interaction of this sediment particle with the flow (Zhai et al., 2021).

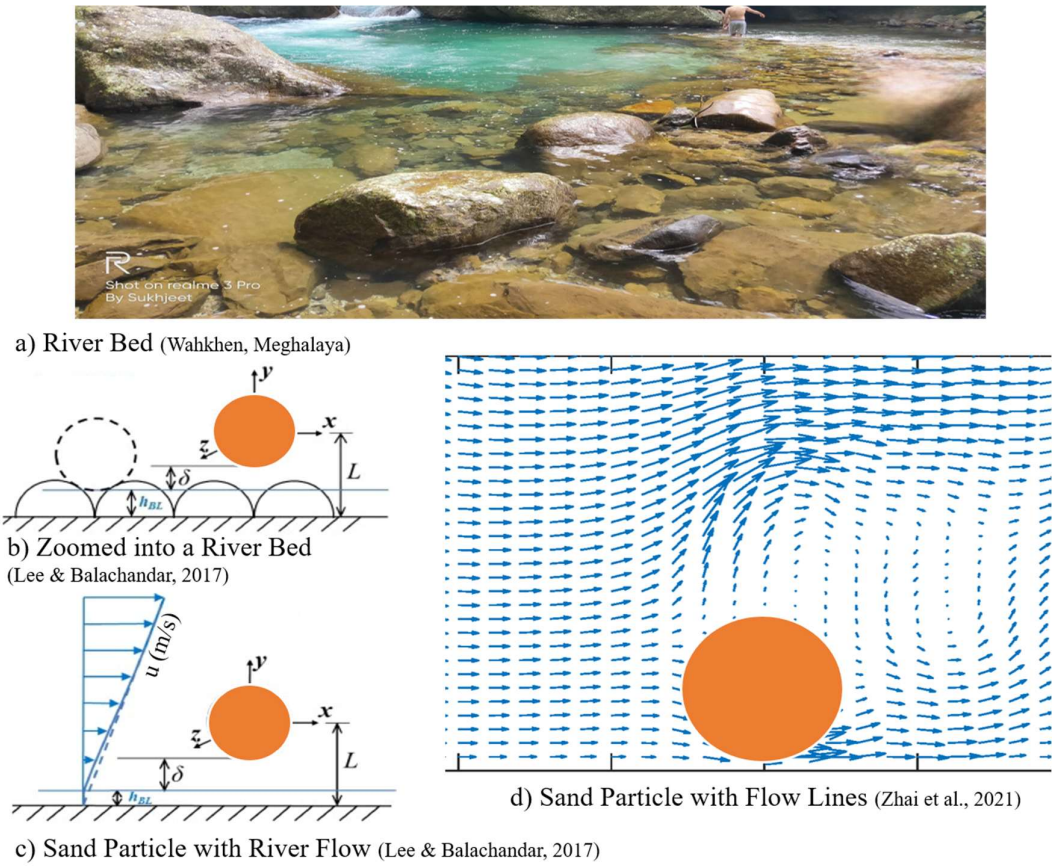

Figure 1.1: Interaction of Sediment Particle with River Flow

The flowing water in the rivers imparts shear stresses on the bed material, which shall be the driving force (Fluvial Action), as shown in Figure 1.2. These forces help the sediment overcome the resisting forces, such as friction, due to its submerged weight and the interlocking forces. The interlocking forces are difficult to predict as they would differ from case to case, depending upon the size and shape of the other bed particles. For the convenience of understanding sediment transport and for establishing a comparison between various cases in this study, the bed material was kept to a uniform size. This limits the unpredictable interlockings between different sizes of the sediment. Another driving force is gravity, which acts as per the slope of the channel (Figure 1.2). When both the resisting and driving forces are balanced, the sediment particle is said to be in the incipient condition. This incipient condition is the critical condition in the study of sediment transport. Different scientists give several

criteria to understand this threshold condition, where just a slight increase in the driving force will initialise the movement of the bed material.

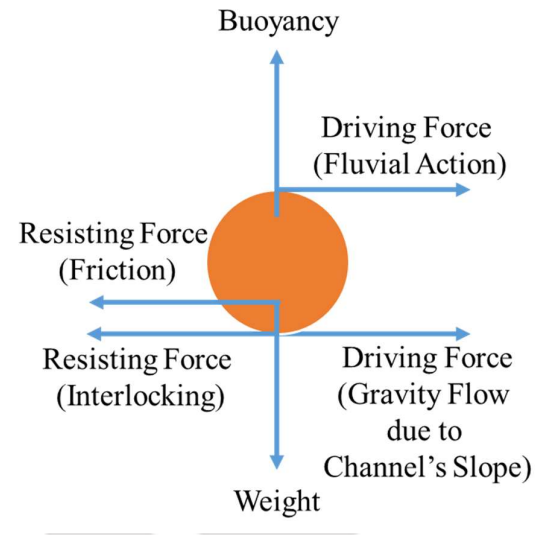

Figure 1.2: Resisting and Driving Forces on an Ideal Sediment Particle at the Riverbed

The force due to the fluvial action increases as the near-bed or near-particle flow velocity increases. The variation of flow streamwise velocity generally follows logarithmic variation in unvegetated sections. The velocity decreases from the top surface till it becomes zero at the fixed boundary of the bed, and so does the strength of the shear stress that helps sediment transport from one point to another point downstream. The shear stress or the force of fluvial action required to move a sediment particle depends on the size of the bed material. As the size of the particle increases, its weight increases, and the velocity of the flow required also increases. A large boulder would require a much higher velocity of the flow to transport the bed material than the fine bed material, as shown in Figure 1.3. The bed material can also be in the suspension or solution phase, which requires minimal flow velocity to carry them downstream. The flow and bed sediment interaction can be explained by the bursting phenomenon, which acts as a hairpin structure (Smith & Metzler, 1983). This phenomenon can be broken down into four types of events, i.e., ejection, entrainment, collapse and sweep. This

starts when a fluid parcel from a slow-moving bottom layer of flow ejects upwards and enters the faster-moving upper layer. It expands, collapses and sweeps back into the bottom layers to transfer the momentum to the bottom layer. These events cause unrest or disturbance in the boundary layers, leading to the movement of the bed particles. These processes can be understood by studying the fluctuations in the three-dimensional flow velocity. Its study is termed a quadrant analysis and is presented in chapters 3, 4, and 5, where we attempt to correlate the strength of depthwise, transverse, and streamwise directions.

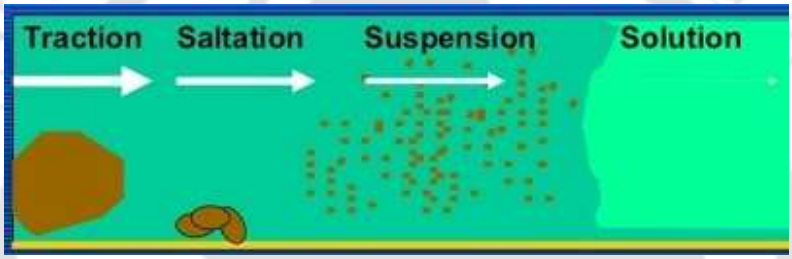

Figure 1.3: Schematic of Sediment Transport Mechanisms in Open Channels. The size of the arrow shows the comparison of flow velocity required to move the respective sediment size as the bed load.

Returning to the pressing issue of sand extraction from riverbeds, this practice has profound and damaging effects on the natural environment. It substantially impacts riverbed and riverbank erosion and alters the river's flow dynamics, leading to a cascade of consequences. Removing sediment from the berm and the adjacent riverbed destabilises riverbanks, making them more prone to collapse. Also, the scarcity of sediment due to dredging creates its deficit downstream, exacerbating erosion and disrupting the delicate balance of the river ecosystem. Furthermore, sand mining changes the riverbed's depth and shape, resulting in flow dynamics shifts, increased turbulence, and altered Thalweg of the rivers. These alterations have far-reaching effects on erosion patterns, sediment transport, and the very structure of the river channel. The ecological impact is profound, leading to the irrevocable destruction of habitats

for riparian and aquatic species. Furthermore, the socio-economic implications pose imminent threats to infrastructure and local livelihoods.

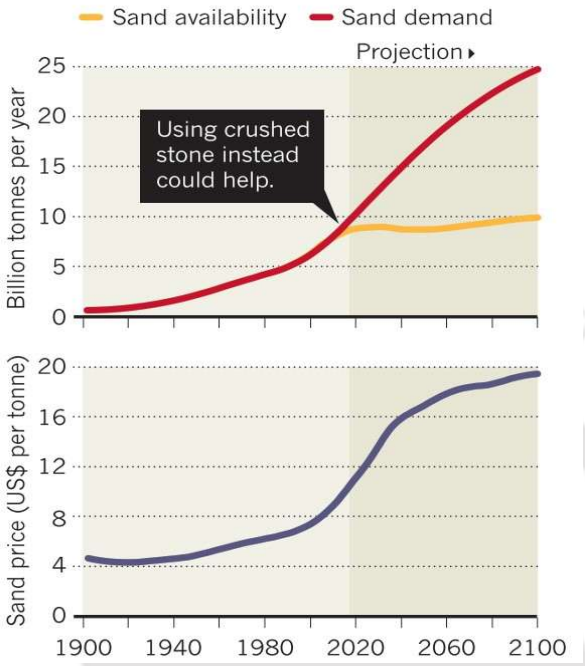

Figure 1.4: Demand of Sand against its supply from 1900 to 2100 (projected) along with the sand prices per tonne (Source: Bendixen et al., Nature 571, 29-31 (2019))

The discussion thus far has revolved around gaining a deep understanding of the issue at hand: the detrimental effects on our rivers, leading to significant harm to life and property, all driven by the relentless pursuit to meet industrial demands. The illicit organisations benefit from this disproportionate demand-to-supply ratio, especially after 2019, as presented by (Bendixen et al., 2019) (Figure 1.4). The widening chasm between supply and demand is driving up the prices of sand, lining the pockets of illegal mining organisations. Given the failure to effectively control illegal mining, it is imperative that we urgently address and mitigate the detrimental impacts of excessive sediment mining from our rivers. This urgent matter demands immediate attention and decisive action.

The researchers have put forth numerous measures to combat the detrimental effects of sediment mining, particularly prevalent in developing nations such as India, China, and Africa. However, the exorbitant costs associated with these solutions pose a significant barrier, considering the limited resources available in these regions. It is imperative to recognize the profound impact of sediment mining on riverbed and riverbank stability and to seek out cost-effective measures for mitigation. This thesis delves deep into unravelling the repercussions of sediment mining on riverbeds and riverbanks, leveraging insights into changes in flow structure in the near bed and near bank zones. Furthermore, it meticulously scrutinizes alterations in sediment transport within laboratory settings, as elucidated in the subsequent chapter. To begin, it's crucial to grasp the complex process that contributes to the failure of a riverbank.

1.2 Riverbank Failure

The riverbank is the sediment material that forms the boundary for the flow. Its failure occurs when it is unable to withstand the flow of a river. The failure of this structure can lead to flooding of the adjacent areas. There are different types of failures, including piping failure, riverbank erosion, mass failure, sliding failure, and undercutting. A typical failure case of the river involves a combination of more than one of these types of failures. The type of sediment of the riverbank and external factors such as riparian vegetation and human actions influence these failures. We will discuss these human actions in detail in the upcoming sections of this chapter. First, it's important to understand the common step in these types of failures, which can be defined as the removal of the stabilizing agent of the riverbank, termed the berm. The fluvial action imparts shear stresses on the sediment in contact with the flow. When the driving forces overcome the resisting forces, these sediment particles travel downstream from their current cross-section. The erosion of the berm leads to decreased support to the riverbank, which collapses and creates a new cross-sectional profile. The failure is generally in such a way that it has new berm material to support the newly formed cross-section. This process

continues until an equilibrium is achieved. However, this equilibrium can only be achieved for specific flow conditions. Since the river flow conditions vary throughout the year, we can observe the riverbank failure as a cyclic process (Figure 1.5).

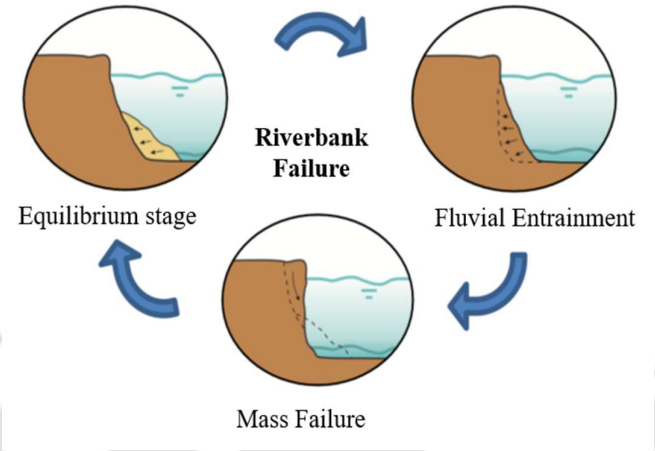

Figure 1.5: Riverbank Failure Process

Upon closely examining the process of riverbank failure, Figure 1.6 offers a visual representation of a typical riverbank. The hatched portion in the figure depicts the impact of fluvial action, which leads to the erosion of the berm. This erosion diminishes the support for the riverbank, thereby weakening the resistive force in the free-body diagram of a Failing Block. Notably, tension cracks become visible in the failing plane at the time of its failure. Furthermore, as the water level rises, the contribution of self-weight in driving forces intensifies due to saturation. Figure 1.6 effectively highlights the significant role played by the angle of the riverbank slope in determining the stability of the riverbank.

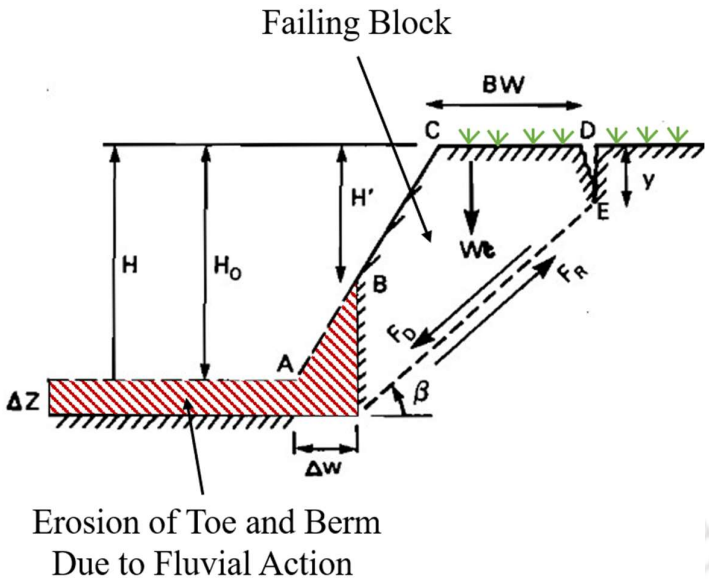

Figure 1.6: Process of Riverbank Failure

In various rivers around the world, one can encounter a rich diversity of riverbank materials, which can be broadly categorized as cohesive and non-cohesive. The manner in which these materials respond to the forces of nature is fascinating. One key determinant of their behaviour is their cohesive strength, which plays a vital role in resisting external forces (Figure 1.6). As the powerful forces of fluvial action gradually erode the existing sediment at the base of the riverbank, it leads to a striking visual of undercutting and erosion. In the case of cohesive material, this erosion process can culminate in mass or beam failure, presenting a dramatic change in the riverbank's structure. Remarkably, cohesive material displays an impressive resilience to riverbank failure compared to non-cohesive material, which yields sliding failure and gradual bank retreat, perpetuated by continuous erosion (Figure 1.7). The varying shear strength of sediment material found in nature introduces a captivating complexity, emphasizing the importance of studying and comprehending the riverbank materials that are more susceptible to fluvial erosion.

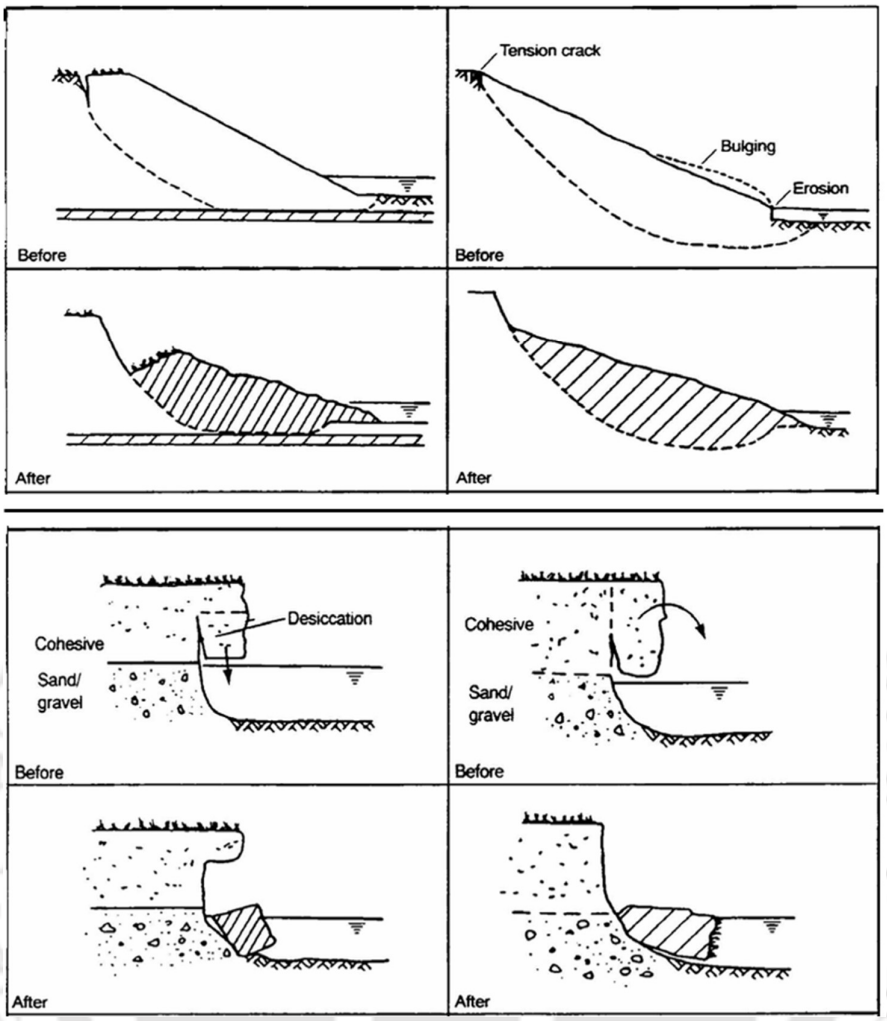

Figure 1.7: Riverbank Failure for Non-Cohesive and Cohesive Bank Material

The failure patterns of non-cohesive and cohesive bank sediment depicted in Figure 1.7 provide evidence of the progressive changes in the riverbank profile. Field observations conducted by (Nasermoaddeli, 2011; Nasermoaddeli & Pasche, 2008) using terrestrial LiDAR to analyze a non-cohesive riverbank profile revealed the cyclic process of riverbank failure (Figure 1.8). The observation commenced with equilibrium profile 1. Fluvial action caused erosion and entrainment, resulting in profile 2. This process persisted until the block began to fail, leading to mass failure and the formation of profile 3. The cycle repeated, and this progression is evident in profiles 4, 5, and 6 in Figure 1.8. To effectively prevent riverbank failures, it is

critical to first understand the underlying causes driving their increase. This understanding will inform the development and implementation of successful mitigation solutions.

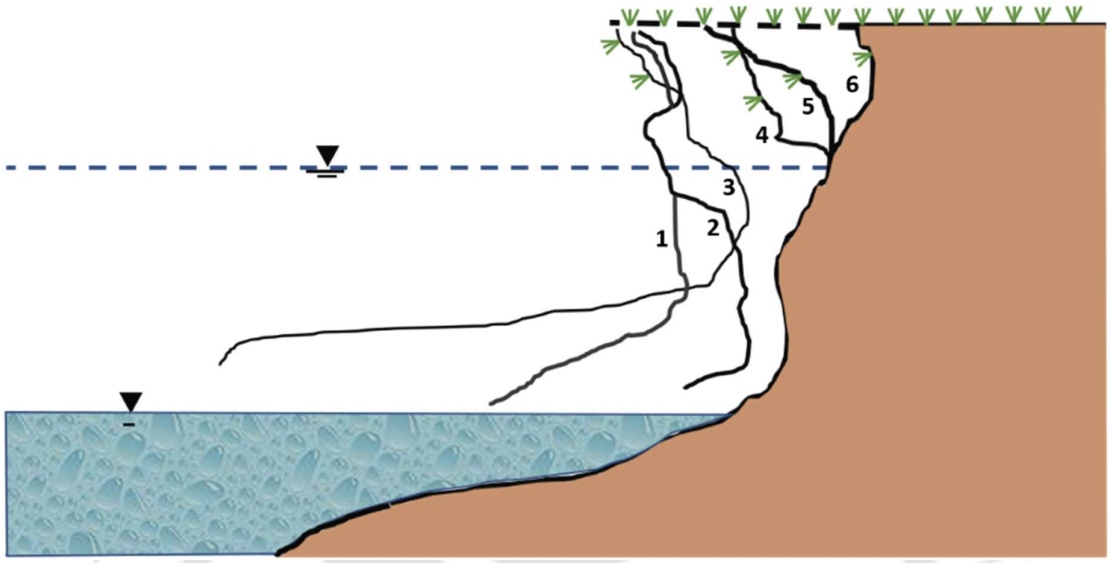

Figure 1.8: Riverbank Failure Profiles due to Fluvial Erosion with time (Nasermoaddeli et al., 2011)

1.3 Uses of Sand

Every year, a substantial 50 billion tons of sand is extracted globally, with a significant portion, approximately 30 billion tons, finding utilization in the construction industry (Padmalal et al., 2008). Beyond construction, sand serves a critical role in land reclamation, as evidenced by the remarkable expansion of Singapore's national area by over 20% between 1960 and 2017, primarily driven by its status as one of the world's largest importers of sand with respect to its land area (Lade, Deshpande, et al., 2019). Additionally, high-silica frac sand plays a pivotal role in oil extraction from shales. Furthermore, sands boasting an exceptionally high silica content of over 99% are harnessed in the manufacturing processes of microchips and optical lenses, underlining the diverse and indispensable uses of this natural resource. Glass industry also uses sand as the raw material. Returning to its usage in the construction industry, which has the maximum portion of sand consumption, we need to understand the available resources of sand.

Figure 1.9: Characteristics of Sand Particles from a) Deserts b) Rivers

The vast majority of sand is found in deserts, with a smaller quantity located in riverbeds. The primary distinction between the two lies in how they are formed or broken down into smaller particles. Desert sand is weathered by the wind, resulting in a round shape, while riverbed sand is formed from the breakdown of large rocks due to the action of flowing water, giving it an irregular shape (Figure 1.9). This irregular shape offers a significant advantage in creating strong bonds with cement in concrete. Sand, a natural resource, is traded among several countries, with a total trade value of 2.33 billion USD, as illustrated in Figure 1.10. Different continents are marked in different colors. Areas located near rivers have convenient access to sand, making extracting sand from rivers more cost-effective than transporting sand. The mechanical removal of the sand from the rivers is termed sediment dredging or sediment mining. In the following sections, we will see different methods to dredge sand from rivers.

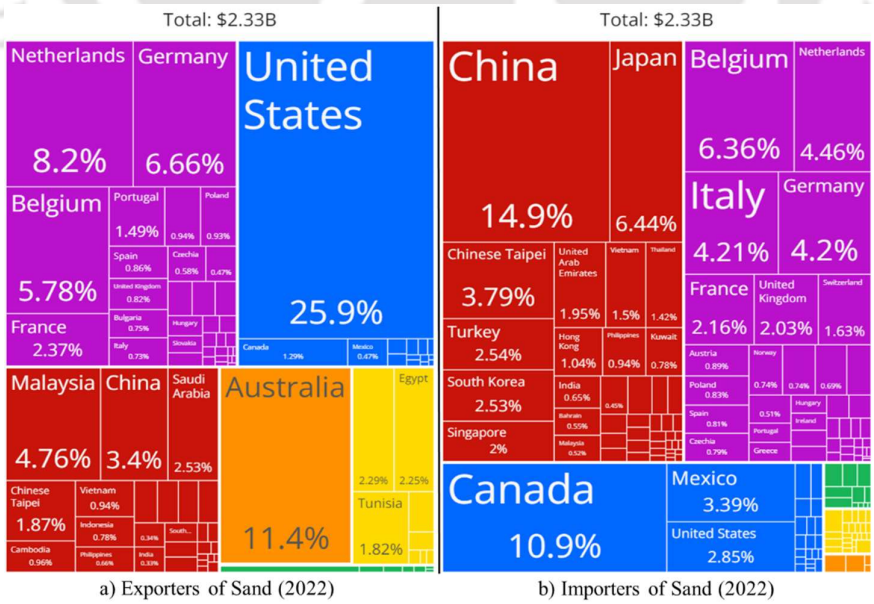

Figure 1.10: Worldwide Trade of Sand in the Year 2022 (source: Observatory of Economic Complexity (OEC))

1.4 Types of Sediment Mining

Sediment mining refers to the extraction of various types of sedimentary material from the Earth for numerous industrial and construction purposes. These materials include gravel, sand, silt, clay, rare earth elements, and heavy minerals. Sediment mining uses different methods depending on the type of sediment being targeted and its intended use. In this thesis, we focus on the sediments mined from the rivers. Rivers contain bed loads of different sizes ranging from boulders in the steep mountainous regions and fine sand in the plain regions. It also contains fine sediment in the form of a suspended load. Below are the types of sediment mining from rivers and their vicinity. Dredging is the process of removing sediment from water bodies to deepen waterways, clear accumulated sediments, or prepare land for reclamation projects. There are three main methods: mechanical dredging, hydraulic dredging, and auger dredging. Dredging disrupts aquatic ecosystems by displacing organisms, releasing toxic substances, and increasing water turbidity, negatively affecting water quality and aquatic life.

1.4.1 Gravel Mining

Gravel mining extracts coarse sedimentary material from quarries or riverbeds, primarily used in the construction of roads, bridges, and drainage systems. It includes open-pit mining, which uses heavy machinery to remove soil and extract gravel, causing significant landscape scars and environmental disturbances. Riverbed gravel mining disrupts natural water balance, leading to erosion and negative impacts on aquatic life. Both methods contribute to extensive land degradation, habitat destruction, erosion, dust emissions, and downstream water quality issues, significantly altering river morphology and harming ecosystems, particularly affecting species dependent on stable riverbeds.

1.4.2 Sand Mining

Sand is one of the most widely used natural resources, with demand driven primarily by the construction industry. Sand mining refers to removing sand from various environments such

as rivers, beaches, dunes, and the seabed. In this thesis, we focus on sand dredging from the riverbed and its effects on the stability of the riverbank. Sand is used in producing concrete, glass, and ceramics, as well as in large-scale land reclamation projects. The various sources used to obtain the sand are discussed below.

1. **Riverbed Sand Mining**: This method involves the extraction of sand from the beds and banks of rivers and streams. Riverbed sand is highly sought after because it is often composed of irregular shapes and rough grains, making it ideal for use in concrete and mortar. The process typically involves scooping or dredging the sand using heavy machinery such as excavators or suction dredgers. Removing sand from rivers disrupts their natural flow, erodes banks, and alters watercourse patterns. These disruptions can lead to flooding and loss of life and infrastructure. It also has serious consequences for the benthic life (Grygoruk et al., 2015).

2. **Beach and Dune Sand Mining**: This method focuses on removing sand from coastal beaches and sand dunes. Coastal areas, particularly beaches, are natural buffers that protect inland regions from storm surges, tides, and coastal flooding. Mining this sand for use in construction and industrial applications depletes natural coastal defences, increasing vulnerability to erosion and storm damage (Nairn et al., 2004).

3. **Marine Sand Mining**: Marine sand mining involves the dredging of sand from the seabed. The process usually takes place in shallow coastal waters, bays, and offshore areas. Marine sand is used for major infrastructure projects, particularly in land reclamation, where it is deposited to create new land or extend coastal areas. This type of mining typically involves the use of large suction dredgers that extract sand from the seabed and pump it onto barges for transport. The environmental impact of marine sand mining is profound, as it disrupts seafloor habitats, harming marine life, including shellfish, fish, and seabirds that rely on

these ecosystems for food and breeding. Moreover, the dredging process stirs up sediment plumes, which reduce water clarity and can smother nearby coral reefs and seagrass beds (Nairn et al., 2004).

1.4.3 Silt and Clay Mining

Silt and clay are fine-grained sediments that are often extracted for use in industries such as ceramics, brickmaking, and construction. These materials are also used for manufacturing tiles and pottery and as fillers in construction. The extraction of silt and clay, critical components for various industries, can be conducted through methods like river and floodplain mining and dredging. River and floodplain mining targets the accumulation of these sediments in natural water courses and adjacent areas, involving the removal of topsoil to reach the sedimentary layers. This technique varies in intensity from manual to mechanized operations, though it risks ecological balance by disrupting natural water flow and promoting erosion. Alternatively, dredging, either hydraulic or mechanical, offers an efficient means to harvest silt and clay from water bodies, especially in mitigating sediment accumulation that threatens navigation and flood control. However, this method equally threatens marine ecosystems and risks mobilizing entrapped pollutants. Both methods, while offering practical solutions to sediment extraction, underscore a critical need for sustainable practices to mitigate environmental impacts (Ciszewski & Sobucki, 2022).

1.5 Mining Scenario in India and the World

Sediment mining, commonly referred to as dredging, is the process of extracting materials such as sand, gravel, silt, and clay from riverbeds, lakes, coastal areas, and seabed. This practice is integral to numerous sectors, including construction, land reclamation, navigation, and environmental restoration. While sediment mining offers economic benefits and infrastructural support, its consequences are often severe and long-lasting. Globally, this practice has been associated with significant environmental damage, biodiversity loss, social unrest, and the

exacerbation of natural disasters (Rentier & Cammeraat, 2022). Countries like India are especially affected, where both legal and illegal mining operations create complex environmental and governance challenges (Padmalal et al., 2008).

1.5.1 Sediment Mining/Dredging in India

India's extensive river networks, expansive coastlines, and booming construction sector have fueled an enormous demand for sedimentary materials, particularly sand. This demand has made sediment mining a critical activity. The increasing prices due to the new imbalance between supply and demand have fostered unregulated and often illegal mining operations, leading to significant social, environmental, and governance issues (Bendixen et al., 2019). The situation in India highlights the difficult balance between socio-economic development and environmental sustainability. The river and coastal sources of mining sand in India are discussed below.

River Systems: India's major rivers, including the Ganga and Brahmaputra, and their tributaries, are key hotspots for sediment mining, particularly for sand and gravel, which are essential in the construction industry. As India urbanizes rapidly, the demand for these materials has skyrocketed. Riverbed mining in states such as Bihar, West Bengal, and Uttar Pradesh has become widespread and, in many cases, uncontrolled. The extraction of riverbed materials alters the natural hydrology of these rivers, disrupting sediment flow, which can lead to riverbank erosion, sedimentation, and downstream flooding (Padmalal & Maya, 2014). This degradation affects not only the river ecosystems but also the livelihoods of local communities who depend on these waterways for fishing, agriculture, and potable water. Furthermore, excessive sand mining can significantly reduce the river's capacity to recharge groundwater aquifers, which are critical for sustaining agriculture in regions that rely on irrigation (Kondolf et al., 2018).

Coastal Areas: India's coastal areas, such as Maharashtra, Tamil Nadu, and Odisha, experience significant sediment mining to meet the high demand for construction in urban centers. This sediment mining, particularly through coastal dredging, has severe environmental impacts, including the destruction of marine ecosystems, removal of protective sand dunes, and disruption of coastal currents (D. Sharma et al., 2021). As a result, coastal defenses are weakened, making these regions more vulnerable to natural disasters such as storm surges, tsunamis, and rising sea levels, which are exacerbated by climate change (Syvitski et al., 2005). Furthermore, the destruction of critical ecosystems like mangroves further endangers coastal communities.

Regulatory Framework and Challenges in India

Regulatory Framework: Sediment mining in India is governed by several legal frameworks, with the Ministry of Environment, Forest, and Climate Change (Ministry of Environment, 2011) and the Central Pollution Control Board (CPCB) being the primary regulatory bodies. Regulations such as the Environment (Protection) Act of 1986, the Water (Prevention and Control of Pollution) Act of 1974, and the Coastal Regulation Zone (CRZ) Notification of 2011 outline strict guidelines for mining activities in rivers and coastal areas. Additionally, the Mines and Minerals (Development and Regulation) Act of 1957, along with the Sustainable Sand Mining Guidelines of 2016, further emphasize sustainable practices and environmental protection. However, while these laws are robust on paper, enforcement is a significant challenge, particularly at the state level. Weak governance, corruption, and political pressure often allow illegal mining operations to flourish, undermining environmental protection efforts (Mensah & Mattah, 2023).

Illegal sand mining: It has emerged as a critical environmental and socio-economic issue in India, particularly due to its large-scale operations and the involvement of criminal networks,

often referred to as ‘sand mafias’. These groups engage in unauthorized extraction of sand from riverbeds and coastal areas, a practice that violates environmental laws and regulations. Sand mafias operate with impunity across several states, including Uttar Pradesh, Maharashtra, and Tamil Nadu, where they exploit weak governance and systemic corruption. Local officials are frequently bribed to overlook violations, allowing these groups to continue their operations unchecked (Padmalal & Maya, 2014).

The environmental consequences of illegal sand mining are profound. Excessive extraction destabilizes river ecosystems by depleting riverbeds, which accelerates erosion and disrupts the natural flow of water. This not only affects water quality but also destroys agricultural land and wildlife habitats. For instance, the removal of sand has been linked to the decline of riverine species and the reduction of groundwater levels, exacerbating water scarcity in already vulnerable regions (Padmalal & Maya, 2014). The degradation of river systems also leads to the displacement of local communities that depend on these ecosystems for agriculture and potable water.

The socio-economic ramifications are equally significant. Illegal sand mining contributes to deepening inequality in affected areas by empowering criminal groups who exert control through violence and intimidation. The sand mafias' dominance has led to power imbalances within local communities, as they manipulate land and water resources for profit, often at the expense of marginalized groups. Furthermore, the degradation of the environment intensifies poverty by reducing agricultural productivity and access to clean water, compounding the socio-economic vulnerabilities of rural populations (Kumari et al., 2024).

1.5.2 Sediment Mining/Dredging Worldwide

Sediment mining is a global activity that provides the materials necessary for infrastructure development, urban expansion, and maintaining navigable waterways. However, it also comes

with significant environmental and social costs. Various regions across the world are engaged in sediment extraction for economic reasons, but unregulated or poorly managed mining activities have led to severe ecological degradation (Peduzzi, 2014). We shall look at the mining scenario region-wise.

1. **Southeast Asia**: Countries in Southeast Asia, particularly Vietnam, Indonesia, and Malaysia, are some of the largest contributors to the global sand mining industry. The rapid urbanization in these countries has led to massive demand for construction materials, especially sand, used in building infrastructure and land reclamation projects. In Indonesia, sand mining has become so intensive that several islands have disappeared as their sediments were extracted for use in other countries (Kurniawan et al., 2020). In Vietnam, sediment extraction from the Mekong River has caused significant ecological disruption, threatening the river's delta and impacting food security, as millions rely on the Mekong for agriculture and fisheries (Bravard et al., 2013).

2. **North America**: In the United States, sediment mining and dredging play a critical role in maintaining the country's vast network of ports and inland waterways. The Mississippi River, for example, requires regular dredging to maintain shipping channels and prevent flooding in surrounding areas (Meade & Moody, 2010). The Great Lakes also see significant sediment mining to maintain harbors and prevent coastal erosion. However, dredging in these areas has raised concerns about releasing pollutants trapped in sediment and destroying aquatic habitats that support regional biodiversity (Allan et al., 2013).

3. **Europe**: Europe, particularly the Netherlands, is renowned for its advanced sediment management practices. As a low-lying country, the Netherlands has historically depended on dredging to maintain land against sea encroachment. Dutch dredging companies, such as Royal Boskalis Westminster and Van Oord, are global leaders in sustainable dredging

technologies (Meulen et al., 2019). In addition to land reclamation, these companies are known for implementing eco-friendly techniques to minimize environmental impact, including sediment recycling and habitat restoration projects. However, despite its reputation for sustainable practices, the Netherlands still faces challenges related to the long-term ecological impacts of continuous dredging.

4. **Middle East**: In the Middle East, countries like the United Arab Emirates and Qatar have used sediment mining to construct large artificial islands, including the famous Palm Jumeirah in Dubai. These projects have contributed significantly to the region's economic development, boosting tourism and real estate. However, the environmental costs have been substantial. Coastal erosion, habitat loss, and the destruction of marine ecosystems have raised concerns about the sustainability of such mega-projects (Jones, 2019). The extraction of sand for construction has also caused geopolitical tensions, as neighboring countries face environmental degradation due to the depletion of sand reserves.

Regulatory Framework and Challenges

International bodies such as the International Maritime Organization (IMO) have set guidelines for sediment mining and dredging to ensure environmental sustainability and minimize ecosystem disruption (Arnaud-Fassetta, 2013). Additionally, national governments enforce their own environmental regulations to limit the negative impacts of sediment extraction. For instance, in Europe, the Water Framework Directive requires countries to ensure that dredging does not significantly impact the health of water bodies. In North America, the U.S. Environmental Protection Agency (EPA) and the U.S. Army Corps of Engineers are responsible for regulating dredging activities, ensuring that they comply with environmental protection standards. However, enforcement of these regulations remains a challenge,

especially in regions where economic interests outweigh environmental concerns. Some of the case studies are presented below.

1.5.3 Case Studies

1. **Singapore**: Singapore's aggressive land reclamation efforts have heavily relied on importing sand from neighboring countries like Cambodia, Malaysia, and Vietnam. These activities have sparked both environmental and geopolitical controversies, as the excessive extraction of sand has led to the degradation of river systems and coastal areas in these source countries (Hackney et al., 2020). In response, several countries have imposed bans on sand exports to Singapore, forcing the city-state to explore alternative methods for land reclamation, including the use of recycled materials and other innovative technologies like Polders, deep cement mixing (DCM), geotextile tubes filled with sediment, lumpy clay as a fill (Tan et al., 2011).

2. **China**: The Yangtze River, one of the longest rivers in the world, has been a focal point for sediment mining in China. As the country rapidly urbanizes, the demand for sand and gravel has grown, resulting in large-scale extraction from the river and its tributaries. This mining has altered the river's hydrology, leading to increased flooding and disruption of ecosystems (Wu et al., 2016). In response, the Chinese government has implemented stricter regulations to curb sediment mining in the Yangtze, including establishing protected areas and promoting river restoration projects.

3. **Netherlands**: The Netherlands stands out as a global leader in sustainable dredging practices. Dutch companies like Royal Boskalis Westminster and Van Oord have developed advanced technologies that minimize environmental damage during sediment extraction. These companies have been instrumental in the development of eco-friendly dredging techniques, such as using dredged materials to restore wetlands and build artificial

sand dunes for coastal protection (van Rijn, 2016). The country's emphasis on sustainability is driven by the need to protect its low-lying land from sea-level rise and coastal erosion, making it a model for balancing economic development with environmental stewardship.

1.6 Effects of Sediment Mining on a River System

Sediment mining, particularly within river systems, involves the extraction of sand, gravel, silt, and other materials from riverbeds and adjacent areas. This practice has profound and multifaceted effects on the river environment, hydrological dynamics, geomorphology, ecology, socio-economics, hydrogeology, and climate. The following section provides an exhaustive exploration of these impacts, highlighting the intricate interactions and long-term consequences of sediment mining.

1.6.1 Alteration in Rivers

1. **Channel Deepening**: Sediment mining often entails deepening river channels to increase the capacity for material extraction. This deepening modifies the flow dynamics of the river by increasing the flow velocities. The resultant faster flow can cause downstream erosion, leading to the potential undermining of riverbanks and infrastructure. Over time, this alteration can significantly change the natural flow regime, affecting sediment transport and deposition patterns.

2. **Flow Disruption**: The removal of sediments disrupts the natural flow patterns of rivers. Sediments play a crucial role in regulating the flow distribution and the seasonal variations of river discharge. Their extraction can lead to altered water distribution, impacting both upstream and downstream ecosystems. This disruption affects the river's ability to maintain its natural hydrological cycle, leading to unpredictable fluctuations in water availability and flow patterns.

Changes in Sediment Transport

1. **Sediment Budget Imbalance**: Sediment mining can create imbalances in the sediment budget of a river system. Extracting sediments reduces the natural sediment supply, leading to deficits downstream. This imbalance can result in riverbed incision, where the riverbed is eroded deeper, and increased bank erosion. The changes in sediment load can alter the river's ability to sustain its shape and stability, impacting the river system's physical and biological characteristics.

2. **Aggradation and Degradation**: The alteration in sediment load due to mining can lead to two significant phenomena: aggradation and degradation. Aggradation involves the accumulation of sediments in certain areas, causing the riverbed to rise. Conversely, degradation refers to the erosion of the riverbed, which can lead to the lowering of the channel bed. Both processes affect the stability of the river channel, influencing sediment transport and the river's overall morphology.

1.6.2 Geomorphological Impacts

Riverbank Erosion

1. **Increased Erosion**: The removal of sediments from the riverbed lowers the base level of the river, which can exacerbate riverbank erosion. As the base level decreases, the river's erosive power increases, leading to the erosion of riverbanks. This erosion can undermine infrastructure such as roads, bridges, and residential properties located near the riverbanks, posing significant risks to human safety and property.

   Increased flow velocities from sediment mining lead to undermining of the riverbank's base or "toe." This undermining results in progressive erosion of the bank face, where the unsupported upper sections collapse as the base is eroded away. This phenomenon exacerbates the instability of riverbanks, leading to ongoing erosion and bank failure (Anderson & Campbell, 2022).

2. **Bank Collapse**: Continued erosion and sediment removal can destabilize the riverbanks, leading to steepened and unstable banks. This instability can result in bank collapses, causing further land loss and damage to adjacent areas. The collapse of riverbanks contributes to the overall degradation of the river environment and affects the stability of nearby infrastructure.

Alteration of River Morphology

1. **Channel Instability**: Prolonged sediment mining can induce significant changes in the morphology of the river channel. The continuous removal of sediments can lead to unstable and shifting channels, altering the river's natural course. This instability can cause unpredictable flooding patterns, leading to increased risks to nearby communities and ecosystems.

2. **Loss of Natural Features**: Sediment mining can lead to the loss of important geomorphological features such as sandbars, river islands, and meanders. These features are crucial for maintaining the river's natural landscape and ecological diversity. Their loss impacts habitat diversity, reduces the complexity of the river environment, and affects the overall ecological health of the river system.

1.6.3 Ecological Impacts

Aquatic Habitat Destruction: Sediment mining alters and destroys critical benthic habitats, leading to habitat loss, reduced biodiversity, and disrupted spawning grounds for fish. This can result in decreased species diversity, disrupted food webs, and degraded water quality due to increased turbidity and pollutant release.

1.6.4 Socio-Economic Impacts

The destruction of aquatic habitats and spawning grounds significantly reduces fish stocks, adversely affecting local fisheries and the livelihoods of communities dependent on them,

leading to economic downturns in fishing sectors. Sustainable management practices become crucial in safeguarding these aquatic resources and supporting the communities that rely on them. Similarly, changes in river flows and sediment mining disrupt irrigation, impairing agricultural productivity by restricting access to essential water resources and degrading soil quality through erosion and sediment deficits, which diminishes crop yields. These challenges threaten food security and the viability of agricultural practices. Additionally, increased riverbank erosion endangers infrastructure such as bridges, roads, and buildings, raising public safety concerns and incurring high maintenance costs. The need for more frequent dredging and maintenance of water infrastructure like dams and reservoirs due to enhanced sedimentation downstream further strains financial resources, complicating effective water infrastructure management.

1.6.5 Hydrogeological Impacts

The removal of sediments from riverbeds diminishes their permeability, adversely affecting groundwater recharge and availability, leading to decreased water tables and negatively impacting groundwater supply and the ecosystems reliant on it. Similarly, sediment dynamics play a crucial role in the discharge rates of springs and the integrity of wetlands, with significant implications for water availability and ecological functions. The practice of sediment mining in river systems introduces a complex array of environmental, hydrological, geomorphological, ecological, socio-economic, hydrogeological, and climatic challenges. This underscores the urgent need for adopting sustainable mining practices, implementing stringent regulations, and developing sophisticated management strategies. It is imperative to find a delicate balance between reaping the economic benefits of sediment mining and ensuring the protection of river ecosystems, a balance that is essential for promoting environmental sustainability and improving community well-being over the long term.

1.7 Effects of Sediment Mining on Riverbank Erosion

Sediment mining, particularly from riverbeds, exerts profound influences on riverbank erosion, with significant ramifications for environmental stability, ecological health, and socio-economic conditions. This section comprehensively explores these effects, presenting detailed analyses and insights into the multifaceted impacts of sediment mining on riverbank erosion.

1. **Channel Instability**: Persistent sediment extraction disrupts the equilibrium of the river channel, causing morphological instability. This instability manifests as unpredictable shifts in the river's course and channel configuration, leading to new erosion-prone areas and altered sediment transport dynamics (Liu et al., 2020). Such instability affects the long-term sustainability of the river's physical structure.

2. **Loss of Natural Features**: The erosion caused by sediment mining often results in the loss of critical geomorphological features such as meanders, sandbars, and river islands. These features play vital roles in maintaining riverine habitat diversity and geomorphological complexity. Their loss can lead to a simplified river structure, which affects the river system's physical and ecological aspects (Peterson & Hughes, 2019).

3. **Riparian Vegetation Loss**: Erosion resulting from sediment mining can destroy riparian vegetation zones, which are crucial for many aquatic and terrestrial species. The loss of vegetation destabilizes riverbanks further and removes critical habitat for species dependent on riparian zones. This destruction leads to a decline in habitat quality and can severely impact local biodiversity (Williams et al., 2021).

4. **Biodiversity Decline**: The destruction of habitats and increased turbidity from erosion can lead to a significant decline in aquatic biodiversity. Species that rely on specific riverine habitats for breeding, feeding, and shelter are particularly vulnerable to these changes. The

resultant decline in biodiversity affects ecosystem functions and services, disrupting ecological balance (Harris & Robinson, 2020).

5. **Increased Sediment Load**: Erosion increases the sediment load in the river, resulting in elevated turbidity levels. High turbidity impairs light penetration, affecting aquatic plants' photosynthesis and overall river health. The increased sediment load also affects fish and other aquatic organisms by reducing habitat quality and altering food availability (Parker et al., 2021).

6. **Pollutant Release**: The mobilization of sediments due to erosion can release previously trapped pollutants, including heavy metals and nutrients, into the water column. This release contributes to water quality degradation and can lead to issues such as eutrophication, harmful algal blooms, and increased toxicity in aquatic systems (Kim & Lee, 2019).

7. **Property and Infrastructure Damage**: Increased erosion can significantly damage property and infrastructure situated along riverbanks. The loss of land and structural damage to bridges, roads, and buildings can have substantial economic implications for local communities. Repair and reconstruction costs can strain public and private finances (Smith et al., 2018).

8. **Agricultural Impacts**: Erosion-induced loss of fertile topsoil from agricultural lands can severely impact crop yields and productivity. The degradation of soil quality reduces agricultural potential and affects food security. Farmers may face increased costs for soil conservation and fertility management (Johnson & Martinez, 2022).

9. **Increased Maintenance Costs**

a) **Bank Protection Measures**: In response to erosion, various bank protection measures such as retaining walls, riprap, and vegetation restoration are often employed. These measures

require substantial financial investment and ongoing maintenance to be effective. The costs associated with these interventions can be significant, impacting local budgets and resources (Brown & Thompson, 2021).

b) **Dredging Needs**: Increased sediment deposition downstream necessitates more frequent dredging to maintain navigable waterways and reservoirs. The costs of dredging operations and the associated logistical challenges can impact water management strategies and budgets (Wilson et al., 2020).

10. **Groundwater Recharge**: Sediment mining and resulting erosion can alter the permeability of riverbeds and banks, impacting groundwater recharge rates. Changes in the river's sediment dynamics can reduce the efficiency of water infiltration into aquifers, affecting groundwater availability (Brown et al., 2022).
11. **Aquifer Depletion**: Reduced river levels due to erosion can lead to diminished groundwater recharge, causing aquifer depletion. This depletion impacts the availability of groundwater resources for various uses, including irrigation and drinking water (Harrison & Adams, 2021).

1.8 State-of-the-Art

Thorne and Tovey (1981) explored the mechanics of bank failure, with a focus on bank toe erosion. Their study identified that undercutting at the toe is the initial phase in many riverbank failure processes. The researchers highlighted the importance of considering not only hydraulic forces but also the geotechnical properties of the bank material.

Simon et al. (1991) introduced a comprehensive approach to understanding the processes leading to riverbank failure in incised streams. Their conceptual model, the "Bank-Stability and Toe-Erosion Model" (BSTEM), allowed for the prediction of the timing and extent of bank failures under varying hydraulic conditions. This model was notable for accounting for the role

of groundwater and hydrological conditions, making it one of the first to comprehensively include the complex interplay between surface and subsurface water in its predictions.

Izumi et al. (1991) conducted an early investigation into cost-effective methods for mitigating riverbank erosion in channels with coarse-grained material. Their approach allowed the channel to reach equilibrium, focusing on the use of physical structures such as jacks, jetties, and dikes to slow the flow near the banks. Through their experiments, they identified a threshold density of these structures that effectively reduced the rate of bank erosion. Additionally, they introduced fine suspended materials into the flow, which slowed down the water further, facilitating the deposition of sediment near the eroded banks. Their study suggested that slowing the flow and introducing fine particles could replenish eroded banks, offering a strategic approach to bank stabilization.

A report **(River Width Adjustment. II: Modeling, 1998)** was built on this foundation by focusing on a comprehensive review of riverbank failure mechanisms, as part of an ASCE task committee's efforts. This committee emphasized the necessity for further validation of laboratory models with field data, highlighting the importance of more robust predictive models for riverbank erosion. Their conclusion underscored the gap between controlled experiments and real-world applications, a recurring theme in riverine research that calls for more integrated, field-based studies.

Couper et al. (2002) advanced the field by developing an in-situ method to measure riverbank erosion using erosion pins, allowing for long-term monitoring at multiple sites in the UK. While the erosion pins allowed for minimal supervision, the researchers acknowledged that the method was intrusive, and that fallen material from higher up the bank often obscured lower-level failures. This methodological limitation, coupled with potential human interference,

pointed to a need for more refined, non-intrusive approaches for studying natural bank erosion processes.

Goring and Nikora (2002) addressed another aspect of the data collection challenge, introducing a three-step technique for filtering noise from Acoustic Doppler Velocimeter (ADV) data. Their method involved categorizing expected signals based on original observations and capping subsequent values with a universal threshold value of acceleration. The approach improved the accuracy of turbulence measurements by replacing data spikes with averaged values, thereby refining the interpretation of flow dynamics near riverbanks—critical for understanding erosion processes more clearly.

Neyshabouri et al. (2002) investigated the influence of pit dimensions on sediment refill rates. Their research demonstrated that pit width, rather than length, had a more significant impact on sediment refill, though they found little effect on downstream turbulence characteristics. This finding emphasizes the localized impact of morphological changes on sediment transport, a factor that needs to be incorporated into larger models of river dynamics.

Debnath et al. (2007) developed an innovative technique using an ultrasonic ranging system to measure the erosion rates of cohesive banks. Their method successfully replicated real-world flow conditions and demonstrated that bed shear stress is a critical factor in erosion processes, particularly in cohesive riverbanks. This work supports the idea that cohesive materials, while generally more resistant to erosion, still exhibit vulnerability under specific stress conditions.

Florsheim et al. (2008) argued for the ecological benefits of natural riverbank erosion, which they claim enhances aquatic habitats. They posited that coarse material from eroded banks can create beneficial structures downstream, contributing to channel complexity and habitat formation. They also criticized rigid structures for controlling erosion, suggesting that these measures disrupt natural processes and downstream ecosystems, an argument that highlights

the need for a balance between human intervention and ecological integrity in river management.

Chuagor et al. (2008) developed a numerical model to simulate the effects of seepage on riverbank stability. Their findings showed a drastic reduction in safety factors, up to 91%, under seepage conditions, highlighting the critical impact of groundwater flow on bank stability and the potential risks to nearby structures. This model stresses the importance of incorporating seepage effects in erosion predictions and infrastructure planning.

(Rinaldi et al., 2008) explored riverbank dynamics in a high-curvature bend, focusing on the gravel riverbeds common in their study area. They found that river discharge during rising and drawdown periods had more profound effects on bank stability than peak flow levels. Their work demonstrated how multi-peaked flow events can exacerbate bank instability through changes in hydrostatic pressure and pore water pressure.

Pizzuto (2009) investigated the role of vegetation in controlling riverbank erosion. His research demonstrated that riparian vegetation significantly influences erosion rates by stabilizing soil through root networks. The study pointed out that vegetation not only reduces surface erosion by anchoring soil but also dissipates flow energy near the banks, reducing hydraulic forces. Pizzuto's work supports the idea of using vegetation as a natural bank stabilization technique, which has become an important consideration in modern river management practices aimed at balancing engineering solutions with ecological restoration.

Darby et al. (2010) developed a numerical model to simulate the effects of vegetation on riverbank stability. Their model incorporated both mechanical and hydrological effects of vegetation and demonstrated that root reinforcement could significantly increase the critical shear stress required to initiate bank erosion. However, they also noted that the beneficial

effects of vegetation could be reduced during high-flow events, when shear stresses exceed the reinforcing capacity of roots, leading to significant erosion even in well-vegetated banks.

A study of unsteady flow conditions in alluvial rivers by **Nasermoaddeli (2011)** identified three dominant bank failure processes: slip failure, undercutting, and cantilever failure. His model was validated through field experiments, which confirmed that initial toe erosion often leads to progressive bank failures. His work also suggested that displaced material from failed banks can temporarily stabilize the riverbed, but strong flows will ultimately erode this stabilizing material, emphasizing the dynamic nature of riverbank erosion.

Papanicolaou et al. (2011) addressed sediment transport and deposition processes related to bank erosion through flume studies that simulated high-flow events. They discovered that bank failures often contributed large amounts of sediment to the channel, which could be deposited downstream, affecting river morphology. Their work provided insights into the feedback loop between bank erosion and sediment transport, highlighting how erosion not only shapes the local bank structure but also influences broader channel dynamics.

Grove et al. (2013) demonstrated that advancements in remote sensing technologies, particularly the use of LiDAR technology, have provided new tools for effectively monitoring erosion. Digital Elevation Models (DEMs) generated from repetitive images allowed them to track long-term morphological changes, such as those caused by floods. However, they acknowledged that in-situ observations remain critical for capturing the full complexity of riverbank erosion events, which highlights the complementary nature of fieldwork and remote sensing.

Rhoads et al. (2013) focused on the influence of human activities, such as urbanization and land-use changes, on riverbank erosion. Their research revealed that increased impervious surfaces in urban areas resulted in more frequent and intense stormwater runoff, which

exacerbated erosion in downstream riverbanks. Their findings have significant implications for urban planning and stormwater management, suggesting that efforts to mitigate riverbank erosion must address both upstream land-use changes and localized bank stabilization techniques.

Xia et al. (2014) explored flow stages and their influence on riverbank failure, expanding on the impacts of cohesive and non-cohesive material properties. They found that cohesive material banks were more resistant to erosion, but stability decreased when flow transitioned from high to low stages due to changes in confining pressure. These findings, coupled with the observation of reduced sediment load downstream of the Three Gorges Dam, reinforce the role of sediment dynamics in bank stability.

M. Hui Yu et al. (2015) further investigated the process of lateral channel migration as a driver of bank erosion, examining the role of shear stress in triggering erosion in both cohesive and non-cohesive materials. Their flume experiments revealed that bank failure typically starts at the water surface for non-cohesive materials but begins at the toe for cohesive banks. Their observations corroborated earlier findings by **Nasermoaddeli (2011)** and advanced our understanding of shear stress profiles in riverbank erosion.

A. Sharma & Kumar (2017b) utilized Acoustic Doppler Velocimetry (ADV) and ultrasonic ranging systems (URS) to capture turbulence characteristics in fluvial environments. Their comprehensive use of Reynolds Shear Stress, mixing length, and quadrant analysis provided deep insights into the turbulent forces that drive bank erosion, emphasizing the importance of understanding turbulence in riverbank stability models.

B. Barman et al. (2018) extensively worked on exploring the effects of sediment mining pits on the downstream flow structure. They observed an increase in turbulence parameters as the flow passed through the sandpit. Further, they (B. Barman et al., 2019a) have worked with

different shapes of the sediment mining pits. Their (B. Barman et al., 2020) study also included the study of the migration of pits, which infers that a pit can migrate from one location to another location downstream. This could have serious consequences for the benthic environment located downstream of the mining location.

Bhattacharya et al. (2019) explored the influence of sand mining on river morphology in Bengal. They observed that mining activities disrupted the natural sediment balance, resulting in "hungry water" downstream of mining sites. This led to increased shear stress and morphological shifts in both the upstream and downstream river sections, highlighting the interconnectedness of human activities and natural river dynamics.

Zhao et al. (2020), Lade et al. (2020) and Lade & Kumar (2020) further explored the interaction of mining with turbulence, focusing respectively on the effects of bank height and mining pits on downstream flow. Their studies underscore the need for comprehensive modeling approaches that incorporate both natural and anthropogenic factors in riverbank stability predictions. The importance of understanding turbulence at various scales and its impact on structures, such as piers and riverbanks, was further echoed in these studies, highlighting a critical area for future research. **Lade et al. (2021)** emphasized that the distance of the mining pit from the riverine structure of interest has a direct effect on the enhancement of the turbulence parameters. Their study focused on understanding the effects of mining on different types of piers.

Liu et al. (2022) and Valyrakis et al. (2021) studied the role of glass tubes as rigid vegetation to understand the turbulence parameters near the riverbank. Their studies are limited to the fixed riverbank and fixed riverbed adjacent to the bank. This limits the understanding of river morphology and turbulence structure in the continuously varying dynamics of the rivers. Another limitation exists with the extent of the vegetation used to mitigate the riverbank

erosion. They have limited the extent of the rigid vegetation till the end of the slope of the riverbank. This thesis describes the importance of the extent of these solutions and discusses enhanced stresses at the interface of the vegetated and unvegetated sections.

Yang et al. (2023) emphasized that riverbank erosion, especially in regions with non-cohesive soil, is not yet fully understood. This ongoing research gap underscores the complexity of natural processes and the need for further investigation to better comprehend and mitigate riverbank erosion impacts.

1.9 Need for Research

Researchers (Arai et al., 2018; Debnath et al., 2007; Zhao et al., 2020) have conducted studies on riverbank erosion using experimental and field analyses. However, these studies have limitations, such as focusing on small test samples and other studies involving compacting test samples before experimentation, which do not reflect real-world scenarios. The existing research primarily focuses on observing the results and processes of riverbank erosion rather than investigating the causes and quantifying the turbulence parameters involved. There is a significant gap in the literature regarding the effects of sand mining on the turbulence characteristics of flow close to the riverbanks. Previous studies have been conducted at arbitrary angles without considering soil characteristics like the angle of repose. Incorporating this information could help propose stable cross-section slopes to mitigate riverbank erosion. Furthermore, no studies have recommended optimal mining pit locations to enhance riverbank stability. Although Lade et al. (2020) suggested locations for mining pits to minimize effects on piers, comprehensive guidelines for riverbank stability remain lacking.

In the research gap of the study of riverbank erosion, Shu et al. (2019) observed changes in sand profile with a rigid bed. G. A. Yu et al. (2020) and Yu Minghui et al. (2016) studied erosion using two different soils, while Okeke et al. (2020) focused on studying riverbank

failures in field conditions. Valyrakis et al. (2021) used artificial vegetation at the slope with fixed riverbanks and riverbeds, which did not provide a complete understanding of the riverbank erosion process.

In sediment mining cases, B. Barman et al. (2018, 2019b); B. Barman & Kumar (2023) found that sandpit affects downstream flow's turbulence properties and demonstrated 3D turbulence in the Anisotropy Invariant map. Ghosh et al. (2016) suggested that the Thalweg of the river is shifting towards the mining sites.

Lade et al. (2020); Lade, Deshpande, et al. (2019) studied the effects of changes in flow structure due to sediment mining on bridge piers. They observed increased scouring depths, lateral erosion, and increased foundation exposure as the pit moved closer to the piers. Channel dredging increases the values of shear stresses near the bed at the cylinder front and increases the peak of higher-order turbulence by about 15% at the rear of the cylinder (Lade et al., 2022). Higher streamwise Reynolds shear stresses (RSS) are also generated in the near-bed region immediately downstream of the pier (Lade et al., 2019). Severe transverse erosion at the pier base, as well as lowering of the channel bed upstream of the pier, was observed because of channel dredging (Lade et al., 2020).

Bariteau et al. (2013) showed the long-term effects of stabilization, establishing that nature-based solutions can be effective. Fernandes et al. (2020) used pitching to protect the riverbank, but it may be costly. Yang and others showed that vegetation can help maintain the boundaries.

This research gap helped establish the aim of this thesis, which is to examine flow structure and morphological changes of different riverbank slopes due to mining pits. Additionally, we have studied the effects of the pit's proximity on the riverbank's stability and explored the performance of nature-based solutions under dredged conditions.

1.10 Objectives of the Study

I. To study the changes in flow structure and morphological changes due to an upstream mining pit on riverbank stability with different slopes.

- To understand the effects of sediment mining on Deep vs Shallow Rivers.
- To understand the effects of sediment mining on different riverbank slopes.

II. To understand the effects of the location of a mining site and the dredging volume on the stability of the riverbank morphology and explain its explanation based on the turbulence parameters of the flow.

- To understand the effects of the proximity of the sandpit on a cross-section of interest.
- To understand the effects of increasing volume of dredging on a cross-section of interest.

III. To explore green solutions for Riverbank Erosion Protection in Dredged Channels by studying the morphological changes due to the combined effect of riverbank vegetation and upstream sandpit.

- To understand the effects of natural, flexible, grown vegetation as a mitigation measure to control riverbank erosion under dredged conditions.
- To understand the effects of natural, rigid stems hammered into the soil as a mitigation measure to control riverbank erosion under dredged conditions.

1.11 Organization of the Thesis

Chapter 1 introduces the readers to the cyclic process of riverbank failure and retreat. It attempts to understand the increasing cases of riverbank failure by relating it to increasing illegal sediment mining cases. It showcases the previous research done by the researchers and then lays out the research gap to establish the aims of this thesis.

Chapter 2 takes the readers through the details of the Flume and the instruments used for carrying out the work in this thesis. It shows the preparation of the test sections and the steps involved in data collection. It also presents the different experimental setups for the following chapters. It will help readers understand the methodology involved in understanding the aspects of riverbank failure due to sediment mining.

Chapter 3 presents the turbulence parameters in the vicinity of the riverbank. It also shows the changes in the morphology of an asymmetrical alluvial channel due to the upstream sediment mining pit. First, it establishes whether a deep or a shallow channel is affected more by a sandpit. Second, it attempts to understand the stability of riverbank cross-sections with different riverbank slopes. It will help readers to understand and quantify the effects of sediment mining on an alluvial channel.

Chapter 4 explores the effects of the sediment mining pit due to its proximity to a section of interest. It also attempts to understand the changes in turbulence parameters and channel morphology due to the increasing volume of dredging from the riverbed. It helps readers understand its adverse effects if sediment mining is not regulated.

Chapter 5 showcases the use of nature-based solutions to mitigate the effects of sediment mining on riverbank erosion. It quantified the near-bank and near-bed turbulence parameters for a deep understanding of the combined effects of sediment mining and the mitigation measures. The readers will be able to understand which kind of vegetation would be suitable for the mitigation measures to be effective.

Chapter 6 concludes the work of the thesis and lays out the recommendations for the development in the field of river research. It also proposes future research work that can be carried out to advance the riverbank erosion mitigation measures.

Appendix I illustrates the turbulence structure of the flow at the interface between the vegetated and unvegetated sections. This study helped identify the necessary extent of riverbank protection measures to enhance the stability of the riverbank, particularly at its toe.

2. Methodology

2.1 Overview

This chapter presents insights into the test setup preparation and data collection for more than 90 experiments performed in this thesis to understand the effects of sediment mining on riverbank stability and explore its mitigation measures. It will take readers through the experimental flume, instruments used for the study of three-dimensional flow velocity measurements, riverbed morphology, and sediment transport.

2.2 Experimental Setup

2.2.1 The Flume

The experimental flume of 17.20 m with glass side walls has been set up at the Water Resources Laboratory in the Department of Civil Engineering at the Indian Institute of Technology Guwahati, Guwahati, India. The width of the flume is 1 m, and the available flow depth is 0.7 m. It is a tilting flume with a longitudinal slope of 0.0019 for all the experiments conducted for this thesis. It is a recirculating flume that intakes water from a large underground sump of 60 m^3 capacity. It is transferred to an overhead tank using 3 centrifugal pumps of 7 KW each. The overhead tank helps maintain a constant head to the inflow of the flume. Upon entrance of flow into the flume using a 0.2 m diameter pipe, it passes through the baffle walls that help remove any unsteady local fluctuations from the flow and provide a smooth entrance to the flow. A length of 5 m has been left between the entrance and the test section for the development of flow (Lade, Mihailović, et al., 2019). The test section consisted of a 5 m length, which was followed by a sediment collector tank of 0.4 m length and 1 m width. It accumulates all the sediment that travels from the test section. The collected sediment is then dried at 108 degrees Celsius. This obtained sediment can be compared for different cases presented in this thesis. The flow then passes over the tailgate, which helps maintain the required flow depth for each

experiment. The flow then passes through a 0.5 m wide rectangular notch that helps determine the flow rate. The flow then joins the underground sump through the drains. A sand bed of 0.15 m is laid throughout the flume without any external compaction or drops. The details of the sand used for sand preparation is discussed in the following sections of the thesis.

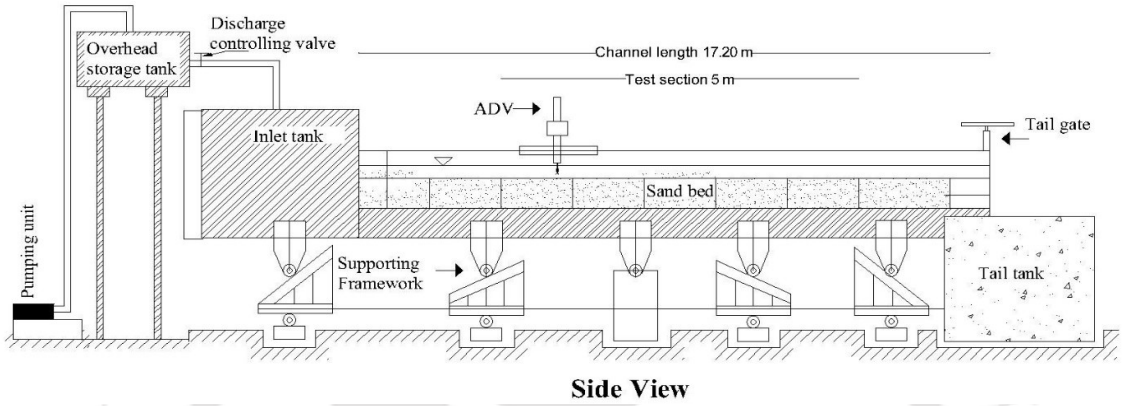

Figure 2.1: The Flume (Side View)

2.2.2 Channel Bed Material and Preparation

The sand bed of 0.15 m thickness has been laid from the entrance of the flume till the sediment collector tank is placed downstream of the test section. In the trial runs for the experiments, the sandbed erosion was always less than 0.05 m, which indicates that the bed thickness was sufficient. The bed material is prepared of uniform sand with a median size (d_{50}) of 1.1 mm for the experiments performed for chapters 3 and 4. This sand can be classified as poorly graded coarse sand. The uniform size of the sediment helps keep the resisting force due to interlocking to be approximately the same for all the cases of experiments, as discussed in Figure 1.2. For Chapter 5, the sand used is of the median size of 0.23 mm and can also be classified as poorly graded sand. This sand was obtained from the Brahmaputra River, which is located close to the institution. The size distribution of both the bed material has been presented in Figure 2.2. The average data of three samples obtained from sieve analysis has been presented in Table 2.1.

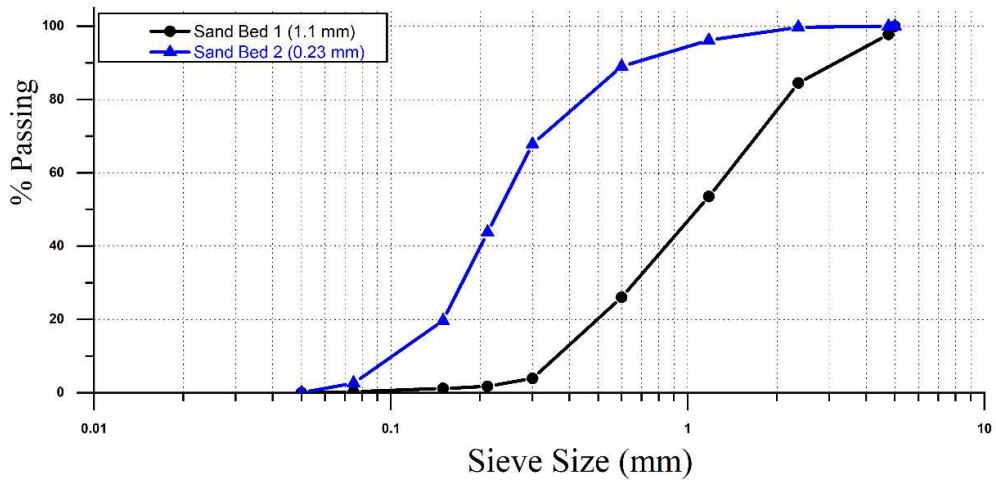

Figure 2.2: Sieve Analysis of Sandbed materials on a semi-logarithmic scale

The classification of sand based on the particle size using sieve analysis of oven-dried samples of both sandbed 1 and sandbed 2 suggests their classification to be coarse sand and fine sand, respectively. The uniformity coefficient (C_u) is less than 6, and the coefficient of curvature (C_c) is close to or less than 1, which indicates that both sandbed materials are uniformly graded. Here, D_{10}, D_{30}, D_{50}, and D_{60} represent 10%, 30%, 50%, and 60% finer material out of the total sample.

Table 2.1: Sandbed particle size classification

	Sand Bed 1	Sand Bed 2
D_{50}	1.106 ~ 1.1 mm	0.228 ~ 0.23 mm
D_{10}	0.382	0.107
D_{30}	0.653	0.176
D_{60}	1.317	0.254
C_u	3.45	2.37
C_c	0.85	1.15

The channel bed was prepared by placing the sand with a thickness greater than the required 0.15 m without any drops. The channel was flooded to achieve natural compaction. The water was drained, and the top of the sandbed was trimmed using the iron mould, as shown in Figure 2.3. The same steps were repeated to prepare the bed material for each experiment.

Figure 2.3: Channel Bed Preparation

2.2.3 Sediment Mining Pit

An irregularly shaped mining pit has been cut from the upstream of the test section. The depth of the pit has been kept at 50% (7.5 cm) of the depth of the bed (15 cm) (Figure 2.10). The literature suggests that the shape of the pit has a negligible effect on the changes in the turbulence parameters. It is the width-to-length ratio of the mining pit. The mining pit has been kept of the same dimensions for all the cases in order to establish a comparative analysis among different cases without worrying about the changes due to different width-to-length ratios of the mining pit. It is to be noted that it is impossible to predict the dimensions of the illegal and indiscriminate dredging. However, to understand the effects of dredging, the irregularly shaped pit has been created in the upstream of the test section. The excavated volume of the pit was $0.05m^3$.

2.2.4 Flow Rate Measurement

The flow rate measurement for all the experiments was done using the rectangular notch of width, L=0.5 m, which was placed downstream of the flume. The flow (Q) -depth (H) relation, $Q = \frac{2}{3} C_D \sqrt{2g} L H^{\frac{3}{2}}$ was used to find flow rate in m^3/s, where g is the acceleration due to gravity (m/s^2). The calibration resulted in a coefficient of discharge, C_D value of 0.82. The head at the notch was found to be 6 cm, 8.5 cm, and 10.6 cm for the discharge of 18, 30, and 42 L/s.

Figure 2.4: Rectangular Notch to Measure Flow Rate

2.3 Instruments and Data Collection

This section will help readers understand the operation of the instruments involved in 3D instantaneous velocity measurements, morphological study and sediment transport analysis.

2.3.1 Acoustic Doppler Velocimeter (ADV)

It is an instrument that works on the principle of Doppler's effect. It emits acoustic signals and studies the changes in the received signal to find the instantaneous velocity of the fluid parcel situated 5 cm below the emitter. The sample size of the fluid parcel ranges from 0.5 to 1 cm^3

(Figure 2.5). The ADV used in this thesis work was made by Nortek. It is a down-looking four-probe model that works at the maximum frequency of 200 Hz. One of its probes, marked with a red ribbon, must be aligned with the streamwise direction of the flow. The SNR (signal-to-noise ratio) must be maintained above 10, and the correlation coefficient must be more than 75 to achieve minimum noise in the signal (Caroppi, Västilä, et al., 2020). A minimum of 120 s of velocity time series were recorded at 100 Hz for each location. The measured velocities u, v, and w correspond to velocities along the X, Y, and Z axes or along the flow, cross-section, and depth, respectively. The velocity readings exhibited spikes of noise. To obtain a clean velocity time series, we utilized the despiking method based on the acceleration threshold approach (Arora, Patel, Srinivasulu, et al., 2023). Figure 2.6 illustrates the velocity power spectra of the streamwise velocities and frequency f at a location in the inner layer of the main channel flow. Figure 2.4 presents the power spectral density function of the raw (red) and postprocessed (blue) velocity time series. Kolmogorov's theory suggests that the acceleration threshold value should be determined through trial and error and should fall between 1 and 1.5, in order for the velocity power spectra in the inertial subrange of isotropic turbulence to follow the "-5/3" law (Pu et al., 2017). Due to the presence of two solid barriers close to the probe, the data obtained at the bank slope displayed higher spikes, particularly. To minimize errors when collecting data near the bank slope, we extended the time series. The manufacturer-provided ADV has an accuracy of 0.5%.

The given sample rate shall give 12,000 samples at all the points in the test section. Figure 2.6(b and c) shows the convergence analysis performed to understand how many samples are sufficient to average out the fluctuations obtained in the readings. The ratio of the average of first N values to the ratio of 12000 samples is observed. As the ratio comes close to 1, it means that the number of samples obtained is sufficient to obtain average values of the turbulence parameters. The convergence analysis revealed that the streamwise velocity data reached

convergence at 7000 samples with an error percentage of less than 2%, while the RSS data converged at 9000 samples with an error percentage of less than 4%. This indicates that 12,000 sample readings at an observation point were adequate to maintain the error within the acceptable range.

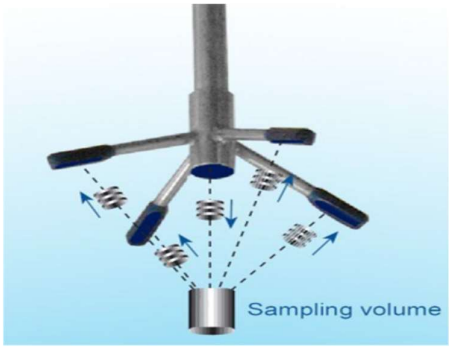

Nortek ADV User Interface

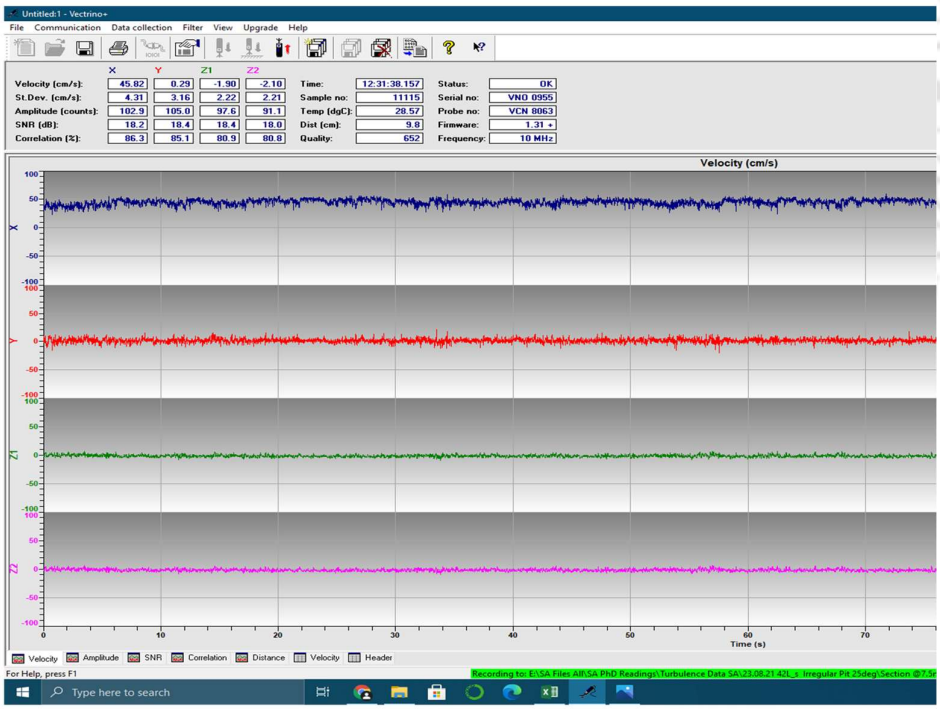

Figure 2.5: Acoustic Doppler Velocimeter (ADV); Working of ADV with Sampling Volume; User Interface

Figure 2.5 shows the probe of ADV installed on a trolley and deployed in the water during an experiment. The user interface of ADV shows the values of SNR and correlation coefficient. The four analogue signals shown here are the readings obtained from the instrument. The signals from the top (X, Y, Z1, and Z2) display the streamwise, transverse and depthwise (1 and 2) velocity instantaneous readings. The depthwise readings 1 and 2 help in correlating with the streamwise and transverse velocity.

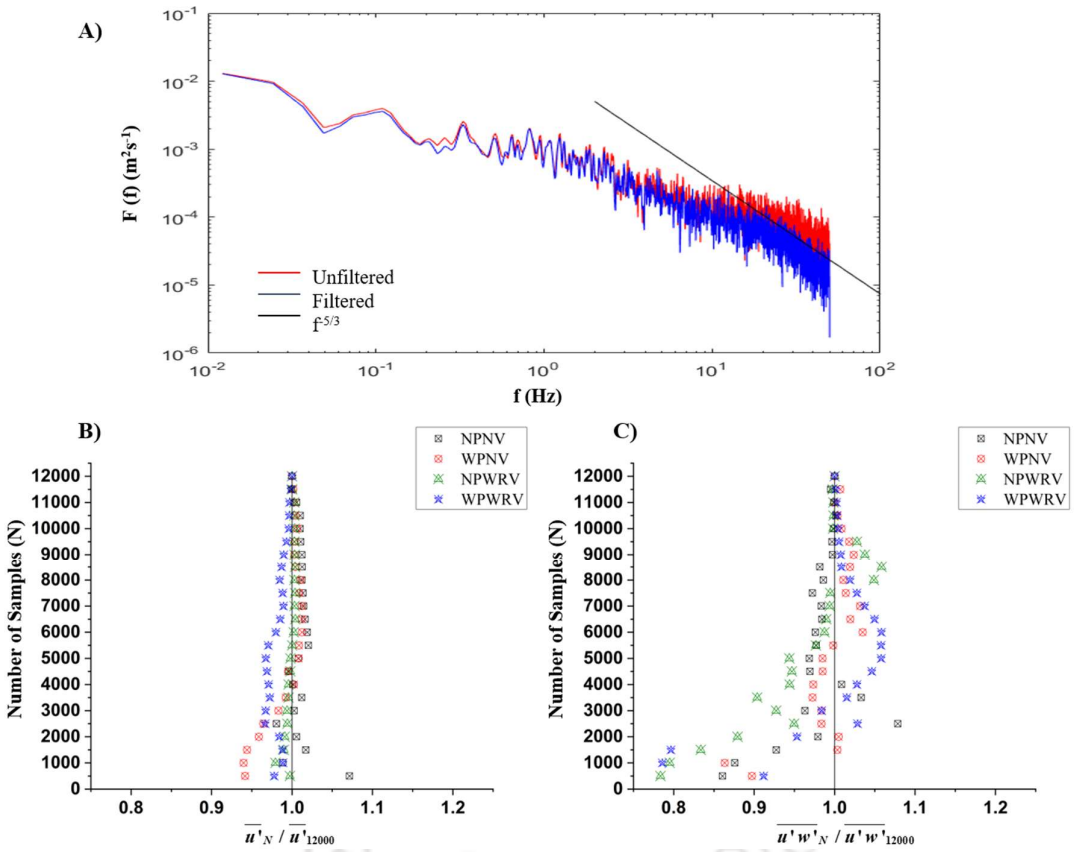

Figure 2.6: Velocity Power Spectra and Convergence Analysis

The velocity readings obtained are instantaneous readings (u, w, v) that can be split into an average component and a fluctuating component (u', w', v') for streamwise, depthwise, and transverse directions, respectively. This splitting of instantaneous readings is termed as Reynolds Averaging. Table 2 lists the velocity measurement uncertainties for the observed readings using ADV, which are in the acceptable range.

Table 2.2: Standard Deviation and Uncertainty analysis of ADV readings

(m/s)	u	v	w	$(u'u')^{0.5}$	$(v'v')^{0.5}$	$(w'w')^{0.5}$
Standard Deviation	$4.16x10^{-3}$	$9.01x10^{-4}$	$3.88x10^{-4}$	$1.23x10^{-3}$	$1.45x10^{-3}$	$2.68x10^{-4}$
Uncertainty %	0.27	0.08	0.05	0.04	0.057	0.024

2.3.2 Ultrasonic Ranging System (URS)

The Seatek ultrasonic ranging system, operating at a frequency of 5MHz, was utilized to measure bed elevations along the centerline of the test section in order to analyze the impact of a pit on bank erosion and sediment movement dynamics. This system consists of five cylindrical transducers enclosed in stainless steel, each measuring 25.4mm in length and 13mm in diameter. Data from all the transducers was collected using a data logger connected to a computer via the designated channel. Five URS transducers were deployed, each with specific placements for monitoring different aspects. One transducer was positioned 0.3m from the wall to track changes in bed level, while another was placed 0.6m from the wall to observe the bank. The remaining three transducers are situated at distances of 0.35m, 0.42m, and 0.55m from the glass wall to monitor the starting of the berm, the initial location of the toe, and the berm ending at the bank, respectively. The system was set to record bed elevations at 10Hz and was mounted on an electric motor-operated trolley capable of moving at a constant speed along the test section. The trolley was equipped with two single-speed motors (Johnson Geared Motor 300 RPM 12v DC Gear for Robotics) at its rear wheels, enabling remote operation at a fixed speed. Bed elevations were recorded at 0, 5, 12, and 24-hour intervals along the riverbank sections as the trolley traversed from the beginning to the end of the observation region of the test section. Figure 2.7(A) presents the photograph of the transducers installed on the moving trolley. These are installed so that they are in contact with the surface of the water. Figure 2.7(B and C) shows the screenshot of the settings that can be changed in the URS as per the requirement of the

experiment. The readings obtained present the distance of the transducer from the water's top surface to the surface of the bed. To obtain the absolute bed level, these readings are subtracted from the water's top surface level.

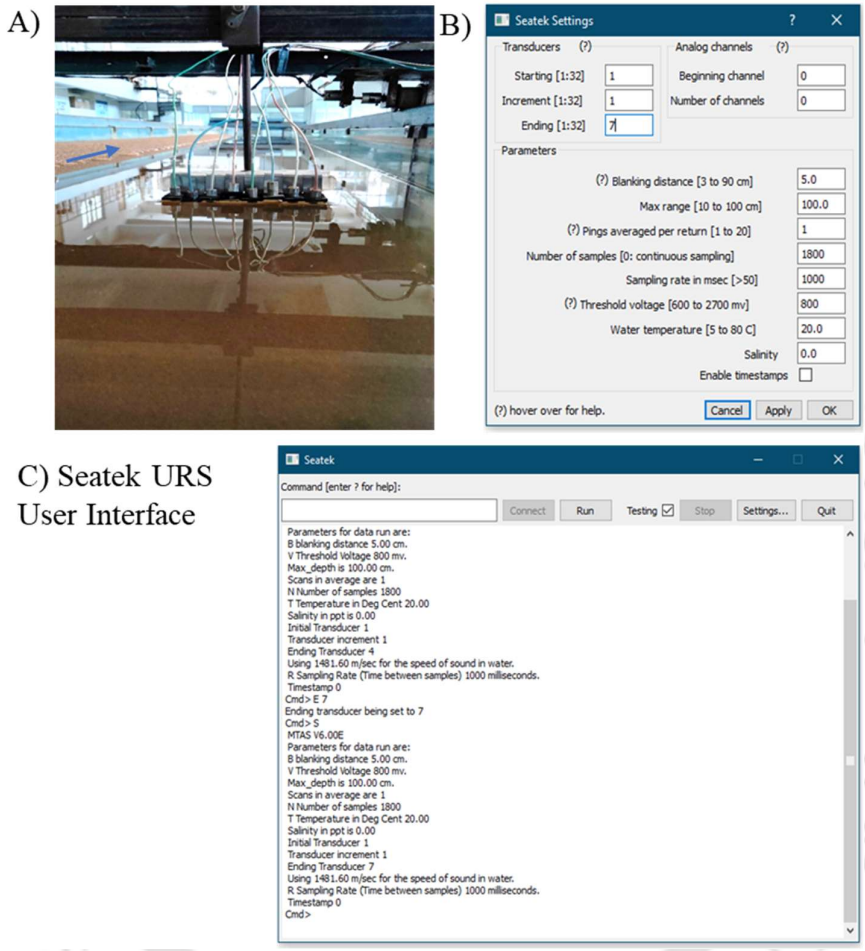

Figure 2.7: Ultrasonic Ranging System

2.3.3 Sediment Collector Tank

The sediment collector tank is a container placed downstream of the test section. Its dimensions are 0.4 m in length, 1 m in width, and 0.15m in depth. The transporting sediment is trapped in this container, which is collected after the end of the experiments to compare the sediment transport for each case of the experiments. Figure 2.8 presents the collected sediment after an experimental run of 24 hours for the case of No Pit and a 31-degree riverbank slope. Keeping all other parameters the same except the changing cases of different types of pit helps

understand how the introduction of sandpit has changed the sediment transport capacity of the test section.

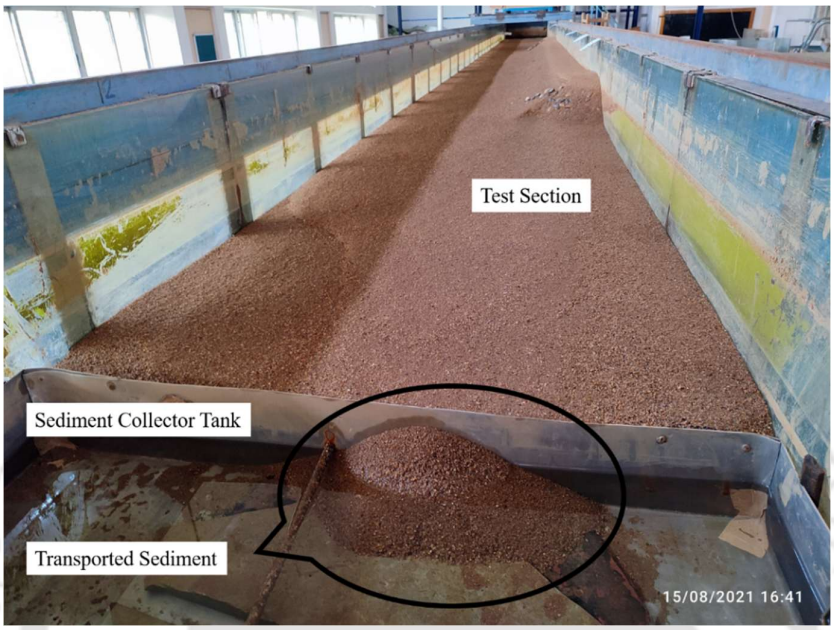

Figure 2.8: Sediment Collector Tank

2.3.4 Digital Point Gauge

A digital point gauge (Figure 2.9) was used to facilitate the measurement of flow depth and to track the morphological changes after the flow of water had been stopped. This instrument helps track the final morphological profiles of the riverbank slope with a lateral distance of 2 cm between two readings, which is maintained using a steel ruler. The accuracy of the instrument for measuring depth was 0.1 mm.

Figure 2.9: Digital Point Gauge

2.4 Experimental Setup

The experiments were conducted in the flume at the Indian Institute of Technology Guwahati, India, using different instruments, as discussed in sections 2.2 and 2.3. The thesis has established three main objectives, as discussed in section 1.10. Different sets of experiments were conducted to fulfil these objectives, which are discussed below.

Objective 1A: To understand the effects of sediment mining on shallow and deep rivers.

The rivers can be classified into shallow or deep rivers. It can either be two different rivers or two different stretches of the river upstream and downstream. or it may even be at the same cross-section. The experiments were conducted to check whether shallow rivers or deep rivers are affected more by sediment mining. Here, two different cross-sections were prepared with a riverbank slope of 31 degrees and different flow depths, as shown in Figure 2.10. The flow depths were maintained at 0.14 m and 0.23 m, which resulted in the top width-to-depth (B/H) ratio being 5.85 and 3.42, respectively. This satisfies the criteria of the classification of channel B/H>5 for wide and B/H<5 for narrow channels (X. Li et al., 2018). The preparation of an asymmetric test section with a riverbank on one side and a glass wall on the other side helped in understanding the near-bank stresses even in wider channels, even with experimental constraints. The preparation of the riverbank has been kept the same as the preparation of the riverbed, i.e., placing the sand without any drops or any external compaction and then flooding the channel to give a natural compaction to the sand. The wooden mould helped trim the excess sand and provided the desired slope and dimensions of the riverbank every time.

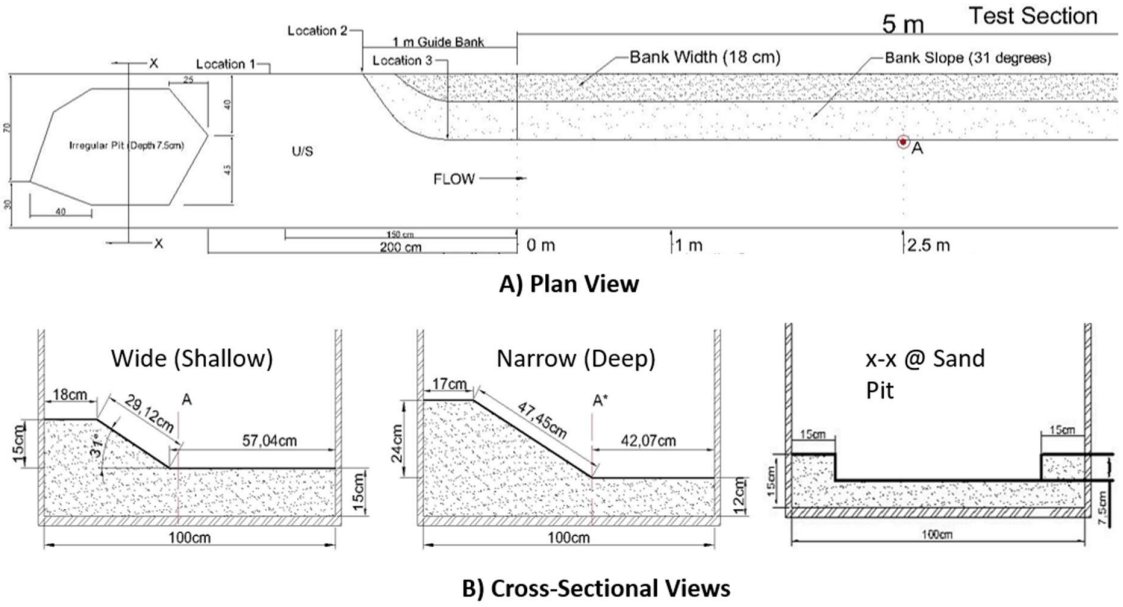

Figure 2.10: A) Plane View of the test section with upstream sandpit; B) Cross-sectional views of Wide (Shallow), Narrow (Deep), and upstream sandpit of 7.5cm depth and 70cm width.

Figure 2.11 presents the experimental photographs for this objective of narrow vs wide channels. Each column shows the riverbank test section from the front and top view without and with the sediment pit. The irregularly shaped pit has been dredged, and the shape and volume have been kept constant for all the experimental cases. The results of turbulence parameters and morphological changes are discussed in the following chapter.

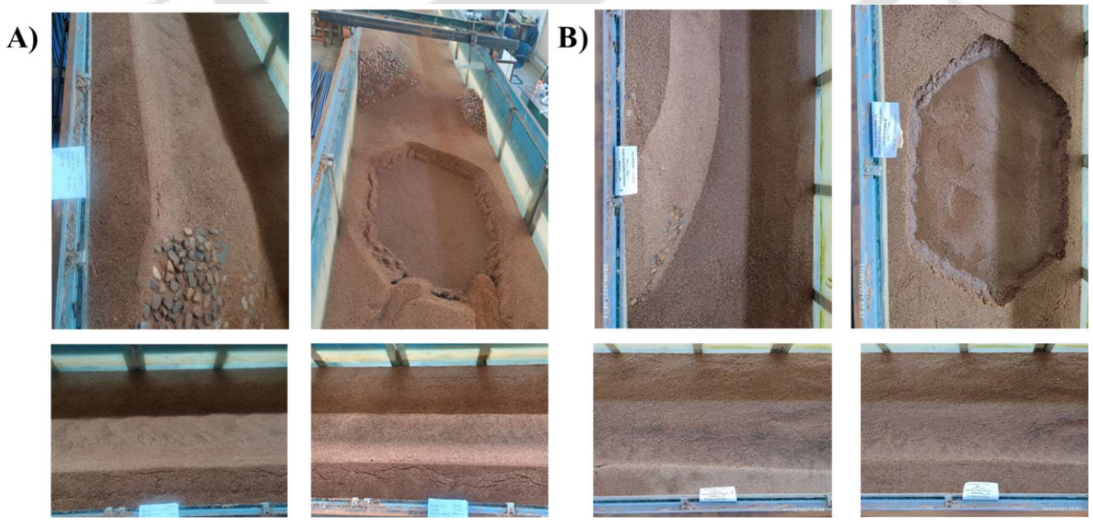

Figure 2.11: Photographs of Experimental Setup A) Wide (shallow) channel; B) Narrow (deep) channel showing riverbank without and with upstream sediment pit

After understanding the effects of sediment mining on the riverbanks of shallow and deep rivers, it is important to further analyse which riverbank slope is affected more by sediment mining.

Objective 1B: To understand the effects of sediment mining on different riverbank slopes.

Steady flow experiments were conducted on a section of the riverbank with three different inclinations: 25, 31, and 40 degrees, on one side of the flume, with discharge rates of 0.018, 0.03, and 0.042 cubic meters per second. A flow depth of 0.14 meters was consistently maintained by adjusting the tailgate. The riverbank's top width was set at 0.18 m, as the maximum erosion observed at the top width, even at the highest discharge, did not exceed 0.1 m. A guide bank, measuring 1 meter in length with stone pitching, was designed to gradually widen from zero to match the riverbank's dimensions and was positioned 6 meters from the entrance of the flume. Throughout these experiments, no external sediments were introduced. (Tay et al., 2015). The experiments were run for 24 hours each.

Three different discharges were used to carry out these experiments. The incipient condition was observed at the discharge of 0.032 m^3/s. The dimensions of the pit were the same as used in previous sections. The experimental conditions are given in Table 2.3. An irregular mining pit of 7.5 cm depth was dug upstream of the test section (Figure 2.12) to simulate channel dredging. At the end of every test, water was drained out slowly, and morphology at location 5 was recorded using a digital depth gauge. The transport of sediments from the channel and bank-derived sediments due to erosion occurred in the form of a bed load. The transported sediments were deposited in the bedload box at the end of the flume. The weight of this bedload was carefully recorded using an electronic weighing scale after oven-drying it for 24 hours.

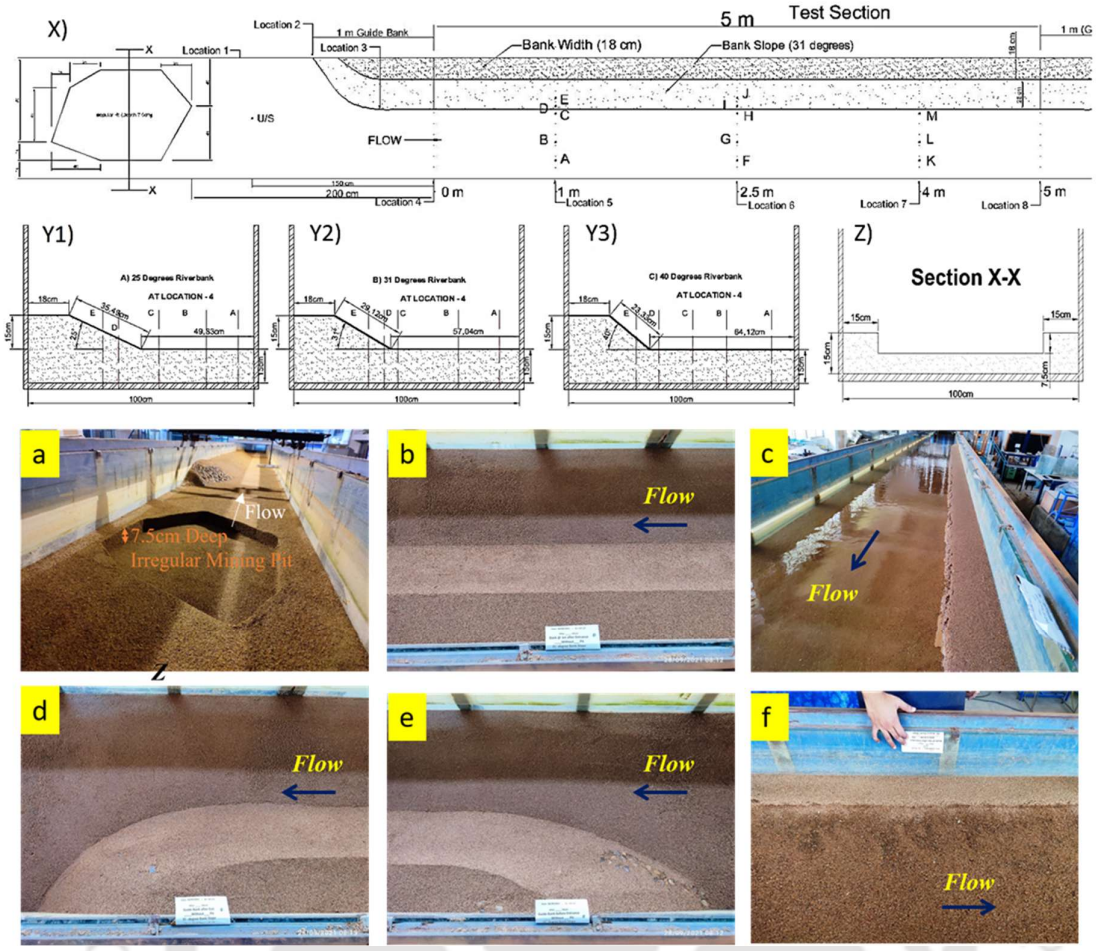

Figure 2.12: Experimental Setup W) side view of the flume X) Plan View of the 5 m test section with a sandpit upstream and observation points A-M Y) cross-sectional views of different slopes at location 4 that is, at the starting of the test section and section X-X at the location of the sandpit. Snapshot of the experiments (a) Irregular sand pit upstream of the riverbank section (b) riverbank test section seen from the top (c) flow in the test section during the experiment (d) downstream side guide bank (e) upstream side guide bank (f) Bank slope erosion at the end of the experiment.

Now, we can understand that sediment mining has direct effects on the riverbed and riverbank's toe, and we can quantify the turbulence and morphological changes. The effects of different locations of mining pits are essential and will be studied in the following section.

Table 2.3: Hydraulic Conditions for Experiments of Objective 1B to study the effects of Sediment Mining on Different Riverbank Slopes

S. No.	H_{bank} (m)	Riverbank Slope (Degrees)	H_{Flow} (m)	Q (m^3/s)	Pit	Re	Fr
1-3	0.15	25 (Gentle)	0.14	0.018, 0.03, 0.042	No Pit	24944	0.41
4-6	0.15	25 (Gentle)	0.14	0.018, 0.03, 0.042	With Pit	24944	0.41
7-9	0.15	31 (Angle of Repose)	0.14	0.018, 0.03, 0.042	No Pit	24840	0.39
10-12	0.15	31 (Angle of Repose)	0.14	0.018, 0.03, 0.042	With Pit	24840	0.39
13-15	0.15	40 (Steep Slope)	0.14	0.018, 0.03, 0.042	No Pit	24722	0.37
16-18	0.15	40 (Steep Slope)	0.14	0.018, 0.03, 0.042	With Pit	24722	0.37

Objective 2A: To understand the effects of the proximity of the sandpit on a cross-section of interest.

A critical aspect in the formation of rules and regulations for sediment dredging is fixing or allotting the location of dredging for legal vendors. The study of the effects of proximity of a mining pit on a cross-section of interest is very important. This experimental setup was designed with three conditions of sediment mining pit i.e., No Pit (NP 31), Instream Pit (INS 31), and Upstream Pit (USP 31). The riverbank slope angle has been fixed at 31 degrees because of the deductions from the previous objective, which tells us that a riverbank cross-section is least affected when the riverbank slope is at the angle of repose. This helped eliminate the failure of riverbanks due to the geotechnical properties of the sand, thereby focusing on the changes in turbulence characteristics of flow due to sediment mining pits. Figure 2.13 shows

the plan view and cross-sections of the given cases of sandpits, as well as photographs of the experimental setup.

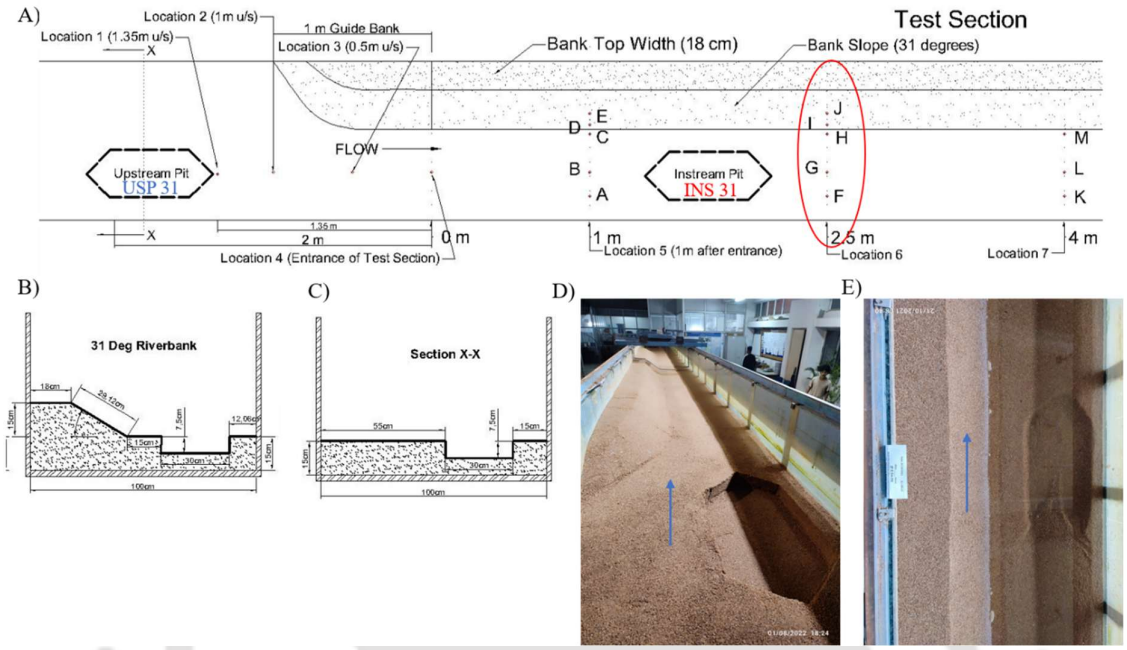

Figure 2.13: Experimental Setup for understanding the effects of the proximity of a pit on a section of interest A) Plan View; B) C/S of Instream Pit; C) C/s of Upstream small pit; Photographs of Test Section with D) Upstream small pit E) Instream Pit

Objective 2B: To understand the effects of increasing volume of dredging on a cross-section of interest.

Another aspect of preparing the regulations is allocating the extent of dredging or dredging volume to a legal vendor. A set of experiments was conducted to understand how the increasing volume of the sediment dredging affects the riverbank stability at a downstream cross-section of interest (marked in red in Figure 2.14). The cases include No Pit (NP 31), Small Pit (SP 31), and Large Pit (LP 31), as shown in Figure 2.14. The cross-section of interest is located 1 m downstream of the start of the test section. The cross-sectional geometry of the riverbank test section has been kept the same as in the previous case. The experiments were performed at the discharge rates of 0.018, 0.03, and 0.042 m^3/s for 24 hours for each case.

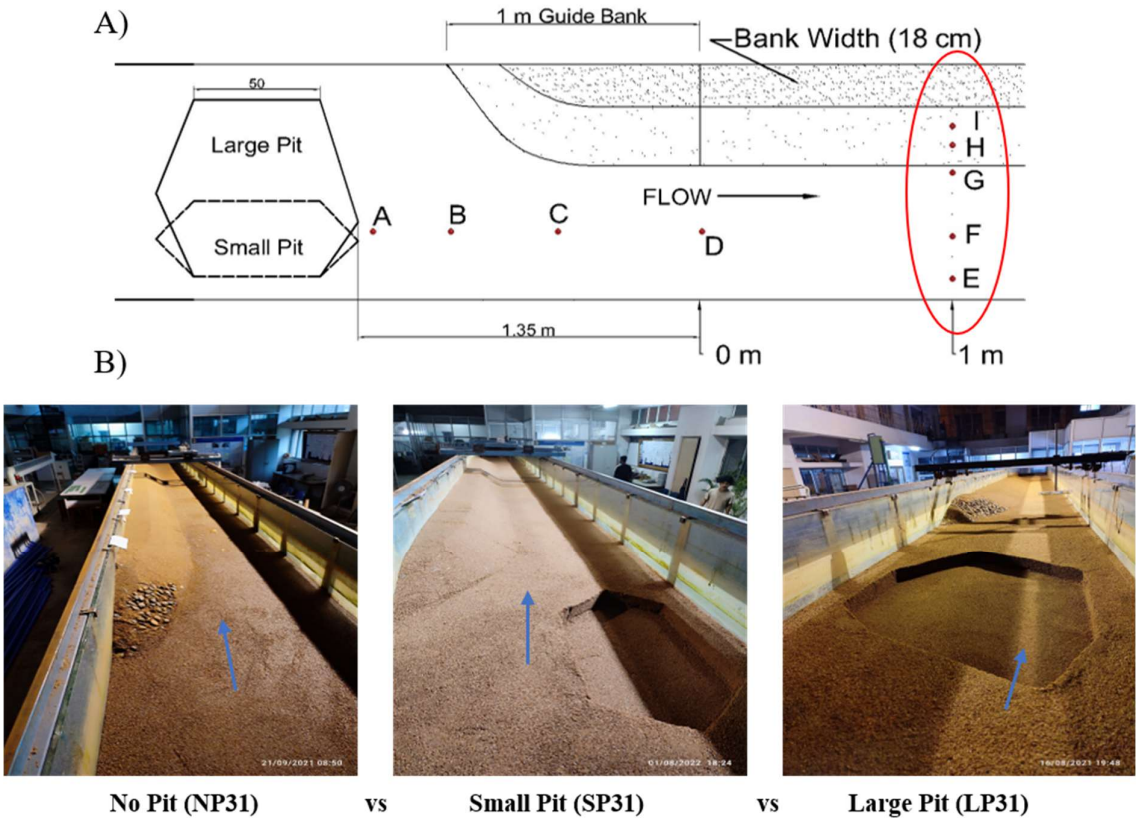

Figure 2.14: Experimental Setup for understanding the effects of the increasing volume of dredging on a section of interest A) Plan View; B) Photographs of Test Section of No Pit, Small Pit, and Large Pit

Objective 3A: To understand the effects of natural, flexible, grown vegetation as a mitigation measure to control riverbank erosion under dredged conditions.

After studying the effects of sediment mining on riverbank stability for various cases, this thesis explores nature-based solutions to mitigate riverbank erosion. In this objective, we shall look at the flexible vegetation planted at the riverbank slope and also beyond the toe of the riverbank to protect the riverbank from increased stresses at the interface of the flow and vegetation (Arora, Patel, Srinivasulu, et al., 2023).

In the conducted study, an asymmetric section of a riverbank was meticulously constructed in a sand medium, situated precisely 7 m from the entrance point of the flume's water. It was

designed so that the water flow would enter the flume and achieve a fully developed state. The experiment was set up to ensure that turbulent flow conditions were established over a 5 m stretch within the test section. This particular riverbank section featured a channel characterized by two side slopes; however, for the purpose of this study, only one of those slopes was constructed. This decision was grounded in the hypothesis that the flow structure would remain identical for both symmetrical halves, a notion supported by previous studies (Knight & Demetriou, 1983; Shiono & Knight, 1991). The riverbank test section extended over a total length of 5 m, as depicted in Figure 2.15. Further details of the riverbank's cross-section, spanning this 5 m length, reveal a top width of 0.18 m and an unsupported side slope height of 0.15 m. Moreover, the riverbank slope, or angle of repose, was determined to be 31°, a configuration illustrated in Figure 2.15. To facilitate a smooth transition of flow, tapered width guide banks were strategically placed at both the commencement and termination points of the test section. These guide banks were designed to gradually transition from zero to the full width of the riverbank before returning to zero, ensuring a controlled modification of flow width throughout the experimental setup.

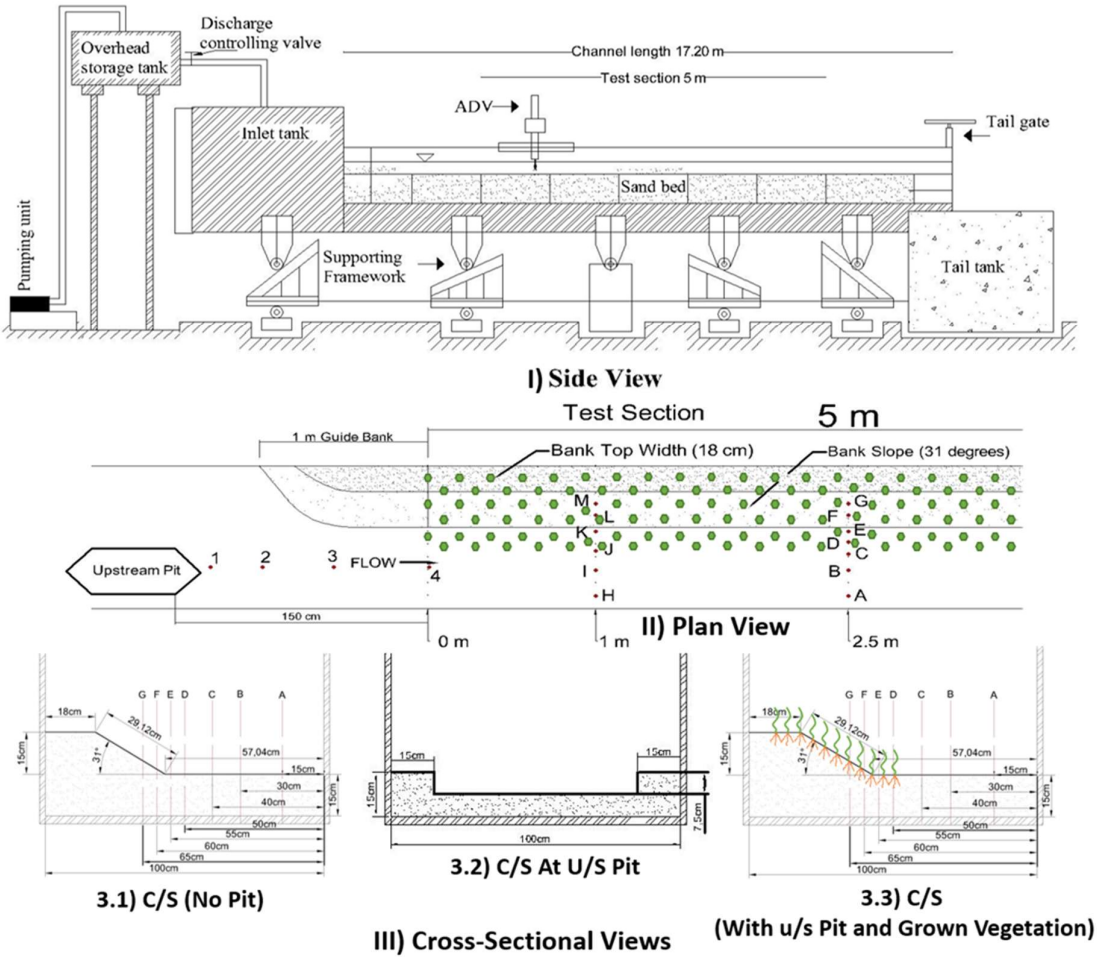

Figure 2.15: Side view of the experimental setup; b) top view of test segment showing an upstream pit and vegetation starting at 0 m (entrance); and cross-sectional view of c) no u/s pit & no vegetation case; d) with u/s pit and no riverbank vegetation; e) with u/s pit and with riverbank vegetation up to half width of the total cross-section.

In investigating the effects of sand mining pits on riverbank vegetation, a series of experiments was designed to compare growth conditions under different scenarios. The primary comparison was between cases with and without the presence of a pit, maintaining a constant flow discharge of 0.03 m^3/s in both instances. For a more nuanced understanding, a third case was introduced wherein pearl millet seeds (*Pennisetum Glaucum*) were sown with the intent to observe any potential mitigation effects the vegetation may have on the consequences arising from the sand mining pit. This phase allowed for a growth period of 15 days, details of which are depicted in Figure 2.16(a). The methodology for sowing took into consideration the need to minimize the impact of vortices at the vegetation-water interface, leading to the decision to sow from the

riverbank top to halfway down the test section. This approach also included extending the sowing area past the toe location, set at 0.43 m, as a measure to counteract any adverse effects. The seeds were systematically placed in linear holes and watered, a process illustrated in Figure 2.16(b), with the spacing between these lines set at 9 cm in adherence to established literature, aiming to achieve a sparse vegetation density (J. Barman & Kumar, 2022b, 2022a; Mossa et al., 2017; Zong & Nepf, 2010).

Following a 15-day growth period, the vegetation reached a height of 0.3 m, effectively doubling the height of the riverbank. This growth milestone marked the vegetation's suitability as flexible emergent vegetation, showcased in Figure 2.16(d,e). The vegetation possessed slender leaves with thin edges, an adaptation potentially beneficial for its survival and function in the studied context. Measurements conducted across different cross-sections yielded an average vegetation spacing of ly = 0.09 m, as recorded in Table 2.5, with the spacing along the flow direction being slightly less, at lx = 0.081 m. The resultant average spacing, $\Delta s = 0.0855$ m, falls within the category of sparsely dense vegetation as defined by (Nepf, 2012). Post-experiment evaluations revealed that the uprooted vegetation had roots extending beyond 0.15 m in length, a finding detailed in Figure 2.16(f). Table 2.4 presents the test conditions and the cases of sandpit and flexible vegetation considered for conducting these experiments.

Table 2.4: Experimental conditions of flow and cases considered

Sr. No.	Pit/Vegetation	Case	Discharge (m^3/s)
1	No pit, No vegetation	Incipient Condition	0.02
2	No pit, No vegetation	I	0.03
3	With pit, No vegetation	II	0.03
4	With pit, With vegetation	III	0.03

Table 2.5: Vegetation Spacing at Different Cross-Sections in the Test Section

Location in Test Section	Spacing (cm) (C/C)	Avg. Spacing at the Cross-section
Entrance	6, 9, 6, 5, 11, 5.5, 11.5	7.72
1 m after Entrance	5.5, 6, 8, 7.5, 6, 8, 7	6.86
2 m after Entrance	6.5, 10, 7, 10.5, 7, 9	8.33
3 m after Entrance	8, 7, 12, 9, 11, 10, 7.5	9.21
4 m after Entrance	6, 8, 10, 12, 8, 9	8.83
Exit of Test Section	8.5. 9, 7, 10, 11	7.58
	Avg Overall Spacing	8.09 ~ 8.1 (cm)

Further analysis was conducted 2.5 m downstream of where the flow entered the test section, involving the collection of depth-based turbulent velocity data at seven points along a riverbank cross-section. This data collection aimed to enhance the understanding of flow dynamics in the presence of the introduced vegetation, contributing to a broader comprehension of the interactions between riverbank erosion processes and vegetation growth patterns.

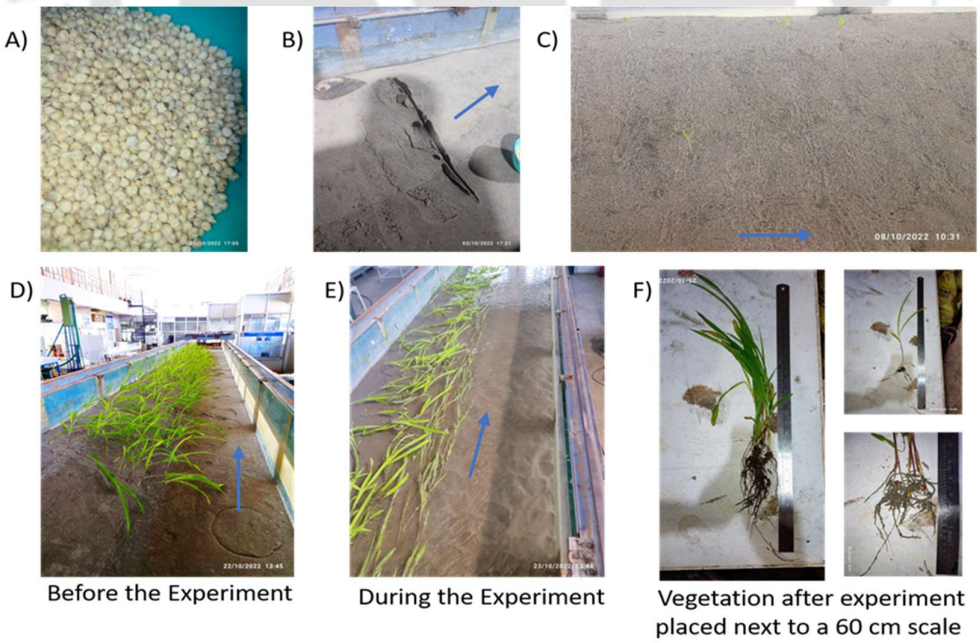

Figure 2.16: A) Picture of pearl millet seeds before sowing; B) sowing at a c/s; C) visible growth in 5 days; D) full growth of vegetation in 15 days; E) during the experimental run; F) plant length averaged at 0.25 m and root length averaged 0.15 m.

Objective 3B: To understand the effects of natural, rigid stems hammered into the soil as a mitigation measure to control riverbank erosion under dredged conditions.

The test segment measured 5.0 m in length, along with guide banks for smooth flow entry and exit (Figure 2.17). The riverbank guide banks start from zero width and gradually increase to match the width of the top of the riverbank. The riverbank's cross-section measured 0.18 m in top width, 0.15 m in unsupported side slope height, and the width of the main channel was 0.58 m, as shown in Figure 2.17. The flow depth (h) was maintained at 0.14 m. The Froude's number was within the sub-critical range (Table 2.6). Within the context of fluvial dynamics research, a comprehensive experimental study was conducted to investigate the impact of upstream anthropogenic alterations, specifically sand mining pits, on sediment transport and riverbank erosion processes. This study meticulously designed four distinct experimental setups within a sediment channel to analyze the interplay between hydraulic conditions and riverbank stability. The experimental configurations were as follows: a control setup without an upstream mining pit (NPNV), a variant featuring an irregularly shaped upstream mining pit with a depth of 0.075 meters (WPNV) as depicted in Figure 2.18A and B, and two additional setups that replicated the no-pit (NPWRV) and with-pit (WPWRV) conditions, respectively, augmented with the introduction of rigid natural vegetation cylinders of perennial reed (Phragmites karka) along the riverbank within the test section, illustrated in Figure 2.18C to E.

The experiments were designed to achieve a constant flow discharge of 0.03 cubic meters per second, thereby facilitating the observation of sediment dynamics under steady hydraulic conditions without the necessity of excavating a pit. This setup allowed for an in-depth analysis of how the flow interacted with the riverbank and bed, inciting erosion under varied experimental conditions. A state of quasi-equilibrium regarding sediment transport was attained within two hours from the inception of the experimental runs, with the experiments

continuing until sediment movement ceased, ensuring a consistent exposure to fluvial activity for a duration of 24 hours for each trial.

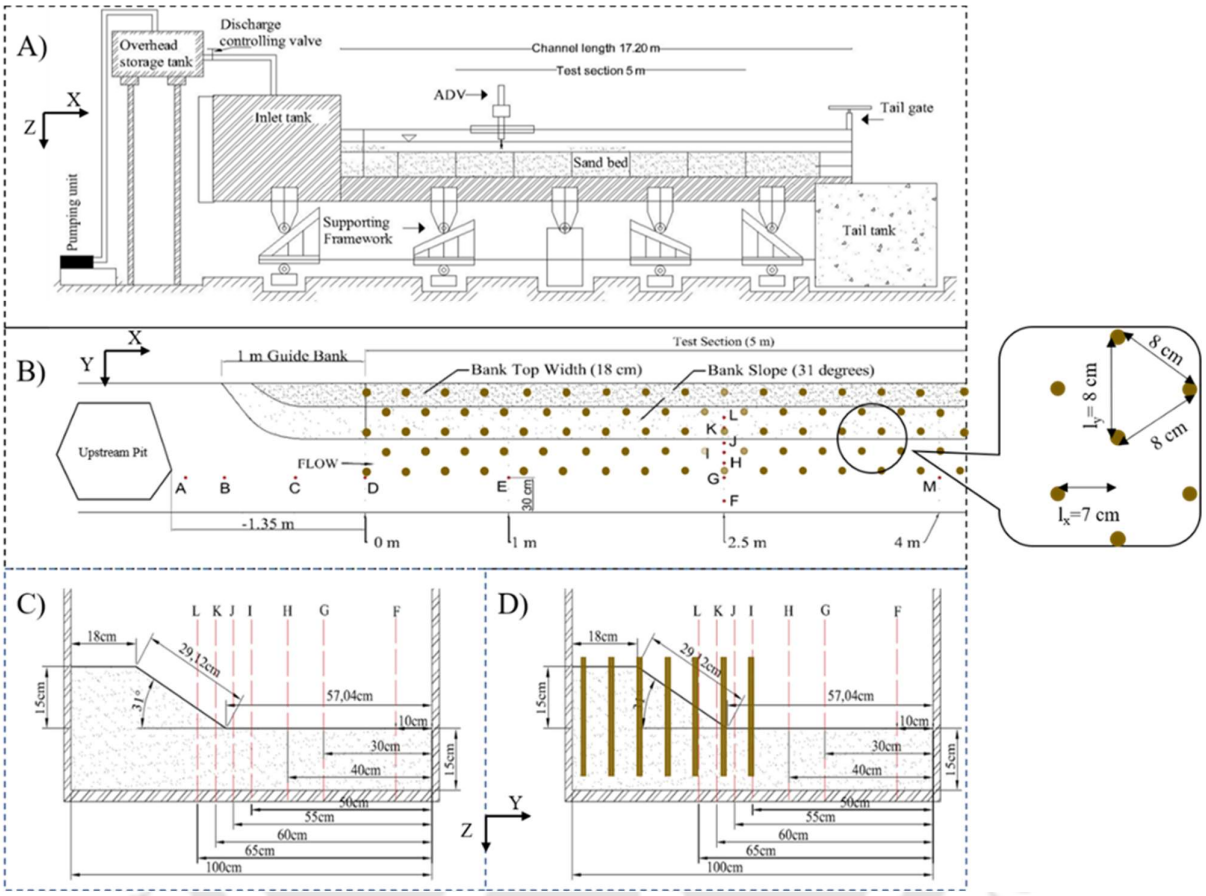

Figure 2.17: Laboratory setup presenting (A) side view; (B) top view with upstream pit and rigid vegetation in staggered pattern; (C) cross-section at 1 m after entrance into the test section without vegetation; (D) cross-section with rigid vegetation.

A particular focus was placed on the dredging scenario, where an irregularly shaped upstream pit, with dimensions of 0.075 meters in depth, 0.7 meters in width, and 0.85 meters in length, was excavated, terminating 1.35 meters upstream of the test section, as shown in Figure 1B. The selection of an asymmetrical pit structure was intentional, aimed at mirroring the heterogeneous shapes often encountered in sand mining operations within riverine environments. This approach ensured a fair comparison of turbulence characteristics across all experimental cases by maintaining consistent pit dimensions and shapes throughout the study.

The experiments involving the with-pit configuration proceeded with the same flow discharge rate of 0.03 cubic meters per second as the no-pit scenario. To explore the combined effects of sand mining pits on sediment dynamics and the potential erosion mitigation attributes of vegetation, natural cylindrical stems, with diameters ranging from 0.01 to 0.015 meters, were embedded into the riverbank, as depicted in Figure 1D. These cylinders, representing rigid stems of perennial reed (*Phragmites Kharka*), were vertically installed from the top of the bank to the midpoint of the test section (Y = 0.5 m), achieving a penetration depth of 0.14 meters into the sand bed, illustrated in Figure 2.18F. Drawing upon existing literature, these stems were uniformly spaced at 0.08 meters from center to center in a staggered arrangement to attain optimal vegetation density, with spacing measurements corroborated through plant density assessments across various cross-sections, yielding an average longitudinal spacing of l_X ~ 0.07 meters within the test segment.

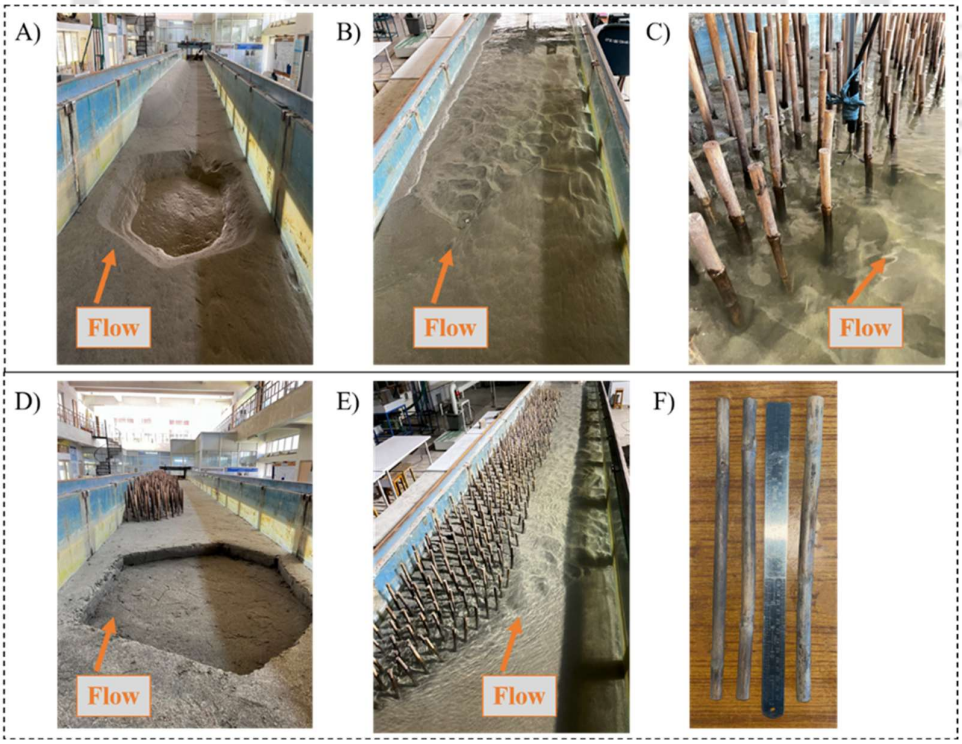

Figure 2.18: Pictures of experimental setup (A) case WPNV, which will be NPNV without sediment pit at given location; (B) during the experimental run for no-vegetation cases showing eroded riverbank; (C) usage of ADV probe in cases of vegetated riverbank; (D) case WPWRV which will be NPWRV without sediment pit at given location; (E) during the experimental run of vegetated riverbank showing stable riverbank profile (F) stems of rigid vegetation kept next to 30 cm steel scale.

Table 2.6: Experimental Conditions for understanding usage of natural rigid stems as a mitigation measure to control riverbank erosion under dredged conditions

S. No.	Pit/Vegetation	Case Name	Discharge (m^3/s)	Froude's No.
1	No Pit, No Vegetation	Incipient Condition	0.023	0.239
2	No Pit, No Vegetation	NPNV	0.030	0.307
3	With Pit, No Vegetation	WPNV	0.030	0.291
4	No Pit, With Rigid Vegetation	NPWRV	0.030	0.366
5	With Pit, With Rigid Vegetation	WPWRV	0.030	0.349

With the given test conditions and experimental setups, this thesis attempts to explain and quantify the near-bank and near-bed turbulence along with the morphological changes for different cases of riverbank under dredged conditions. The following chapter shall take the readers through the results obtained for these cases and it will attempt to correlate the morphological changes with the turbulence characteristics of flow.

3. Turbulence Structure and Morphological Changes Due to an Upstream Sand Pit

In the study of the effects of sediment mining on riverbank stability, we first need to understand different types of rivers by classifying them into a narrow (deep) or a wide (shallow) river based on the top width-to-depth ratio, as discussed in section 2.4.

3.1 Introduction

Rivers exhibit significant variability in their morphological characteristics, which directly influence hydrodynamic behaviours and erosion processes. Two distinct types of river morphologies often observed are wide (shallow) rivers and narrow (deep) rivers, as discussed before in section 2.4. River systems are characterized by their dynamic hydromorphological properties, with significant alterations observed in the riverbed and banks, highlighting the critical nature of riverbank erosion (Ghosh et al., 2016). This process not only affects the flow of water and sediment distribution within the river system but also has a profound socio-economic impact on communities residing in nearby floodplains. Triggered when the shear stress induced by the river's flow on bank sediments exceeds the resistance to particle movement, riverbank erosion leads to the expansion of the river's cross-section. This, in turn, decreases flow velocity and sediment settlement, potentially altering the river's Thalweg (Arafat et al., 2015; Zhu et al., 2008). Such changes continue until an equilibrium is reached concerning the cross-section for a specific discharge rate, which is subject to the river's discharge dynamics, making riverbank erosion an ongoing process. The eroded material contributes to sediment deposition downstream, where the capacity for flow turbulence and resuspension is lower, thereby influencing meander formation, material transport, and lateral channel migration (Dehghani et al., 2013; Lawler et al., 1997). Furthermore, the stability of riverbanks over years or decades is indispensable for the restoration of riparian vegetation and ecology, although this can be compromised by both natural phenomena—such as seepage,

changing water levels, and freeze-thaw cycles—and human activities, including deforestation, gravel extraction, and river training works (Briggs et al., 2021; Emberson, 2017).

Riverbank erosion naturally unfolds due to the flow near the riverbank, driven by mechanisms such as toe failure, undercutting, and tension cracks, which eventually lead to beam failure. This erosion is mainly attributed to three processes: fluvial erosion, mass failure, and subaerial processes. Subaerial processes involve the bank sediments' wetting and drying, freeze-thaw cycles, etc., weakening the bank slope. While these processes do not directly erode the bank, they facilitate erosion through the other mechanisms. Mass failures happen when the sediment's weight's shear force exceeds the sediment's shear strength, with cohesive bank forces adding to the shear strength and stability. Fluvial erosion is the direct consequence of flow impacting the bank sediments, with the flow structure and near-bank stresses causing erosion (Couper & Maddock, 2001). Studies have highlighted soil particle size distribution and the stress from water flow as critical to the erosion process (Majumdar & Mandal, 2022), finding that uniform bank soil results in more erosion due to increased seepage flow thanks to greater pore spaces. Anthropogenic activities like sand mining, dam construction, and the removal of riparian vegetation have been noted to exacerbate erosion by altering flow parameters (Midgley et al., 2012). The geotechnical properties of riverbank soil and their impact on bank stability have been examined, with experiments indicating toppling failure is prevalent in overhanging banks (Samadi et al., 2013). For cohesive soils, the accumulation of eroded mass at the bottom can temporarily halt further destabilization until this material is again eroded by the flow (Osman & Thorne, 1988). Field studies on cohesive soil banks have observed the accumulation of failed mass at the toe, leading to subsequent failures and erosion by fluvial actions (Thorne & Tovey, 1981b). Research has pointed out that erosion in cohesionless soil banks, like those along the Ganga in India's Malda District, is due to fine, uniform soil that increases porosity and horizontal flow, leading to destabilization (Majumdar & Mandal, 2022). Laboratory

experiments by Nardi et al. (2012) on sandy soil banks observed partial failures and berm formation at the toe during water level rises, highlighting a reduction in apparent cohesion (Arai et al., 2018; Nardi et al., 2012; Thi & Minh, 2019). Erosion rates have been measured using erosion pins and intermittent readings (Couper et al., 2002). In Nepal's Siwalik Hills, studies showed failure in the most erodible sand layer, with increased erosion from freeze-thaw cycles noted (Kimiaghalam et al., 2015). It has been found that vegetation near the bank can affect flow velocity and stress, potentially destabilizing the bank through toe scouring, despite vegetation's role in increasing turbulence and mixing (Li et al., 2022; Liu et al., 2017; Meftah et al., 2014; Valyrakis et al., 2021; Yang et al., 2018). Tension cracks have been observed in non-cohesive soil riverbanks (Arai et al., 2018; Liang et al., 2015). All studies concur that cohesive riverbanks are stronger than non-cohesive ones (Arai et al., 2018; Daneshfaraz et al., 2021; Roy et al., 2020). While riverbank erosion leads to the loss of fertile lands, it also contributes sediments to the river, which can create productive lands downstream over time, suggesting that erosion can have beneficial aspects for riverine ecosystems and downstream land fertility (Florsheim et al., 2008).

The practice of extracting sand from riverbeds, known as river sand mining, has seen a dramatic increase in recent years to satisfy the burgeoning needs of the construction industry. The method of pit excavation for instream sand mining has gained popularity due to the desirable irregular shapes and rough texture of the soil particles for construction purposes. Environmental Impact Assessment (EIA) studies indicate that the long-term adverse effects of sand mining outweigh its short-term advantages for society. Various researchers have attempted to quantify sand mining using remote sensing, satellite imagery, and local authority reports (Bravard et al., 2013; Gruel & Latrubesse, 2021), yet accurate estimations are hindered by illegal mining activities. The practice of extracting sand from riverbeds is lucrative, offering quick profits with minimal risk or repercussions for those involved. EIA studies have

highlighted increased turbulence in downstream water flow (B. Barman et al., 2019b, 2019a; Daneshfaraz et al., 2021; Lade & Kumar, 2020; Neyshabouri et al., 2002; Padmalal & Maya, 2014), leading to enhanced erosion or scouring of river structures (Lade & Kumar, 2020; Li et al., 2020), necessitating protective measures. While these erosion control efforts can reduce damage at specific sites, they may also amplify turbulence downstream, potentially compromising the safety of downstream structures by exceeding their designed stress limits (Chu-Agor et al., 2008). Therefore, a broader, more long-term strategy is essential for erosion control (Florsheim et al., 2008).

Sand mining also causes the Thalweg line, which defines the deepest part of a riverbed, to shift toward the mining site, destabilizing the riverbank's base. The creation of burrow pits from mining activities near rivers can transform land use and cover, encroaching upon adjacent agricultural lands and threatening the stability of nearby riverbank structures (Nwobodo et al., 2021; Okeke et al., 2020). The displaced sand from the banks and bed tends to fill these excavated areas (Wahaba et al., 2019). Extensive mining along significant portions of the river can reduce the depth of the water flow, accelerating erosion at the riverbank's base and potentially leading to structural failure. Such failures could involve large sections of the riverbank, as much as 70,000 m^3, resulting in severe flooding during high-flow conditions (Liang et al., 2015). Human activities, including sand mining, can either exacerbate or mitigate these flood risks. Thus, the impact of upstream excavation on riverbanks warrants thorough investigation. Research indicates that bank erosion and resultant changes may intensify with climate change, despite predominant fluctuations in river flow (Liang et al., 2015; Shu et al., 2019).

The formation of riverbanks is a gradual natural phenomenon, influenced by the settling of soil at various angles of inclination. These varying slopes of the riverbanks can result from factors such as the river's sinuosity, erosion, and the accumulation of sediments along the banks. Past

studies have highlighted the issues caused by fluvial entrainment, electrochemical processes, and the composition of riverbank materials in the erosion dynamics. Nonetheless, the significant removal of sand and gravel from riverbeds also deserves attention for its potential impact on riverbank erosion. Research indicates that mining operations can modify the flow patterns and turbulence within the river, which, in turn, can drastically affect the erosion of riverbanks, particularly through fluvial processes, as turbulence directly influences the stresses on bank sediments. Given the widespread practice of riverbed extraction, its effects on riverbank erosion are crucial for determining suitable protective measures. There exists a noticeable research gap regarding the fluvial erosion of riverbanks caused by flow interactions. Our understanding of how human activities, such as sand extraction, influence riverbank erosion is still developing and requires further investigation. This study aims to explore how sand mining pits affect the fluvial erosion process and the stability of riverbanks through physical model experiments. We examined the hydromorphological changes and erosion of non-cohesive riverbanks in an erodible channel featuring a mined pit. The study analyzed the impact of the pit on the flow dynamics in the main channel and adjacent to the riverbank, focusing on turbulent parameters. The insights gained from analyzing turbulence and the erosion of the riverbank at the end of the experiments made in the present study are discussed in this section.

3.2 Effects of Sediment Mining on Narrow (Deep) vs Wide (Shallow) Rivers

Based on the generalized Physical Model, experimental studies were conducted on both narrow and wide channels to measure the three-dimensional instantaneous velocity using the acoustic Doppler velocimeter, as presented in objective 1A in the previous chapter. The data obtained were then analyzed to compare the distribution of stream-wise velocity and Reynolds shear stress in wide and narrow channels. Further studies were conducted employing quadrant analysis, to reveal the flow characteristics. The results of the studies for wide and narrow

channels are then compared to understand the difference in flow behaviour in both scenarios. The results confirmed that the streamwise velocity gradient near the bank of the narrow channel is steeper than that measured at the bank of the wide channel. The results obtained in the laboratory experiments are similar to Reynolds (Re) and Froude's (Fr) numbers in the real field conditions. Reynolds number governs the ratio of inertial to viscous forces, influencing turbulence, boundary layer development, and momentum transfer. Ensuring Re similarity allows for accurately producing key flow phenomena such as velocity profiles, turbulence intensities, and secondary flow structures, particularly near boundaries where viscous effects are pronounced (Najafzadeh & Oliveto, 2022). Froude number, on the other hand, characterizes the balance between inertial and gravitational forces, making it essential for replicating free-surface flows, wave dynamics, and flow transitions between subcritical and supercritical states. Fr similarity is particularly crucial for studies involving open-channel flows, hydraulic jumps, or energy dissipation, where gravitational forces dominate (Aung et al., 2023). Together, Re and Fr similarity provides a comprehensive framework to replicate the interaction between internal flow dynamics and surface flow behavior (Heller, 2011).

Similar observations can be made for normalized transverse velocity profiles, depthwise velocity profiles and Reynolds Shear Stress profiles (Figure 3.1). The transverse velocity profile and depthwise velocity profile of the wide channel have been observed to be positive values, whereas it has been found to be negative values for the narrow channel. Analysis of bed shear stress at the bank of narrow and wide channels confirmed that the bed shear stress for the wide channel near the bank is much higher than the narrow channel.

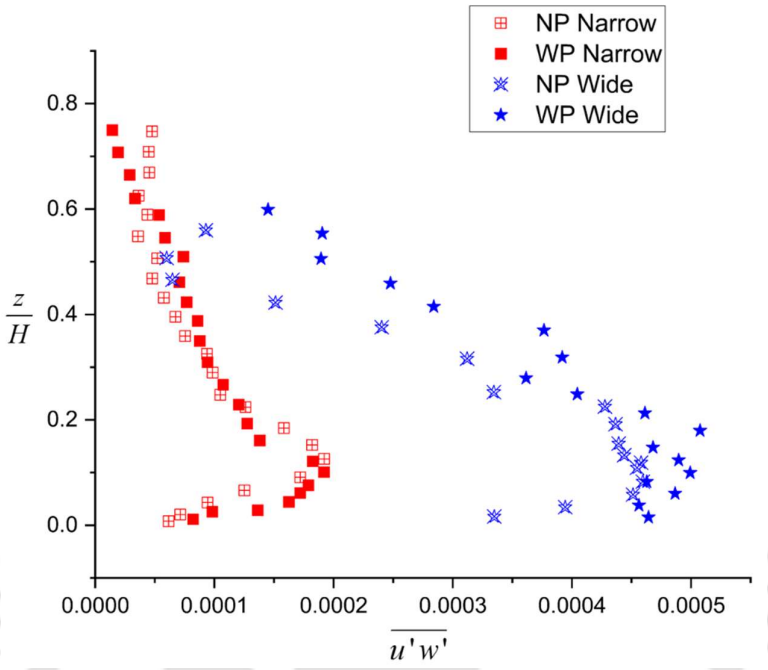

Figure 3.1: Streamwise Reynolds Shear Stress for Wide and Narrow Channels under Dredged Conditions. NP stands for No-pit and WP stands for with-pit. The pit is located upstream of the test section.

Quadrant analysis reveals that the contribution of all the events decreases progressively with an increase in hole size. It was also observed that when the hole size 'H' becomes large, only contributions due to ejections Q2 and sweeps Q4 exist (Figure 3.2). Thus, predicting that the ability of sediment to get transported as bedload is more near the bank in both narrow and wide channels due to the rush of high streak flow towards the bed causes higher momentum exchange near the bed.

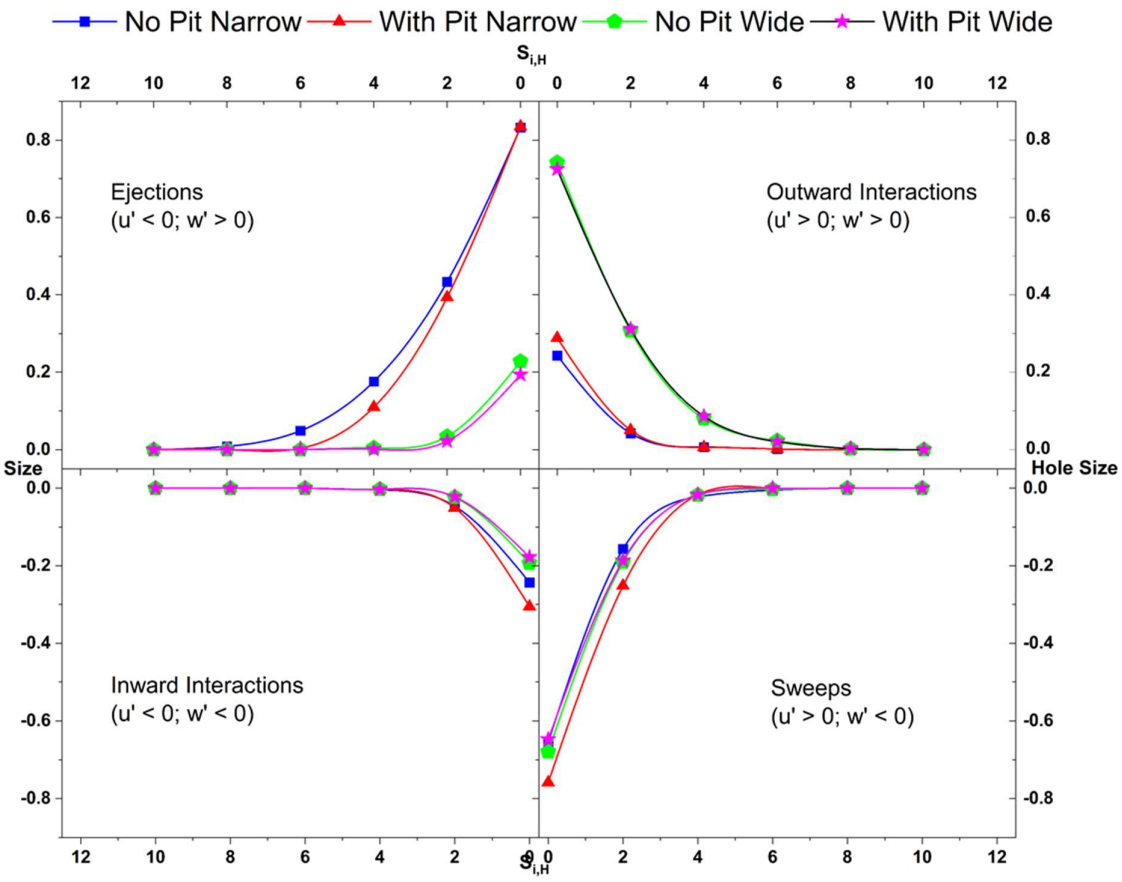

Figure 3.2: Quadrant Analysis at a depth of z/H~0.2 for the cases of Narrow and Wide Channels under Dredged Conditions

This study examines the nature of turbulence and morphological changes in a narrow channel as compared to a wide channel. This will help us understand the hydrodynamic behaviour of the flow in a deep channel. The Reynolds shear stress near the bank for wide channels is 1.5 times higher than the narrow channels. The bed shear stress for the narrow channel is found to be 0.00032 (m^2/s^2), while for the wide channel is 0.00062 (m^2/s^2). This confirms that the bed shear stress for the wide channel near the bank is 93.75 % higher than that of the narrow channel. Hence, we can conclude that wide channels are more sensitive to sediment mining than narrow (deep) channels.

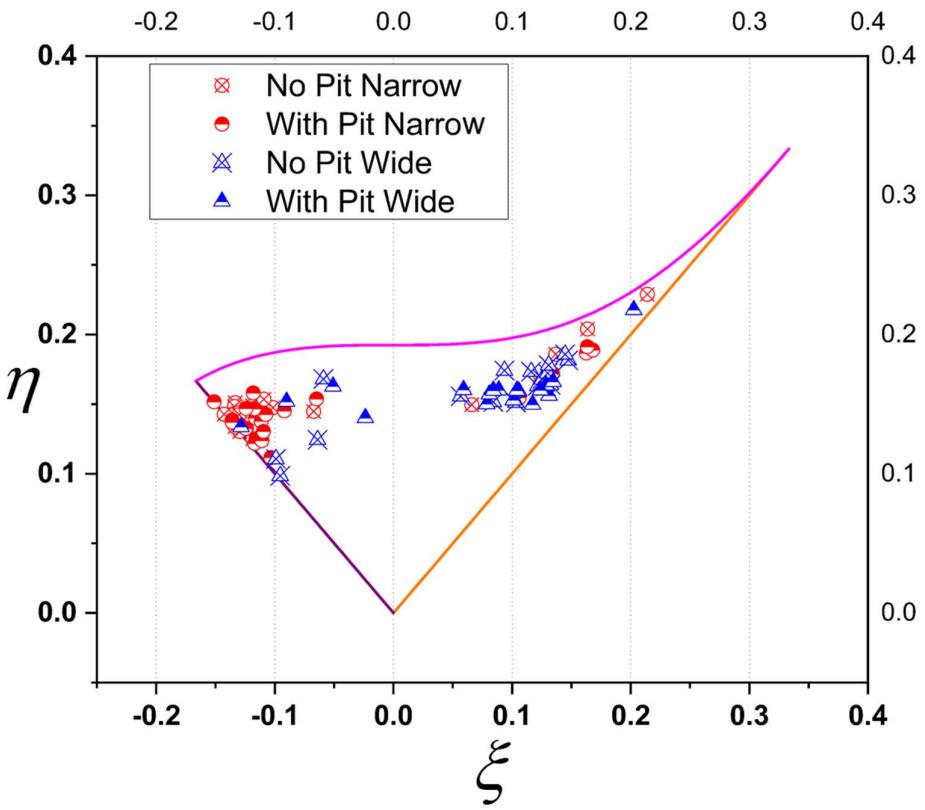

Figure 3.3: Anisotropy Invariant Map representing the relation between degree and nature of anisotropy for Narrow and Wide Channels under dredged conditions.

In an Anisotropy Invariant Map (AIM), the vertical axis, η [–II (positive or zero)] represents the degree of anisotropy, and the Horizontal axis ξ [III] corresponds to the nature of anisotropy (Figure 3.3). It can be calculated using Reynolds stress anisotropy tensor, $b_{ik} = \frac{\overline{u_i' u_i'}}{2k} - \frac{\delta_{ik}}{3}$, where '$\delta_{ik}$' is a Kronecker delta function, 'k' is the turbulent kinetic energy, 'i, k' denotes the streamwise and depthwise direction, 'u'' is the velocity fluctuation in streamwise direction (A. Sharma & Kumar, 2021). Here, $II = -b_{ik}b_{ik}/2$ and $III = b_{ij}b_{jk}b_{ki}/3$. The points for the narrow channel are concentrated on the left boundary, which suggests 2-dimensional turbulence, whereas the points for the wide channel are concentrated on the right boundary, which means 1-dimensional turbulence. This supports the fact that there will be more sediment transport in the case of the wide channels. Now, the mining pit has shifted the points towards the origin,

which suggests 3-D turbulence, making things supportive for sediment transport further downstream. The left boundary, as identified by Choi & Lumley, (2001), represents a pancake-shaped turbulence, where one component of TKE is smaller than the other two that are equal. On the other hand, the right boundary represents a cigar-shaped turbulence, where one component of TKE is larger than the other two.

3.3 Effects of Sediment Mining on Riverbank Stability with Different Slopes

To study the flow structure in the entire cross-section of the riverbank, the velocity measurements at A, B, C, D, and E for all the test cases were analysed at location 5. The flow structure was studied by analysing the turbulence parameters such as mean velocity distribution, Reynolds stress distribution, and turbulent kinetic energy distribution across the riverbank cross-section. A 5 cm wide zone near the glass wall is excluded in the results to remove the side-wall effects (Tay et al., 2015). Also, morphological adjustments in the cross-section of the riverbank occurring on account of the flow structure at location 5 at the end of the experiment were studied. The test cases' results are presented, and process understandings are discussed in this section.

3.3.1 Mean Velocity Field

According to Reynolds decomposition, turbulent velocities are the sum of two components, i.e., mean ($\bar{u}$, $\bar{v}$, and $\bar{w}$) and fluctuating (u', v', and z') given by equation 1

$$\bar{u} = \frac{1}{n}\sum_{i=1}^{n} u_i \; ; \; \bar{v} = \frac{1}{n}\sum_{i=1}^{n} v_i \; ; \; \bar{w} = \frac{1}{n}\sum_{i=1}^{n} w_i \qquad 01$$

Mean streamwise velocities $\bar{u}$ Along with the flow depth (z/h) in the riverbank is plotted in 4. The transverse velocity vectors resulting from mean secondary velocity distribution ($\bar{v}$, $\bar{w}$) in the riverbank is shown in Figure 3.5. In the case of 25º riverbank (gentle slope), mean turbulent velocity profiles ($\bar{u}$) in the main-channel portion are logarithmic, with the inner layer extending

to z/h = 0.2-0.25. Also, transverse velocities in the main channel have substantial magnitudes and directions away from the bank. These transverse velocities have lower magnitudes in the near-bank flow. In the case of a sand pit upstream, the mean streamwise velocity distribution is almost similar for this slope. However, slight variations in the secondary flow are evident (Figure 3.5). The direction of the mean transverse is towards the slope in the near bank flow on the upstream channel pit. For the 31º riverbank (angle of repose), the pit alters the mean streamwise velocities in the riverbank flow. In the main channel, the pit caused bed sediment erosion and a slight increase in the water depth. Therefore, mean streamwise velocities are lowered in the outer layer ($z/h > 0.25$) in the case of a channel pit, as seen in profiles A and B in Figure 3.4(K). Berm formation occurs at the edge of the slope. Near-bed mean streamwise velocities at this location (profile C) are higher in the case of a pit. In the case of a steep riverbank (40º slope), mean streamwise velocities in the main channel as well as at the edge of the slope (profiles A, B, and C) show higher magnitudes, especially in the inner layer in the case of a pit. For steep slopes, strong recirculation in the transverse direction is observed in main–channel flow due to the pit. In the near-bank region (location C), pit dredging has resulted in higher mean streamwise velocity gradients. It implies that the pit will increase the viscous shear in the boundary layer formed in the near-bank flow (Lade et al., 2021).

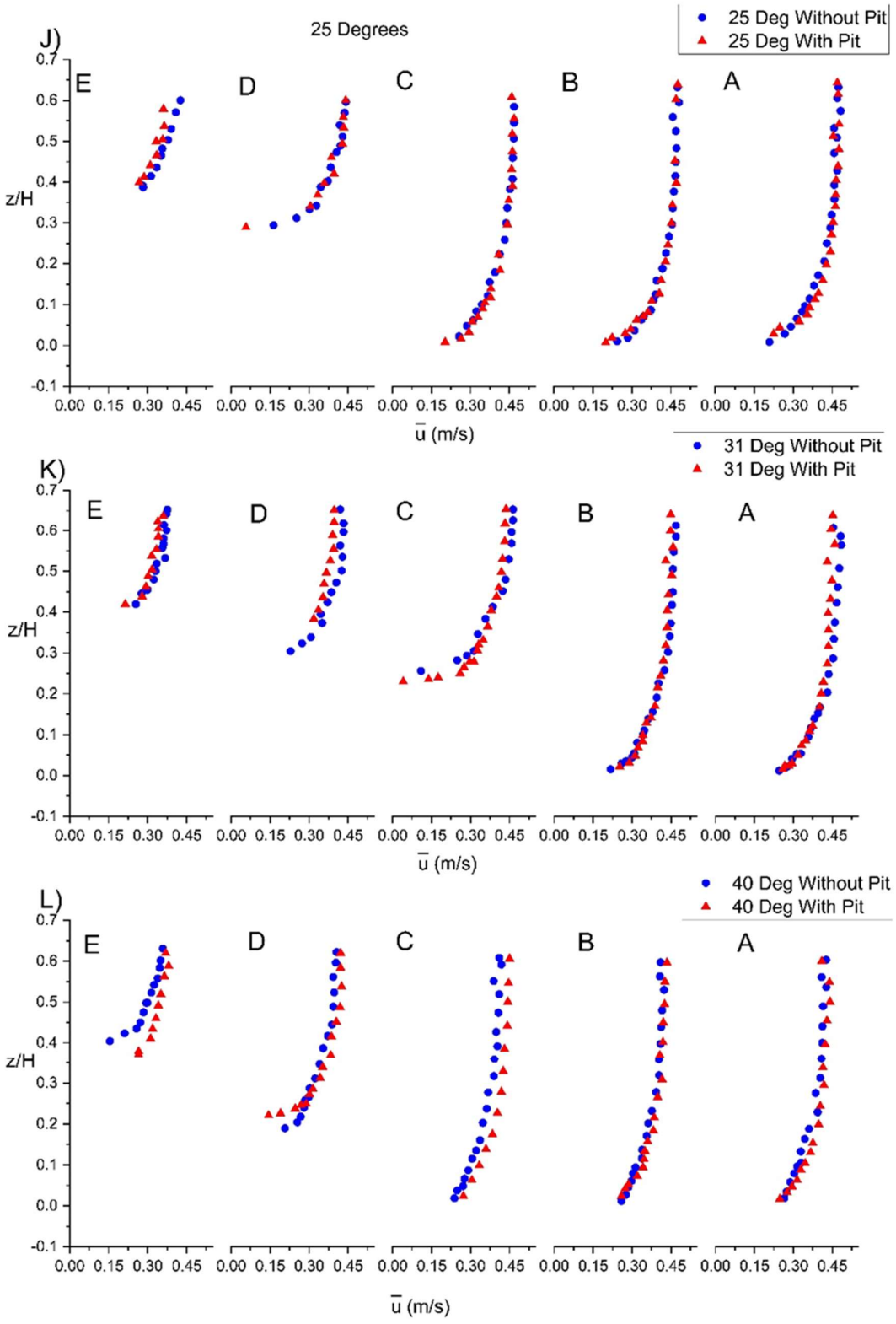

Figure 3.4: Mean streamwise velocity ū distribution at A, B, C, D, and E points at location 5 in the riverbank for three riverbank slopes without pit vs with pit, respectively

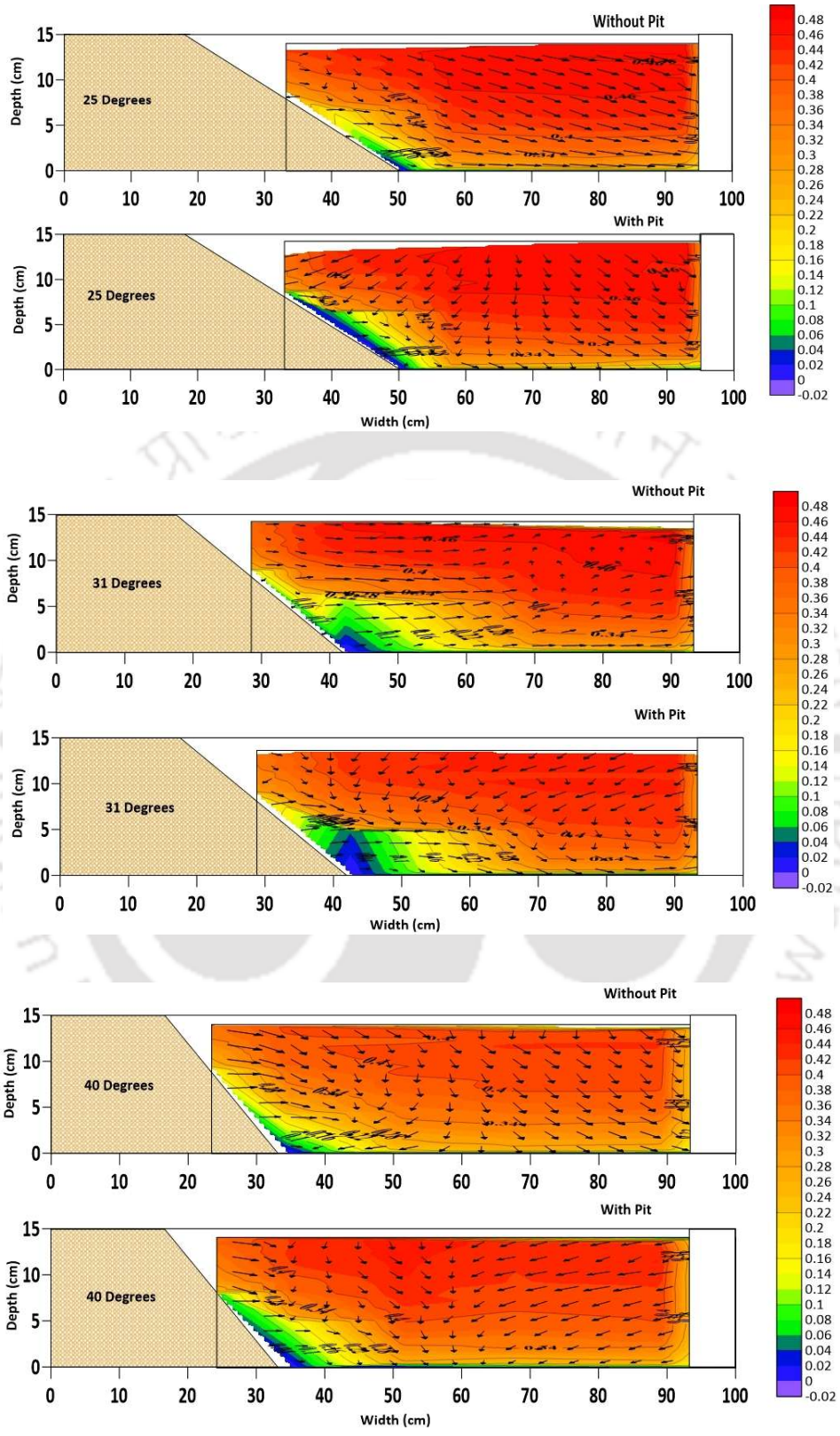

Figure 3.5: Resultant mean cross-sectional velocity vectors as secondary flow with contour of streamwise velocity for all three riverbank slopes without pit and with pit, respectively

3.3.2 Turbulent Kinetic Energy

The temporal mean turbulent kinetic energy distribution in the riverbank cross-section is shown in Figure 3.6. Temporal mean Turbulent Kinetic energy at a point in the Eulerian reference frame is given by $TKE = \frac{1}{2}\left(\overline{u'^2} + \overline{v'^2} + \overline{w'^2}\right)$. It has the contribution of turbulent eddies in the anisotropic integral scale to the isotropic Taylors micro-scale and Kolmogorov's scale. Energy-containing eddies are created due to the riverbank roughness as well as the secondary flow interactions in the toe region due to the bank slope. For gentle bank slope (25º), TKE is concentrated in the near-bed region of main-channel flow and near-bed region on the slope. It is evident from Figure 3.6 that secondary flow within the riverbank is remarkably stronger for steeper angles, which leads to greater velocity fluctuations, especially in the toe flow region. Therefore, the magnitude of TKE concentration in the near-bank flow or toe region in 20-25 % greater for 31º and 40 º bank slope. For bank slope equal to the angle of repose (31º), the pit causes increased TKE concentration in the main-channel boundary layer and decreased TKE concentration on the sloping bank sediments. Also, The TKE distribution extends up to the flow surface, which indicates that the pit creates a greater fluctuation in the top flow layer in the riverbank. It also implicitly indicates that the turbulent eddies of higher velocity scales are formed in the outer layer of riverbank flow in the pit case. For steep slopes, the TKE concentration was observed near the toe of the bank. The magnitudes of this TKE concentration zone near the tow region increased due to the pit.

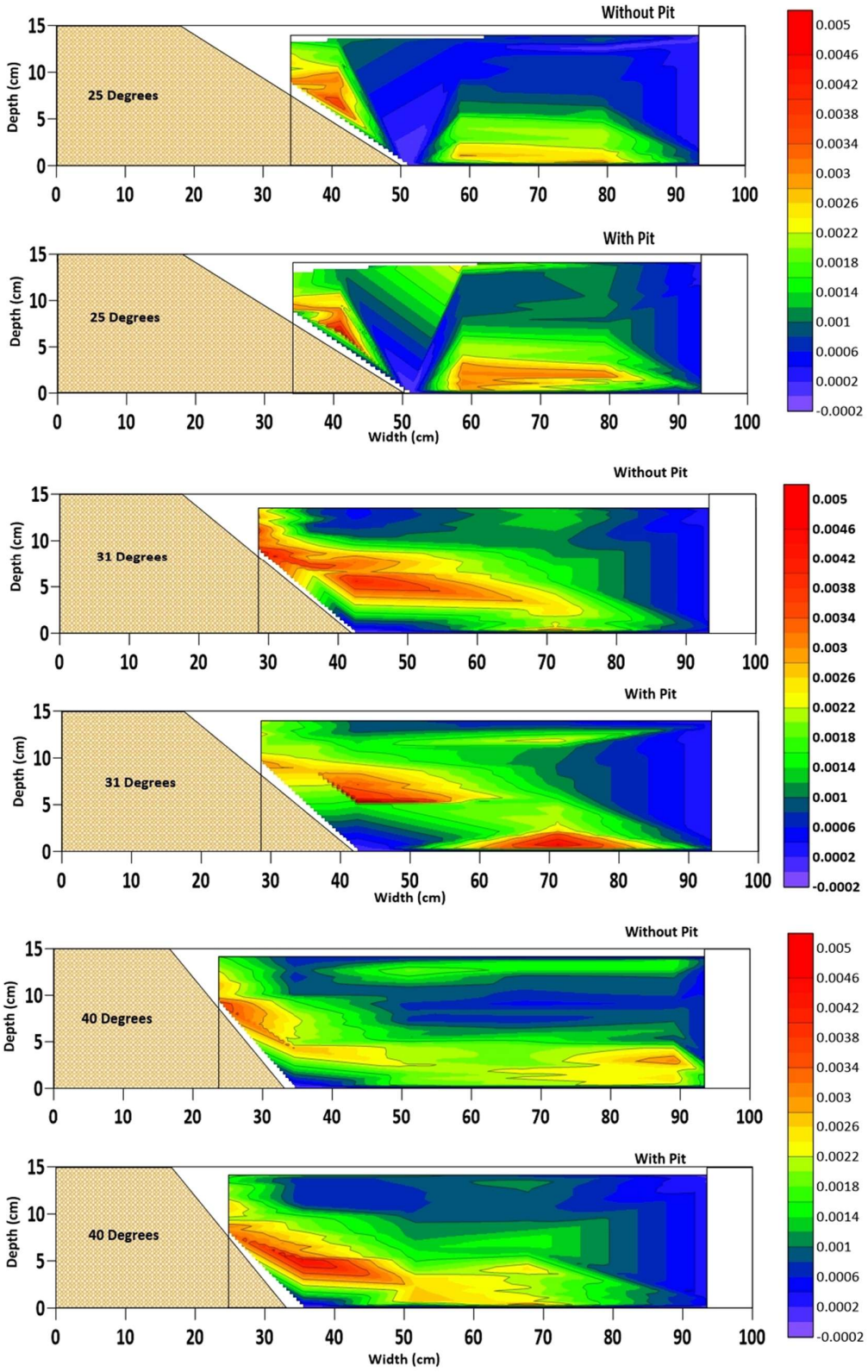

Figure 3.6: Contour of Turbulent Kinetic Energy (k) distribution in the Riverbank for all three slopes without pit vs with pit, respectively.

3.3.3 Reynolds Shear Stresses

For all the test cases, flow through the riverbank section is fully rough turbulent as Re > 10,000 and $R_e^* > 70$. Here, 'R_e^*' is a dimensionless particle Reynolds number which can be defined using shear velocity 'u_*' m/s, mean particle diameter 'd_{50}' m, and kinematic viscosity 'ν' m^2/s, as $R_e^* = \frac{u_* d_{50}}{\nu}$. It indicates that the flow near the particle is turbulent (Lade & Kumar, 2020). Turbulent velocities recorded in the flow are Eulerian measurements. In the Cartesian coordinate system, Reynolds stresses on all three planes, *X-Y*, *Y-Z*, and *Z-X,* are shown in Figure 3.7. As the Riverbank sediments lie on the *X-Y* plane, the turbulent shear stresses acting on it become significant as these stresses directly cause the movement and deposition of sediments. These two turbulent shear components acting on the plane of sediments in streamwise and transverse directions are τ_{Z-X} and τ_{Z-Y} respectively. The streamwise Reynolds shear stress distribution $\tau_{Z-X} = -\rho\overline{u'w'}$ (J. Barman & Kumar, 2022b) in the riverbank section is shown in Figure 3.8. The contours of transverse Reynolds shear stress $\tau_{Z-Y} = -\rho\overline{v'w'}$ in the riverbank are shown in Figure 3.9.

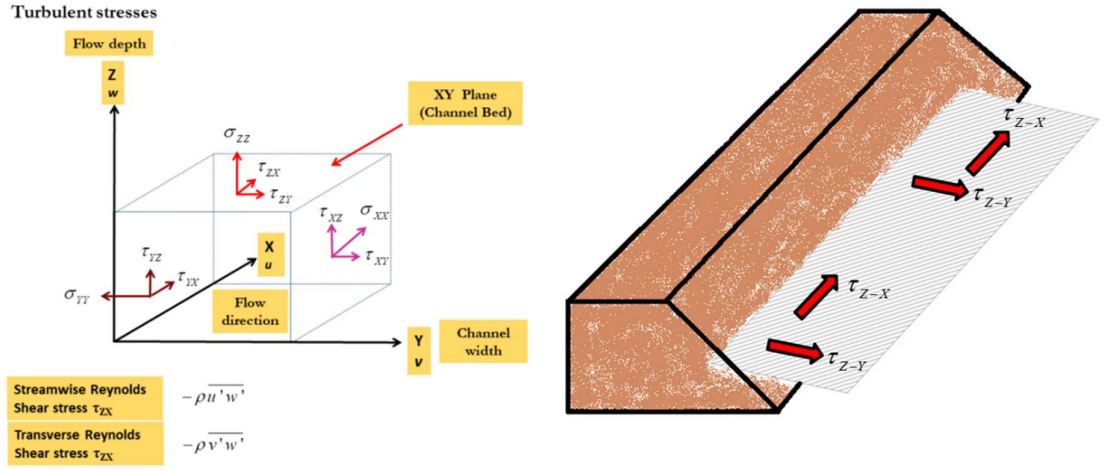

Figure 3.7: Reynolds stress tensor acting in the riverbank flow

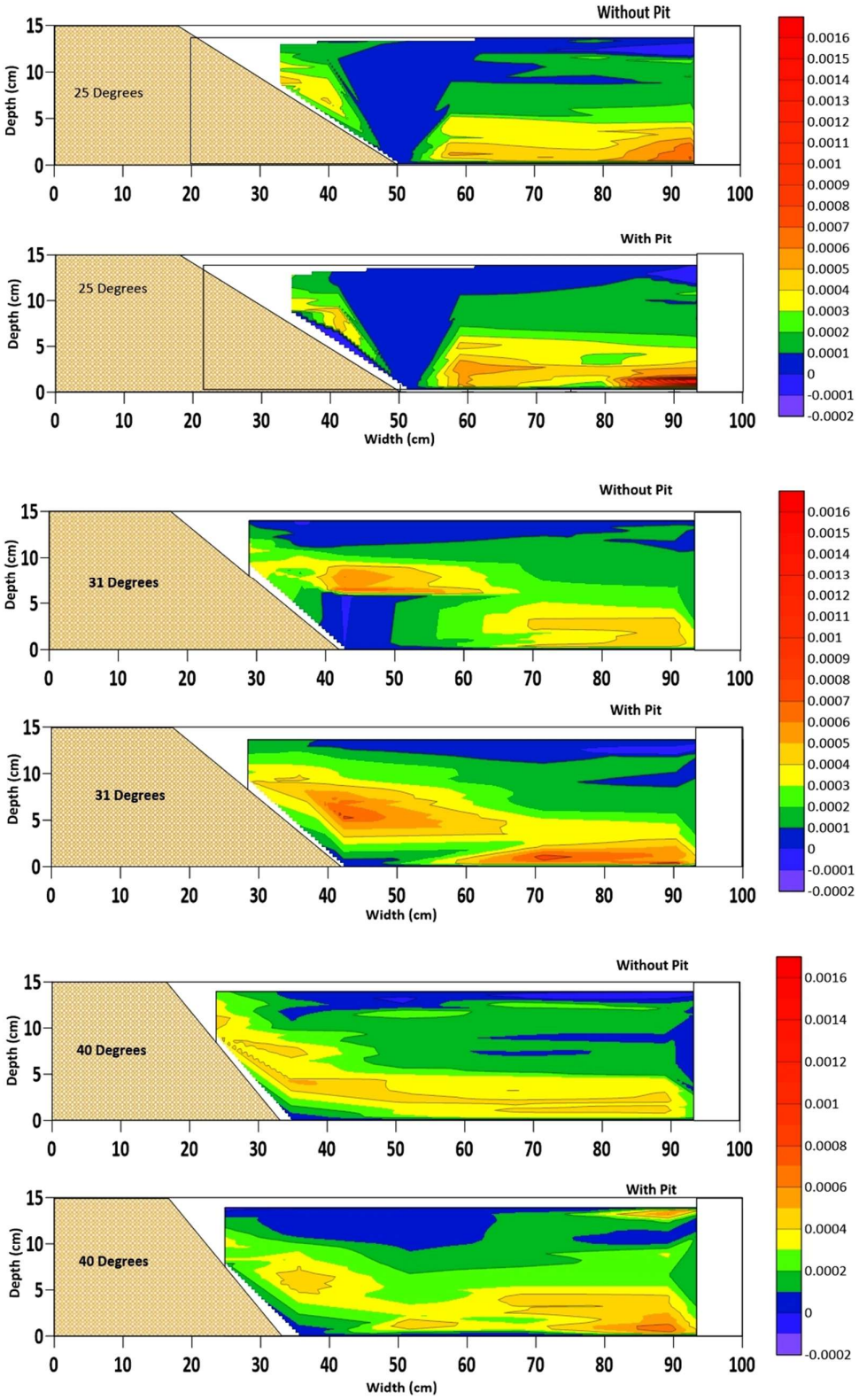

Figure 3.8: Contour plot of the Streamwise Reynolds shear stress τ(Z-X) in the cross-section at location 5 for all three riverbank slopes without and with pit, respectively

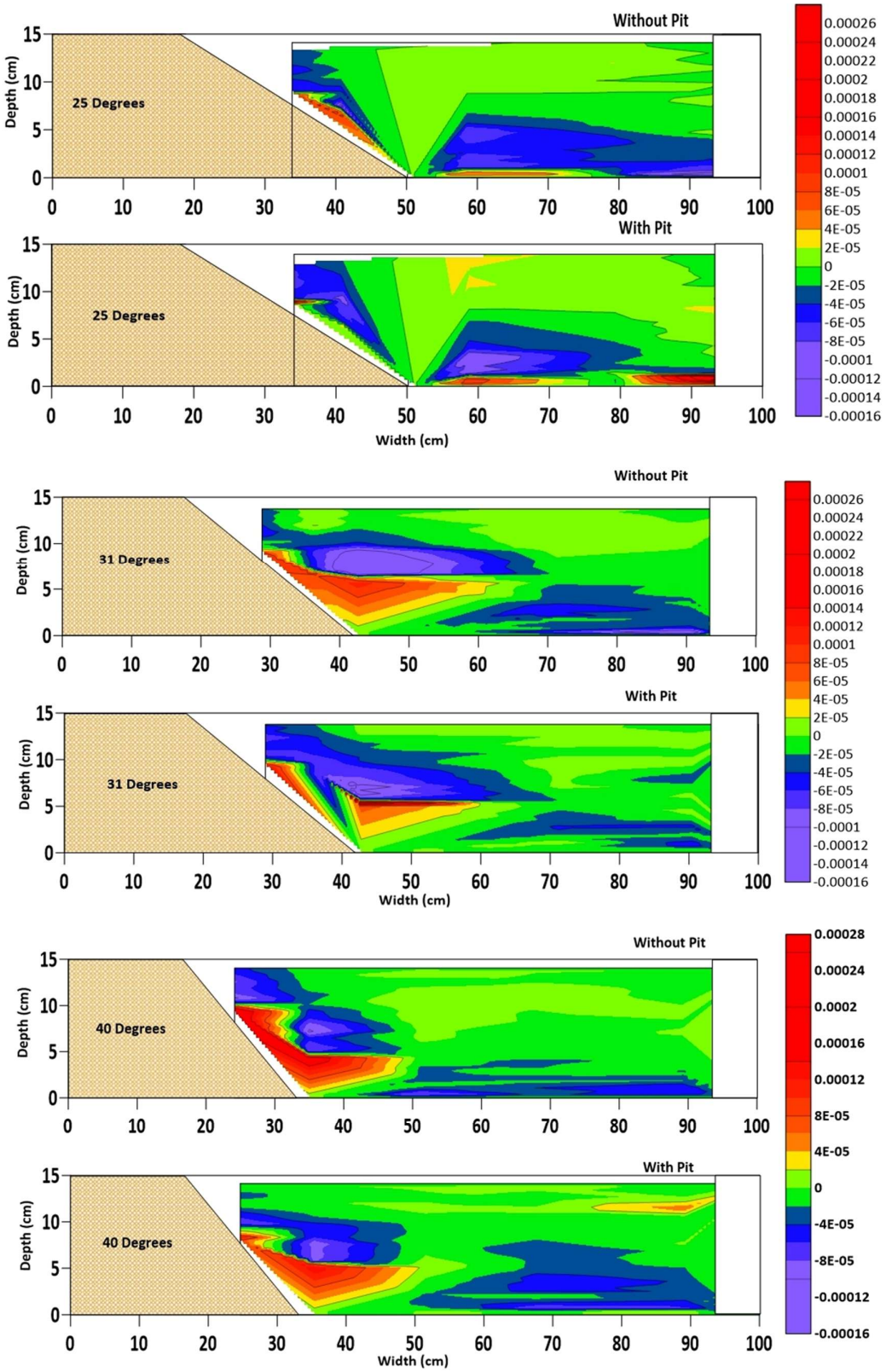

Figure 3.9: Contour plot of the Transverse Reynolds shear stress $\tau_{(Z\text{-}Y)}$ in the cross-section at location 5 for all three riverbank slopes without and with pit, respectively

The two important mechanisms of riverbank failures are a mass failure and fluvial erosion (Masoodi et al., 2019). The action of flow causes the fluvial erosion of the riverbank. The transport of streamwise momentum across the flow depth in the riverbank is responsible for streamwise Reynolds shear stresses (τ_{Z-X}) acting on the sediments in the channel portion and the bank portion. Similarly, the transport of transverse momentum across the flow depth causes transverse Reynolds shear stress τ_{Z-Y} on the sediments. It is evident from

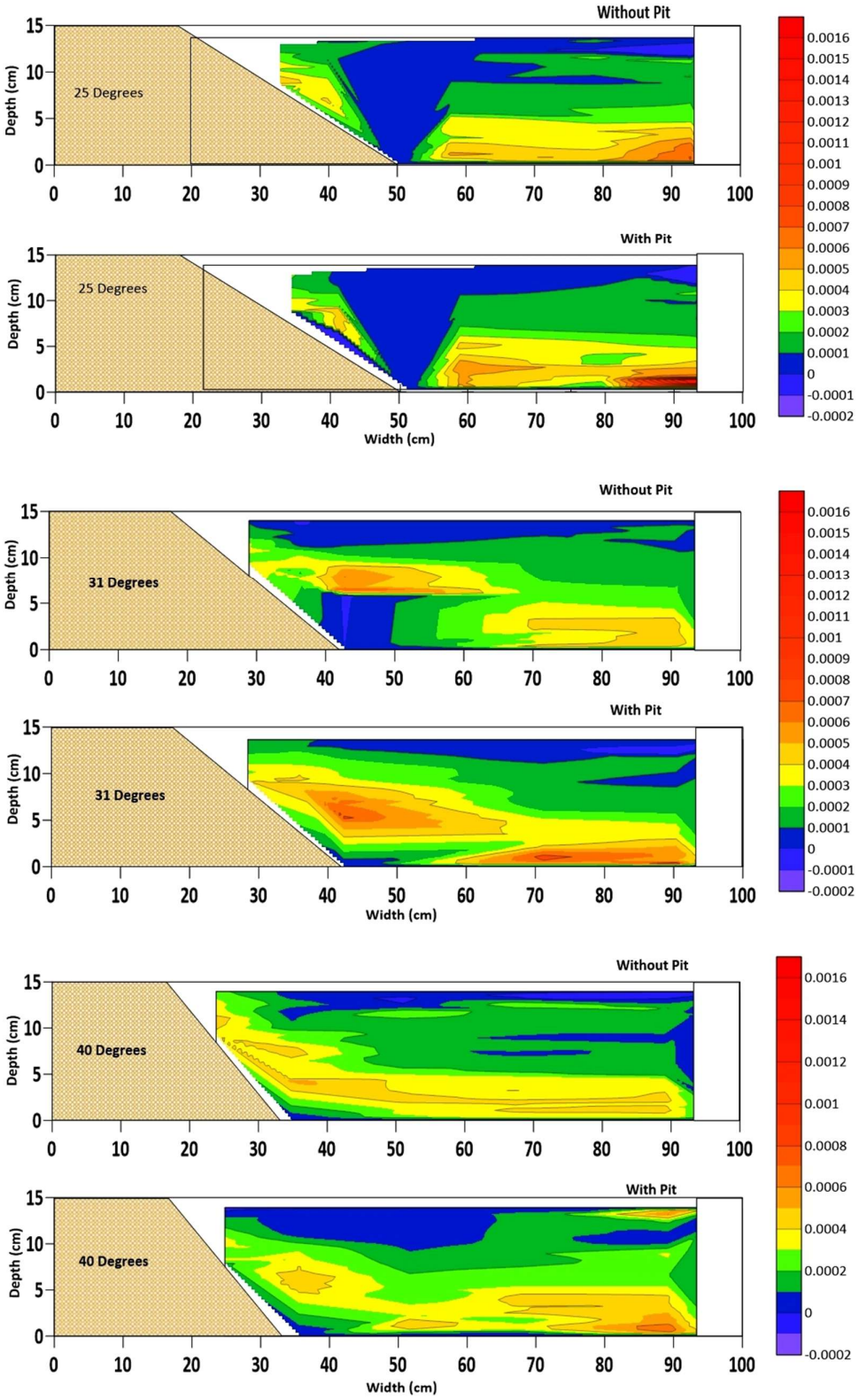

that for all three slopes, streamwise Reynolds shear stresses (τ_{Z-X}) are higher in the inner layer

at A, B, and C. For 31º and 40º slopes, pit excavation increases the streamwise Reynolds shear stresses (τ_{Z-X}) in the inner layer within the main channel, which is responsible for sediment transport. Also, the transverse Reynolds stresses τ_{Z-Y} near the bed, in the main channel, flow increases due to the pit excavation. Thus, the main-channel erosion and channel bed degradation occur for these riverbank slopes due to excess streamwise and transverse Reynolds stresses. In the riverbank flow, τ_{Z-Y} near the toe of the bank increases with the increase of the sloping angle. A close observation of Figure 3.9 indicates that τ_{Z-Y} in the near bank flow, i.e., at the toe of the slope, increases due to pit excavation. For steep riverbank slopes (40º), τ_{Z-Y} is maximum and concentrated in the flow zone near the toe, which causes excess transport of sediments and berm erosion occurs progressively. Therefore, for a steep slope, the berm formed at the toe, which provides slope stability, gets progressively eroded due to the excess transverse stresses developed due to the pit.

Flow on the bank slope governs the slope's sediment movement and fluvial erosion after the sliding failure. In the case of a sand pit, the streamwise and transverse turbulent shear stresses on the slope are significantly lower than in the no-pit case (

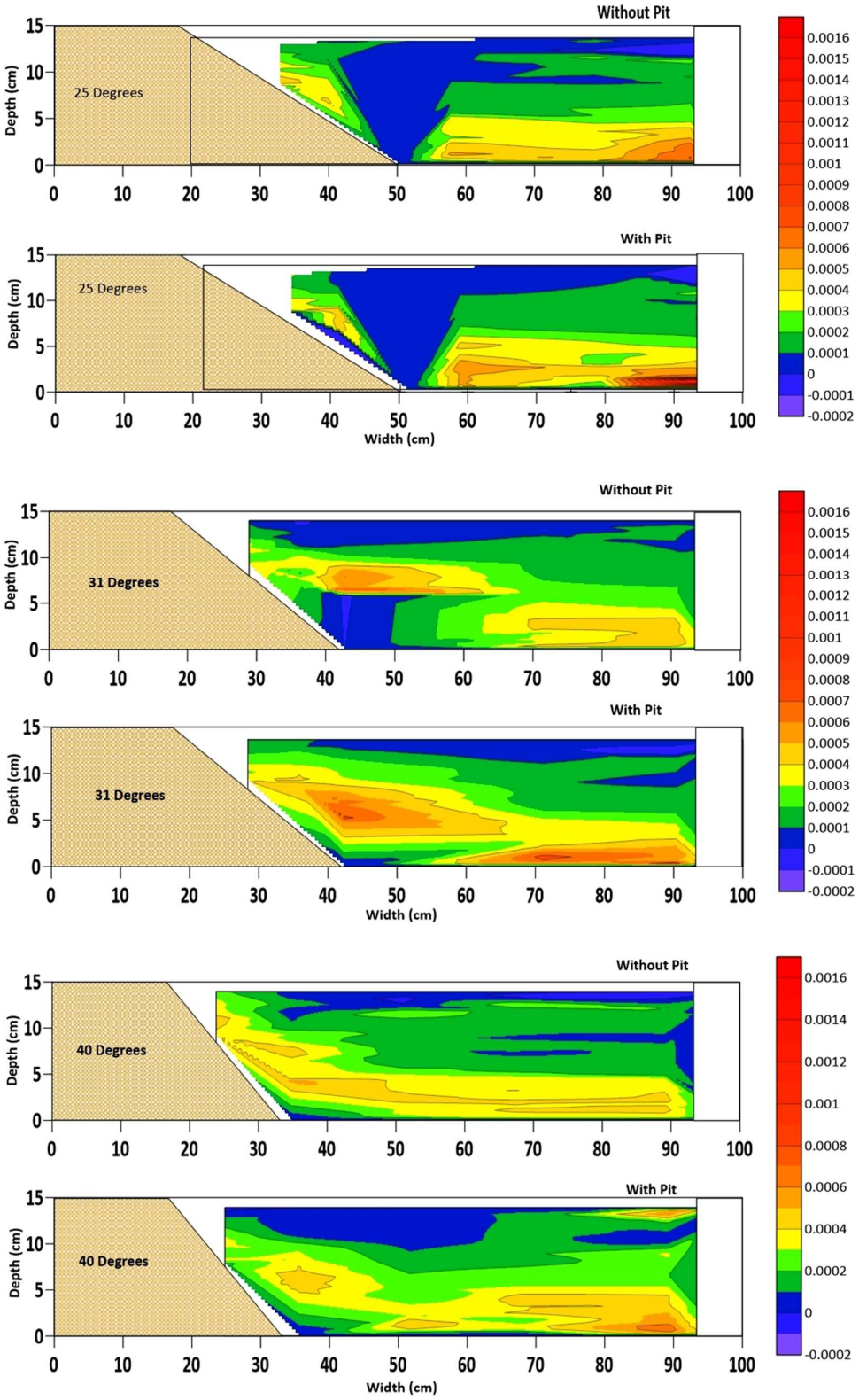

and Figure 3.9). Therefore, fluvial erosion of the slope is lesser in the case of the pits for 25º

and 31º slopes. For steep slope (40º), the sliding failure of the bank itself is significant for both with pit and without pit case, and hence fluvial erosion and slope failure are almost equal in both cases.

3.3.4 Turbulence Intensities

The turbulent normal stresses acting on the fluid element represent the turbulence intensities in the flow. Turbulence intensities in the streamwise (σ_u), transverse (σ_v) and vertical (σ_w) directions along the non-dimensional depth (z/h) at point C are shown in Figure 3.10. It represents the near-bank flow region at the toe of the riverbank, where berm formation occurs. Turbulence intensities in the toe flow region reveal crucial information about the secondary flow in the riverbank. The magnitude of turbulence intensities in the transverse (σ_v) and vertical direction (σ_w) in the toe region of the bank are of the same order of magnitude as that of the streamwise direction for all the slopes. Thus, secondary flow is significant in sediment movement and deposition of the berm formation that occurs at the toe region. For all three slopes, the turbulence intensities are concentrated in the inner layer of near-bank flow. With the increase in the bank slope, the depthwise zone of maximum turbulence intensities also increases [from z/h – 0.2 for gentle slope (25º) to z/h – 0.35 for steep slope (40º)]. For a gentle slope (25º), pit excavation slightly increases the streamwise intensity in the inner layer by about 30 %. However, the effect of the pit is more pronounced in the transverse and vertical intensities. The average increase in σ_v and σ_w was about 22.6% and 21.7 %, respectively. For 31º slopes, intensities in all three directions increase in the outer layer (z/h > 0.2) due to the channel pit. The average increase in σ_u, σ_v and σ_w was about 52%, 38% and 43%, respectively. For steep riverbank (40º), the profile of σ_u in the case of a pit is almost similar to the no pit case. However, the secondary flow alterations are evident as the σ_v and σ_w in the inner layer escalate in a pit case.

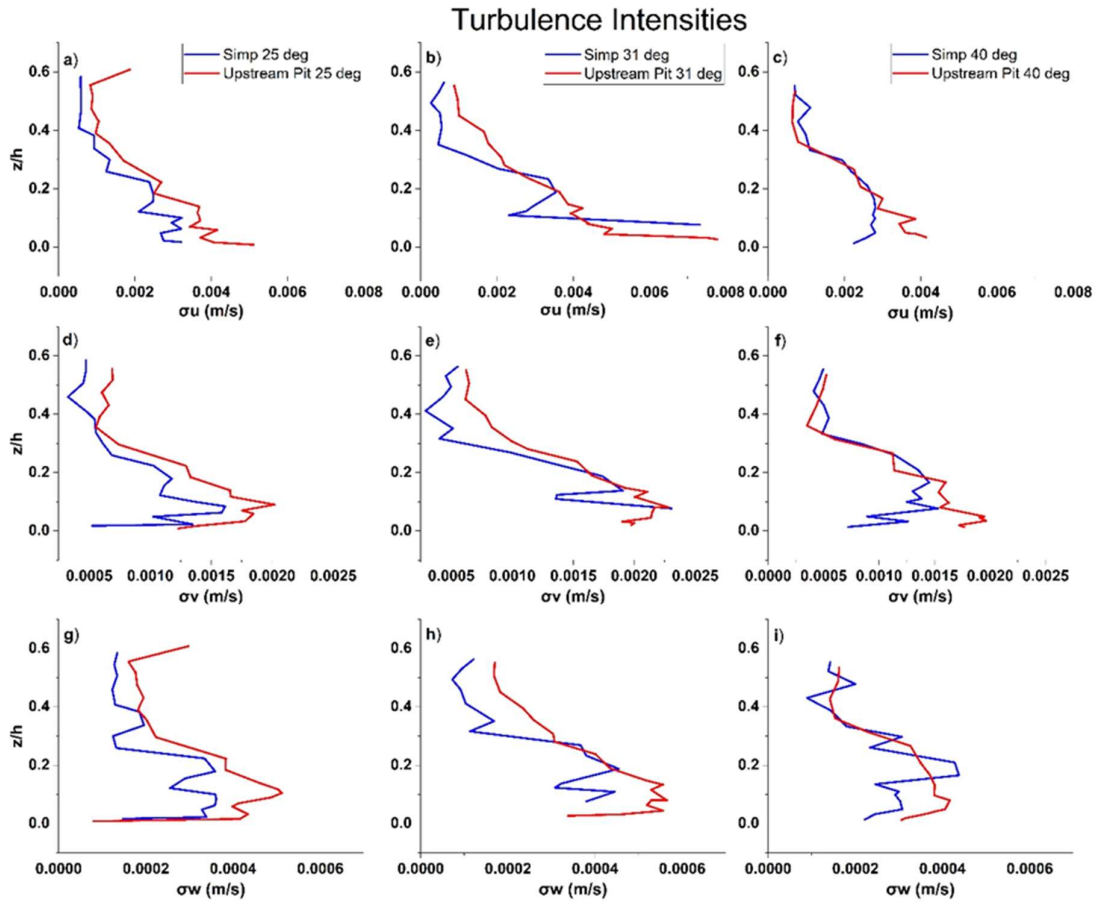

Figure 3.10: Streamwise (a-c), transverse (d-f) and downward (g-i) Turbulence Intensities at location 5-C for riverbank slope of 25°, 31°, and 40° without pit and with pit, respectively.

3.3.5 Bursting

The streamwise momentum transport normal to the riverbed plane (X-Y plane) causes a time-averaged Reynolds shear stress $-\rho\overline{u'w'}$ on the plane. This time-averaged RSS is a resultant of 4 types of turbulent bursts on $u' - w'$ plane. These four types of bursting events are [Q1] Outward interactions ($u' > 0,\ w' > 0$); [Q2] Ejections ($u' < 0,\ w' > 0$); [Q3] Inward interactions ($u' < 0,\ w' < 0$), and [Q4] Sweeps ($u' > 0,\ w' < 0$) **(Nakagawa & Nezu, 1977).** Based on the conditional statistics of u' and w', the contribution of all 4 type of bursting events to the total Reynolds shear can be calculated by Equation 3.2.

$$RSS_{Q1} = -\rho\overline{u'w'}_{[+u',+w']};\ RSS_{Q2} = -\rho\overline{u'w'}_{[-u',+w']}$$
$$RSS_{Q3} = -\rho\overline{u'w'}_{[-u';-w']};\ RSS_{Q4} = -\rho\overline{u'w'}_{[+u',-w']} \quad 3.2$$

The fractional contribution of all four bursting events in total RSS magnitudes across the riverbank is presented in Figure 3.11. In order to avoid redundancy, the results of the 31º riverbank have been discussed. The contours of fractional contribution suggest that the RSS generation on account of any bursting event is not uniform throughout the riverbank cross-section, owing to strong secondary flow. Careful investigation of Figure 3.11 reveals that in main-channel flow (bed width 60 cm – 90 cm on X axis), Outward interactions and Inward interactions are dominant in generating the RSS within the inner layer. However, in the outer layer, Ejections and Sweeps generate greater RSS. If we focus on near bank flow (bed width 30 cm – 60 cm on X axis), maximum RSS close to sediments is due to Ejections followed by Outward interactions. In the upper flow layer, however, outward and Inward interaction events occur over a large flow area and generate RSS. It is interesting to note that Sweep events contribute the least to the total RSS, especially in the near-bank flow. Channel pit affects the turbulence bursting events occurring across the riverbank flow. In the main-channel flow, Outward interactions and Inward interaction events are amplified in the inner flow layer. In the outer layer, the contribution of outward interactions and inward interaction also slightly increased, while the ejection contribution decreased in the with-pit case. Pit excavation increases the RSS generation from sweep events in the near bank flow at the berm location. As sweep events are associated with greater sediment mobility, pit excavation can be erosive in the near-bank and berm areas. Thus, pit excavation alters the bursting events across the riverbank flow, implying variation in the nature of turbulence.

The fractional contributions discussed in Figure 3.11 provide the overall effect of each respective bursting event encompassing all the bursts, week or strong. Therefore, it cannot sample stronger events out of weaker ones. In order to find the stronger and more dominant

bursting events, hole analysis is adopted. In this method, the hyperbolic hole (H) region is superimposed on the $u'w'$ plane, and only the events outside this hole region (stronger events) are computed. This region is given by:$|u'w'| = H(\overline{u'u'})^{0.5}(\overline{w'w'})^{0.5}$. The fractional contribution of a particular bursting event outside the hole region is computed by Equations 3.3 and 3.4.

$$\langle u'w' \rangle_{i,H} = \lim_{T\to\infty} \frac{1}{T} \int_0^T u'(t)w'(t)\lambda_{i,H}(z,t)dt \qquad 3.3$$

Where $\lambda_{i,H}(z,t)$ is called a detection function defined as:

$\lambda_{i,H}(z,t)$ =1, if $u'w'$ is in quadrant i, and if $|u'w'| \geq H(\overline{u'u'})^{0.5}(\overline{w'w'})^{0.5}$ 3.4

$\lambda_{i,H}(z,t) = 0$, otherwise

A sample hole size analysis at a point in near-bank flow for 31º riverbank slope is shown in 3.12. For higher hole sizes, stronger ejection events occur due to the pit excavation. Such stronger ejection bursts are observed for hole sizes as high as 6. Thus, due to the sandpit, stronger ejection bursts provide a mechanism of sediment movement near the bank toe.

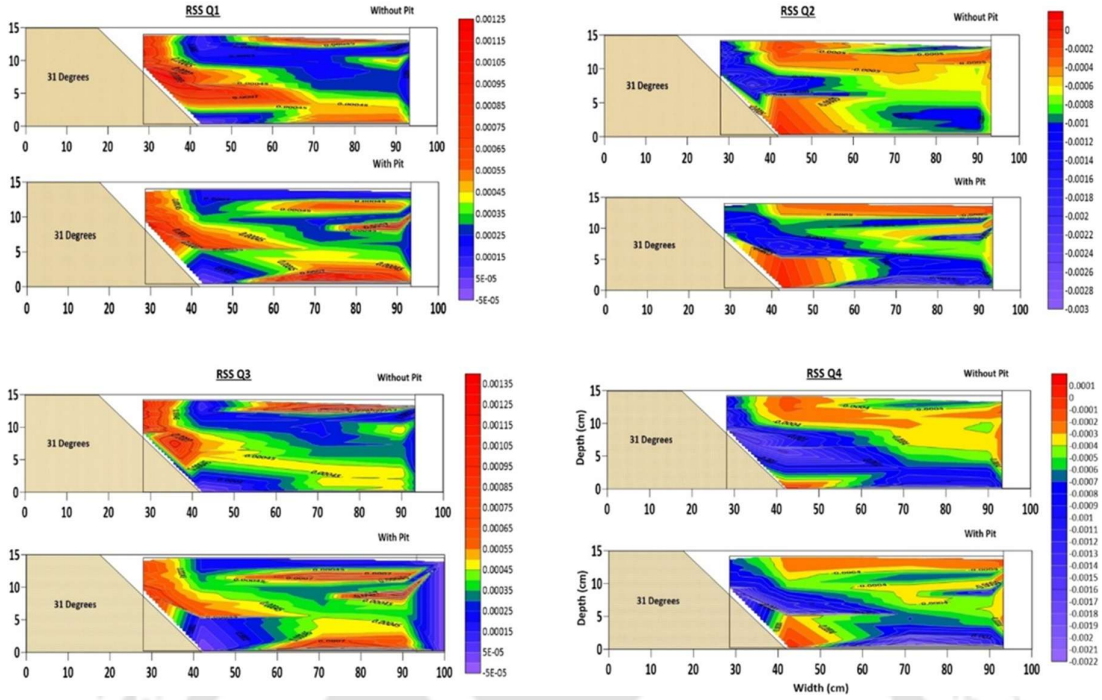

Figure 3.11: Temporal mean distribution of streamwise RSS magnitudes due to all 4 types of bursting events across 31° riverbank cross-section at location 5 without pit vs with pit, respectively

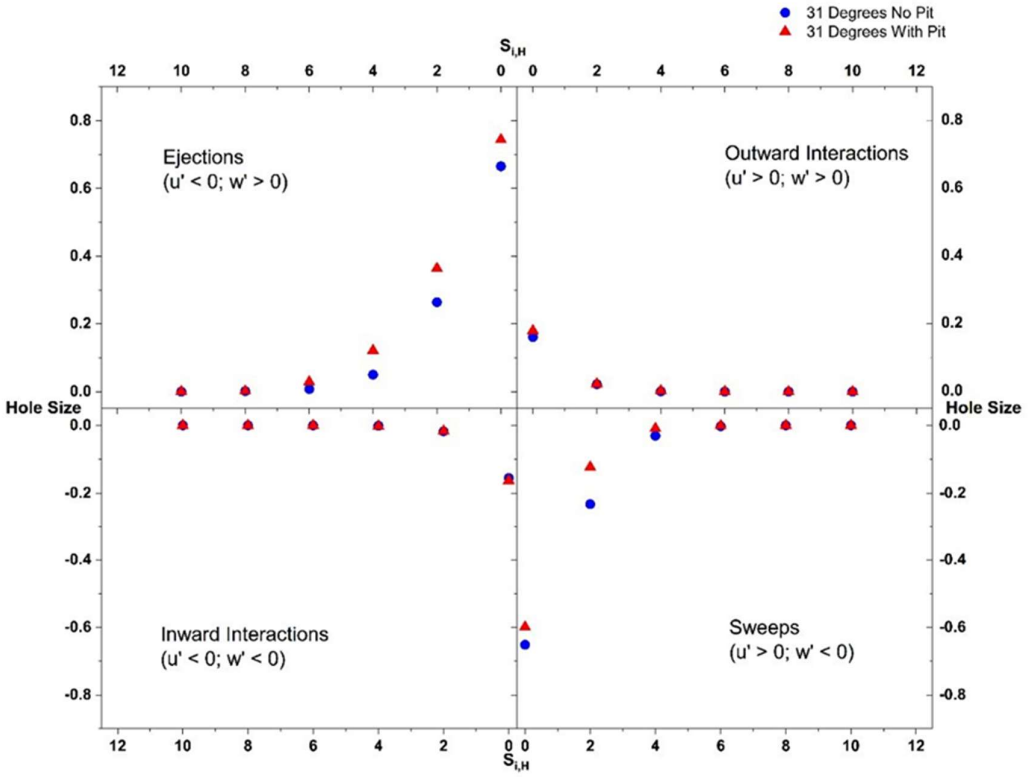

3.12: Quadrant hole analysis of τ_(Z-X) in the near-bank flow of 31° riverbank at point C of location 5 without pit and with pit. It represents momentum carried normal to the main flow direction by stronger events of all types of bursts.

3.3.6 Riverbank Morphology

The cross-sections of the riverbank for all the test cases after 24 hours of steady flow passing through them are plotted in Figure 3.14. In this study, three bank slopes have been tested, i.e., 25º (flatter than the angle of repose of the sediments), 31º (equal to the angle of repose), and 40 º (steeper than the angle of repose). The initial top width for all the cases was 18.0 cm. In 25º and 31º cases, initially, sliding failure occurred along the slope, and the formation of the berm at the toe of the riverbank was observed. This berm formed at the toe provides lateral stability to the riverbank slope. Also, the bank-derived sediments were deposited in the main channel, causing channel aggregation. Later, fluvial erosion was prominent where the streamwise and lateral stresses exerted by the near bank flow caused the transport of sediments from the berm and channel portion. The riverbank top width available after erosion, in the case of 25º and 31º, was around 15 cm and 12 cm, respectively.

Excavating sand pit supplements the streamwise momentum and lateral momentum transport normal to the flow direction downstream, causing greater Reynolds shear stresses on the sediment plane *X*-*Y* (Figure 3.8 and Figure 3.9). At the quasi-equilibrium state, the effect of the sand pit was negligible on the 25º riverbank. However, in the case of the 31º slope, the bank-derived sediments deposited in the main channel were progressively eroded because of enhanced turbulent shear stresses exerted by the main channel flow. Therefore, the main channel bed level at the quasi-equilibrium was lowered by about 1.2 cm. It increased the exposed height of the slope, which is critical for bank stability. Also, streamwise and lateral turbulent shear stresses exerted by the near bank flow lead to the progressive erosion of the berm. Berm height is significantly lowered by pit excavation. The average berm area at the toe was decreased by 27%, due to pit action. This implies that the stability of the riverbank downstream of the pit may decrease if it is subjected to unsteady flows in the future. It is clearly evident that in the case of a sand pit, the bank failure planes above the berm are closer to the

original slope (for slopes up to the angle of repose). Hence, lesser bank sediments are eroded during pit excavation. One of the reasons for this effect may be that the flow erosivity is concentrated in the channel and near the toe flow. In the case of a 40º riverbank slope, sliding failure occurred initially for both without and with pit cases. Bank sediments could not deposit sufficiently near the toe on account of a steep slope. The berm height was almost half compared to 25º and 31º cases. In the case of the pit, the main channel lowered by 2.8 cm for 20 cm of the channel at the centre, but the riverbank was almost the same as in the no-pit case. This indicates that failure slopes steeper than the angle of repose is governed by gravity forces compared to fluvial action. So, in such cases, pit excavation has a negligible impact on the equilibrium morphology of the riverbank slope. The bed and bank-derived sediments that get transported were collected in the bedload box. The percentage increase in the bedload transport due to sandpit was found to be 15 %, 8.34 %, and 17.74 % for 25º, 31º, and 40º riverbank slopes (Figure 3.13). Channel dredging clearly leads to increased mobility of riverbank sediments.

Figure 3.13: Sediment Transported through the Test Section in 24 Hours of the Experimental Run

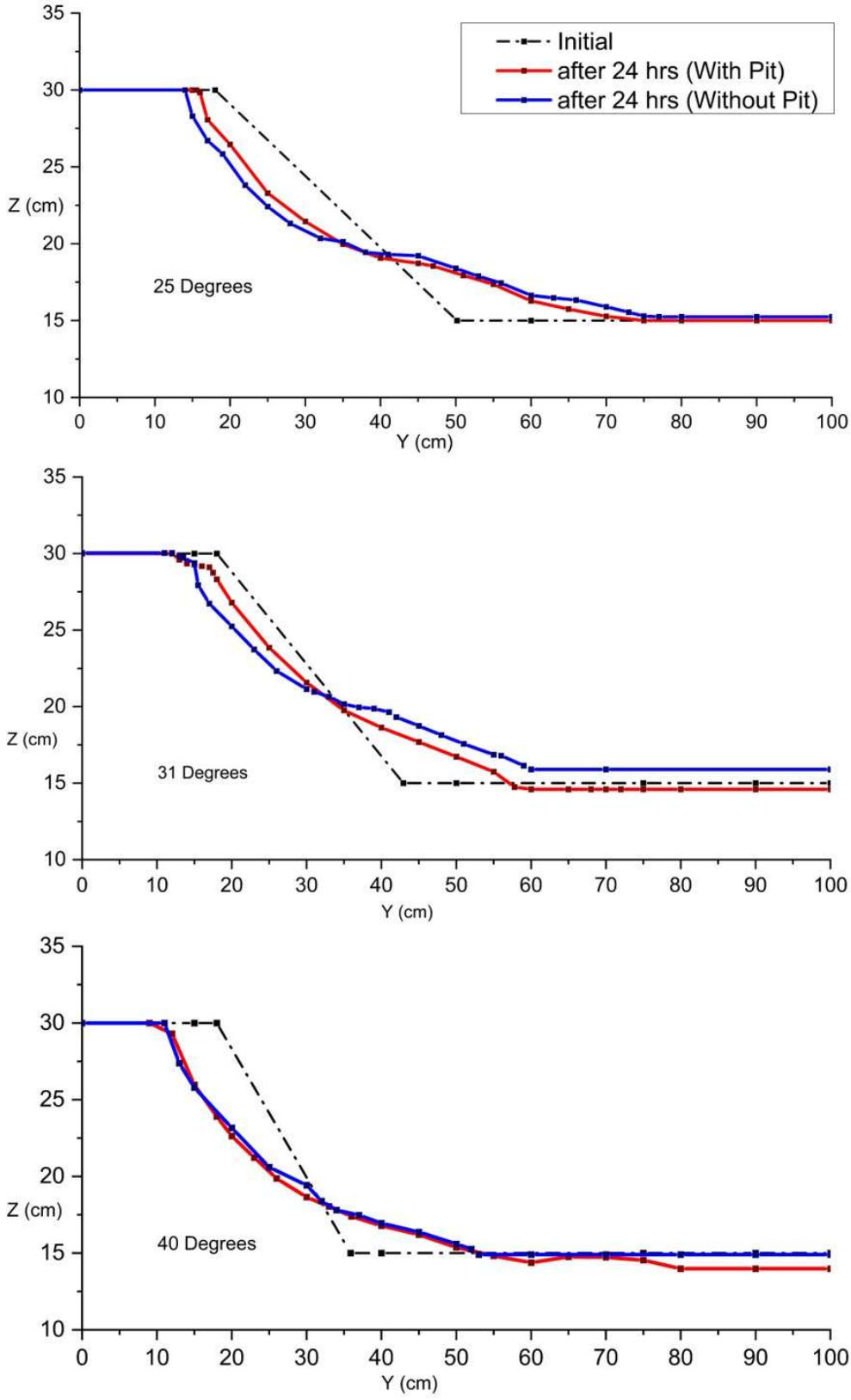

Figure 3.14: Cross Section P-Q (location 5) at the starting (initial) and at the end of the experiment (24 hours) for all three riverbank slopes without and with pit, respectively

3.4 Conclusions

Experiments were conducted in a laboratory flume to study the riverbank erosion and failure processes in an excavated channel. The hydromorphological response of the riverbank to the upstream sand pit was analysed based on turbulence statistics and quasi-equilibrium riverbank morphologies. The understanding of the process derived from the study is given below.

1. The cohesionless riverbanks subjected to steady zero-pressure gradient flow undergo sliding failure initially, and later, the fluvial erosion was observed progressively. Berm formation occurs at the toe region, which supports the bank's slope. The morphological adjustments cease to continue, and the riverbank section reaches a quasi-equilibrium state.
2. Channel pits upstream have notable effects on riverbank hydromorphology. Sandpits cause amplified turbulent shear in the near-bed flow of the main channel, which is responsible for erosion bed degradation. The berm, which provides stability at the toe, also undergoes erosion.
3. Sand pit alters the nature of turbulence bursting events across the entire riverbank. Statistics of the fractional contribution of various bursting events show that outward and inward interaction events have been amplified in the inner layer of the main channel flow. The pit also causes greater sweep event RSS generation in the berm area at the toe of the riverbank. However, in this flow region, pit excavation causes stronger ejection events, which may be responsible for sediment mobility and berm erosion at the toe.
4. In the upper flow layer of the riverbank, TKE and turbulence intensities increase, which indicates greater mixing and transport across the flow depth due to the channel pit.

5. On the sloping portion, the turbulent shear and normal stresses decrease due to the pit. Hence, lesser bank sediments from the slope are derived in the channel due to pit excavation.

Based on the above conclusions, it becomes important to consider the impact of channel dredging activities in the context of riverbank stability and erosion. The fluvial erosion characteristics of the riverbank are due to the channel pit being a complex dynamic process, and fluvial elements such as seepage, vegetation characteristics, etc., may become significant. These factors are not considered in this study, but they are important avenues for future research.

4. Effects of Proximity of Sediment Pit and Dredging Volume on the Riverbank Stability

This chapter of the thesis attempts to understand the effects of sediment mining pits on the stability of the riverbank due to their proximity. It will also quantify the increase in turbulence parameters and morphological changes due to increasing the volume of dredging. It is attempted to understand if and how the sandpit affects the riverbank stability and contributes to formulating guidelines for sediment dredging from rivers.

4.1 Introduction

Rivers are complex systems that respond to every activity occurring naturally or anthropogenically. This response can be observed upstream and downstream of the affected river segment. The river acts as a lifeline to the earth's system by acting as a transporting agent of essential elements to the beneficiaries in the earth's biosphere (Florsheim et al., 2008). The river erodes the beds of the upstream mountains while moving down a steep slope. It transports the high-nutrient and rough-surfaced sediment and deposits it downstream into the plains. While it enriches the surroundings for agriculture and supplies water for various purposes, the transported sediment is perfect for use as a construction filling material in the exponential urbanization in the 21st century. The extraction of sand and gravel from the riverbeds and floodplains has become a major supply channel of aggregates to the construction sector (Padmalal et al., 2008; Rentier & Cammeraat, 2022; Sanchis-Ibor et al., 2017). Although controlled dredging is justified for the nation's socio-economic development, the ever-increasing demand for construction-grade sediment and profit margin has caught ravenous organizations' attention (Mensah & Mattah, 2023). The dredging changes the cross-sectional shape and stability of a stream channel. It enhances the effects of hydraulic erosion and further decreases the stability of the cross-section (Barman et al., 2017; Barman et al., 2018; Barman et al., 2019a; Barman et al., 2019b). Bank instabilities and erosion due to instream channel

mining may be aggravated due to simultaneous fluvial phenomena such as seepage, changes in pore water pressure, changes in the stage of the river, and other anthropogenic activities (Lade et al., 2021; Lade, Deshpande, et al., 2019; Lade & Kumar, 2020; Patel et al., 2022; A. Sharma & Kumar, 2018).

River transports sediments in the form of bedload when flow characteristics such as velocities and bed shear stresses exceed the incipient conditions. It flows continuously and achieves a regime condition with no overall deposition or erosion unless a strong/large-scale natural event or anthropogenic activity disrupts the river's balance. The river sets on to achieve a new quasi-equilibrium by depositing the incoming sediment upstream or shifting its flow path (Lawler et al., 1997; Thorne & Tovey, 1981). The replenishment of the dredged pit begins with the regularly flowing sediment. This prevents the sediment from flowing downstream and depletes the sediment in the downstream riverbed. The intensity of the river's reaction directly depends on the level of anthropogenic action (Arora, Lade, et al., 2023; Arora, Patel, Lade, et al., 2023; Kramm, 2020; Rentier & Cammeraat, 2022; Roy et al., 2020). The dissemination of the riverbank is a source of sediment downstream and helps the river regain its quasi-equilibrium. The riverbank regeneration occurs during flood retrieval or high-stage but low discharge. The eroded bank faces a higher probability of failures such as toe failure, deep cracks, cavity formation, and mass failure. Near-bank dredging is sometimes practiced, threatening the bank's safety, mainly led by toe failure. Tension cracks depend on soil properties such as cohesion, sediment size, and distribution (Debnath et al., 2007; Roy et al., 2019). The river's dynamic stage in different seasons significantly impacts sedimentation and transportation (Nardi et al., 2012). The high velocity of the flow at the low stage contributes to the undercutting of the riverbanks. The expansion of the lateral cavity, formed during improper mining in the riverbank, depends upon the fluctuations in the flow and aspect ratio of the cavity (Juez et al., 2018). The failed riverbank will lead to floods in the local area, destroying the local

infrastructure and inflicting loss of fertile land, lives, and property. This would also affect the downstream structures and aquatic life. Various bank protection measures, such as the installation of spur dykes, river training works, and flood passage grounds, are adopted by the government. These methods involve significant capital investment for numerous rivers in the country, and such capital is not available in developing nations. The developing nations then lose significant amounts of fertile land, causing indirect losses to the nation for profit to some covetous organizations (Duan et al., 2019; Khan et al., 2021; Mensah & Mattah, 2023).

(Benedet et al., 2013; Benedet & List, 2008) researchers have contributed to the study of the extent of mining and its effects on coastal erosion. (Haghnazar & Saneie, 2019) have extensively worked on laboratory experiments to study the filling rate of the sediment pit in series. (B. Barman et al., 2017, 2020, 2022) have explained that the mining pit migrates with time. (Lade et al., 2020) have shown the effects of the proximity of the pit on the scour development in the vicinity of the bridge pier. However, the effects of the proximity of the sandpit on the riverbank stability are not fully understood. This section covers the laboratory experiments conducted in a flume with upstream and downstream pits, and its effects on riverbank stability have been quantified.

4.2 Effects of the Proximity of Sediment Pit on the Stability of the Riverbank

The experiments were conducted in the laboratory flume for three different discharges in the setup, as discussed in Section 2.4. The dimensions of the sediment pit and its locations have been presented in Figure 2.13. The slope of the riverbank has been kept at 31 degrees for all three cases, as it has been established that the riverbanks are relatively stable if the angle of the riverbank slope is its angle of repose. The contours of the longitudinal variation of the average streamwise velocity at the centre of the main channel have been presented in Figure 4.1. It is evident that the sandpit affects the flow. It mainly affects the flow in the near-bed region, which propagates upwards as the distance increases, which is clearly visible in Figure 4.1 upon

comparing the cases from A to C. Re-orientation of the high-velocity flow is considerably more as the pit moves closer to the center of the test section.

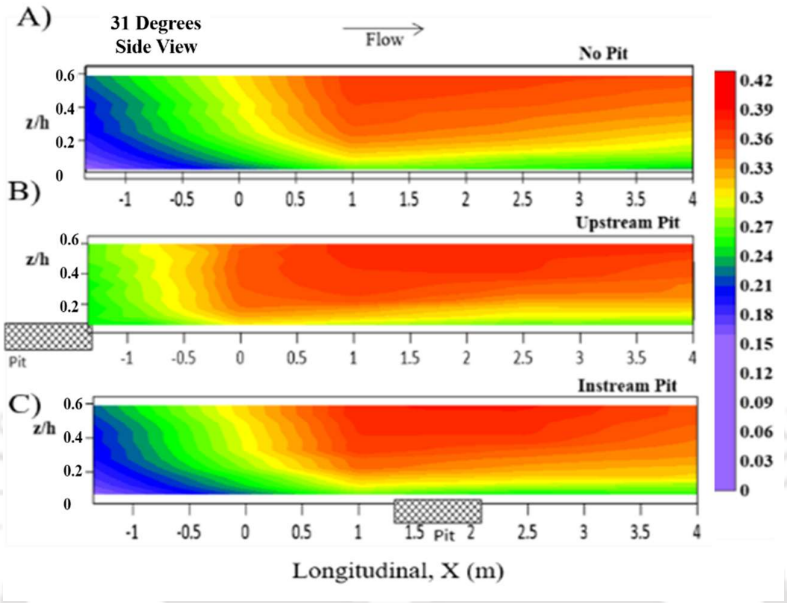

Figure 4.1: Longitudinal Variation of the Average Streamwise Velocity (m/s) with Different Locations of the Sandpit A) No Pit; B) Upstream small pit; C) Instream small Pit.

Further, the study of variation of Reynolds shear stress (RSS) has been presented in Figure 4.2. The increase in RSS at the centre of the test section in the case of the instream pit is observed to be 72%. This shall cause an increase in the sediment transport capacity of this zone. The section in interest lies at the X=2.5 m, which means there will be significant changes in the morphology. For the upstream case, the increase in shear stresses immediately after crossing the pit is visible in Figure 4.2. This shall destabilize the near-bed sediment and transport it downstream. In the following sub-section, we will see how it has affected the morphology of the cross-section of interest.

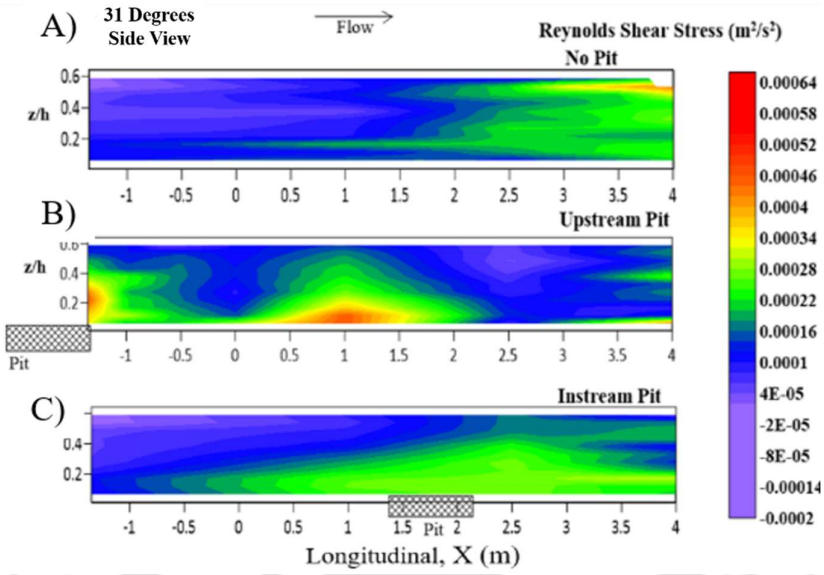

Figure 4.2: Longitudinal Variation of Reynolds Shear Stress (m^2/s^2) due to A) No Pit; B) Upstream small pit; C) Instream small pit

The Turbulent Kinetic Energy (TKE) doubled its magnitude for the depth z/h<0.3. The increased TKE values suggest an increase in the turbulence levels of the flow, which necessarily means the increased sediment transport activity. The magnitude of the TKE is less in the case of the upstream pit in Figure 4.3 because of the cross-section there before the start of the riverbank.

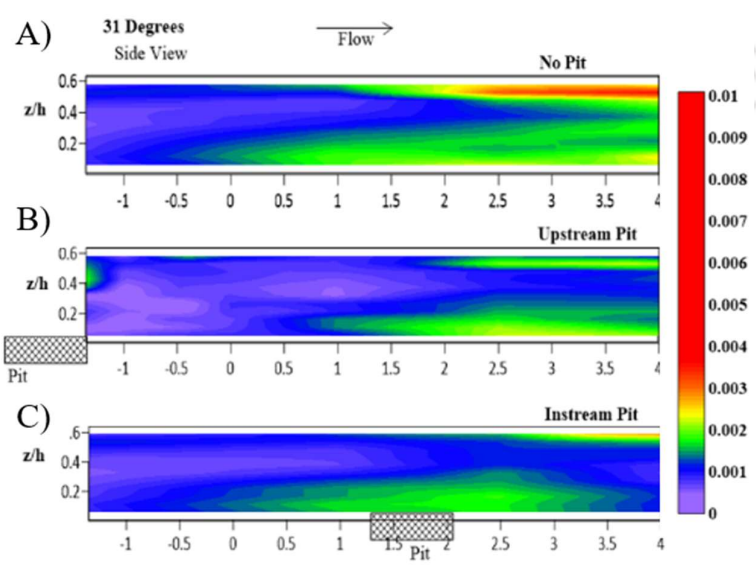

Figure 4.3: Contours of Turbulent Kinetic Energy (m^2/s^2) in A) No Pit; B) Upstream small pit; C) Instream small pit.

The morphological changes in the riverbank cross-section due to the experimental flow of 24 hours for all three cases are presented in Figure 4.4. The dashed line shows the initial profile, and green shows the case if there was no sediment mining. The effects of the instream pit (in red) are similar to the cases presented in the previous chapters. This causes erosion of the test section. In the study of the effects of the upstream pit, the anticipated result is the erosion of the cross-section. However, the blue line shows the aggradation of the test section. It has been possible due to the increased RSS and TKE in the near-bed region.

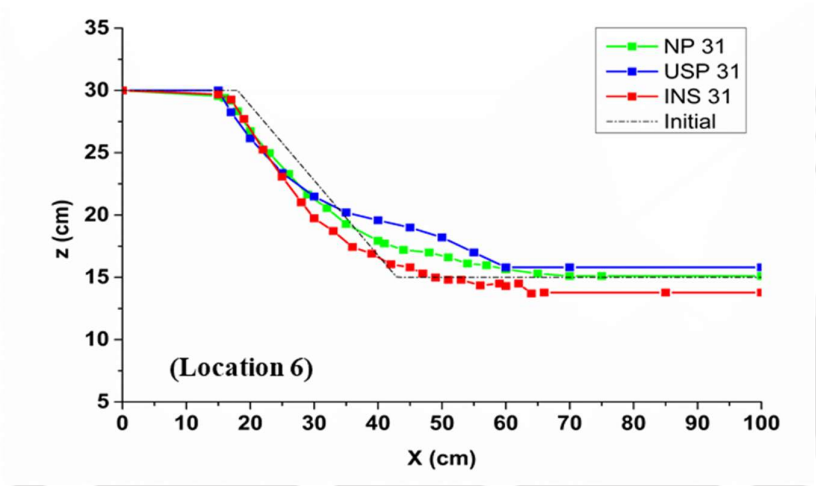

Figure 4.4: The Morphological changes at the cross-section located at the centre of the test section or the cross-section of interest.

4.3 Effects of Increasing Sediment Mining Pit Volume on Riverbank Stability

The study of the effects of increasing sediment dredging volume is essential in setting up the regulations for allocating mining sites to vendors. The experiments were conducted using the setup shown in Chapter 2. The average streamwise velocity variation along the depth of the centre of the test section is provided in Figure 4.5. The average streamwise velocity in the near-bed region ($z/H<0.2$) showed a slight increase of 5% and 4% for the cases of small upstream pit (SP 31) and large upstream pit (LP 31) compared to no-pit (NP 31), respectively.

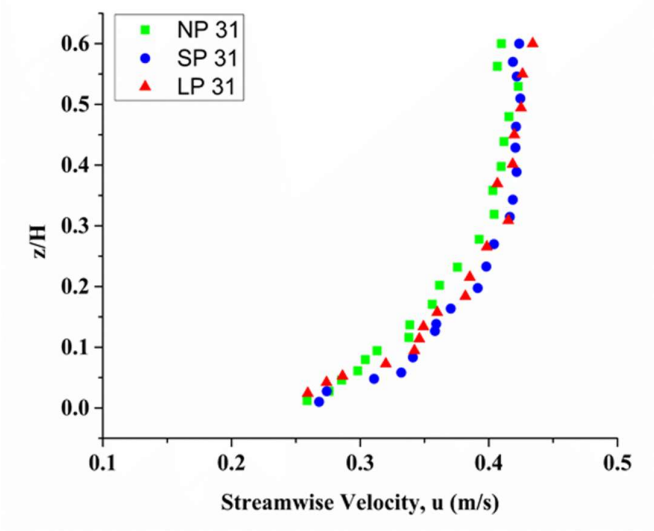

Figure 4.5: Average Streamwise Velocity variation along the depth at the center of the cross-section of interest.

Figure 4.6 presents the variation of RSS along the depth at the center of the cross-section. It clearly shows the increase in the near-bed shear stresses as the mining volume is increased from No Pit to Small Pit to Large Pit. The increase in near-bed average RSS was 24% and 80% for the SP 31 and LP 31 cases, respectively, upon increasing the mining volume by 2.34 times. This indicates that there will be increased shear stresses acting on the sediment due to the fluvial action. This causes an increase in the sediment transport capacity of a channel.

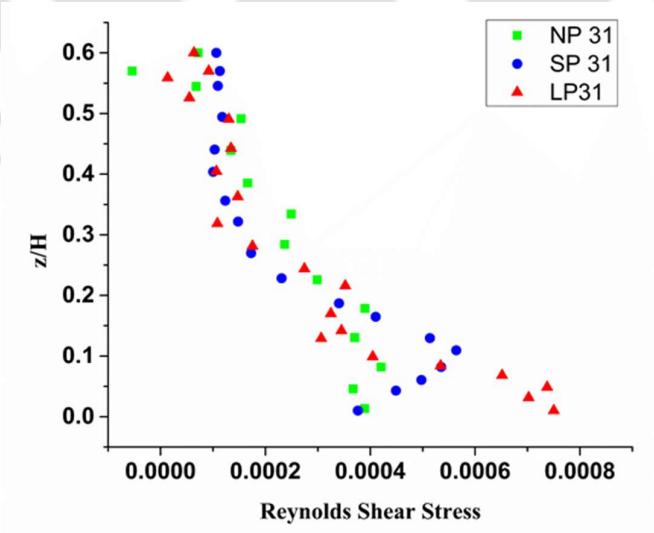

Figure 4.6: Average Reynolds Shear Stress at the center of the cross-section of interest.

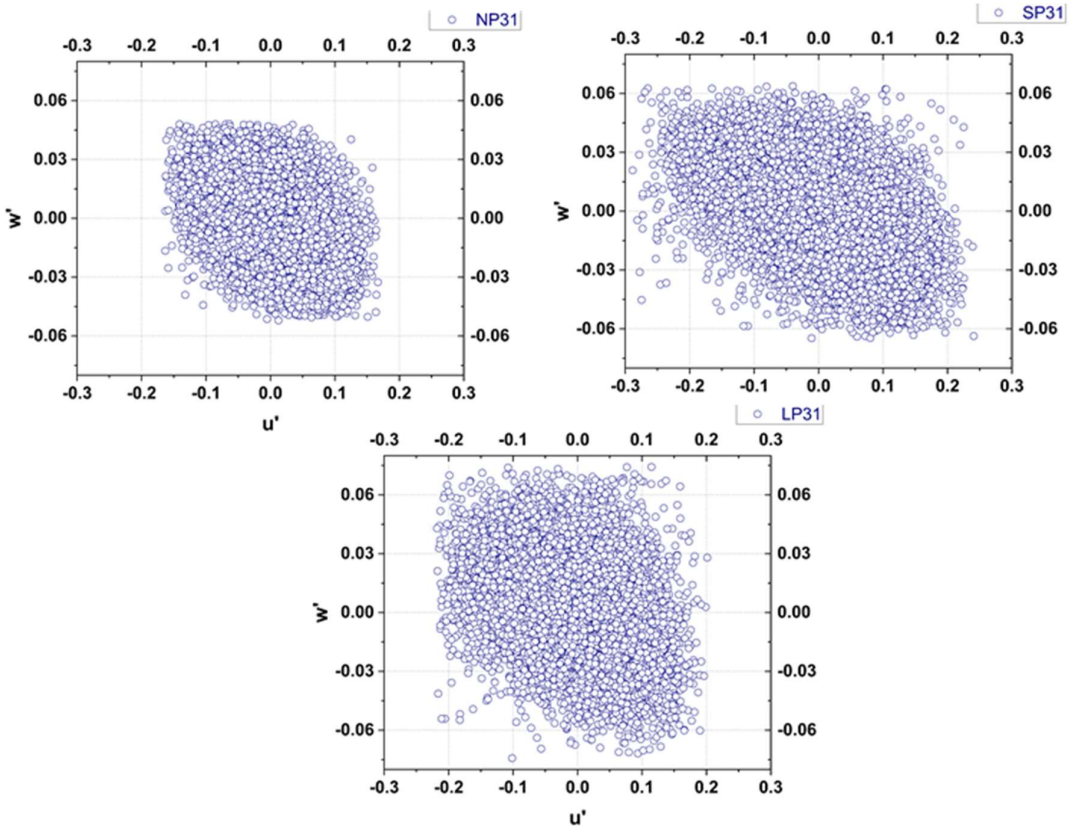

Figure 4.7: Quadrant Analysis with fluctuation events at the center of the cross-section of interest at z/H ~ 0.2

Figure 4.7 presents the quadrant analysis for the given three cases of sediment mining. It is a plot between the fluctuation component of the instantaneous velocity for each sample of the observed 12000 readings at a given depth of z/H ~ 0.2. It can be seen that as the volume of dredging increases, the strength of the depthwise velocity fluctuation (w') component with respect to its streamwise fluctuation component (u'). This indicates the presence of stronger downward and upward flow at the given point. This causes increased destabilisation of the sediment present at the bed, causing greater sediment transport. The increased sediment transport means increased destabilisation of the entire downstream section, which may affect the riverine structures and increase riverbank toe erosion, leading to riverbank failures.

Figure 4.8 shows the morphological changes in the cross-section of interest due to fluvial action from 24 hours of the experimental run. As the volume of dredging increases from No Pit (green)

to Small Pit (blue) to Large Pit (red), the erosion of the cross-section increases. The erosion area was 15.1 cm2 for the SP 31 case as compared to the NP 31 case. The erosion area increased by 4 times (60.8 cm2) upon increasing the mining volume by 2.34 times. The erosion of the toe of the riverbank is clearly visible in the cases of increased sediment mining. This indicates the urgent need for the regulations to allocate the extent of sediment mining.

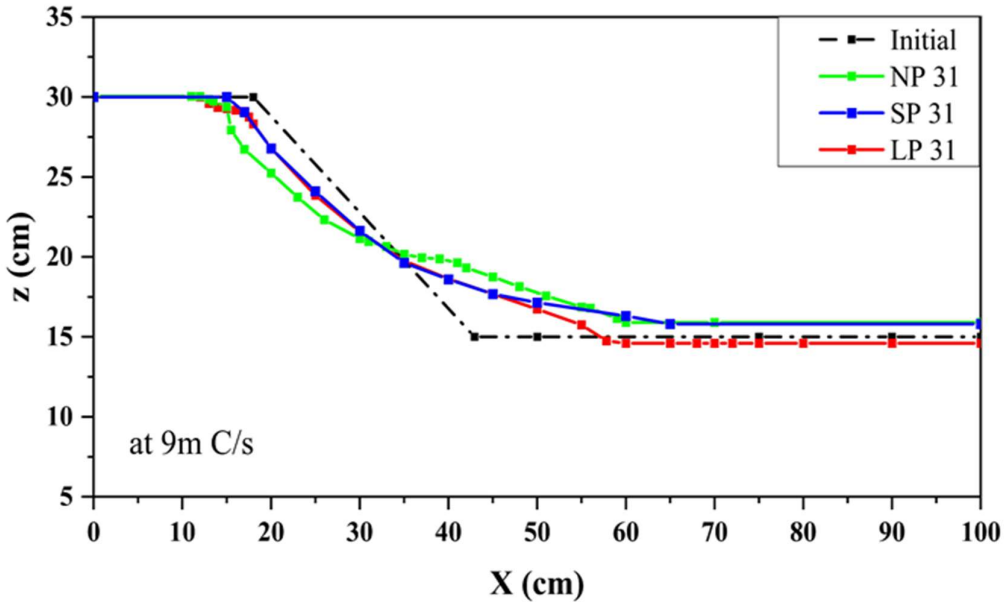

Figure 4.8: Morphological changes of the cross-section of interest after 24 hours of the experimental run.

4.4 Conclusions

We found that the pit at a closer distance created havoc by eroding 15% of the riverbed and the berm. However, the far pit had caused aggradation at the cross-section. This was because the eroded particle would settle in the downstream. So, it was clear to us that it is not merely erosion everywhere. It is the instability or increased sediment transport in the channel due to mining. The following conclusions can be drawn based on these experiments.

- The upstream small pit (USP 31) showed deposition compared to the no-pit case (NP 31) at the location 4 m after its downstream end.

- This has occurred due to the erosion of the zone -1.5 m < X < 2.5 m, which has transported downstream due to fluvial action.
- The cross-section with an instream small pit (INS 31) showed erosion of 2 cm (13.33%) of the channel bed.
- Although the average streamwise velocity remains the same, the re-orientation of the high-velocity region is stronger close to the pit.
- TKE suggests that the affected depth increased from z/H<0.2 to z/H<0.3 as the pit moved close.
- The average streamwise velocity in the near-bed region (z/H<0.2) showed a slight increase of 5% and 4% for the cases of small upstream pit (SP 31) and large upstream pit (LP 31) compared to no-pit (NP 31), respectively.
- The increase in near-bed average RSS was 24% and 80% for the SP 31 and LP 31 cases, respectively, upon increasing the mining volume by 2.34 times.
- The erosion area was 15.1 cm2 for the SP 31 case as compared to the NP 31 case. The erosion area increased by 4 times (60.8 cm2) upon increasing the mining volume by 2.34 times

This study emphasizes the detrimental effects of sediment mining pits. It illustrates how unplanned and insensitive mining practices can jeopardize the stability of riverbanks. A more thorough understanding of the relationship between the proximity of a sandpit and the volume of dredging necessitates additional research involving various sizes of mining pits and sand extraction at different distances from the relevant cross-section. Nonetheless, this study establishes a solid foundation for recognizing the significance of both the location and size of sediment mining activities in the vicinity of sensitive areas with critical infrastructure, such as bridges.

5. Nature-Based Solutions to Mitigate Riverbank Erosion

5.1 Introduction

Riverbank erosion affects the stability of a river. The cross-section of the river changes as various factors like stream flow, unstable slopes, cracks, seepage, and anthropogenic activities affect the riverbanks. The sediment received from the banks may differ from the sediment present at the riverbed, which brings heterogeneity to the sediment transport occurring at the riverbed (Majumdar & Mandal, 2022). Apart from making the sediment transport problem more complex, the instability of the riverbank may lead to catastrophic events like floods (Jugie et al., 2018). A weakened or eroded riverbank at a particular location would be more susceptible to failure when the flood water passes through the river. A failed riverbank would indicate channel migration and loss of precious land surface (Arora, Lade, et al., 2023; M. hui Yu et al., 2015). The river migration affects various water exchange infrastructural projects installed close to the riverbanks, such as water supply for a nearby community or dumping treated wastewater (Benedet et al., 2013). Anthropogenic activities like near shore constructions, river encroachments, bridge construction, port construction, and sediment mining have been done for decades. While all other activities are being controlled to some extent by the governments, various illegal operators are taking up sediment mining operations (Duan et al., 2019; Rentier & Cammeraat, 2022). Many agencies have reported the extent of mining to be as high as 3.5 Million tons in 1 year (Ciszewski & Sobucki, 2022). To minimise the damaging effects of sediment dredging done in the past on the riverbank, the choice of action shifts towards stabilising factors like installation of rocks in different sizes, spurs, grouping, river training structures, and increasing the riparian vegetation with suitable and locally available vegetation (Chen et al., 2019; Hartwig et al., 2016; S. Kang et al., 2021; Krishna Prasad et al., 2016; Patel et al., 2022; Patel & Kumar, 2023).

Studies have emphasised that riparian vegetation protects the banks in two ways, mainly root action and altering the river flow (Okeke et al., 2020). Previous research has established that the root extent of riparian vegetation significantly stabilises the riverbank. A riverbank with deeply rooted vegetation would stay stabilised till the zone of failure has not passed further down than the roots of the vegetation (Okeke et al., 2020). The selection of vegetation depends on the root system, and only large-scale bedform erosion can cause vegetation to uproot or fail. In further extreme cases, the entire riverbank and riparian vegetation will fail (Okeke et al., 2020). The other action of riverbank vegetation in contact with the river flow is to deflect the flow from the riverbank towards the unvegetated part of the cross-section to achieve the minimum resistance to the flow. The deflection of flow away from the bank helps decrease erosion due to fluvial action, which is the main component of riverbank erosion (Yang et al., 2018). Other than the positive effects of deflecting the flow away, there are two main adverse effects, i.e., a slight rise in the water level is observed in the vegetation zone, which occurs as the flow tries to overcome the resistance to vegetation in the flow area. This will be critical when the flow water level is near the flood stage (Arora et al., 2023c; M. Liu et al., 2022; Zeng et al., 2022). The other problem will be with increased riverbed erosion of the main channel (Arora et al., 2023(a,b), Yang et al., 2018).

For vegetation to significantly affect the riverbank stability and river flow, various researchers have studied different types of vegetation and different densities of their plantations (Barman & Kumar, 2022b; Lama et al., 2020; Liu et al., 2021; Liu et al., 2017; Nepf, 1999; Siniscalchi et al., 2012). To minimise the cost of artificial plantation of suitable vegetation, the optimised density of the plantation needs to be achieved. Many researchers have worked with various densities of different types of vegetation and have provided a classification of the density of vegetation depending upon the height of vegetation (h) and its frontal area (a) in the flow to be (Barman & Kumar, 2023; Guo et al., 2021; Luhar et al., 2008; Nepf, 2012). Previous studies

have concluded that increasing the density of the vegetation will lead to increasing velocity in the main channel (Valyrakis et al., 2021). The nature of vegetation plays an important role. Rigid vegetation has not proved to be as resistant to the flow as flexible vegetation (Caroppi et al., 2021). Further, large and blunt vegetation would accumulate the debris and other solid waste flowing in the rivers (Osman & Thorne, 1988). Flexible, bladed vegetation with deep roots, locally available, weather tolerant, moisture tolerant, and fast-growing vegetation should be best suited for controlling riverbank erosion and stabilising the riverbank. We have selected pearl millet (Pennisetum glaucum) vegetation for our study due to its fast-growing rate, deep enough roots for shallow banks, bladed leaves, and valuable production crop.

The increased velocity will have more significant morphological effects on the main channel by supporting sediment transport (Arora et al., 2023c; Nezu & Sanjou, 2008). The vegetation density in nature can be zero, sparse, or dense (Li et al., 2023). An unvegetated riverbank section would have no protection and be highly susceptible to high flow rates. Dense vegetation would support the riverbanks within its limits and deflect maximum flow away from the banks. While this benefits the banks, it accelerates the flow in the main channel, causing severe riverbed erosion. A striking balance of the vegetation density as sparse vegetation would be helpful, which will prevent riverbank erosion and also not cause damage to the main channel. Such vegetation shall be sowed one month before the expected monsoon season along the entire length of the riverbank to be protected. At this time, dropped water levels will have exposed riverbanks. In some time, the plants shall gain enough height to deflect the water away from the banks and the roots deep enough to strengthen the riverbank soil. In case of flood events or high flow rates, vegetation should protect the riverbank. Otherwise, it shall yield crops and cattle for the nearby farmers.

Lab studies have been conducted to study the changes in flow structure due to sand mining pit, which, in principle, agrees with the increased fluctuations in instantaneous velocity and

enhanced sediment transport capacity downstream of the sandpit (Barman et al., 2020, 2022; Barman & Kumar, 2023). Further researchers have studied the effects of a sandpit on engineering structures like piers, oblong piers, and tandem piers (Lade et al., 2020, 2021, 2022). Previous research has been carried out studying the effects of mining pits on the riverbanks (Arora et al., 2023a; Thompson, 2023). Only a few researchers have explored the positive effects of vegetation on the riverbanks (Chen et al., 2019; Valyrakis et al., 2021). However, understanding the potential of a vegetated riverbank as a preventive measure to the bank erosion caused by the combined effects of fluvial erosion and upstream sediment mining is yet to be explored. Here, we are studying the flow characteristics after the flow has crossed the pit and how the presence of the pit has affected the flow in the test section, and then we compare the morphological changes on the river bank and bed when the bank is vegetated with the grown vegetation of pearl millets due to its flexible and bladed leaves. This study bridges the gap in understanding these effects by evaluating if the riverbank erosion prevention nature of grown flexible, bladed vegetation and root action can subside the effects of the sand mining pit present upstream of the test section.

In this study, we have analysed the longitudinal and cross-sectional changes in the flow structure. The study also investigated the morphodynamic response of a riverbank section (channel section with side slope) to a mining pit excavated upstream and the negation effects due to vegetation coverage on the riverbank. The discharge selected for these experiments is 0.03 m3/s. The experiments were conducted on the discharge of 0.03 m3/s, whereas the incipient condition was achieved at 0.02 m3/s. The turbulent characteristics of the 0.03 m3/s have been presented in this study, which has significant sediment transport for the test period of 24 hours. This will help us understand how a patch of vegetation can affect the stability of the downstream riverbank while the anthropogenic issue of sand mining is present.

5.2 Effects of Natural, Flexible, Grown Vegetation as a Mitigation Measure to Control Riverbank Erosion Under Dredged Conditions

To understand the flow structure in the whole test segment of the riverbank, the velocity readings were taken at the cross-section 2.5 m after entrance into the test section at points 'A-G' for all the test cases. Also, the longitudinal changes in the flow structure were observed at the centre of the main channel at 0.3 m from the right glass wall. The flow structure was deliberated by analysing the turbulence parameters such as mean velocity distribution, Reynolds stress distribution, and turbulence intensities distribution in the riverbank test segment. A 0.05 m wide region near the glass wall is omitted in the outcome profiles to eliminate the side-wall effects. Also, morphology alterations in the cross-section of the riverbank occurring due to the flow hydrodynamics at the entrance of the test section at the end of the experiment were studied. In this part, the results of the test cases are provided, and process workings are assessed.

5.2.1 Mean Velocity

Reynolds decomposition states that the turbulent velocities streamwise (u), transverse (v), and depthwise (w) are the entirety of two components: mean ($\overline{u}$, $\overline{v}$, and $\overline{w}$), and their fluctuating velocity components (u', v', and w'). The contour of mean streamwise velocity against the flow depth (z/h) in the riverbank is given in Figure 5.1 for longitudinal variation and in Figure 5.2 for cross-sectional variations. In all three cases, for longitudinal changes, streamwise velocity profiles (u) are in the main-channel segment and are logarithmic, with the inner layer reaching $z/h = 0.15 - 0.25$.

The sandpit changes the mean streamwise velocities in the riverbank flow in upstream pit scenarios, as shown in Figure 5.1. In the primary channel, the sandpit prompted bed sediment erosion and slightly increased water depth. Therefore, In the event of a channel pit, mean

streamwise velocities are reduced in the outer layer ($z/h > 0.2$). The velocity increases downstream of the flow in the region $z/h < 0.2$, as seen in longitudinal profile B compared to profile A of Figure 5.1. In case III, the flow acceleration in the main channel occurs due to vegetation, as shown in profile C of Figure 5.1. At the cross-section, the near bed and near bank streamwise velocity for the case of the upstream pit is more than the no-pit case, as shown in Figure 5.2(A & B). In case III, the increase in streamwise velocity in the main channel is attributed to vegetation at the riverbank, as shown in profile C of Figure 5.2.

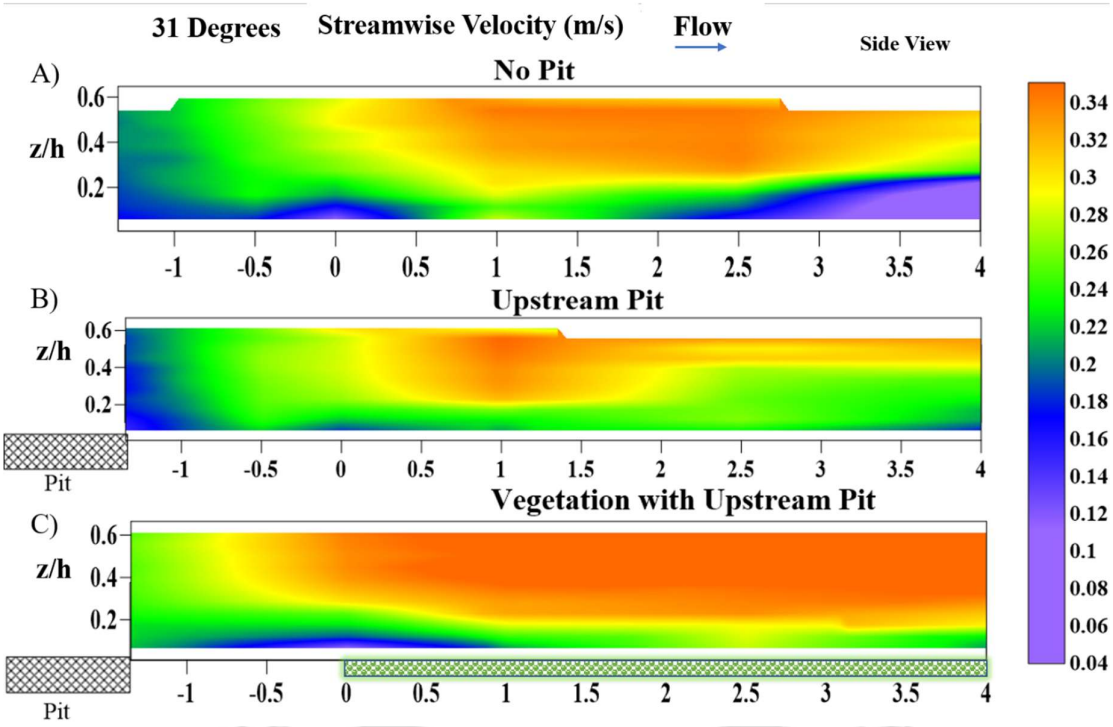

Figure 5.1: Streamwise velocity profiles along the length of flow for the cases of A) No Pit, No Vegetation; B) U/s Pit, No Vegetation; C) U/s Pit, Vegetation zone (marked in green at the horizontal axis) for discharge of 0.03 m^3/s

The near-bank streamwise velocity has decreased due to the sandpit, but the near-bed velocity has seen a sharp rise related to the no-pit case, as shown in Figure 5.2. This increase will help transport the eroded sediment of the berm and riverbed further downstream. It will help prevent riverbank erosion for now, but it will cause a greater unsupported height of the riverbank, as

established in previous research (Arora et al., 2023a; Arora et al., 2023b). The zone, $0.4 < z/h < 0.6$, has slightly increased as the top of flexible vegetation aligns with the flow. Even this increase in near-bank velocity can be reduced if the vegetation density increases (Barman & Kumar, 2023; Kang, 2013). It implies that the composure of the riverbank, even with the increased streamwise velocity, is due to the root action of the vegetation. While the pit has caused a decrease of streamwise velocity in the outer layer ($z/h > 0.2$), the vegetation accelerates the flow in the main channel, which can be seen as the neutralising effect of sediment mining.

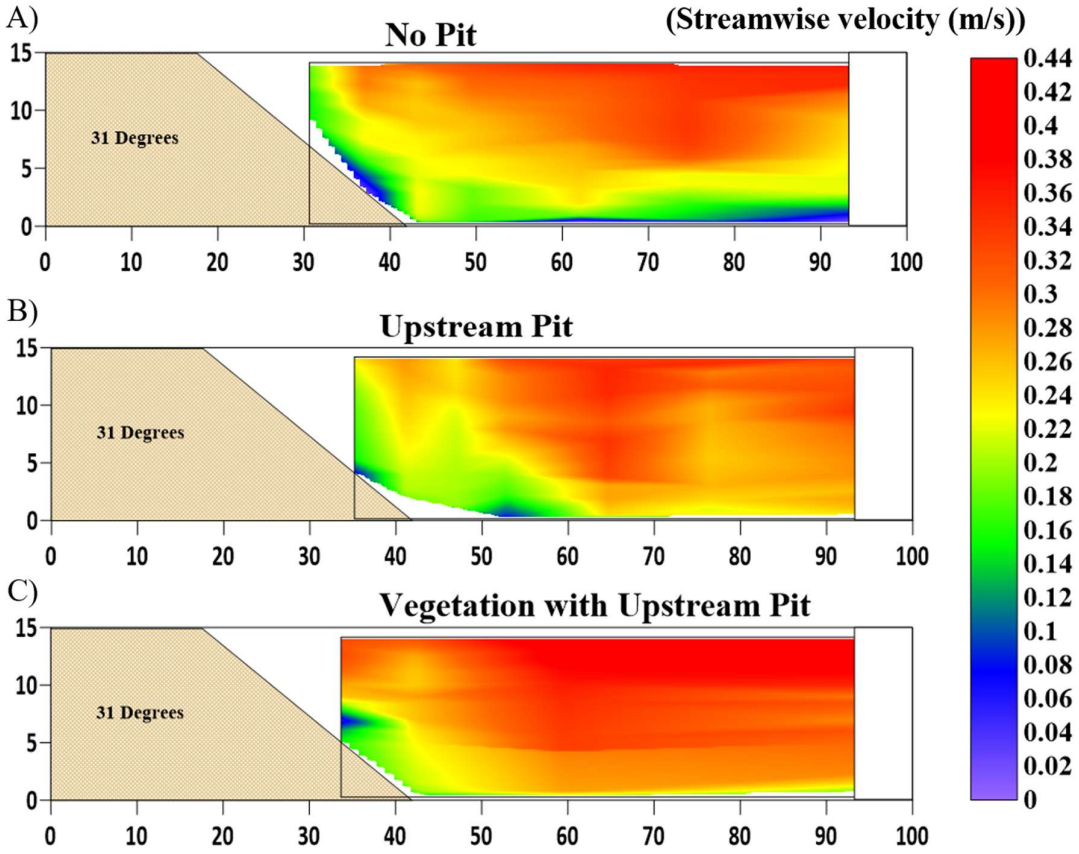

Figure 5.2: Streamwise velocity (m/s) profiles of flow at the cross-section of 2.5 m after entrance into the test section for the cases of A) No Pit, No Vegetation; B) U/s Pit, No Vegetation; C) U/s Pit, Vegetation for discharge of 0.03 m^3/s

5.2.2 Reynolds Shear Stress

In every test condition, the flow in the riverbank segment is highly turbulent and rough with $\mathrm{Re} > 10,000$. Eulerian measurements of the flow's turbulent velocities are used. Reynolds stresses on the planes X-Y and Y-Z in the Cartesian coordinate system are depicted in Figure 5.3, Figure 5.4, and Figure 5.5, showing longitudinal and cross-sectional variations. The turbulence shear forces acting on the riverbank sediments are essential as they lay on the X-Y plane because these stresses directly influence the movement and deposition of sediments. These two turbulent shear components, which are operating in opposite streamwise and transverse directions on the plane of sediments, are τ_{Z-X} and τ_{Z-Y}, respectively. The streamwise Reynolds shear stress distribution $\tau_{Z-X} = -\rho(\overline{u'w'})$ (Pu, 2021; Barman & Kumar, 2022a) in the riverbank segment is given in Figure 5.3. Figure 5.4 illustrates the riverbank's transverse Reynolds shear stress contours where u' and w' are obtained from the experimental readings using ADV, as mentioned in section 2.2 above. Mass collapse and fluvial erosion are the two leading causes of riverbank failures (Masoodi et al., 2019). The riverbank is eroded by fluvial activity as a consequence of flow. Streamwise Reynolds shear stresses (τ_{Z-X}) applied on the sediments on the channel bed and bank sections are caused by streamwise momentum's passage over the riverbank's flow depth (Arora & Kumar, 2024b).

According to the cross-section profiles of Figure 5.5, the shear stress has increased close to the area of the berm, which accelerates the berm's erosion. Longitudinal Profiles A and B of Figure 5.3 reveal that the pit may have decreased shear stress. Due to the riverbank's increased unsupported height, mass failure will result from the erosion of the stabilising berm. According to Figure 5.5(c), scenario III's region of strong shear stresses has moved away from the riverbank. Due to pit excavation, the inner layer of the main channel encounters an increase in streamwise Reynolds shear stresses (τ_{Z-X}), which causes the material to migrate.

Transverse Reynolds stresses along the bed of the primary channel flow are also made worse by the pit excavation, as shown in Figure 5.6. The transverse RSS variation from negative to positive will increase turbulence and flow intermixing. Therefore, high streamwise and transverse RSS shifts sediment loads and contributes to the degradation of these riverbank slopes' channel banks and main-channel erosion (Dian et al., 2022). Detailed analysis of Figure 5.2 demonstrates that pit excavation increases flow near the bank or at the slope's base. Flow on the bank slope controls silt movement and fluvial erosion on the slope after the slide fails. The slope's streamwise and lateral turbulence shear stress is much less in the sand pit scenario than in the no-pit scenario (Figure 5.5 and Figure 5.6). This results in higher erosion of the riverbeds but less river erosion of the hillside where the pits are. Compared to instances I and II, transverse shear stress in case III has increased in the main channel. However, it is unidirectional, resulting in less random movement of the flow, keeping it fixed in drifting away from the riverbank.

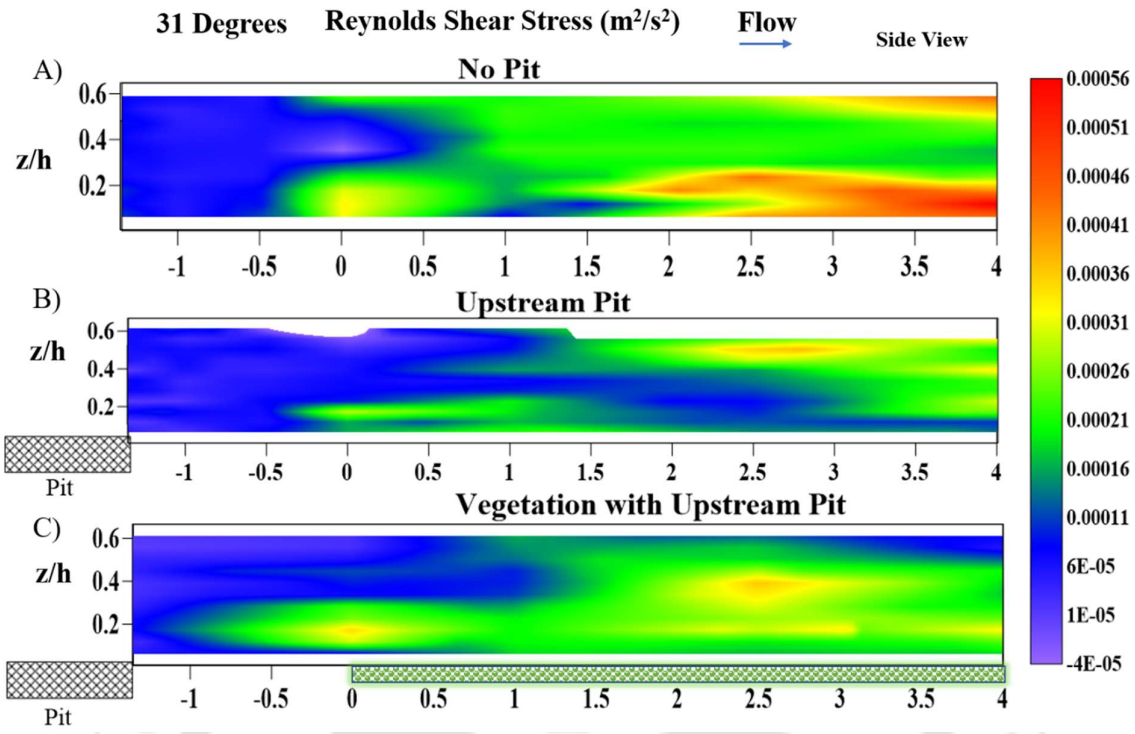

Figure 5.3: Reynolds Shear Stress (m^2/s^2) profiles along the length of flow for the cases of A) No Pit, No Vegetation; B) U/s Pit, No Vegetation; C) U/s Pit, Vegetation for discharge of 0.03 m^3/s

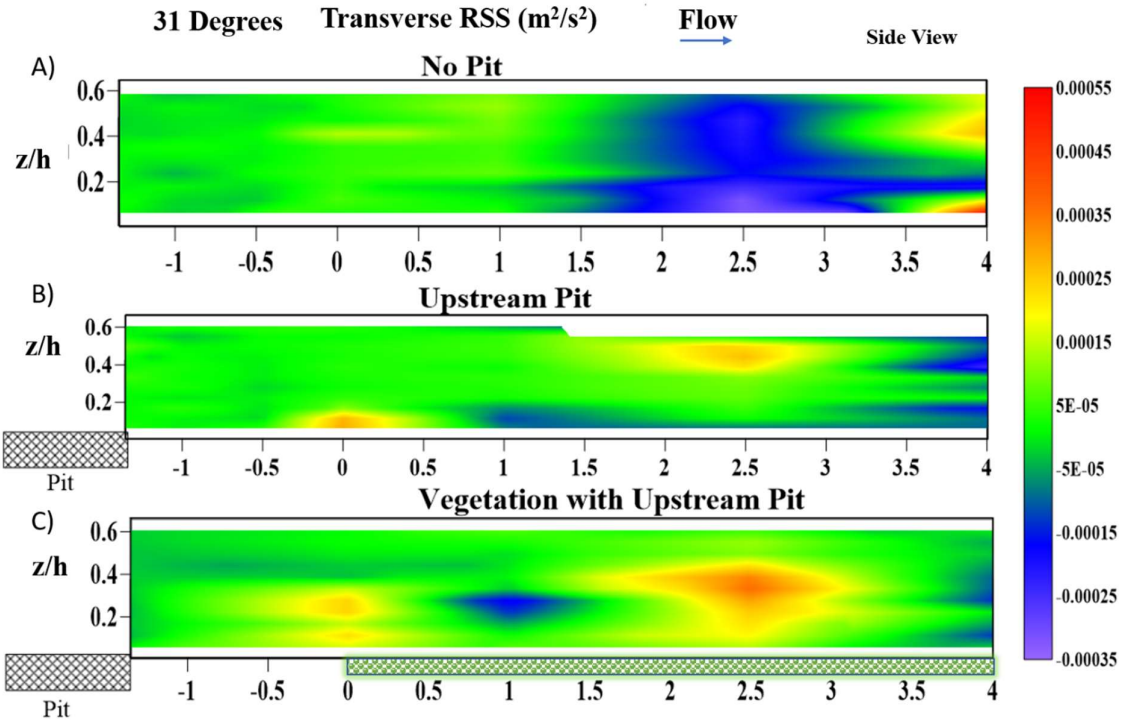

Figure 5.4: Transverse Shear Stress (m^2/s^2) (τ_{Z-Y}) profiles along the length of flow for the cases of A) No Pit, No Vegetation; B) U/s Pit, No Vegetation; C) U/s Pit, Vegetation for discharge of 0.03 m^3/s

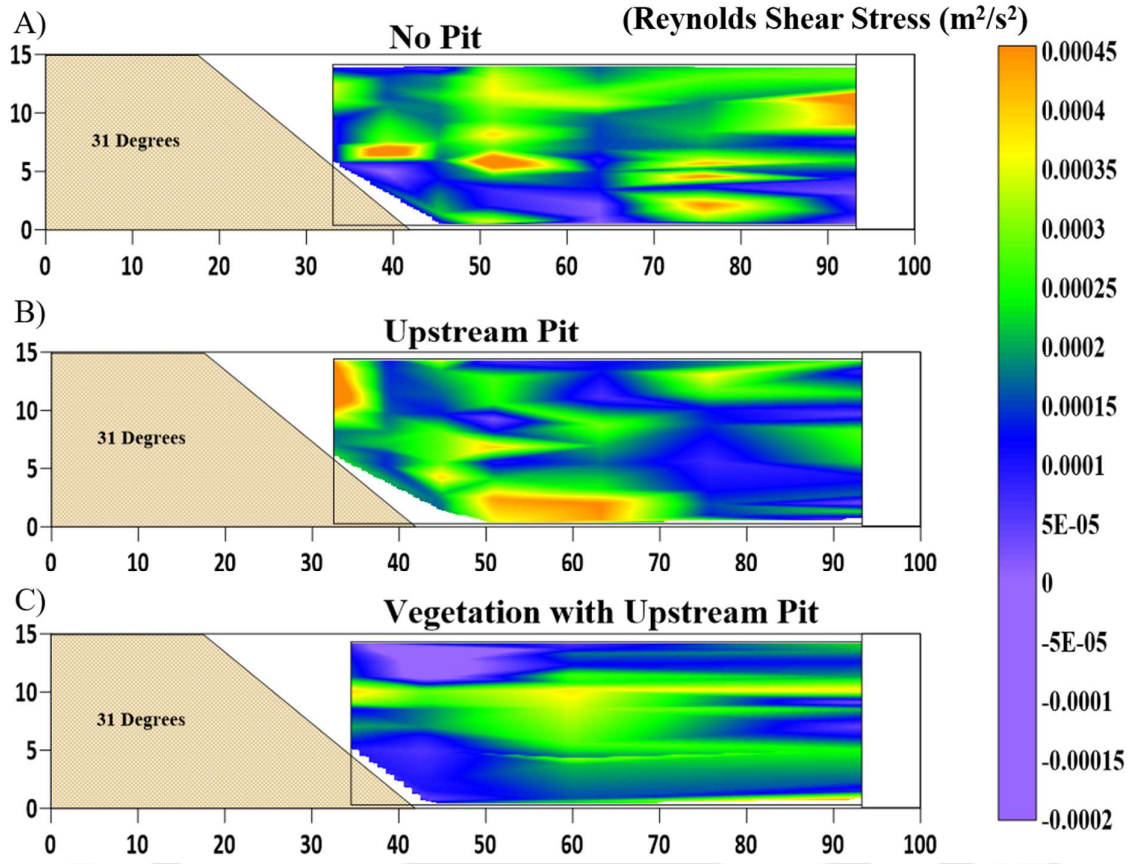

Figure 5.5: Reynolds Shear Stress (m^2/s^2) (τ_{Z-X}) profiles of flow at the cross-section 2.5 m after entrance into the test section for the cases of A) No Pit, No Vegetation; B) U/s Pit, No Vegetation; C) U/s Pit, Vegetation for discharge of 0.03 m^3/s.

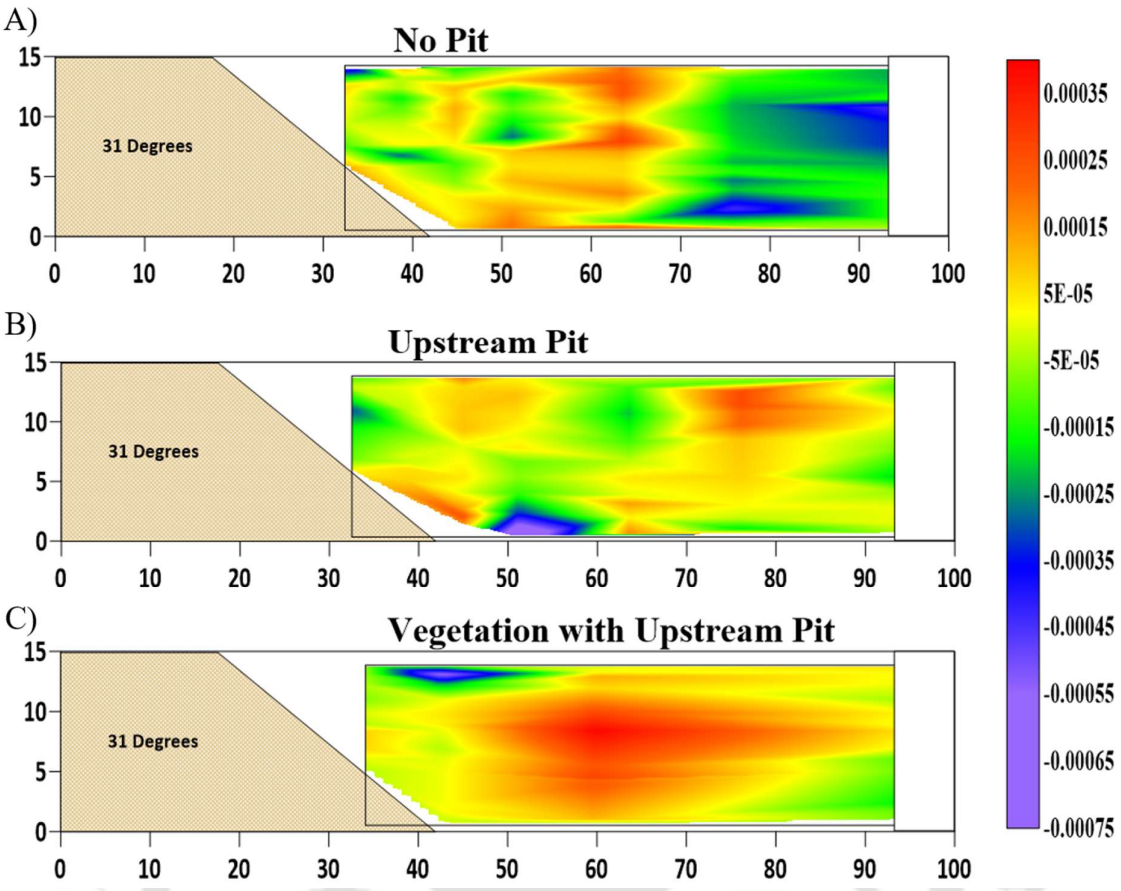

Figure 5.6: Transverse Shear Stress (m^2/s^2) (τ_{Z-Y}) profiles of flow at the cross-section 2.5 m after entrance into the test section for the cases of A) No Pit, No Vegetation; B) U/s Pit, No Vegetation; C) U/s Pit, Vegetation for discharge of 0.03 m^3/s.

5.2.3 Turbulence Intensity Profiles

The turbulence normal stresses applied to the fluid element represent the turbulence intensities in the flow. Figure 5.7 depicts the intensity of the turbulence 2.5 m after entering the test section in the streamwise ($\sigma_u = \overline{u'u'}$), vertical ($\sigma_w = \overline{w'w'}$), and transverse ($\sigma_v = \overline{v'v'}$) directions along the non-dimensional depth (z/h) where u', w' and v' have been obtained from the experimental readings using ADV as elaborated in section 2.2 above. The toe flow region's turbulence intensity provides key details about the secondary flow down the riverbank. In the

toe area of the bank, the extent of turbulence intensities in the transverse (σ_v) and vertical (σ_w) directions are similar to those in the streamwise direction for all cases.

Therefore, secondary flow plays a crucial role in sediment transport and the deposition of the berm that forms in the toe zone. The inner layer of the near-bank flow is where the turbulence intensities are focused in all three scenarios. The pit's impact, however, is more noticeable in the vertical and transverse intensities. The increase in streamwise turbulence intensity in Figure 5.7(c) is due to vegetation at the riverbank. Due to the sandpit, the average surge in σ_v and σ_w was about 15.9% and 20.2%, respectively. In case III, the near-bank turbulence intensities were pacified, whereas the values became consistent in the main channel, which may be due to the flow training to move away from the bank in the main channel.

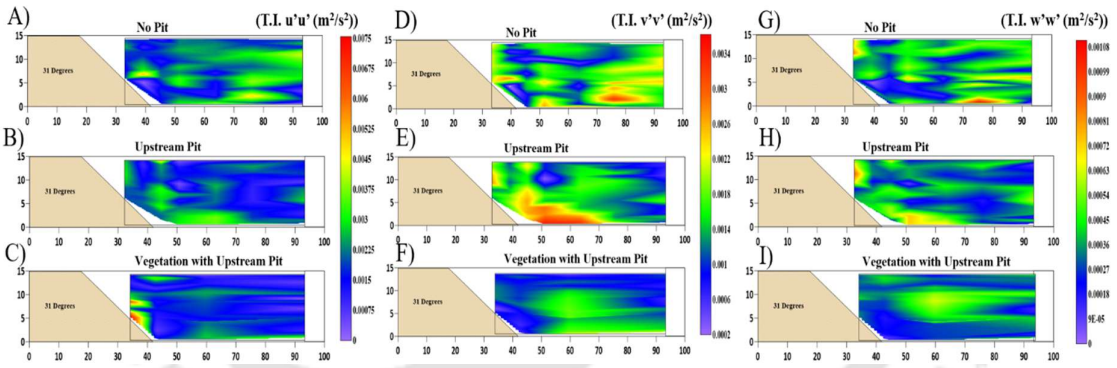

Figure 5.7: Turbulence Intensity (TI) (m^2/s^2) profiles of flow at the cross-section 2.5 m after entrance into the test section (A, D, G) No Pit, No Vegetation case; (B, E, H) U/s Pit, No Vegetation C, F, I) U/s Pit, Vegetation for discharge of 0.03 m^3/s where A-C) streamwise TI; D-F) Transverse TI; G-I) Depthwise TI.

5.2.4 Morphological Changes in Cross-Sectional Profile

Figure 5.8 shows the cross-sections with the riverbank for each test condition after 24 hours of constant flow across them. Three examples were evaluated in this investigation, each with a 31° angle (the same as the angle of repose). For all cases, the starting top width was 0.18 m. The point gauge readings have been plotted at four cross-sections of the test section. The entire

bank's top was eroded within 24 hours of the experimental run. The entrance of the test section (Figure 5.8) has been affected the most due to its proximity to the upstream pit. The pit has caused increased erosion of the berm for width $0.3m < y < 0.55m$. Additional Reynolds shear stresses are imposed on the sediment plane X-Y due to sand pit excavation, which augments downstream streamwise momentum and transverse momentum transport normal to the flow direction. The aggradation of the segment, $0.6m < y < 0.85m$, may be due to the sediment flow from the upstream berm. The segment $0.85m < y < 1m$ shows erosion of case II to be much more than case I. Figure 5.8(B) suggests more significant erosion of the bank due to the sand pit as compared to the case I, while the entire cross-section has almost leveled, which shows greater instability induced by the sediment pit to the downstream section. Figure 5.8(C) supports the results from previous research that the riverbed faces the direct effects of the sandpit, whereas the riverbank has decreased erosion. However, the bank would now face increased unsupported height (Arora et al., 2023b). Figure 5.8(D) shows the aggradation in the entire cross-section for case II as compared to case I, which shows the increased sediment transport rate due to the sediment mining pit. There is not much doubt that channel dredging increases the mobility of riverbank sediments. In all profiles of Figure 5.8, the vegetated section has shown stability even more than the 'no pit' case. The concept of inducing stability by nullifying the effects of sandpit has been overcome much more than expected owing to the vegetated riverbank's combined root action and flow deflection properties. In case III, the downstream section presented in Figure 5.8(C) and (D) has not seen much aggradation because the sediment from the bank has stayed composed due to the vegetation.

While studying the effects of vegetation to negate the instability caused by the sand dredging operation, even the sparse vegetation has proven to be highly effective. This means there is scope for reducing the vegetation density required to balance the effects of sediment mining operations. We propose to decrease the density of the vegetation further as the study aims not

to disrupt the natural balance of the river system but to negate the effects of the anthropogenic activity of sediment mining.

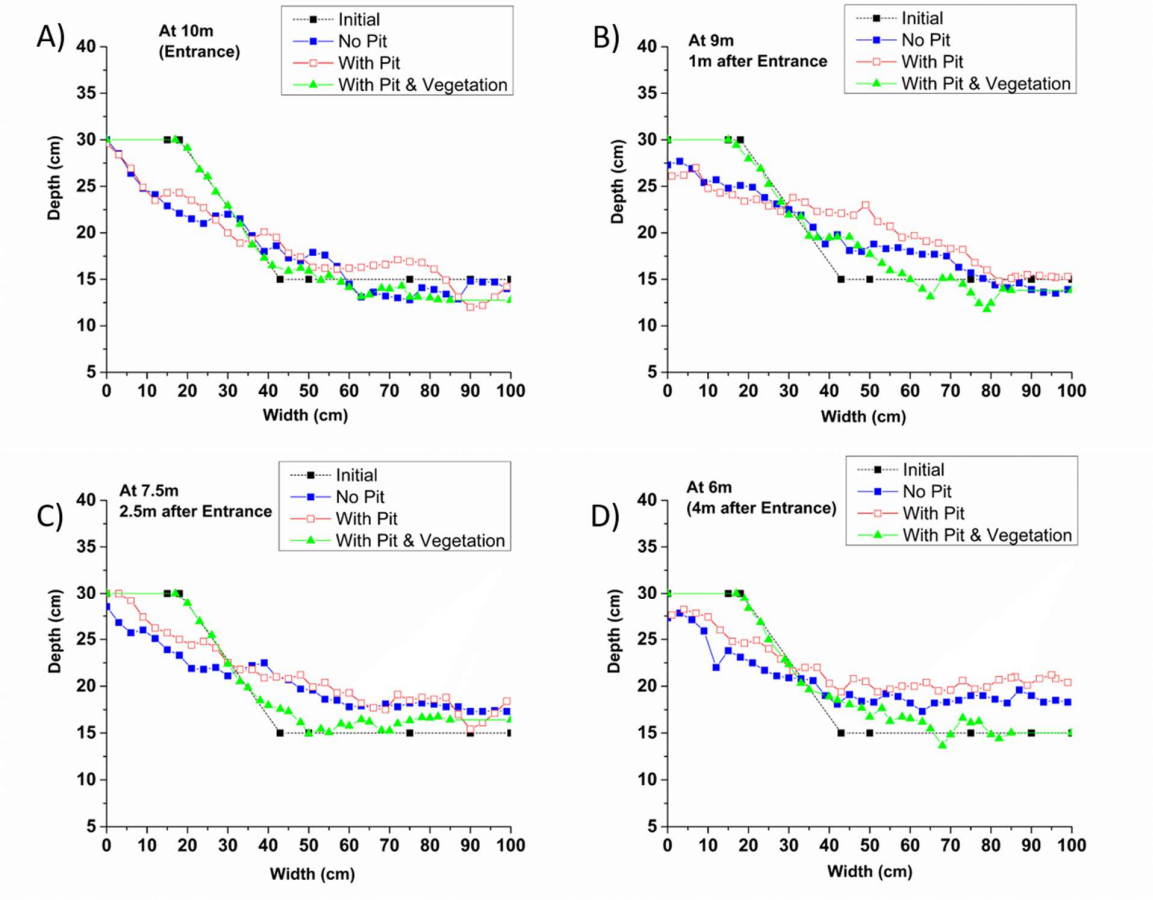

Figure 5.8: Morphology at the cross-section A) Entrance of test section; B) 1 m after entrance; C) 2.5 m after entrance; D) 4 m after entrance into the test section after 24 hours of the experimental run at a flow rate of 0.03 m^3/s. The black dashed line represents the initial cross-section just before the experiments start.

5.3 Effects of Natural, Rigid Stems as a Mitigation Measure to Control Riverbank Erosion Under Dredged Conditions

The flow structure was studied using streamwise velocity variations, Reynolds shear stress (RSS), transverse RSS, and Turbulent Kinetic Energy (TKE). The instantaneous velocity data for the entire flow depth was obtained longitudinally at $Y = 0.7m$ and at the cross-section 2.5 m after entering the test section at points 'A-M' for each test case to comprehend the flow

structure across the whole riverbank test segment. The result profiles exclude a 0.05 m wide zone next to the glass wall to exclude the side-wall impacts. Additionally, morphological changes in the riverbank's cross-section, 2.5 m after the start of the test segment and along the length $Y = 0.7m$ caused by flow, were examined for all four cases. This section presents the test case findings and discusses their effects on the morphological changes of the test segment.

5.3.1 Mean Velocity

According to Reynolds decomposition, the mean ($\overline{u}$, $\overline{v}$, and $\overline{w}$) and its fluctuating velocity components (u', v,' and w') make up the whole of the turbulent velocities streamwise (u), transverse (v), and depthwise (w). Figure 5.9 (A, B) shows the variation of streamwise velocity along the vegetated riverbank's depth at $Y = 0.45m$ and at $Y = 0.7m$, respectively, for no-pit (NPWRV) and upstream-pit (WPWRV) cases. The streamwise velocity seems to be constant for the entire depth in the vegetated zone of the riverbank cross-section ($Y = 0.45m < 0.5m$). The logarithmic law is followed in the unvegetated part of the test section ($Y = 0.7m > 0.5m$). An increase in near-bed streamwise velocity in the unvegetated main channel was observed due to the sandpit, which, in contrast, decreased in the vegetated riverbank zone. This indicates further slowing down of the near-bank flow, which will help mitigate the fluvial erosion of the bank. However, the increased difference in velocity at the interface in the near-bed zone ($z/h < 0.2; Y = 0.5m$) will eventually result in more shear stresses and vortices formation (Li et al., 2022). This increased turbulence at the interface will erode the berm at the riverbank toe. Figure 5.9(C) presents the variation of the streamwise velocity along the cross-section at the intervals of $\Delta Y = 0.03m$ at a fixed depth $z/h = 0.25$. It helps understand the pattern of change in velocity in the vegetated zone ($0m < Y \leq 0.5m$), unvegetated zone ($0.5m < Y < 1m$), and at their interface for both the cases of no-pit and with-pit. It can be inferred that the streamwise velocity in the vegetated zone further decreased for the with-pit case. At the same time, a slight

increase is observed in the main channel, which would help mitigate the fluvial erosion of the riverbank, but at the cost of increased erosion in the main channel (Arora & Kumar, 2024a).

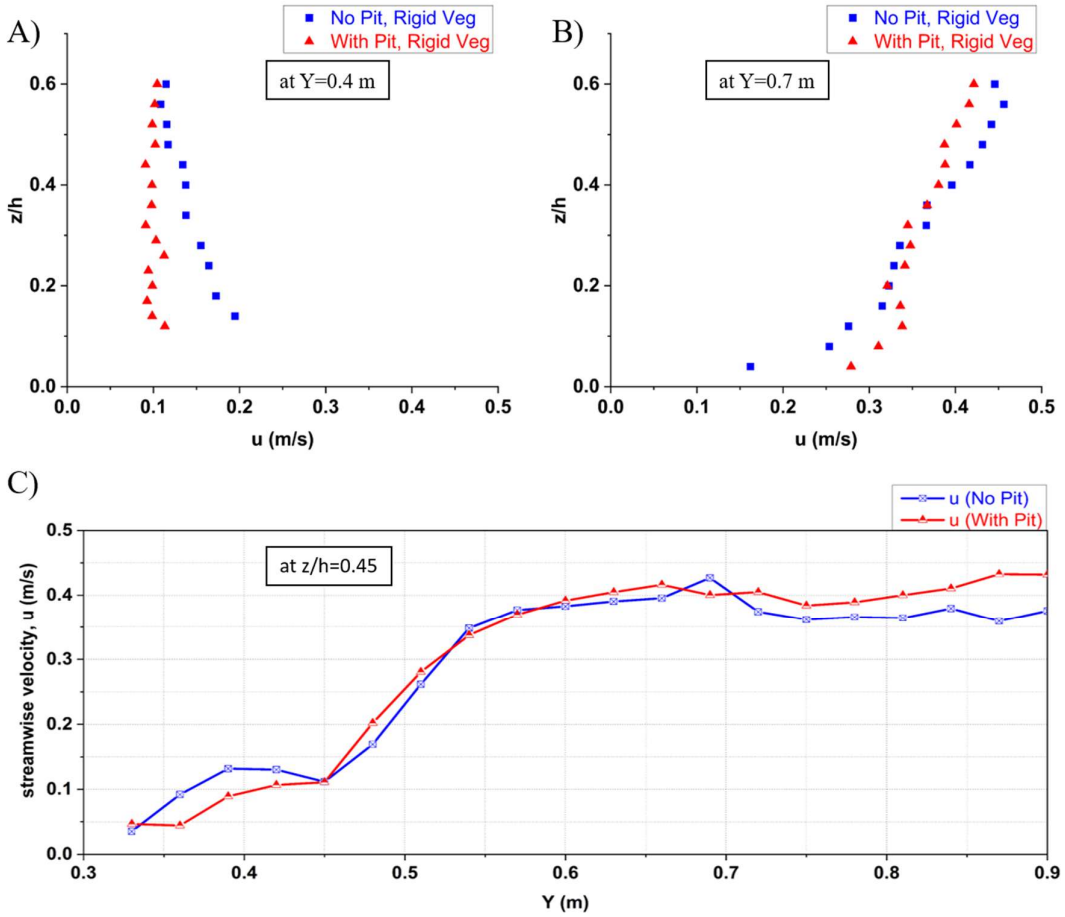

Figure 5.9: Streamwise velocity variation of the cases of NPWRV and WPWRV A) at the location J, Y=0.4 m, within the vegetated segment; B) at the location G, Y=0.7 m, at the center of the main channel; C) across the cross-section, at a depth of z/h=0.45, at a distance of 3 cm apart from each other

Figure 5.10 depicts the contours of the streamwise velocity (m/s) at the cross-section 2.5 m after the entrance of the test segment for all four cases of this study, along with a common color scale for its magnitude. An apparent increase in near-bed streamwise velocity for both no-vegetation (Figure 5.10(A, B)) and with-rigid-vegetation (Figure 5.10(C, D)) due to the sand pit can be observed. Also, the sand pit has caused a reduction in the near-bank streamwise velocity. These changes cause training of flow away from the bank and cause movement of the riverbeds and berms' eroded material downstream. For the ongoing current flow conditions, it

will assist in stopping riverbank erosion, but as prior studies have shown, it will result in a higher unsupported height of the riverbank for the upcoming seasons (Arora et al., 2023a; Arora et al., 2023b). Higher mean streamwise velocity gradients result from sand dredging in the near-bank zone (location K). It suggests that the boundary layer created in the near-bank flow would experience more viscous shear due to the pit (Lade et al., 2021).

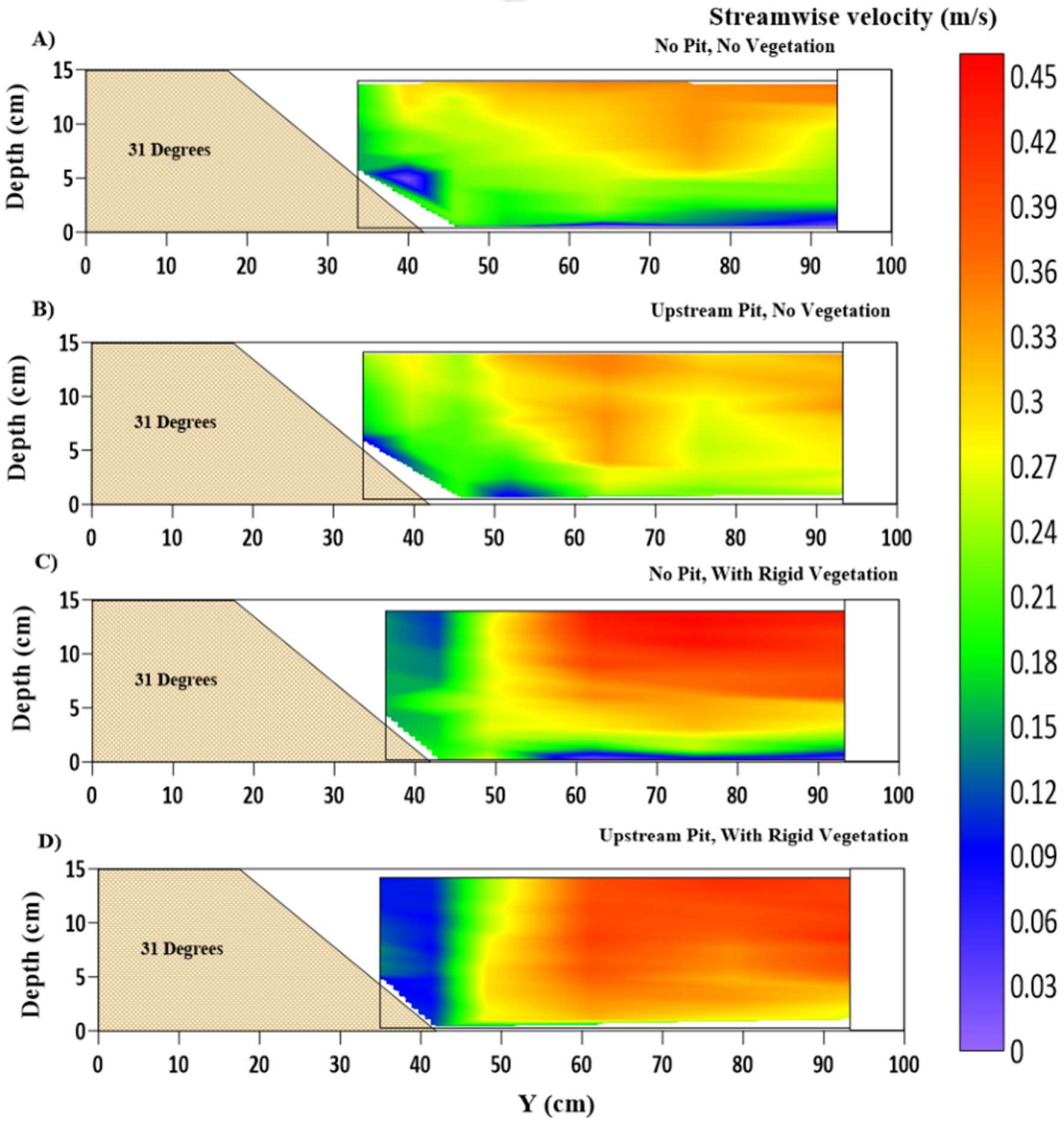

Figure 5.10: Contour of mean streamwise velocity ($\bar{u}$) (m/s) fluctuations at the cross-section located 2.5 m after the beginning of the test section, where A) NPNV; B) WPNV; C) NPWRV; D) WPWRV

Figure 5.11 shows the longitudinal variation of the streamwise velocities versus the normalized flow depth (z/h) in the riverbank, located in the main-channel section at $Y = 0.7m$, with the

inner layer reaching $z/h = 0.1-0.25$. In with-pit settings, the sandpit in the main channel caused bed sediment erosion and a slight rise in water depth. Consequently, mean streamwise velocities in the outer layer ($z/h > 0.2$) decrease in the case of a channel pit. In the region ($z/h < 0.2$), the velocity increases downstream of the sandpit, as shown in Figure 5.11B and 11D. The increase in the near-bed streamwise velocity due to the sandpit is evident in Figure 5.11(A, B). However, this increase in streamwise velocity is more in the cases of vegetated riverbanks as the main channel has to accommodate the flow diverted away from the riverbank by the vegetation. As seen in profile 6C, the vegetation along the riverbank causes an increase in the streamwise velocity as the flow constricts from the rectangular cross-section before the start of the test segment ($-1.35m < X < 0m$). In the case of WPWRV, as seen in profile 11D, riverbank vegetation causes the flow to accelerate in the main channel, while the sandpit causes acceleration in the near-bed region. The WPWRV case in Figure 5.11D ($Y = 0.7m$) has a higher streamwise velocity beyond the entrance of the test section ($X > 0m$) due to the presence of an upstream sediment pit, which causes a slight increase of head when the flow crosses the pit as observed by the previous researchers (Lade et al., 2020, 2021; Barman et al., 2020).

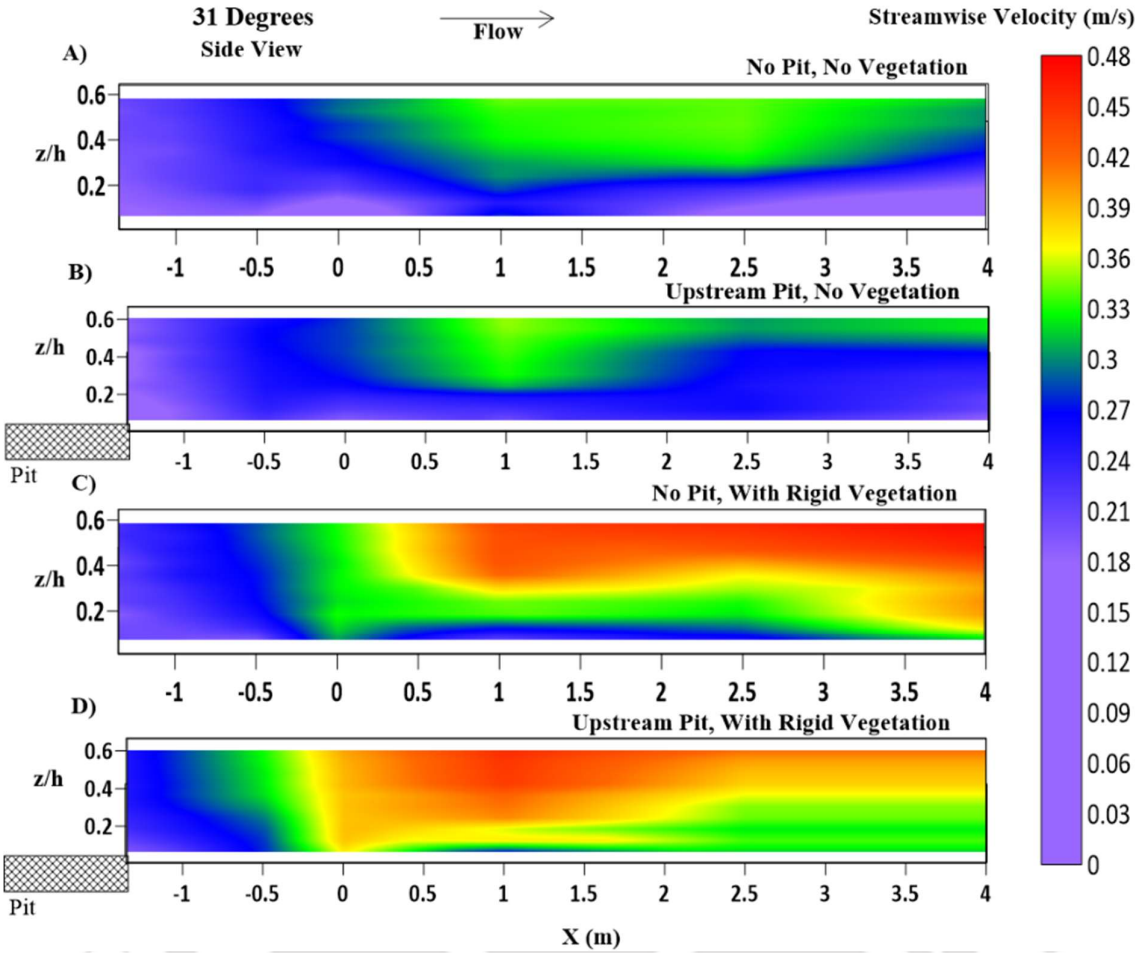

Figure 5.11: Contour of mean streamwise velocity ($\bar{u}$) (m/s) variations, at Y=0.7m, at the center line of the main channel representing A) NPNV; B) WPNV; C) NPWRV; D) WPWRV

5.3.2 Reynolds Shear Stress (RSS)

In every test condition, the flow in the riverbank segment is highly turbulent and rough $R_e > 10,000$. Eulerian measurements of the flow's turbulent velocities are used in this study. It refers to the instantaneous velocity observations taken at the given sections. Flow on the bank slope controls silt movement and fluvial erosion on the slope after the sliding failure. Mass collapse and fluvial erosion are the two leading causes of riverbank failures (Masoodi et al., 2019). The turbulence shear forces acting on the riverbank sediments are essential as they lay on the X-Y plane because these stresses directly influence the movement and deposition of sediments. These two turbulent shear components, operating in streamwise and transverse

directions on the X-Y plane of sediments, are τ_{Z-X} and τ_{Z-Y}, respectively, where $\tau_{Z-X} = -\overline{u'w'}$ and $\tau_{Z-Y} = -\overline{u'v'}$ (m^2/s^2). Here, u' and w' are obtained from the experimental readings using ADV, as mentioned in section 2.2 above. These shear forces give the sediment a push in the streamwise and transverse directions, respectively. This helps the sediment particles to overcome the forces of resistance. If the shear forces are sufficient enough to reach the incipient condition, then the sediment particles start moving. Reynolds stresses contours on the plane X-Y in the streamwise direction in the Cartesian coordinate system are depicted in Figure 5.12 and Figure 5.13, showing cross-sectional and longitudinal variations, respectively. The NPNV case in Figure 5.12A suggests a zone of high shear stresses concentrated in the outer layer zone ($z/h > 0.2$). The near bank RSS causes riverbank erosion, which has flattened the cross-sectional profile, as shown in Figure 5.17. The WPNV case in Figure 5.12B shows the concentration of the high-RSS region in the near bed zone ($z/h < 0.2$), which leads to increased sediment migration. The streamwise RSS at the berm location ($0.4m < Y < 0.6m$) has increased significantly due to the presence of the upstream sandpit, which leads to unstable slopes and increases the unsupported height of the riverbank. The high fluctuations in streamwise RSS in Figure 5.12(C and D) suggest intermixing of the flow moving downwards (positive values) and upwards (negative values), respectively. These fluctuations have become stronger in the WPWRV case than the NPWRV case, leading to higher turbulence in the flow and, eventually, increased riverbed erosion volume, as shown in Figure 5.18(C and D).

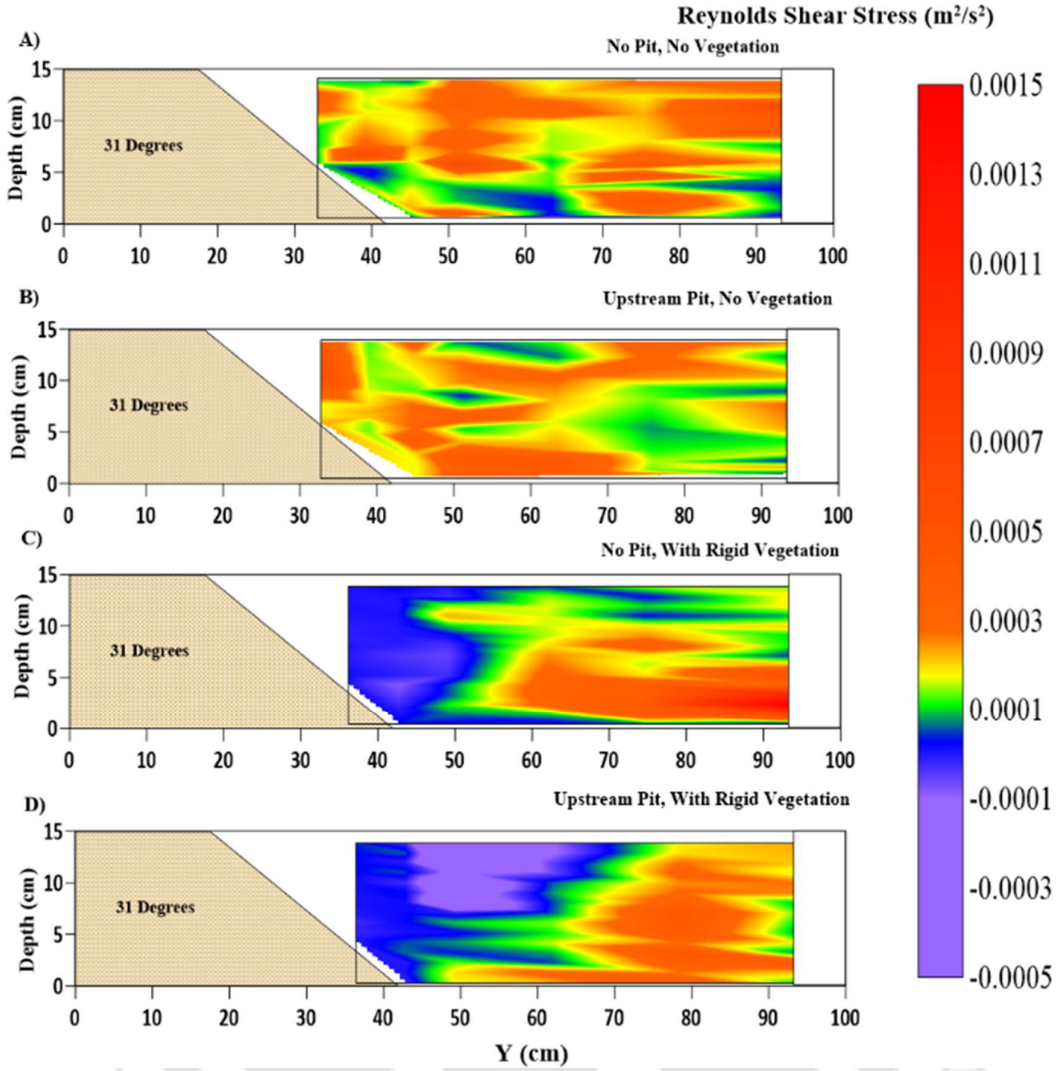

Figure 5.12: Contour of Reynolds shear stress (m2/s2) variations at the location of 2.5 m after the beginning of the test section representing A) NPNV; B) WPNV; C) NPWRV; D) WPWRV

Longitudinal Profiles of RSS at $Y = 0.7m$, in Figure 5.13(A and B) reveal that the pit causes a decrease in streamwise RSS at the center line of the cross-section while it has increased significantly in the near-bank region, as seen in Figure 5.12(A and B). The presence of vegetation in NPWRV and WPWRV cases was observed to have higher streamwise RSS in the main channel as compared to the NPNV and WPNV cases due to the increased flow velocity and its fluctuations in the unvegetated main channel of the test segment. The upstream sediment pit has shown an evident increase in the streamwise RSS, as seen in Figure 5.13D, compared to Figure 5.13C, which assists the sediment transport. The lateral or transverse shear stresses

become an important factor in studying flow characteristics in a vegetated test segment as flow moves away from the riverbank slope in the lateral direction.

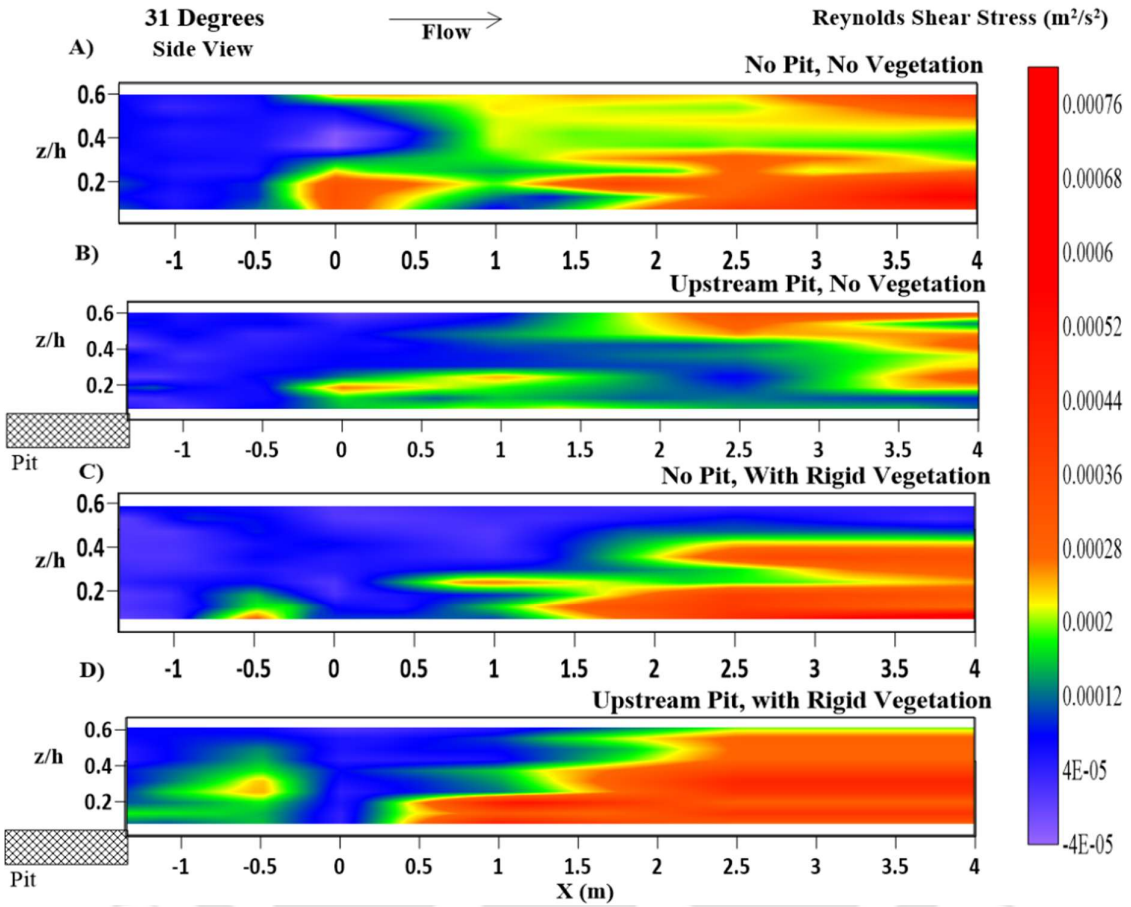

Figure 5.13: Contour of Reynolds shear stress (m2/s2) longitudinal variations, at Y=0.7m, at the center line of the main channel representing A) NPNV; B) WPNV; C) NPWRV; D) WPWRV

5.3.3 Transverse Reynolds Shear Stress (RSS)

The contours of transverse RSS ($\tau_{Z-Y} = -\overline{u'v'}$) across the cross-section are presented in Figure 5.14. The transverse RSS, with fluctuating components of streamwise and transverse velocities, highlights the lateral stresses acting in the cross-section, gives vital details of the flow structure, and helps understand the morphological behavior of the riverbank and riverbed. It should be noted that the transverse RSS and streamwise RSS are similar, which states the importance of studying the transverse RSS in this setup. The highly fluctuating transverse RSS in Figure 5.14 represents the higher inter-mixing of the flow in the cross-section. This destabilizes the cross-

sectional profile of the riverbank and riverbed by causing increased sediment instability and its transport in the lateral direction. Figure 5.14A, positive transverse RSS in $0.35m < Y < 0.7m$ suggests the lateral stresses in the flow in the direction away from the riverbank towards the main channel. The upstream sediment pit in Figure 5.14B has caused a decrease in the transverse RSS as it increases the streamwise RSS, as shown in Figure 5.12B. The rigid vegetation on the riverbank at $Y \leq 0.5m$ causes the formation of vortices by creating a velocity gradient in the vegetated and unvegetated segment, as shown in Figure 4C. The vegetation has led to very high transverse RSS in the zone $Y > 0.6m$, which has adverse effects on the stability of the main channel, as seen in Figure 5.17. Although the sediment pit in the WPWRV case, as shown in Figure 5.17D, has alleviated the transverse stress in the main channel, it has led to a sharp increase of transverse RSS near the riverbank. It may have occurred due to the increased streamwise fluctuations in the flow due to the pit's presence. Therefore, high streamwise and transverse RSS shifts sediment loads and contributes to the degradation of these riverbank slopes' channel banks and main-channel erosion.

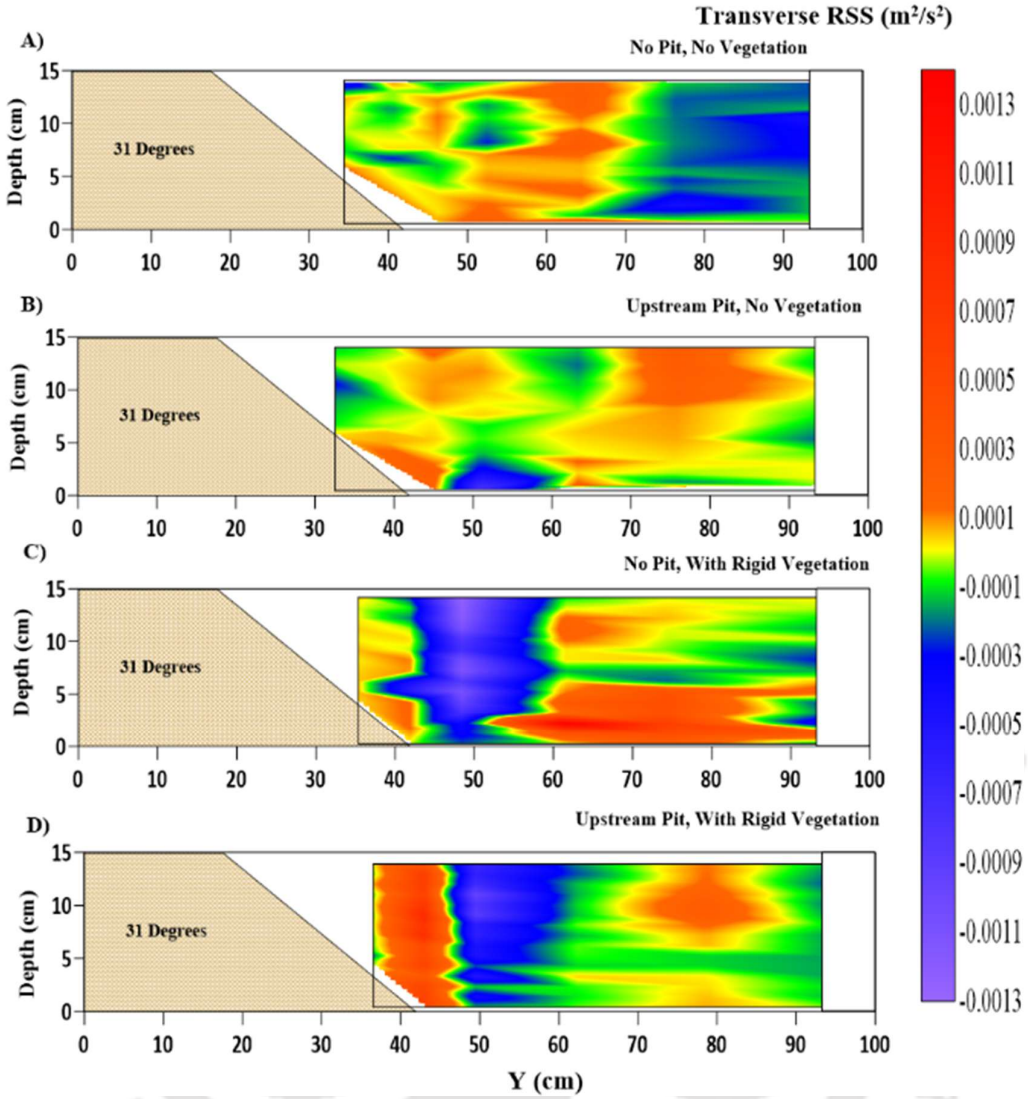

Figure 5.14: Contour of transverse shear stress (m2/s2) variations at the location of 2.5 m after the beginning of the test section representing A) NPNV; B) WPNV; C) NPWRV; D) WPWRV

5.3.4 Turbulent Kinetic Energy (TKE)

The TKE, $k = 0.5 \times (\overline{u'u'} + \overline{v'v'} + \overline{w'w'})$, at the cross-section for all four cases, has been presented in Figure 5.15. The TKE represents the sum of flow intensities in three directions of flow. Increased TKE values shall indicate an increase in the overall turbulence energy of the flow. This indicates an increase in the sediment erosion capacity of the flow. The turbulent kinetic energy is distributed unevenly across the cross-section. However, it is consistent throughout the depth at different cross-section points and with higher turbulence in the main

channel for the NPNV case (Figure 5.15A). The upstream pit has caused an increase in the turbulence at the location of the berm for the WPNV case (Figure 5.15B). It has caused a shift of the high turbulence region towards the near-bed region. It would cause an increase in the erosion of the berm and bed. It would lead to the increased unsupported height of the bank, which supports the results of previous studies (Arora et al., 2023b). Figure 5.15C suggests a sharp increase in turbulence levels at the location of the vegetation interface ($Y = 0.5m$) for the case NPWRV. The higher turbulent kinetic energy near the bed may have occurred due to the increased contribution of the lateral components of TKE. Figure 5.15D shows higher turbulence at the interface and the near-bed region of the main channel for $Y > 0.7m$. The decreased depthwise turbulence at $Y = 0.6m$ may have happened due to the simultaneous occurrence of the vegetated riverbank and the upstream sandpit and resulted in less erosion as seen in Figure 5.17C at $Y = 0.6m$.

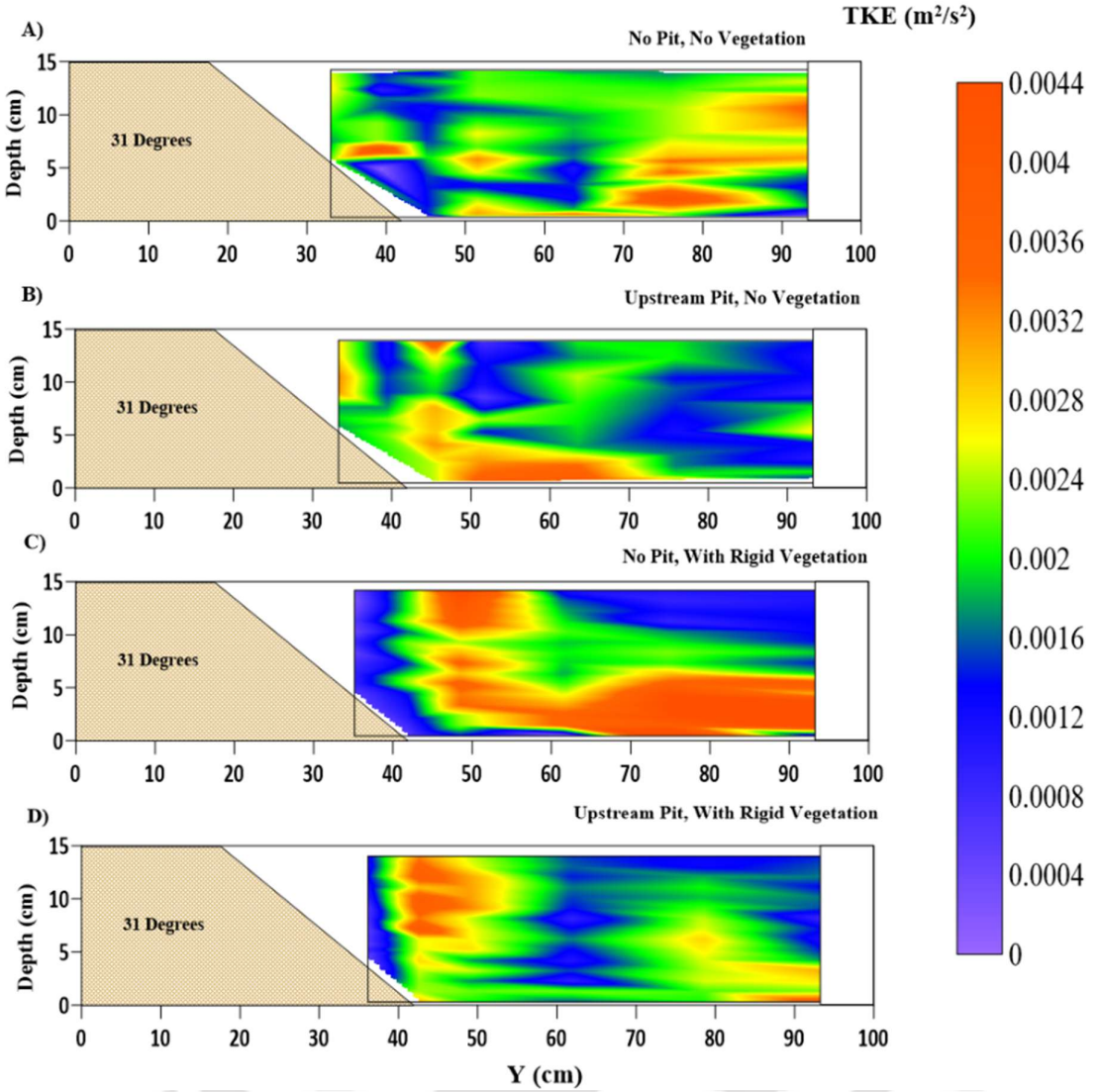

Figure 5.15: Contour of Turbulent Kinetic Energy (TKE) k (m2/s2) variations at the location of 2.5 m after the beginning of the test section representing A) NPNV; B) WPNV; C) NPWRV; D) WPWRV

Figure 5.16 shows the longitudinal variation of the TKE in the main channel at the location $Y = 0.7m$. The NPNV case suggests a higher TKE region in the main channel, which occurs in a natural channel. The shift of TKE levels from low (green) ($-1.35m < X < 0m$) to high (red) ($X > 0m$) in Figure 5.16A is due to the gradual change in the rectangular cross-section to the test section with the riverbank of 31° slope, which has happened due to constriction of the flow. The WPNV case shows low TKE levels throughout as compared to the NPNV case as the high turbulence region towards the berm as the flow interacts with the berm formed at

the toe of the riverbank, causing its erosion, as shown in Figure 5.15C. The NPWRV case (Figure 5.16C) shows an apparent increase of the TKE in the main channel as the flow diverts away from the vegetated riverbank towards the unvegetated segment. The WPWRV case in Figure 5.16D shows a slight increase in turbulent kinetic energy ($-1.35m < X < 0m$) as the flow leaves the sediment pit. The longitudinal trend of TKE suggests high turbulence in the main channel region, which shows a clear shift away from the riverbank region. This leads to the decreased erosion of the riverbank but at the cost of excessive erosion of the main channel, as seen in morphological readings presented in Figure 5.17 and Figure 5.18 in the following sub-section.

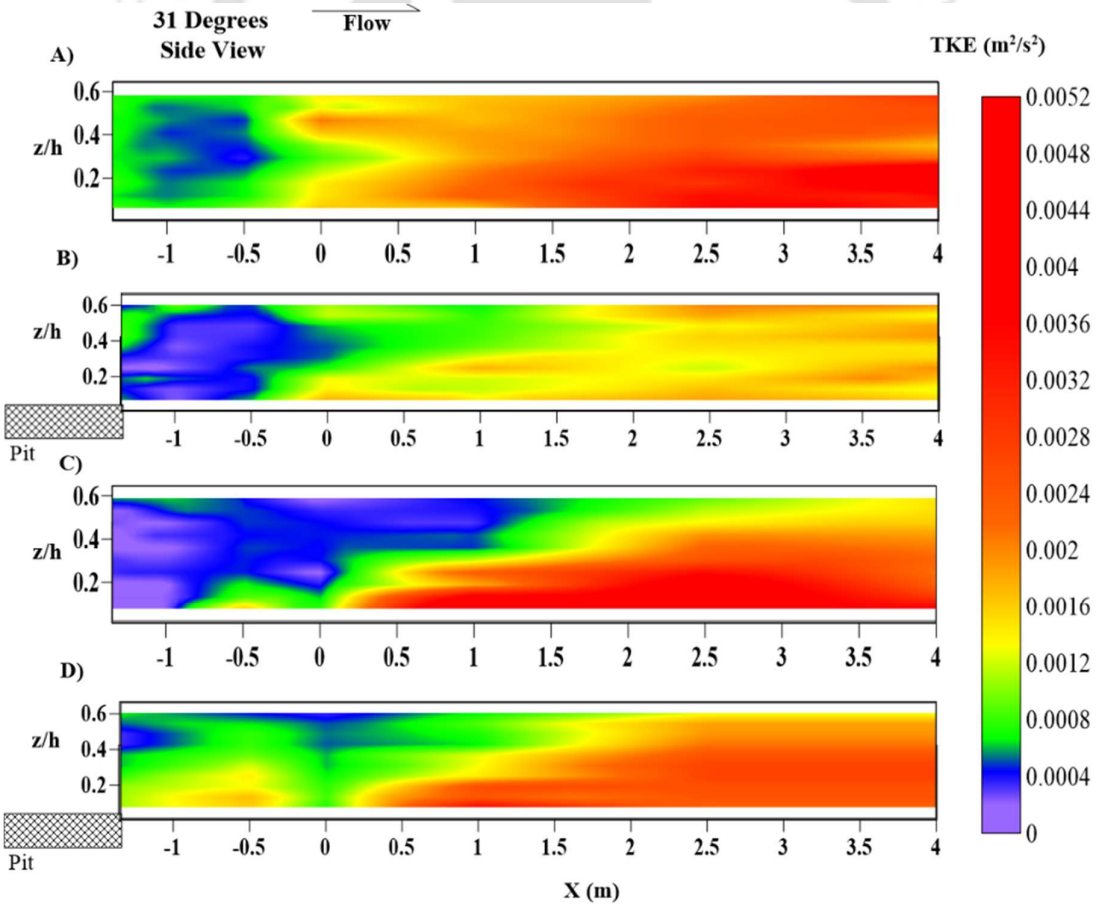

Figure 5.16: Contour of Turbulent Kinetic Energy (TKE) k (m2/s2) longitudinal variations, at Y=0.7m, at the center line of the main channel representing A) NPNV; B) WPNV; C) NPWRV; D) WPWRV

5.3.5 Channel Morphology

Figure 5.17 shows the cross-sections with the riverbank for each test condition after 24 hours of constant flow rate of $Q = 0.03 m^3/s$ through the test section. Four illustrations were evaluated in this investigation, each with a 31° angle (the same as the angle of repose). The point gauge readings have been plotted at four cross-sections of the test section. For all cases, the starting top width of the riverbank was 0.18 m. The entire bank's top was eroded within 24 hours of the experimental run for cases NPNV and WPNV (Figure 5.17). The entrance of the test section (Figure 5.17A) has been affected the most due to its proximity to the upstream pit and the convergence of the flow into the test section. The pit has caused increased berm erosion, as seen in Figure 5.17(A and C). Additional Reynolds shear stresses are imposed on the $X-Y$ sediment plane due to sand excavation, which augments downstream streamwise and transverse sediment transport.

Figure 5.17(A and B) suggests more significant bank erosion in the WPNV case due to the presence of a sand pit compared to the case NPNV (Lade et al., 2020; Arora et al., 2023a). The aggradation of the downstream segment for the cases NPNV and WPNV in Figure 5.17(B, C, and D), $Y > 0.4m$, has occurred due to the sediment transported from the upstream segments by depleting the upstream bank, berm, and bed. The entire cross-section has almost leveled, which shows greater instability induced by the sediment pit to the downstream section. Figure 5.17(C) supports the results from previous research that the riverbed faces the direct effects of the sandpit, whereas the riverbank has decreased erosion. However, the bank would now face increased unsupported height for the upcoming years (Arora et al., 2023(a, b)). This suggests the instability in the selected test section without introducing vegetation on the riverbank.

In all profiles of Figure 5.17, the vegetated sections have shown cross-sectional stability even more than the NPNV case, which is considered here as the reference when anthropogenic

interference, such as sediment mining, has not occurred. The concept of inducing stability by nullifying the adverse effects of sandpit has been overcome more than expected, owing to the vegetated riverbank's flow deflection properties. However, the main channel (unvegetated), $Y > 0.5m$, has seen much higher erosion in cases of NPWRV and WPWRV due to the increased streamwise velocity, RSS, and transverse RSS, as discussed in previous sub-sections. The erosion of more than 67% of the sand bed in the main channel has been observed. The riverbank maintained its profile throughout the test segment, due to which the eroded sediments could not settle in the test segment, which was seen in the cases of NPNV and WPNV. In the case of NPWRV, the downstream section presented in Figure 5.17(C and D), $Y > 0.45m$, has not seen much aggradation because the sediment from the upstream bank and berm has stayed composed due to the vegetation.

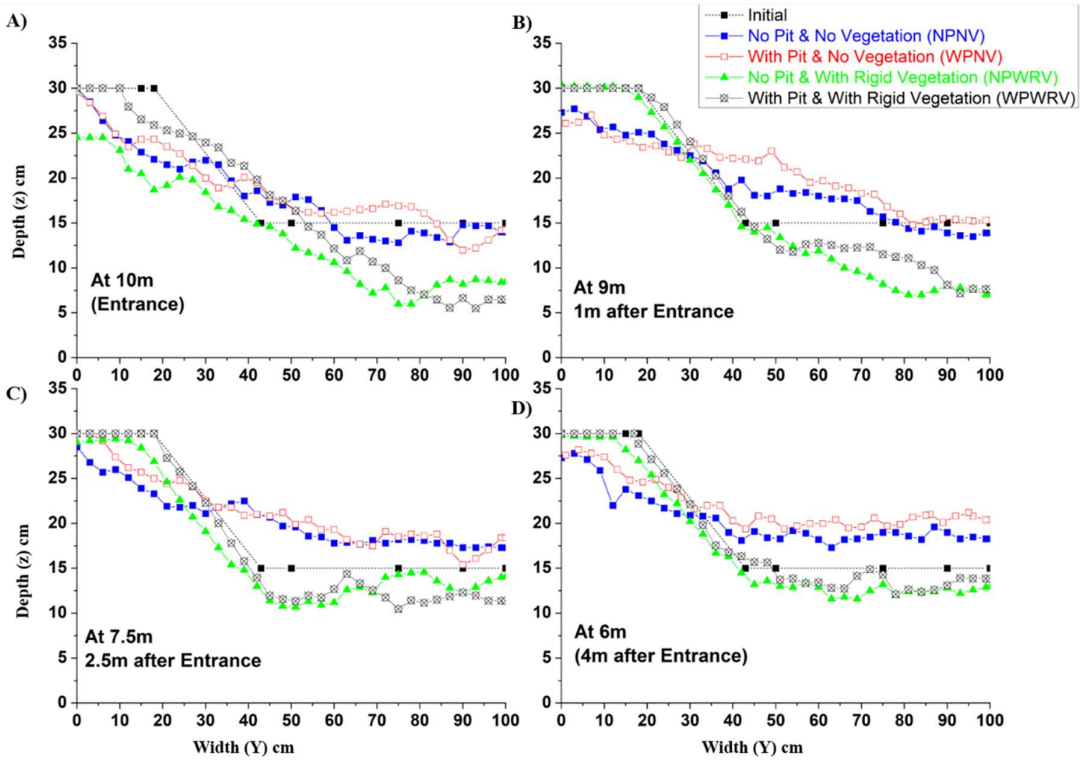

Figure 5.17: Cross-sectional profile after 24 hours experimental run using point gauge for the cases of NPNV, WPNV, NPWRV, and WPWRV at A) entrance; B) 1 m after entrance; C) 2.5 m after entrance; D) 4 m after entrance into the test section along with the given initial profile of the cross-section

Figure 5.18 represents the erosion (in yellow) and aggradation (in red) of the bed profile along the flow length at $Y = 0.7m$ due to the flow action of 24 hours for the initial profile. The test segment lies in $10m < X < 5m$, where the brown dotted texture represents the extent of rigid vegetation on the riverbank. Figure 5.18A for the case NPNV shows slight erosion in the zone, which occurred when the flow entered the test section. The downstream zone $X < 9m$ experiences more aggradation than erosion due to the sediment supply from the eroded riverbank in the test segment. Similar aggradation is observed in the WPNV case, but a slight shift of the sediment pit has been observed, which agrees with the previous research (Barman et al., 2019). Since the riverbank has maintained its profile in the NPWRV and WPWRV cases, the main disruption can be seen in the main channel. Figure 5.18(C and D) represents the center line of the main channel. The erosion from the main channel in the test segment peaks at 0.075 m at the entrance of the test section for both cases. However, the WPWRV case observed higher erosion volume than the NPWRV case in the test segment in $5m < X < 10m$. The observed erosion areas in the test segment at the center line $Y = 0.7m$ for NPWRV and WPWRV were measured to be 0.01565 m^2 and 0.01685 m^2, respectively. The increment of 7.66% in the erosion at the center line of the main channel shows the effects of the upstream sediment pit, which has caused an increase in shear stresses and turbulent kinetic energy of the flow, as discussed in the previous sub-sections. The data suggests that removing sediment from a river can have a significant impact on the riverbed and surrounding banks downstream. Additionally, if vegetation is introduced to combat this issue, it may further impact the main channel. This

highlights the necessity for continued monitoring and regulations by stakeholders including local communities, government agencies, and environmental organizations.

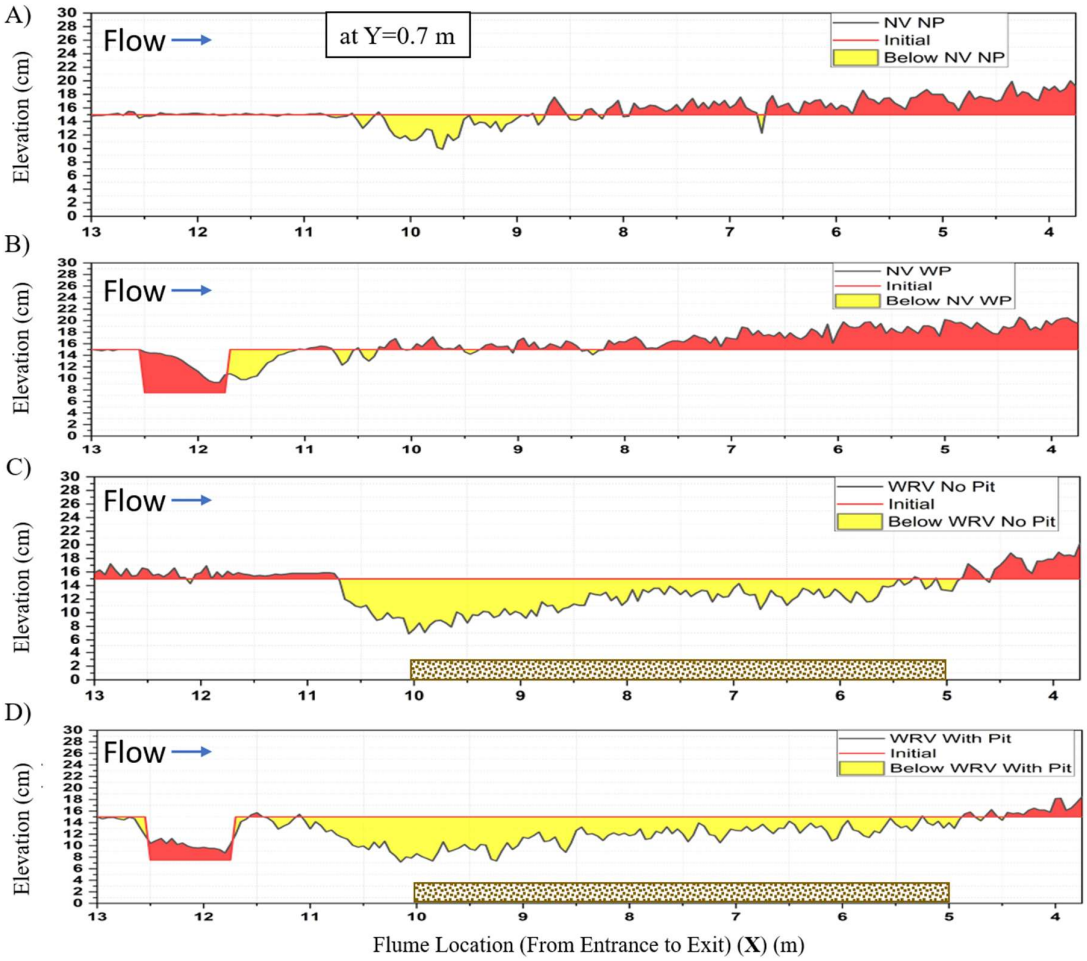

Figure 5.18: Bed elevation profile at Y=0.7 m at the center line of the main channel of cases A) NPNV; B) WPNV; C) NPWRV; and D) WPWRV using point gauge after 24 hours experimental run. The area in yellow represents the erosion, and the area in red represents the aggradation of the bed with respect to the given initial profiles. The brown dotted pattern represents the extent of rigid vegetation in the test segment.

5.4 Conclusions

The flow structure of the four scenarios with nomenclature, no pit & no vegetation (NPNV); with upstream pit & no vegetation (WPNV); no pit & with rigid vegetation (NPWRV); and with upstream pit & with rigid vegetation on the riverbank (WPWRV) were examined. While the vegetation increased the streamwise velocity in the outer layer of the main channel, its combination with the upstream sediment pit influenced the near-bed streamwise velocity

profile by increasing the streamwise velocity, resulting in increased sediment transport. Rigid emergent vegetation positioned equidistant in the riverbank zone reduced the streamwise velocity close to the riverbank. The rigid vegetation caused a slight increase in the head as flow in the vegetated segment tried to overcome the resistance. Increased near-bed streamwise shear stresses, brought forth by the sandpit, have accelerated sediment movement from the upstream test section to the downstream test section.

On the other hand, the vegetation did not change the near-bed shear stress but instead raised the shear stress in the outer layer. However, The combination of sandpit and riverbank vegetation caused high shear stress in the main channel, leading to its instability. Due to the sediment pit, the transverse shear stress increased in the entire cross-section, especially near the bed. It leads to the lateral transport of sediment, which assists in destabilizing the sediment particles and, eventually, reduces stability in the channel cross-section by downstream transport of the bedload with the flow. The rigid vegetation showed sharp changes from positive at the bank, negative at the interface, and positive in the main channel. The changes became even steeper with the combined effect of vegetation and sediment pit, suggesting the instability of the main channel. The upstream sediment pit caused an increase in the TKE in the near bed zone for the case WPNV as compared to the NPNV case. The location of the increased TKE was the same as that of the berm of the riverbank, leading to its erosion and eventual increased unsupported height of the riverbank. This can lead to mass failure in the upcoming season or can cause undercutting before the overhang failure. The vegetation caused an increase in TKE from the interface to the main channel. The turbulent kinetic energy for the cross-section and longitudinal section of the WPWRV case was more than that of the other three cases, which has occurred due to considerable contributions of 3D fluctuations in the flow with combined effects of vegetation and an upstream sediment pit.

The morphology of the NPNV and WPNV showed erosion of the entire bank and further aggradation in the sediment at the riverbed. This led to the approximate leveling of the whole cross-section and increased bed elevation in the downstream part of the test segment for these two cases of no vegetation. This led to the compulsion to introduce riverbank erosion prevention measures like riverbank vegetation. The NPWRV and WPWRV helped the cross-section maintain its profile throughout the test segment, but the diversion of flow away from the bank led to increased erosion of more than 67% of the riverbed in the main channel. However, the overall profile of the downstream cross-sections showed a stable riverbank with slight variation in the riverbed profile of the main channel, which necessarily means that there was not much effect on the conveyance capacity or the thalweg of the channel. The longitudinal profile of the morphological study at the center line of the main channel presented the slight forward movement of the sandpit, which aligns with the previous research. The increased aggradation downstream for the WPNV case compared to the NPNV suggests increased instability due to the sediment pit. The findings pertaining to the morphological alterations resulting from sediment dredging underscore the significance of effective regulation of dredging activities by local authorities. Such measures are essential to mitigate the potential environmental impacts of dredging and ensure sustainable development in affected areas.

The riverbank with the installed dense rigid vegetation faced minimal change, even with an upstream sandpit. The rigid vegetation contributed to the bank's increased stability but at the cost of instability of the riverbed and increased sediment transport in the main channel. Over the long term, the presence of these rigid stems will serve to protect the riverbank from erosion, while concurrently leading to an increase in sediment transport within the main channel. It is anticipated that an equilibrium state will eventually be reached, provided that there is a sustained supply of sediment from upstream. The primary contribution of this study would be to supplement the hypothesis that, as shown in the results section, rigid vegetation would have

protected the riverbank but would have compromised the main channel bed profile due to the enhanced flow rate in the main channel. Conversely, sparsely planted vegetation would have been more beneficial in protecting riverbanks while maintaining the profile of the overall cross-section from the eroding effects of upstream sediment mining pit.

This chapter has provided valuable insights into the potential of nature-based solutions for mitigating the negative effects of sediment mining. An important takeaway from this study is that simply planting vegetation on riverbanks does not offer a sustainable long-term solution to the issue of riverbank failure. The presence of vegetation can have adverse effects on the near-toe region, where the vegetated and unvegetated areas meet, as detailed in the appendix of this thesis. It is important to note, however, that this study is constrained by the width limitations of the experimental setup, which may have restricted our understanding of the combined effects of sediment mining and nature-based solutions.

6. Conclusions and Recommendations

This study has been carried out to understand and quantify the effects of sediment mining pits on riverbank stability. We have understood, through literature, that there have been increasing cases of riverbank failures. We could identify one of the reasons why illegal and indiscriminate sediment mining is practised throughout India and many parts of the world and how it affects riverbank erosion. We then explored the existing guidelines laid out by various agencies in India and all over the world. We found that the guidelines are vague and lack specifications and a complete understanding of the effects of sediment mining on riverbank erosion. Therefore, we conducted more than 90 experiments in the laboratory with at least one repetition for the reliability of the tests. The following conclusions can be drawn from this study that can benefit the readers to get a better understanding of the issue and its possible resolutions using nature-based solutions.

6.1 Effects of Sediment Mining on Riverbank Stability

Experiments were conducted in a laboratory flume to study the riverbank erosion and failure processes in an excavated channel. The hydromorphological response of the riverbank to the upstream sand pit was analysed based on turbulence statistics and quasi-equilibrium riverbank morphologies. The understanding of the process derived from the study is given below.

1. The cohesionless riverbanks subjected to steady zero-pressure gradient flow undergo sliding failure initially, and later, the fluvial erosion was observed progressively. Berm formation occurs at the toe region, which supports the bank's slope. The morphological adjustments cease to continue, and the riverbank section reaches a quasi-equilibrium state.

2. Channel pits upstream have notable effects on riverbank hydromorphology. Sandpits cause amplified turbulent shear in the near-bed flow of the main channel, which is responsible

for erosion bed degradation. The berm, which provides stability at the toe, also undergoes erosion.

3. Sand pit alters the nature of turbulence bursting events across the entire riverbank. Statistics of the fractional contribution of various bursting show that Outward and Inward interaction events have amplified in the inner layer of the main channel flow. The pit also causes greater sweep event RSS generation in the berm area at the toe of the riverbank. However, in this flow region, pit excavation causes stronger ejection events, which may be responsible for sediment mobility and berm erosion at the toe.

4. In the upper flow layer of the riverbank, TKE and turbulence intensities increase, which indicates greater mixing and transport across the flow depth due to the channel pit.

5. On the sloping portion, the turbulent shear and normal stresses decrease due to the pit. Hence, lesser bank sediments from the slope are derived in the channel due to pit excavation.

Based on the above conclusions, it becomes important to consider the impact of channel dredging activities in the context of riverbank stability and erosion. The fluvial erosion characteristics of the riverbank due to the channel pit is a complex dynamic process, and fluvial elements such as seepage, vegetation characteristics, etc., may become significant. These factors are not considered in this study, but they are important avenues for future research.

6.2 Effects of the Proximity and size of the Mining Pit on the Riverbank Stability

We found that the pit at a closer distance created havoc by eroding 15% of the riverbed and the berm. However, the far pit had caused aggradation at the cross-section. This was because the eroded particle would settle in the downstream. So, it was clear to us that it is not merely erosion everywhere. It is the instability or increased sediment transport in the channel due to mining. The following conclusions can be drawn based on these experiments.

• The upstream small pit (USP 31) showed deposition compared to the no-pit case (NP 31) at the location 4 m after its downstream end.

• This has occurred due to the erosion of the zone -1.5 m < X < 2.5 m, which has transported downstream due to fluvial action.

• The cross-section with an instream small pit (INS 31) showed erosion of 2 cm (13.33%) of the channel bed.

• Although the average streamwise velocity remains the same, the re-orientation of the high-velocity region is stronger close to the pit.

• TKE suggests that the affected depth increased from z/H<0.2 to z/H<0.3 as the pit moved close.

• The average streamwise velocity in the near-bed region (z/H<0.2) showed a slight increase of 5% and 4% for the cases of small upstream pit (SP 31) and large upstream pit (LP 31) compared to no-pit (NP 31), respectively.

• The increase in near-bed average RSS was 24% and 80% for the SP 31 and LP 31 cases, respectively, upon increasing the mining volume by 2.34 times.

• The erosion area was 15.1 cm2 for the SP 31 case as compared to the NP 31 case. The erosion area increased by 4 times (60.8 cm2) upon increasing the mining volume by 2.34 times

6.3 Nature-Based Solutions to Mitigate Riverbank Erosion

The flow structure of the four scenarios with nomenclature, no pit & no vegetation (NPNV); with upstream pit & no vegetation (WPNV); no pit & with rigid vegetation (NPWRV); and with upstream pit & with rigid vegetation on the riverbank (WPWRV) were examined. While the vegetation increased the streamwise velocity in the outer layer of the main channel, its combination with the upstream sediment pit influenced the near-bed streamwise velocity

profile by increasing the streamwise velocity, resulting in increased sediment transport. Rigid emergent vegetation positioned equidistant in the riverbank zone reduced the streamwise velocity close to the riverbank. The rigid vegetation caused a slight increase in the head as flow in the vegetated segment tried to overcome the resistance. Increased near-bed streamwise shear stresses, brought forth by the sandpit, have accelerated sediment movement from the upstream test section to the downstream test section.

On the other hand, the vegetation did not change the near-bed shear stress but instead raised the shear stress in the outer layer. However, The combination of sandpit and riverbank vegetation caused high shear stress in the main channel, leading to its instability. Due to the sediment pit, the transverse shear stress increased in the entire cross-section, especially near the bed. It leads to the lateral transport of sediment, which assists in destabilizing the sediment particles and, eventually, reduces stability in the channel cross-section by downstream transport of the bedload with the flow. The rigid vegetation showed sharp changes from positive at the bank, negative at the interface, and positive in the main channel. The changes became even steeper with the combined effect of vegetation and sediment pit, suggesting the instability of the main channel. The upstream sediment pit caused an increase in the TKE in the near bed zone for the case WPNV as compared to the NPNV case. The location of the increased TKE was the same as that of the berm of the riverbank, leading to its erosion and eventual increased unsupported height of the riverbank. This can lead to mass failure in the upcoming season or can cause undercutting before the overhang failure. The vegetation caused an increase in TKE from the interface to the main channel. The turbulent kinetic energy for the cross-section and longitudinal section of the WPWRV case was more than that of the other three cases, which has occurred due to considerable contributions of 3D fluctuations in the flow with combined effects of vegetation and an upstream sediment pit.

The morphology of the NPNV and WPNV showed erosion of the entire bank and further aggradation in the sediment at the riverbed. This led to the approximate leveling of the whole cross-section and increased bed elevation in the downstream part of the test segment for these two cases of no vegetation. This led to the compulsion to introduce riverbank erosion prevention measures like riverbank vegetation. The NPWRV and WPWRV helped the cross-section maintain its profile throughout the test segment, but the diversion of flow away from the bank led to increased erosion of more than 67% of the riverbed in the main channel. However, the overall profile of the downstream cross-sections showed a stable riverbank with slight variation in the riverbed profile of the main channel, which necessarily means that there was not much effect on the conveyance capacity or the thalweg of the channel. The longitudinal profile of the morphological study at the center line of the main channel presented the slight forward movement of the sandpit, which aligns with the previous research. The increased aggradation downstream for the WPNV case compared to the NPNV suggests increased instability due to the sediment pit. The findings pertaining to the morphological alterations resulting from sediment dredging underscore the significance of effective regulation of dredging activities by local authorities. Such measures are essential to mitigate the potential environmental impacts of dredging and ensure sustainable development in affected areas.

The riverbank with the installed dense rigid vegetation faced minimal change, even with an upstream sandpit. The rigid vegetation contributed to the bank's increased stability but at the cost of instability of the riverbed and increased sediment transport in the main channel. Over the long term, the presence of these rigid stems will serve to protect the riverbank from erosion, while concurrently leading to an increase in sediment transport within the main channel. It is anticipated that an equilibrium state will eventually be reached, provided that there is a sustained supply of sediment from upstream. The primary contribution of this study would be to supplement the hypothesis that, as shown in the results section, rigid vegetation would have

protected the riverbank but would have compromised the main channel bed profile due to the enhanced flow rate in the main channel. Conversely, sparsely planted vegetation would have been more beneficial in protecting riverbanks while maintaining the profile of the overall cross-section from the eroding effects of upstream sediment mining pit.

6.4 Future Work and Recommendations

The following recommendations can be drawn from this study:

- If there is a limited budget, use it to change the riverbank slope to its angle of repose.
- The sediment mining should be limited to outside the rivers, at the barrages/dams/sediment bypass tunnels.
- Preventive measures such as riverbank vegetation should be installed till beyond the toe of the riverbank.
- Although dense riverbank vegetation seems to be an easy solution to riverbank erosion, keeping the density low will prevent excessive damage to the riverbed near the riverbank.
- Flexible riverbank vegetation would perform better in protecting the river cross-section.
- Rigid riverbank vegetation (artificial or natural) can be installed as an emergency measure for forecasted floods.
- Sandpits can be used as sediment traps at international borders, which has no international law regarding mining potential.

Future Scope:

- The rate of replenishment of mining pits allows time for replenishment after mining in that area.
- Study of the Extent of protection measures beyond the toe of the riverbank.

- Usage of submerged vegetation as the riverbank protection measure under dredged conditions.
- Study the effects of water depth variation on the riverbank stability to understand the effects of sudden drawdown under dredged conditions.
- A similar study including a suspended load and pulsating supply of external sediment.

Bibliography

Aberle, J., & Smart, G. M. (2003). The influence of bed material roughness on the turbulence structure of flow over gravel beds. *Water Resources Research*, *39*(6), 1137. https://doi.org/10.1029/2001WR001072

Anjum, N., & Tanaka, N. (2020). Hydrodynamics of longitudinally discontinuous, vertically double layered and partially covered rigid vegetation patches in open channel flow. *River Research and Applications*, *36*(1), 115–127. https://doi.org/10.1002/rra.3546

Arafat, Y., Saleh Pallu, M., Maricar, F., & Lopa, R. T. (2015). Morphology evolution of lower Jeneberang River, Indonesia. *International Journal of Earth Sciences and Engineering*, *8*(5), 2011–2016.

Arai, R., Ota, K., Sato, T., & Toyoda, Y. (2018). Experimental investigation on cohesionless sandy bank failure resulting from water level rising. *International Journal of Sediment Research*, *33*(1), 47–56. https://doi.org/10.1016/j.ijsrc.2017.08.002

Arora, S., & Kumar, B. (2024a). Effect of emergent vegetation on riverbank erosion with sediment mining. *Scientific Reports*, *14*(1), 1–17. https://doi.org/10.1038/s41598-024-61315-9

Arora, S., & Kumar, B. (2024b). The riverbank vegetation for mitigating the adverse effects of sediment dredging. *Ecohydrology*, *17*(5). https://doi.org/10.1002/eco.2656

Arora, S., Lade, A. D., & Kumar, B. (2023). Higher-order turbulence statistics and multiscale characterization of morphodynamics in a riverbank section with an upstream mining pit. *Physics of Fluids*, *35*(6), 66607. https://doi.org/10.1063/5.0159014

Arora, S., Patel, H. K., Lade, A. D., & Kumar, B. (2023). Turbulence structure and bank erosion process in a dredged channel. *River Research and Applications*, *December 2022*, 1–16. https://doi.org/10.1002/rra.4100

Arora, S., Patel, H. K., Srinivasulu, G., & Kumar, B. (2023). Turbulent Characteristics at Interface of Partly Vegetated Alluvial Channel. *International Journal of Civil Engineering*, *0123456789*. https://doi.org/10.1007/s40999-023-00890-w

Aung, H. H., Onorati, B., Oliveto, G., & Yu, G. (2023). Riverbed Morphologies Induced by Local Scour Processes at Single Spur Dike and Spur Dikes in Cascade. *Water (Switzerland)*, *15*(9). https://doi.org/10.3390/w15091746

Banerjee, S., Ertunc, O., & Durst, F. (2008). Anisotropy Properties of Turbulence. In *13th WSEAS International Conference on Applied Mathematics*.

Banerjee, S., Krahl, R., Durst, F., & Zenger, C. (2007). Presentation of anisotropy properties of turbulence, invariants versus eigenvalue approaches. *Journal of Turbulence*, *8*, 1–27. https://doi.org/10.1080/14685240701506896

Bariteau, L., Bouchard, D., Gagnon, G., Levasseur, M., Lapointe, S., & Bérubé, M. (2013). A riverbank erosion control method with environmental value. *Ecological Engineering*, *58*, 384–392. https://doi.org/10.1016/j.ecoleng.2013.06.004

Barman, B., Barman, J., & Kumar, B. (2022). Fractal dimensions of hydraulic parameters in sand mined alluvial channel. *Water Supply*, *22*(6), 6143–6156. https://doi.org/10.2166/ws.2022.204

Barman, B., & Kumar, B. (2023). Quantification of turbulent flow anisotropy in an alluvial channel mining pit. *Marine Georesources and Geotechnology*, *41*(2), 211–220.

https://doi.org/10.1080/1064119X.2022.2025504

Barman, B., Kumar, B., & Sarma, A. K. (2018). Turbulent flow structures and geomorphic characteristics of a mining affected alluvial channel. *Earth Surface Processes and Landforms*, *43*(9), 1811–1824. https://doi.org/10.1002/esp.4355

Barman, B., Kumar, B., & Sarma, A. K. (2019a). Dynamic characterization of the migration of a mining pit in an alluvial channel. *International Journal of Sediment Research*, *34*(2), 155–165. https://doi.org/10.1016/j.ijsrc.2018.10.009

Barman, B., Kumar, B., & Sarma, A. K. (2019b). Impact of sand mining on alluvial channel flow characteristics. *Ecological Engineering*, *135*(November 2018), 36–44. https://doi.org/10.1016/j.ecoleng.2019.05.013

Barman, B., Sarma, A. K., & Kumar, B. (2020). Mining pit migration of an alluvial channel: experimental and numerical investigations. *ISH Journal of Hydraulic Engineering*, *26*(4), 448–456. https://doi.org/10.1080/09715010.2018.1501775

Barman, B., Sharma, A., Kumar, B., & Sarma, A. K. (2017). Multiscale characterization of migrating sand wave in mining induced alluvial channel. *Ecological Engineering*, *102*, 199–206. https://doi.org/10.1016/j.ecoleng.2017.02.021

Barman, J., & Kumar, B. (2022a). Flow behaviour in a multi-layered vegetated floodplain region of a compound channel. *Ecohydrology*, *15*(4), 1–17. https://doi.org/10.1002/eco.2427

Barman, J., & Kumar, B. (2022b). Turbulence in a compound channel with the combination of submerged and emergent vegetation. *Physics of Fluids*, *34*(4). https://doi.org/10.1063/5.0086739

Batalla, R. J., & Vericat, D. (2009). Hydrological and sediment transport dynamics of flushing flows: Implications for river management in regulated rivers. *River Research and Applications*, *25*(4), 297–314. https://doi.org/10.1002/rra.1233

Bebina Devi, T., Sharma, A., & Kumar, B. (2019). Flow characteristics in a partly vegetated channel with emergent vegetation and seepage. *Ecohydrology and Hydrobiology*, *19*(1), 93–108. https://doi.org/10.1016/j.ecohyd.2018.07.006

Ben Meftah, M., De Serio, F., Malcangio, D., & Mossa, M. (2016). Resistance and boundary shear in a partly obstructed channel flow. *River Flow - Proceedings of the International Conference on Fluvial Hydraulics, RIVER FLOW 2016*, *September*, 795–801. https://doi.org/10.1201/9781315644479-126

Bendixen, M., Best, J., Hackney, C., & Iversen, L. L. (2019). Time is running out for sand. *Nature*, *571*(7763), 29–31. https://doi.org/10.1038/d41586-019-02042-4

Benedet, L., Finkl, C. W., & Dobrochinski, J. P. H. (2013). Optimization of nearshore dredge pit design to reduce impacts on adjacent Beaches. *Journal of Coastal Research*, *29*(3), 519–525. https://doi.org/10.2112/JCOASTRES-D-12-00126.1

Benedet, L., & List, J. H. (2008). Evaluation of the physical process controlling beach changes adjacent to nearshore dredge pits. *Coastal Engineering*, *55*(12), 1224–1236. https://doi.org/10.1016/j.coastaleng.2008.06.008

Bhattacharya, R., Dolui, G., & Das Chatterjee, N. (2019). Effect of instream sand mining on hydraulic variables of bedload transport and channel planform: an alluvial stream in South Bengal basin, India. *Environmental Earth Sciences*, *78*(10), 1–24. https://doi.org/10.1007/s12665-019-8267-3

Blanckaert, K., & de Vriend, H. J. (2004). Secondary flow in sharp open-channel bends.

Journal of Fluid Mechanics, *498*, 353–380. https://doi.org/10.1017/S0022112003006979

Blanckaert, K., & Graf, W. H. (2004). Momentum Transport in Sharp Open-Channel Bends. *Journal of Hydraulic Engineering*, *130*(3), 186–198. https://doi.org/10.1061/(asce)0733-9429(2004)130:3(186)

Bravard, J.-P., Goichot, M., & Gaillot, S. (2013). Geography of sand and gravel mining in the Lower Mekong River. First survey and impact assessment. *EchoGéo*, *26*.

Briggs, M. K., González, E., Osterkamp, W. R., Shafroth, P. B., & Zamora, F. (2021). Stream Corridor Restoration: In *Renewing Our Rivers* (pp. 13–42). University of Arizona Press. https://doi.org/10.2307/j.ctv1b0fv8d.6

Caroppi, G., Gualtieri, P., Fontana, N., & Giugni, M. (2020). Effects of vegetation density on shear layer in partly vegetated channels. *Journal of Hydro-Environment Research*, *30*, 82–90. https://doi.org/https://doi.org/10.1016/j.jher.2020.01.008

Caroppi, G., Västilä, K., Gualtieri, P., Järvelä, J., Giugni, M., & Rowiński, P. M. (2020). Acoustic Doppler velocimetry (ADV) data on flow-vegetation interaction with natural-like and rigid model plants in hydraulic flumes. *Data in Brief*, *32*, 0–8. https://doi.org/10.1016/j.dib.2020.106080

Caroppi, G., Västilä, K., Gualtieri, P., Järvelä, J., Giugni, M., & Rowiński, P. M. (2021). Comparison of Flexible and Rigid Vegetation Induced Shear Layers in Partly Vegetated Channels. *Water Resources Research*, *57*(3). https://doi.org/10.1029/2020WR028243

Caroppi, G., Västilä, K., Järvelä, J., Rowiński, P. M., & Giugni, M. (2019). Turbulence at water-vegetation interface in open channel flow: Experiments with natural-like plants. *Advances in Water Resources*, *127*(February), 180–191. https://doi.org/10.1016/j.advwatres.2019.03.013

Choi, K. S., & Lumley, J. L. (2001). The return to isotropy of homogeneous turbulence. *Journal of Fluid Mechanics*, *436*, 59–84. https://doi.org/10.1017/S002211200100386X

Chu-Agor, M. L., Fox, G. A., Cancienne, R. M., & Wilson, G. V. (2008). Seepage-induced undercutting and instability of layered streambanks. *Hydrological Processes*, *22*(6), 1325–1337. https://doi.org/10.1002/hyp.6680

Ciszewski, D., & Sobucki, M. (2022). River response to mining-induced subsidence. *Catena*, *214*(December 2021), 106303. https://doi.org/10.1016/j.catena.2022.106303

Couper, P. R., & Maddock, I. P. (2001). Subaerial river bank erosion processes and their interaction with other bank erosion mechanisms on the River Arrow, Warwickshire, UK. *Earth Surface Processes and Landforms*, *26*(6), 631–646. https://doi.org/10.1002/esp.212

Couper, P., Stott, T., & Maddock, I. (2002). Insights into river bank erosion processes derived from analysis of negative erosion-pin recordings: Observations from three recent UK studies. *Earth Surface Processes and Landforms*, *27*(1), 59–79. https://doi.org/10.1002/esp.285

Cramer, C. J. (1999). Implicit Solvation Models: Equilibria, Structure, Spectra, and Dynamics - Chemical Reviews (ACS Publications). *Chemical Reviews*.

Daneshfaraz, R., Ghaderi, A., Sattariyan, M., Alinejad, B., Asl, M. M., & Di Francesco, S. (2021). Investigation of local scouring around hydrodynamic and circular pile groups under the influence of river material harvesting pits. *Water (Switzerland)*, *13*(16), 1–19. https://doi.org/10.3390/w13162192

Darby, S. E., Alabyan, A. M., & Belyaev, V. R. (2010). The influence of riparian vegetation on bank stability: Mechanistic processes and models for prediction. *Earth Surface*

Processes and Landforms, *35*(6), 727–743. https://doi.org/10.1002/esp.1911

Debnath, K., Ghosh, S., & Patra, K. C. (2007). Erodibility of cohesive riverbanks: Laboratory investigation and numerical simulation. *Journal of Hydraulic Engineering*, *133*(9), 1010–1018. https://doi.org/10.1061/(ASCE)0733-9429(2007)133:9(1010)

Dehghani, A. A., Azamathulla, H. M., Hashemi Najafi, S. A., & Ayyoubzadeh, S. A. (2013). Local scouring around L-head groynes. *Journal of Hydrology*, *504*, 125–131. https://doi.org/10.1016/j.jhydrol.2013.09.020

Devi, T. B. (2016). *HYDRODYNAMICS OF VEGETATIVE CHANNEL WITH DOWNWARD SEEPAGE A Thesis submitted Doctor of Philosophy Submitted by Declaration of Authorship*. *126104013*.

Devi, T. B., Sharma, A., & Kumar, B. (2017). Studies on emergent flow over vegetative channel bed with downward seepage. *Hydrological Sciences Journal*, *62*(3), 408–420. https://doi.org/10.1080/02626667.2016.1230673

Duan, H., Cao, Z., Shen, M., Liu, D., & Xiao, Q. (2019). Detection of illicit sand mining and the associated environmental effects in China's fourth largest freshwater lake using daytime and nighttime satellite images. *Science of the Total Environment*, *647*, 606–618. https://doi.org/10.1016/j.scitotenv.2018.07.359

Emberson, R. (2017). Accelerating riverbank erosion. *Nature Geoscience*, *10*(5), 328–328. https://doi.org/10.1038/ngeo2948

Fernandes, L. F. S., Pinto, A. A. S., Terêncio, D. P. S., Pacheco, F. A. L., & Cortes, R. M. V. (2020). Combination of ecological engineering procedures applied to morphological stabilization of estuarine banks after dredging. *Water (Switzerland)*, *12*(2), 1–14. https://doi.org/10.3390/w12020391

Florsheim, J. L., Mount, J. F., & Chin, A. (2008). Bank erosion as a desirable attribute of rivers. *BioScience*, *58*(6), 519–529. https://doi.org/10.1641/B580608

Ghani, W., Barman, J., Patel, H. K., Shah, S. R., & Kumar, B. (2022). Flow Characteristics of a Sinuous Channel with Flexible Banks. *International Journal of Civil Engineering*, *21*(3), 479–490. https://doi.org/10.1007/s40999-022-00789-y

Ghazanfari-Hashemi, R. S., Montazeri Namin, M., Ghaeini-Hessaroeyeh, M., & Fadaei-Kermani, E. (2020). A Numerical Study on Three-Dimensionality and Turbulence in Supercritical Bend Flow. *International Journal of Civil Engineering*, *18*(3), 381–391. https://doi.org/10.1007/s40999-019-00471-w

Ghosh, P. K., Bandyopadhyay, S., Jana, N. C., & Mukhopadhyay, R. (2016). Sand quarrying activities in an alluvial reach of Damodar River, Eastern India: towards a geomorphic assessment. *International Journal of River Basin Management*, *14*(4), 477–489. https://doi.org/10.1080/15715124.2016.1209509

Golder, A. K., Chauhan, S., & Ravi, R. (2021). Synthesis of low-cost bentonite/Duranta erecta's fruit powder imbedded alginate beads and its application in surfactant removal. *Environmental Science and Pollution Research*, *28*(42), 58945–58957. https://doi.org/10.1007/s11356-021-14306-6

Grygoruk, M., Fraak, M., & Chmielewski, A. (2015). Agricultural rivers at risk: Dredging results in a loss of macroinvertebrates. preliminary observations from the narew catchment, Poland. *Water (Switzerland)*, *7*(8), 4511–4522. https://doi.org/10.3390/w7084511

Haghnazar, H., & Saneie, M. (2019). Impacts of pit distance and location on river sand mining

management. *Modeling Earth Systems and Environment*, *5*(4), 1463–1472. https://doi.org/10.1007/s40808-019-00627-6

Harrison, M., & Adams, B. J. (2021). Groundwater depletion due to sediment mining impacts: Case studies and analysis. *Hydrogeology Journal*, *29*(4), 865–880. https://doi.org/10.1007/s10040-021-02310-

Heller, V. (2011). Scale effects in physical hydraulic engineering models. *Journal of Hydraulic Research*, *49*(3), 293–306. https://doi.org/10.1080/00221686.2011.578914

Izumi, N., Egashira, S., & Ashida, K. (1991). Experimental study on riverbank protection using hydraulic structures. *Journal of Hydraulic Engineering*, *117*(7), 882–895. https://doi.org/10.1061/(ASCE)0733-9429(1991)117:7(882)

Juez, C., Thalmann, M., Schleiss, A. J., & Franca, M. J. (2018). Morphological resilience to flow fluctuations of fine sediment deposits in bank lateral cavities. *Advances in Water Resources*, *115*, 44–59. https://doi.org/10.1016/j.advwatres.2018.03.004

Jugie, M., Gob, F., Virmoux, C., Brunstein, D., Tamisier, V., Le Coeur, C., & Grancher, D. (2018). Characterizing and quantifying the discontinuous bank erosion of a small low energy river using Structure-from-Motion Photogrammetry and erosion pins. *Journal of Hydrology*, *563*(June), 418–434. https://doi.org/10.1016/j.jhydrol.2018.06.019

Kang, H., & Choi, S. U. (2006). Turbulence modeling of compound open-channel flows with and without vegetation on the floodplain using the Reynolds stress model. *Advances in Water Resources*, *29*(11), 1650–1664. https://doi.org/10.1016/j.advwatres.2005.12.004

Karimi, S., Bonakdari, H., Karami, H., Gholami, A., & Zaji, A. H. (2017). Effects of Width Ratios and Deviation Angles on the Mean Velocity in Inlet Channels Using Numerical Modeling and Artificial Neural Network Modeling. *International Journal of Civil Engineering*, *15*(2), 149–161. https://doi.org/10.1007/s40999-016-0075-5

Khan, M. A., Sharma, N., & Odgaard, J. (2021). Experimental and Numerical Studies of Velocity and Turbulence Intensities for Mid-Channel Bar. *Water Resources*, *48*(5), 746–762. https://doi.org/10.1134/S0097807821050043

Kimiaghalam, N., Goharrokhi, M., Clark, S. P., & Ahmari, H. (2015). A comprehensive fluvial geomorphology study of riverbank erosion on the Red River in Winnipeg, Manitoba, Canada. *Journal of Hydrology*, *529*, 1488–1498. https://doi.org/10.1016/j.jhydrol.2015.08.033

Knight, D. W., & Demetriou, J. D. (1983). Flood Plain and Main Channel Flow Interaction. *Journal of Hydraulic Engineering*, *109*(8), 1073–1092. https://doi.org/10.1061/(asce)0733-9429(1983)109:8(1073)

Knighton, D. (1998). *Fluvial Forms and Processes: A New Perspective*. Routledge. https://doi.org/10.4324/9780203717763

Kondolf, G. M., Schmitt, R. J. P., Carling, P., Darby, S., Arias, M., Bizzi, S., Castelletti, A., Cochrane, T. A., Gibson, S., & Kummu, M. (2018). Changing sediment budget of the Mekong: Cumulative threats and management strategies for a large river basin. *Science of the Total Environment*, *625*, 114–134.

Kramm, M. (2020). When a River Becomes a Person. *Journal of Human Development and Capabilities*, *21*(4), 307–319. https://doi.org/10.1080/19452829.2020.1801610

Kumari, N., Pandey, S., & Kumar, G. (2024). Sand Mining: A Silent Threat to the River Ecosystem. In *Rivers of India: Past, Present and Future* (pp. 109–132). Springer.

Kurien, S., & Sreenivasan, K. R. (2007). Measures of Anisotropy and the Universal Properties

of Turbulence. *New Trends in Turbulence Turbulence: Nouveaux Aspects*, 53–111. https://doi.org/10.1007/3-540-45674-0_2

Kurniawan, M. A., Andriyanto, I., Arismawan, B., Risyad, A., Wibowo, A. M., & Raharjo, S. A. (2020). Estimation of Potential of Iron Sand in The Eastern Coastal Area of Cilacap Regency Based on The Local Magnetic Anomalies Data. *Journal of Physics: Conference Series*, *1494*(1), 12038.

Lade, A. D., Deshpande, V., & Kumar, B. (2020). Study of flow turbulence around a circular bridge pier in sand-mined stream channel. *Proceedings of the Institution of Civil Engineers: Water Management*, *173*(5), 217–237. https://doi.org/10.1680/jwama.19.00041

Lade, A. D., Deshpande, V., Kumar, B., & Oliveto, G. (2019). On the morphodynamic alterations around bridge piers under the influence of instream mining. *Water (Switzerland)*, *11*(8). https://doi.org/10.3390/w11081676

Lade, A. D., & Kumar, B. (2020). Streambed instabilities around a bridge pier in a dredged channel. *River Research and Applications*, *36*(7), 1360–1365. https://doi.org/10.1002/rra.3629

Lade, A. D., Mihailović, A., Mihailović, D. T., & Kumar, B. (2019). Randomness in flow turbulence around a bridge pier in a sand mined channel. *Physica A: Statistical Mechanics and Its Applications*, *535*, 122426. https://doi.org/10.1016/j.physa.2019.122426

Lade, A. D., Taye, J., & Kumar, B. (2021). Effect of sand mining on the flow hydrodynamics around an oblong bridge pier. *Engineering Research Express*, *3*(4). https://doi.org/10.1088/2631-8695/ac396e

Lama, G. F. C., Errico, A., Francalanci, S., Solari, L., Preti, F., & Chirico, G. B. (2020). Evaluation of flow resistance models based on field experiments in a partly vegetated reclamation channel. *Geosciences (Switzerland)*, *10*(2), 1–17. https://doi.org/10.3390/geosciences10020047

Lawler, D. M., Thorne, C. R., & Hooke, J. M. (1997). Bank erosion and instability. *Applied Fluvial Geomorphology for River Engineering and Management*, 137–172.

Lee, H., & Balachandar, S. (2017). Effects of wall roughness on drag and lift forces of a particle at finite Reynolds number. *International Journal of Multiphase Flow*, *88*, 116–132. https://doi.org/10.1016/j.ijmultiphaseflow.2016.09.006

Li, C. W., & Yu, L. H. (2010). Hybrid LES/RANS modelling of free surface flow through vegetation. *Computers and Fluids*, *39*(9), 1722–1732. https://doi.org/10.1016/j.compfluid.2010.06.009

Li, X., Zhong, D., Zhang, Y. J., Wang, Y., Wang, Y., & Zhang, H. (2018). Wide river or narrow river: Future river training strategy for Lower Yellow River under global change. *International Journal of Sediment Research*, *33*(3), 271–284. https://doi.org/10.1016/j.ijsrc.2018.04.001

Ling, H., Guo, B., Xu, H., & Fu, J. (2014). Configuration of water resources for a typical river basin in an arid region of China based on the ecological water requirements (EWRs) of desert riparian vegetation. *Global and Planetary Change*, *122*, 292–304. https://doi.org/10.1016/j.gloplacha.2014.09.008

Liu, D., Alobaidi, K., & Valyrakis, M. (2022). The assessment of an acoustic Doppler velocimetry profiler from a user ' s perspective. *Acta Geophysica*, *70*(5), 2297–2310. https://doi.org/10.1007/s11600-022-00896-3

Lumley, J. L. (1979). Computational Modeling of Turbulent Flows. In *Advances in Applied Mechanics* (Vol. 18, Issue C). https://doi.org/10.1016/S0065-2156(08)70266-7

Majumdar, S., & Mandal, S. (2022). Assessment of geotechnical properties of the bank sediment to investigate the riverbank's stability along the Ganga river within the stretch of Malda district, West Bengal, India. *Sustainable Water Resources Management*, *8*(2), 1–13. https://doi.org/10.1007/s40899-022-00637-w

Masoodi, A., Majdzadeh Tabatabai, M. R., Noorzad, A., & Samadi, A. (2019). Riverbank Stability under the Influence of Soil Dispersion Phenomenon. *Journal of Hydrologic Engineering*, *24*(3). https://doi.org/10.1061/(asce)he.1943-5584.0001756

Meade, R. H., & Moody, J. A. (2010). Causes for the decline of suspended-sediment discharge in the Mississippi River system, 1940–2007. *Hydrological Processes: An International Journal*, *24*(1), 35–49.

Mensah, J., & Mattah, P. A. D. (2023). Illegal sand mining in coastal Ghana: The drivers and the way forward. *Extractive Industries and Society*, *13*(August 2022), 101224. https://doi.org/10.1016/j.exis.2023.101224

Mera, I., Franca, M. J., Anta, J., & Peña, E. (2015). Turbulence anisotropy in a compound meandering channel with different submergence conditions. *Advances in Water Resources*, *81*, 142–151. https://doi.org/10.1016/j.advwatres.2014.10.012

Midgley, T. L., Fox, G. A., & Heeren, D. M. (2012). Evaluation of the bank stability and toe erosion model (BSTEM) for predicting lateral retreat on composite streambanks. *Geomorphology*, *145–146*, 107–114. https://doi.org/10.1016/j.geomorph.2011.12.044

Ministry of Environment, F. and C. C. (2011). *Coastal Regulation Zone (CRZ) Notification, 2011*. Government of India.

Mossa, M., Ben Meftah, M., De Serio, F., & Nepf, H. M. (2017). How vegetation in flows modifies the turbulent mixing and spreading of jets. *Scientific Reports*, *7*(1), 1–14. https://doi.org/10.1038/s41598-017-05881-1

Naghian, M., Lashkarbolok, M., & Jabbari, E. (2017). Numerical Simulation of Turbulent Flows Using a Least Squares Based Meshless Method. *International Journal of Civil Engineering*, *15*(1), 77–87. https://doi.org/10.1007/s40999-016-0087-1

Nairn, R., Johnson, J. A., Hardin, D., & Michel, J. (2004). A biological and physical monitoring program to evaluate long-term impacts from sand dredging operations in the United States outer continental shelf. *Journal of Coastal Research*, *20*(1), 126–137. https://doi.org/10.2112/1551-5036(2004)20[126:abapmp]2.0.co;2

Najafzadeh, M., & Oliveto, G. (2022). Scour Propagation Rates around Offshore Pipelines Exposed to Currents by Applying Data-Driven Models. *Water (Switzerland)*, *14*(3), 1–25. https://doi.org/10.3390/w14030493

Nakagawa, H., & Nezu, I. (1977). Prediction of the contributions to the Reynolds stress from bursting events in open-channel flows. *Journal of Fluid Mechanics*, *80*(1), 99–128. https://doi.org/10.1017/S0022112077001554

Nandi, K. K., Pradhan, C., Dutta, S., & Khatua, K. K. (2022). How dynamic is the Brahmaputra? Understanding the process–form–vegetation interactions for hierarchies of energy dissipation. *Ecohydrology*, *15*(3). https://doi.org/10.1002/eco.2416

Nardi, L., Rinaldi, M., & Solari, L. (2012). An experimental investigation on mass failures occurring in a riverbank composed of sandy gravel. *Geomorphology*, *163–164*, 56–69. https://doi.org/10.1016/j.geomorph.2011.08.006

Nasermoaddeli, M. H. (2011). Bank Erosion in Alluvial Rivers With Non-Cohesive Soil in Unsteady Flow. *Hamburger Wasserbau-Schriften*, 349.

Nasermoaddeli, M. H., & Pasche, E. (2008). Application of terrestrial 3D laser scanner in quantification of the riverbank erosion and deposition. *River Flow 2008*, *January 2008*, 2407–2416.

Nepf, H. M. (2012). Flow and Transport in Regions with Aquatic Vegetation. *Annual Review of Fluid Mechanics*, *44*(1), 123–142. https://doi.org/10.1146/annurev-fluid-120710-101048

Neyshabouri, M. R., Farhoudi, J., & Habib, Z. (2002). Factors affecting the rate of pit filling by sediments in rivers. *Journal of Hydraulic Engineering*, *128*(3), 321–329. https://doi.org/10.1061/(ASCE)0733-9429(2002)128:3(321)

Nezu, I., Tominaga, A., & Nakagawa, H. (1993). Field Measurements of River Turbulence and Secondary Currents in Straight Rivers. *Doboku Gakkai Ronbunshu*, *1993*(467), 49–56. https://doi.org/10.2208/jscej.1993.467_49

Okeke, C. A. U., Azuh, D., Ogbuagu, F. U., & Kogure, T. (2020). Assessment of land use impact and seepage erosion contributions to seasonal variations in riverbank stability: The Iju River, SW Nigeria. *Groundwater for Sustainable Development*, *11*(January), 100448. https://doi.org/10.1016/j.gsd.2020.100448

Osman, A. M., & Thorne, C. R. (1988). Riverbank Stability Analysis. I: Theory. *Journal of Hydraulic Engineering*, *114*(2), 134–150. https://doi.org/10.1061/(asce)0733-9429(1988)114:2(134)

Padmalal, D., & Maya, K. (2014). *Environmental Science and Engineering Sand Mining Environmental Impacts and Selected Case Studies*.

Padmalal, D., Maya, K., Sreebha, S., & Sreeja, R. (2008). Environmental effects of river sand mining: A case from the river catchments of Vembanad lake, Southwest coast of India. *Environmental Geology*, *54*(4), 879–889. https://doi.org/10.1007/s00254-007-0870-z

Papanicolaou, A. N., Elhakeem, M., & Hilldale, R. C. (2011). Sediment transport and deposition due to riverbank erosion. *Water Resources Research*, *47*(5), W05529. https://doi.org/10.1029/2010WR009159

Park, H., & Hwang, J. H. (2021). A Standard Criterion for Measuring Turbulence Quantities Using the Four-Receiver Acoustic Doppler Velocimetry. *Frontiers in Marine Science*, *8*(August). https://doi.org/10.3389/fmars.2021.681265

Patel, H. K., Arora, S., Lade, A. D., Kumar, B., & Azamathulla, H. M. (2022). Flow behaviour concerning bank stability in the presence of spur dike – A review. *Water Supply*, *00*(0), 1–22. https://doi.org/10.2166/ws.2022.418

Peduzzi, P. (2014). Sand, rarer than one thinks. *Environmental Development*, *11*(208–218), 682. https://doi.org/https://doi.org/10.1016/j.envdev.2014.04.001

Pizzuto, J. E. (2009). Streambank erosion and river-channel evolution: A geomorphological perspective. *River Research and Applications*, *25*(7), 791–804. https://doi.org/10.1002/rra.1167

Pu, J. H., Wei, J., & Huang, Y. (2017). Velocity distribution and 3D turbulence characteristic analysis for flow over water-worked rough bed. *Water (Switzerland)*, *9*(9). https://doi.org/10.3390/w9090668

Rentier, E. S., & Cammeraat, L. H. (2022). The environmental impacts of river sand mining. *Science of The Total Environment*, *838*(April), 155877.

https://doi.org/10.1016/j.scitotenv.2022.155877

Rhoads, B. L., Wilson, D., & Urban, S. (2013). The influence of urbanization on riverbank erosion and channel morphology. *Geomorphology*, *191*, 54–68. https://doi.org/10.1016/j.geomorph.2013.01.011

Rinaldi, M., Mengoni, B., Luppi, L., Darby, S. E., & Mosselman, E. (2008). Numerical simulation of hydrodynamics and bank erosion in a river bend. *Water Resources Research*, *44*(9), 1–17. https://doi.org/10.1029/2008WR007008

Roy, S., Barman, K., Das, V. K., Debnath, K., & Mazumder, B. S. (2020). Experimental Investigation of Undercut Mechanisms of River Bank Erosion Based on 3D Turbulence Characteristics. *Environmental Processes*, *7*(1), 341–366. https://doi.org/10.1007/s40710-019-00417-3

Samadi, A., Amiri-Tokaldany, E., Davoudi, M. H., & Darby, S. E. (2013). Experimental and numerical investigation of the stability of overhanging riverbanks. *Geomorphology*, *184*, 1–19. https://doi.org/10.1016/j.geomorph.2012.03.033

Sanchis-Ibor, C., Segura-Beltrán, F., & Almonacid-Caballer, J. (2017). Channel forms recovery in an ephemeral river after gravel mining (Palancia River, Eastern Spain). *Catena*, *158*(June), 357–370. https://doi.org/10.1016/j.catena.2017.07.012

Sharma, A., & Kumar, B. (2017a). Probability distribution functions of turbulence in seepage-affected alluvial channel. *Fluid Dynamics Research*, *49*(1). https://doi.org/10.1088/1873-7005/49/1/015508

Sharma, A., & Kumar, B. (2017b). Structure of turbulence over non uniform sand bed channel with downward seepage. *European Journal of Mechanics, B/Fluids*, *65*, 530–551. https://doi.org/10.1016/j.euromechflu.2017.05.006

Sharma, A., & Kumar, B. (2018). Sheet flow hydrodynamics over a non-uniform sand bed channel. *International Journal of Sediment Research*, *33*(3), 313–326. https://doi.org/10.1016/j.ijsrc.2018.01.004

Sharma, A., & Kumar, B. (2021). Comparison of flow turbulence over a sand bed and gravel bed channel. *Water Supply*, *00*(0), 1–12. https://doi.org/10.2166/ws.2021.201

Sharma, D., Rao, K., & Ramanathan, A. L. (2021). A systematic review on the impact of urbanization and industrialization on Indian coastal mangrove ecosystem. *Coastal Ecosystems: Environmental Importance, Current Challenges and Conservation Measures*, 175–199.

Shiono, K., & Knight, D. W. (1991). Turbulent open-channel flows with variable depth across the channel. *Journal of Fluid Mechanics*, *222*(HY11), 617–646. https://doi.org/10.1017/S0022112091001246

Shu, A., Duan, G., Rubinato, M., Tian, L., Wang, M., & Wang, S. (2019). An experimental study on mechanisms for sediment transformation due to riverbank collapse. *Water (Switzerland)*, *11*(3). https://doi.org/10.3390/w11030529

Simon, A., & Collison, A. J. C. (2002). Quantifying the mechanical and hydrological effects of riparian vegetation on streambank stability. *Earth Surface Processes and Landforms*, *27*(5), 527–546. https://doi.org/10.1002/esp.337

Simon, A., Curini, A., Darby, S. E., & Langendoen, E. J. (1991). Bank-stability and toe-erosion model: Development and application in the USDA ARS National Sedimentation Laboratory. *Hydrological Processes*, *9*(5), 615–631. https://doi.org/10.1002/hyp.3360090514

Smith, C. R., & Metzler, S. P. (1983). The characteristics of low-speed streaks in the near-wall region of a turbulent boundary layer. *Journal of Fluid Mechanics*, *129*, 27–54. https://doi.org/10.1017/S0022112083000634

Syvitski, J. P. M., Vörösmarty, C. J., Kettner, A. J., & Green, P. (2005). Impact of humans on the flux of terrestrial sediment to the global coastal ocean. *Science*, *308*(5720), 376–380.

Tan, T.-S., Lu, Y.-T., Phoon, K.-K., & Karthikeyan, M. (2011). *Innovative Approaches to Land Reclamation in Singapore*. *January*, 85–102. https://doi.org/10.3850/978-981-07-0188-8_p176

Tay, G. F. K., Kuhn, D. C. S., & Tachie, M. F. (2015). Effects of sedimenting particles on the turbulence structure in a horizontal channel flow. *Physics of Fluids*, *27*(2). https://doi.org/10.1063/1.4907669

Taye, J., & Kumar, B. (2021). Experimental study on near-bed flow turbulence of sinuous channel with downward seepage. *Proceedings of the Institution of Civil Engineers: Water Management*, *174*(4), 173–186. https://doi.org/10.1680/jwama.19.00094

Tennekes, H., & Lumley, J. L. (2020). Spectral Dynamics. In *A First Course in Turbulence*. https://doi.org/10.7551/mitpress/3014.003.0010

Thi, T. D., & Minh, D. Do. (2019). Riverbank stability assessment under river water level changes and hydraulic erosion. *Water (Switzerland)*, *11*(12). https://doi.org/10.3390/w11122598

Thorne, C. R., & Tovey, N. K. (1981a). Stability of composite river banks. *Earth Surface Processes and Landforms*, *6*(5), 469–484. https://doi.org/10.1002/esp.3290060507

Thorne, C. R., & Tovey, N. K. (1981b). Stability of composite river banks. *Earth Surface Processes and Landforms*, *6*(5), 469–484. https://doi.org/10.1002/esp.3290060507

Transactions, S., Mathematical, A., & Oct, V. (2013). *Fixed Point Structures Author (s): T . B . Muenzenberger and R . E . Smithson Published by : American Mathematical Society American Mathematical Society is collaborating with JSTOR to digitize , preserve and extend access to Transactions of the American*. *184*(4), 153–173.

Valyrakis, M., Liu, D., Turker, U., & Yagci, O. (2021). The role of increasing riverbank vegetation density on flow dynamics across an asymmetrical channel. *Environmental Fluid Mechanics*, *21*(3), 643–666. https://doi.org/10.1007/s10652-021-09791-9

van Prooijen, B. C., & Uijttewaal, W. S. J. (2005). Horizontal Mixing in Shallow Flows. In W. Czernuszenko & P. Rowiński (Eds.), *Water Quality Hazards and Dispersion of Pollutants* (pp. 55–68). Springer US. https://doi.org/10.1007/0-387-23322-9_3

Wu, W., Xu, Z., & Chen, J. (2016). Impact of sediment mining in the Yangtze River. *Journal of Hydrology*, *540*, 17–26. https://doi.org/10.1016/j.jhydrol.2016.06.002

Wuppukondur, A., & Chandra, V. (2018). Control of Bed Erosion at 60° River Confluence Using Vanes and Piles. *International Journal of Civil Engineering*, *16*(6), 619–627. https://doi.org/10.1007/s40999-017-0147-1

Xia, H., He, Z., & Zhao, L. (2014). Role of cohesive and non-cohesive materials in riverbank stability: A review of experimental and field data. *Geomorphology*, *208*, 73–85. https://doi.org/10.1016/j.geomorph.201

Xiao, Y., Wang, N., Liang, D., & Liu, J. (2018). Flow Structures in Trapezoidal Compound Channels with Different Side Slopes of Main Channel. *International Journal of Civil Engineering*, *16*(7), 823–835. https://doi.org/10.1007/s40999-017-0212-9

Xiaohui, S., & Li, C. W. (2002). Large eddy simulation of free surface turbulent flow in partly vegetated open channels. *International Journal for Numerical Methods in Fluids*, *39*(10), 919–937. https://doi.org/10.1002/fld.352

Yu, G. A., Li, Z., Yang, H., Lu, J., Huang, H. Q., & Yi, Y. (2020). Effects of riparian plant roots on the unconsolidated bank stability of meandering channels in the Tarim River, China. *Geomorphology*, *351*, 106958. https://doi.org/10.1016/j.geomorph.2019.106958

Yu, M. hui, Wei, H. yan, & Wu, S. bai. (2015). Experimental study on the bank erosion and interaction with near-bank bed evolution due to fluvial hydraulic force. *International Journal of Sediment Research*, *30*(1), 81–89. https://doi.org/10.1016/S1001-6279(15)60009-9

Yu Minghui, Xi, C., Hongyan, W. E. I., Chengwei, H. U., & Songbai, W. U. (2016). Experimental of the influence of different near-bank riverbed compositions on bank failure. *Advances in Water Science*, *27*(2), 176–185. https://doi.org/10.14042/j.cnki.32.1309.2016.02.002

Zhai, H., Jeng, D. S., & Guo, Z. (2021). The role of 2d seepage on sediment incipient motion around a pipeline. *Journal of Marine Science and Engineering*, *9*(6). https://doi.org/10.3390/jmse9060580

Zhang, H., Wang, Z., Dai, L., & Xu, W. (2015). Influence of vegetation on turbulence characteristics and Reynolds shear stress in partly vegetated channel. *Journal of Fluids Engineering, Transactions of the ASME*, *137*(6), 1–8. https://doi.org/10.1115/1.4029608

Zhao, K., Gong, Z., Zhang, K., Wang, K., Jin, C., Zhou, Z., Xu, F., & Coco, G. (2020). Laboratory Experiments of Bank Collapse: The Role of Bank Height and Near-Bank Water Depth. In *Journal of Geophysical Research: Earth Surface* (Vol. 125, Issue 5). https://doi.org/10.1029/2019JF005281

Zhu, Y. H., Lu, J. Y., Liao, H. Z., Wang, J. S., Fan, B. L., & Yao, S. M. (2008). Research on cohesive sediment erosion by flow: An overview. *Science in China, Series E: Technological Sciences*, *51*(11), 2001–2012. https://doi.org/10.1007/s11431-008-0232-4

Zong, L., & Nepf, H. (2010). Flow and deposition in and around a finite patch of vegetation. *Geomorphology*, *116*(3–4), 363–372. https://doi.org/10.1016/j.geomorph.2009.11.020

Appendix-I

Turbulent Characteristics at Interface of Partly Vegetated Alluvial Channel

Abstract

This study investigates the changes in flow structure at the interface of partly vegetated, determining if it is better to have wholly vegetated test sections near the important riverine structures. The research examines the flow behaviour at the interface using transverse flux, turbulent kinetic energy, probability density function and anisotropy. The study found the presence of helical flow downstream of the partly vegetated section, indicated by negative Reynolds shear stress. The lateral acceleration of the flow contributes to large-scale fluctuations, as supported by probability density function analysis and the anisotropy stress tensor. Turbulent kinetic energy (TKE) was higher for the wholly vegetated case due to the presence of 2-D stress components compared to 1-D stress components in the partly vegetated case, as supported by Anisotropy Invariant Map (AIM). Wholly vegetated sections exhibit highly fluctuating transverse flux, indicating greater intermixing rather than unidirectional movement. Based on the findings, it is recommended to opt for a wholly vegetated cover instead of a partly vegetated cover in riverbanks or near structures like bridge piers and river training structures affected by lateral or laterally accelerating flow. This analysis of additional turbulence helps safer designs of critical components of river structures.

Keywords: Partly Vegetated, Wholly vegetated, Turbulent Kinetic Energy, Anisotropy

Introduction

The growth of river vegetation helps address the environmental, flood control, and flow deflection to a desired branch of the channel (Bebina Devi et al., 2019; Golder et al., 2021; Ling et al., 2014; Nandi et al., 2022; Valyrakis et al., 2021; van Prooijen & Uijttewaal, 2005). A river, generally, has a vegetated region and a flow region without vegetation (Xiaohui & Li,

2002). The interface region of the vegetated and unvegetated region observes transverse mixing of the flow coming out of the vegetated region to the unvegetated region to gain the least resistance to the flow. Various researchers have studied turbulence characteristics at the interface region by observing it in the field (Lama et al., 2020), in the experimental setup (Bebina Devi et al., 2019; Ben Meftah et al., 2016; Caroppi et al., 2019; Caroppi, Gualtieri, et al., 2020; Devi, 2016; Mossa et al., 2017), and some have further modeled the flow (Anjum & Tanaka, 2020; Caroppi et al., 2021; Kang & Choi, 2006; Karimi et al., 2017; Lama et al., 2020; C. W. Li & Yu, 2010; Naghian et al., 2017; Xiaohui & Li, 2002). The turbulence enhancement has been linked to the transverse shear produced by the drag of vegetation. Large eddies were found at the interface (Arora, Patel, Lade, et al., 2023; Xiaohui & Li, 2002). (van Prooijen & Uijttewaal, 2005) have found horizontal eddies larger than the depth of flow in the case of shallow flow conditions. Several researchers (Bebina Devi et al., 2019; Devi, 2016; Devi et al., 2017; Patel et al., 2022) worked on seepage effects on flow hydrodynamics in a partly vegetated channel and compared the flow characteristics in partly vegetated with the unvegetated region of the flow. However, the scope of advanced analysis at the interface point of partly vegetated with the wholly vegetated section remains open. (Caroppi et al., 2019, 2021) suggest 40% greater momentum exchange in the case of flexible vegetation than rigid vegetation, and the vortices contained deeper into the flexible vegetation. The current study has considered the effects of emergent flexible vegetation due to its higher efficiency in lateral momentum transfer (Caroppi et al., 2019, 2021).

Researchers have agreed on increased turbulence, lateral transfer of mass, and flow momentum at the interface of the vegetated and unvegetated sections (Anjum & Tanaka, 2020; Bebina Devi et al., 2019; Caroppi et al., 2021; Wuppukondur & Chandra, 2018; Zhang et al., 2015). (J. Barman & Kumar, 2022a, 2022b; Blanckaert & de Vriend, 2004; Blanckaert & Graf, 2004; Ghani et al., 2022; Ghazanfari-Hashemi et al., 2020; Lade et al., 2021; Taye & Kumar, 2021;

Xiao et al., 2018) have suggested the presence of helical flow at the interface of compound channels and the sharp bends. While the vegetation is generally seen to divert the flow, here we study the suitable extent of vegetation installation (or) removal from the vicinity of the structures of interest as different structures would have different tolerance to the turbulence/velocity. The work done by (Bebina Devi et al., 2019) is concentrated on understanding the effects of seepage in a partly vegetated test section, whereas the current study works on determining the additional turbulence occurring in the wholly vegetated test section as compared to the interface of the partly vegetated test section. This would help understand the extent of vegetation suitable for a channel or extension of vegetation beyond riverbanks or near the riverine structures.

Materials and Methods

Experimental Setup

The study was performed in a 17.2 m long and 1m wide recirculating flume, with the sand bed of D_{50}=1.1 mm, at the Water Resources lab, IIT Guwahati, India, with partly and wholly vegetated channels. The test section was 5 m long and 1 m wide, where 0.5 m section was left unvegetated in case of partly vegetated while the other half was vegetated, as shown in Figure 0.1. The observation point for PDF was fixed near the bed at 0.17 z/h, which is also the center point of vegetation (Oryza Sativa bundles placed at 0.1 m center to center spacing) for the fully vegetated case but situated at the interface of the vegetated/unvegetated part of the partly vegetated section where, "z" is the distance of the observation point from the bed and "h" is the distance of highest point of observation from the bed. The flow rate was 0.0326 m^3/s with a water depth of 0.12 m, and the instantaneous velocity readings $u = \overline{u} + u'$ (m/s) were taken at 100 Hz for 120 seconds using Nortek Acoustic Doppler Velocimeter (ADV). The four-probes down looking ADV samples the fluid volume 0.05 m below it. The sample volume is cylindrical in shape with dimension of 0.0055 m height and diameter of 0.006 m. The

transmitter of ADV works on the Doppler effect and the signals emitted towards the sampling volume gets reflected from the sample volume and are received by the probes. The received signal contains noise produced by system or due to the obstructions nearby. The quality of received signal shall be kept in check using Signal to Noise ratio (SNR) and correlation coefficient between the orthogonally placed receivers (Park & Hwang, 2021). The SNR was greater than 10 and correlation coefficient was greater than 70 for all the velocity measurements. Measurements were repeated to assess the uncertainty in ADV measurements and presented in

Table 7. The acceleration threshold of 1-1.5 was considered while removing the noise from the collected ADV data, and decluttered velocity power spectra follow Kolmogorov's -5/3 law (Pu et al., 2017), as shown in Figure 0.2. Free upstream and free downstream points were also studied for velocity and shear stress patterns in both cases to realize the effects of partly and wholly vegetated sections. Turbulent Kinetic Energy (TKE), lateral flow flux, PDF of velocity fluctuations, and Anisotropy at the center of the test section have been analyzed to quantify the changes and to comprehend the flow characteristics at the interface profile in these two cases.

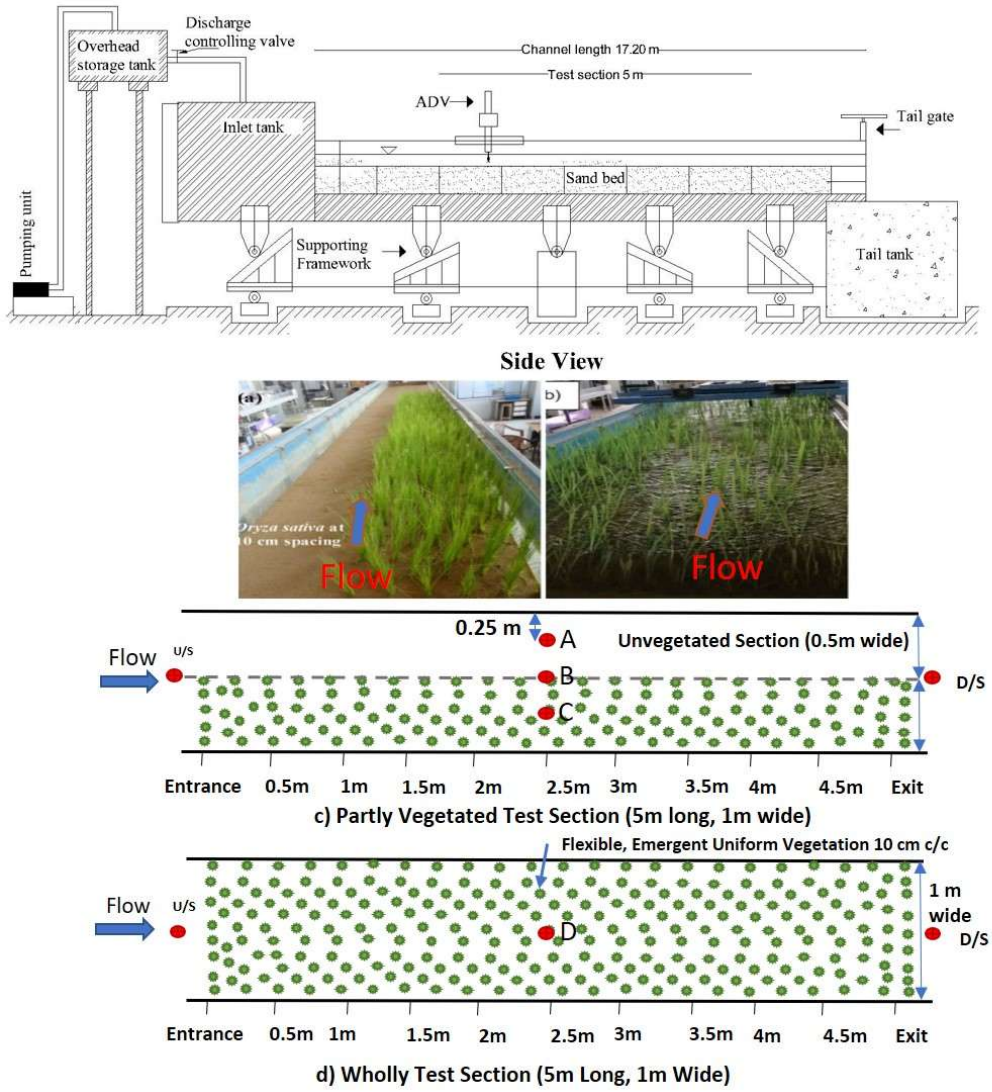

Figure 0.1: Experimental Setup with Side view and pictures of a) Partly Vegetated b) Wholly Vegetated test section and experimental plan of c) Partly vegetated d) Wholly vegetated test section with observation points at the free upstream, the center of the test section and free downstream points for discharge of 0.0326 m^3/s.

Table 7: Uncertainty analysis of Nortek Acoustic Doppler Velocimeter (ADV)

	u	v	w	$(u'u')^{0.5}$	$(v'v')^{0.5}$	$(w'w')^{0.5}$
Standard Deviation	$4.22*10^{-3}$	$9.61*10^{-4}$	$4.27*10^{-4}$	$1.05*10^{-3}$	$1.08*10^{-3}$	$3.11*10^{-4}$
Uncertainty %	0.29	0.05	0.03	0.06	0.069	0.03

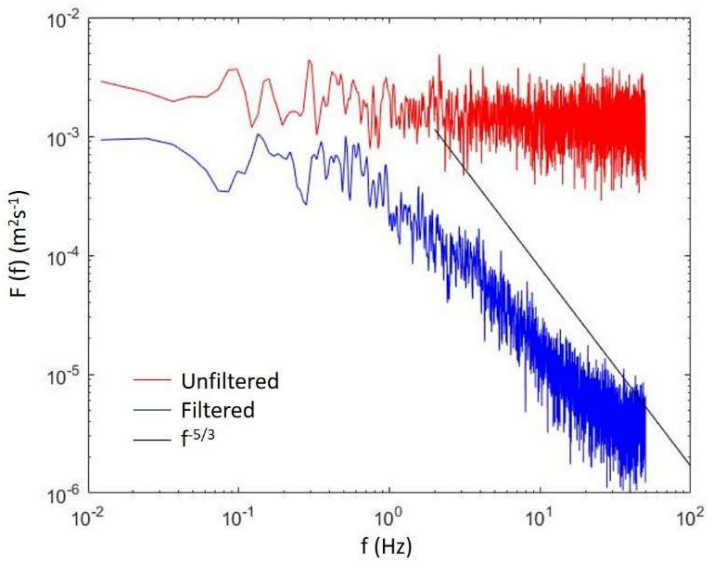

Figure 0.2: Velocity power spectra of raw and processed streamwise velocity time series with Kolmogorov's -5/3 law

Theoretical Background

The probability density function describes the probability of occurrence of the selected random variable at a particular point. Log, normal distribution, or Gaussian distribution can illustrate the probability density function. The distribution methods are based on the finite interval over which the convergence occurs. The primacy of the Gram Charlier series to other series is that it can be applied to series containing intervals where the enactment of convergence is infinite (Transactions et al., 2013). Also, PDFs of the Gram Charlier series are generated given the higher-order moments up to four (Cramer, 1999).

Probability functions for velocities fluctuations

Velocity fluctuations (u', w', v') follow the Gram Charlier series based on exponential distribution at which u', w', and v' are normalized as $\hat{u} = u'/\sigma_u$, $\hat{w} = w'/\sigma_w$ and $\hat{v} = v'/\sigma_v$ where σ_u, σ_w and σ_v are the average streamwise, depth-wise and transverse turbulence intensities, respectively, (A. Sharma & Kumar, 2017b). Turbulence intensities $(\sigma_u, \sigma_v, \sigma_w)$ are calculated

to obtain information regarding the contribution of fluctuating components of velocity to the turbulence production. Mathematically, it can be defined as:

$$\sigma_u = \sqrt{\frac{\sum_1^n (u-\bar{u})^2}{n-1}};\ \sigma_v = \sqrt{\frac{\sum_1^n (v-\bar{v})^2}{n-1}};\ \sigma_w = \sqrt{\frac{\sum_1^n (w-\bar{w})^2}{n-1}}$$

where *u, v* and *w* are the instantaneous velocity components in streamwise and vertical directions, $\bar{u}$, $\bar{v}$ and $\bar{w}$ are the time-averaged velocity components in streamwise and vertical directions, and n is the number of velocity samples recorded.

The probability density function (PDF) for streamwise velocity fluctuation is expressed in the following form of equation $P_{\hat{u}}(\hat{u}) = \frac{1}{2}C_{00}(\exp(-|\hat{u}|)) + \frac{1}{4}C_{10}\hat{u}(\exp(-|\hat{u}|)) - \frac{1}{16}C_{20}(1+|\hat{u}|-\hat{u}^2)(\exp(-|\hat{u}|)) - ....$ (Nakagawa & Nezu, 1977; A. Sharma & Kumar, 2017a) where, $C_{00} = m_{00} = 1$, $C_{10} = m_{10}$ and $C_{20} = \frac{1}{2}m_{20} - 1$. For PDF of downward and transverse velocity fluctuations, $P_{\hat{w}}(\hat{w}) = \frac{1}{2}C_{00}(\exp(-|\hat{w}|)) + \frac{1}{4}C_{01}\hat{w}(\exp(-|\hat{w}|)) - \frac{1}{16}C_{02}(1+|\hat{w}|-\hat{w}^2)(\exp(-|\hat{w}|)) - ....$ where, $C_{01} = m_{01}$ and $C_{02} = \frac{1}{2}m_{02} - 1$. The generating moments (m_{jk}) are obtained from the experimental observations and can be defined as $m_{jk} = \overline{u'^j w'^k}$.

$P_{\hat{v}}(\hat{v}) = \frac{1}{2}C_{00}(\exp(-|\hat{v}|)) + \frac{1}{4}C_{01}\hat{v}(\exp(-|\hat{v}|)) - \frac{1}{16}C_{02}(1+|\hat{v}|-\hat{v}^2)(\exp(-|\hat{v}|)) - ....$ where, $C_{01} = m_{01}$ and $C_{02} = \frac{1}{2}m_{02} - 1$. The generating moments (m_{ij}) can be defined as $m_{ij} = \overline{u'^i v'^j}$.

Results and discussion

The flow characteristics in the test sections of wholly vegetated and partly vegetated test sections were studied by observing instantaneous 3D velocity at free upstream and free

downstream (0.5 m before and after the test section, respectively) and at points A, B, C, and D using parameters such as mean velocity field, Reynolds Shear Stress, TKE, TKE transverse flux, PDF of velocity fluctuations, and Anisotropy at the interface of the partly vegetated test section.

Mean Velocity Field

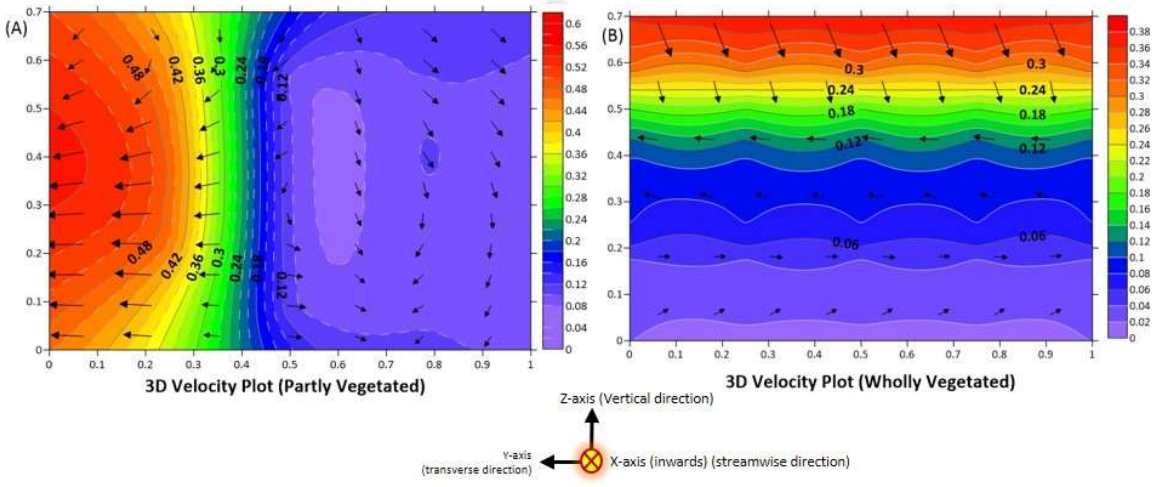

Figure 0.3: Average 3-D Velocity at the center of the test section (A) Partly Vegetated (B) Wholly Vegetated test section with discharge of 0.0326 m^3/s. The colored contour represents magnitude of streamwise velocity. The length and direcion of arrows depicts the strength and direction of secondary flow.

In both partly and wholly vegetated cases, the average streamwise velocity, $\bar{u}$ (m/s), is presented as contours in Figure 0.3, whereas the vectors show the resultant secondary flow movement in the cross-section at the center of the test segment. Figure 0.3(a) shows high flow velocity at the unvegetated part of the test segment with a steep gradient at the interface point, validating it from previous researchers' observations. Figure 0.3(b) has an attenuated flow due to vegetation. The lateral flow represented by the velocity vectors suggests the movement of flow coming out of the vegetated section to the unvegetated section in the case of partly vegetated, whereas intermixing of the flow is found in the wholly vegetated test section. The length of the vectors exhibits the extent of the secondary flow helping visualize the accelerating lateral flow at the interface while moving away from the vegetated part.

The average streamwise velocity of the test segment has increased as the flow passes through the partly vegetated test section due to the partial obstruction present in the field. The unvegetated section helped overcome the resistive forces of the vegetation section, which increased the flow depth in its zone. The difference in flow depth increased the flow's lateral movement and the streamwise velocity downstream of the test segment. In the case of the wholly vegetated test segment, there is no opportunity for the flow to reach any flow area of less flow resistance and achieves higher flow depth to accommodate the incoming flow. As the stems of flexible vegetation has an even higher resistance to the flow than the top of the vegetation, S-shape streamwise velocity has been observed downstream of the wholly vegetated test section, as shown in Figure 0.4.

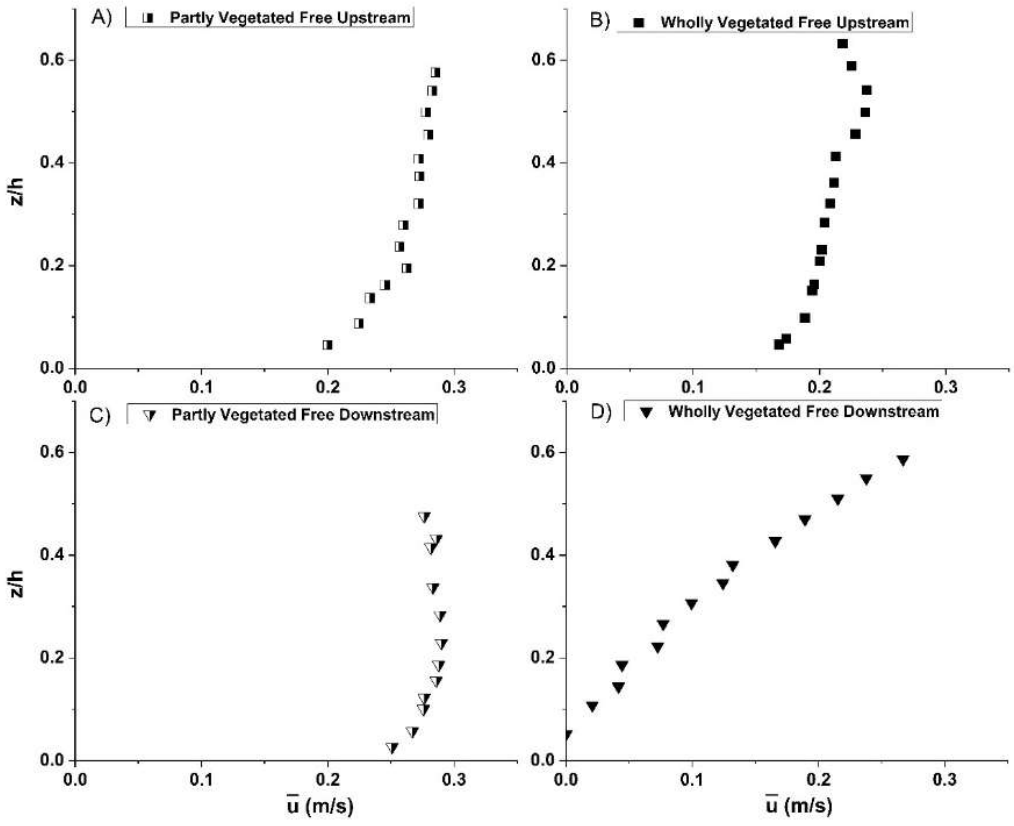

Figure 0.4: Streamwise velocity (m/s) at A) Upstream of the partly vegetated test section B) Upstream of the wholly vegetated test section C) Downstream of the partly vegetated test section D) Downstream of the wholly vegetated test section at the discharge of 0.0326 m^3/s

Reynolds Shear Stresses

For both the test cases, flow is turbulent with R_e > 10,000. Total Reynolds shear stress in the z-x plane ($\tau_{z-x} = -\overline{u'w'}$ m^2s^{-2}) and total transverse shear stress ($\tau_{y-x} = -\overline{u'v'}$ m^2s^{-2}) are presented in Figure 0.5 with the y-axis normalized with total flow depth. The RSS (τ_{z-x}) at the interface of the vegetated/unvegetated plane is much smaller than that if the section is wholly vegetated. The slightly negative RSS in the case of partly vegetated flow suggests the presence of the helical flow due to the intermixing of flows of different flow velocities. The secondary flow in the compound channel is substantial, and its study is essential to understand the flow structure. Transverse shear stress (τ_{y-x}) at the interface of partly vegetated is found to be significant, but it has been observed to be higher in wholly vegetated cases. The additional stresses in the flow at the interface point, due to the lateral flow in the case of partly vegetated, are more than that of the unvegetated test section as per the literature but are much less than that in the case of wholly vegetated flow.

The RSS (τ_{z-x}) at the free upstream and free downstream for both the test cases are presented in Figure 0.6. The RSS at the upstream cases observed its peak at z=0.2h is negligible as compared to the RSS of the flow after passing through the test segment. In the case of the partly vegetated downstream section, $\tau_{z-x} = -\overline{u'w'}$ is negative, which suggests a positive correlation between u' and w'. This depicts the chances of the presence of helical flow due to intermixing of two different layers of the flow of high velocity from the unvegetated and low-velocity flow

from the vegetated section as observed by other researchers in compound channel flow (J. Barman & Kumar, 2022a; Blanckaert & Graf, 2004).

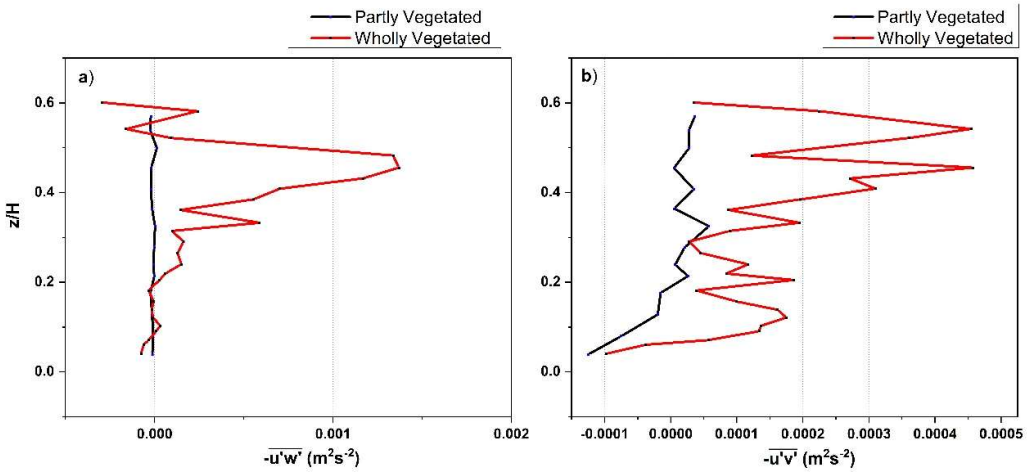

Figure 0.5: a) Reynolds Shear Stress in the z-x plane and b) Transverse Shear Stress in the x-y plane at the center of test sections in both cases at Q=0.0326 m³/s

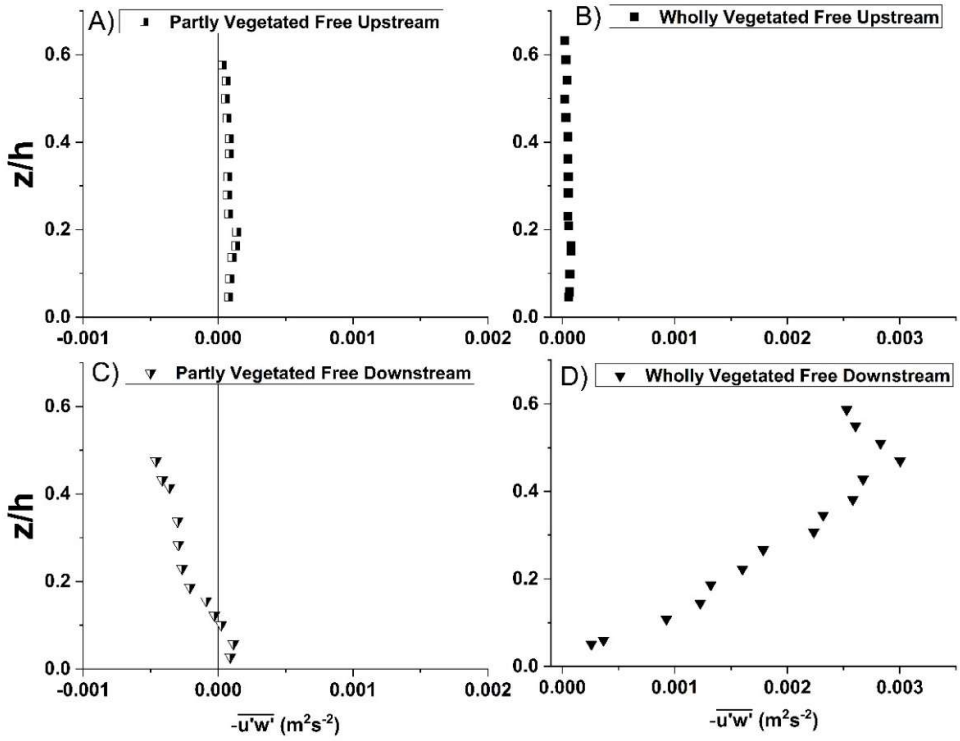

Figure 0.6: Reynolds Shear Stress at A) Upstream of the partly vegetated test section B) Upstream of the wholly vegetated test section C) Downstream of the partly vegetated test section D) Downstream of the wholly vegetated test section at the discharge of 0.0326 m³/s

Turbulent Kinetic Energy Flux

The transverse TKE Flux and turbulent kinetic energy are given as $F_{kv} = 0.75(\overline{v'v'v'} + \overline{u'u'v'})$ and $k = 0.5(\overline{u'u'} + \overline{v'v'} + \overline{w'w'})$, respectively. Transverse TKE flux is positive in most of the sections in the case of the partly vegetated test section suggesting the lateral movement of the flow towards the unvegetated test section. However, in the case of wholly vegetated, it shows intermixing of the flow, which is in line with the literature (Figure 0.7 (a)). The turbulent kinetic energy in Figure 0.7 (b) is also significantly less than that of the wholly vegetated section suggesting higher turbulence in wholly vegetated than partly vegetated, which, however, has more turbulent kinetic energy than a typical unvegetated test section. The surged Turbulent kinetic energy for the wholly vegetated case is due to the interaction of flexible vegetation with the flow.

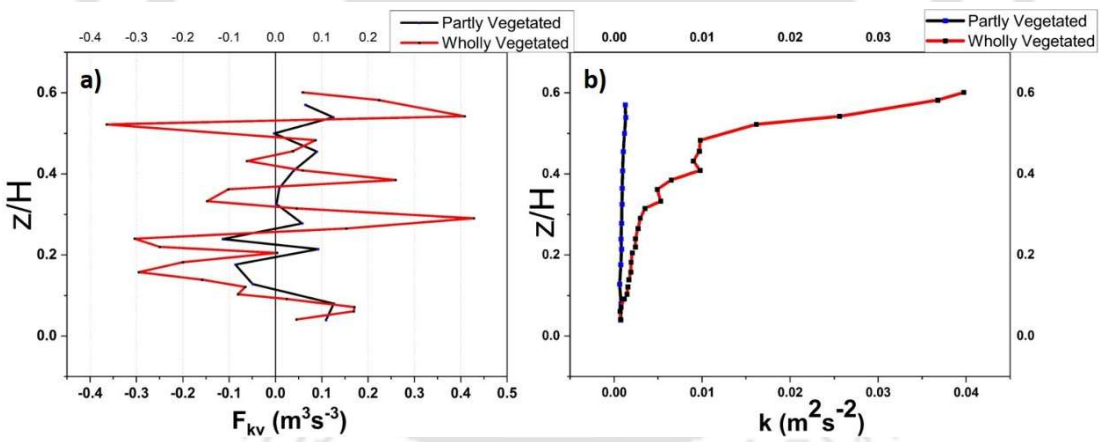

Figure 0.7: a) Transverse TKE Flux (F_{kv}) and b) Turbulent Kinetic Energy (k) for partly vs. wholly vegetated at the center of the test section at Q = 0.0326 m^3/s

Probability Density Function (PDF) of streamwise and transverse velocity

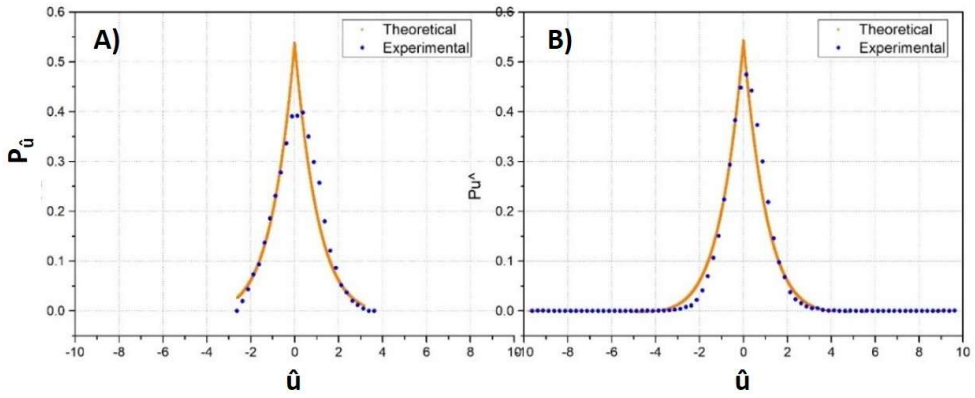

Figure 0.8: PDF of streamwise velocity fluctuations a) Partly vegetated vs. b) Wholly Vegetated at z=0.17h at the center of the test section with the discharge of 0.0326 m^3/s

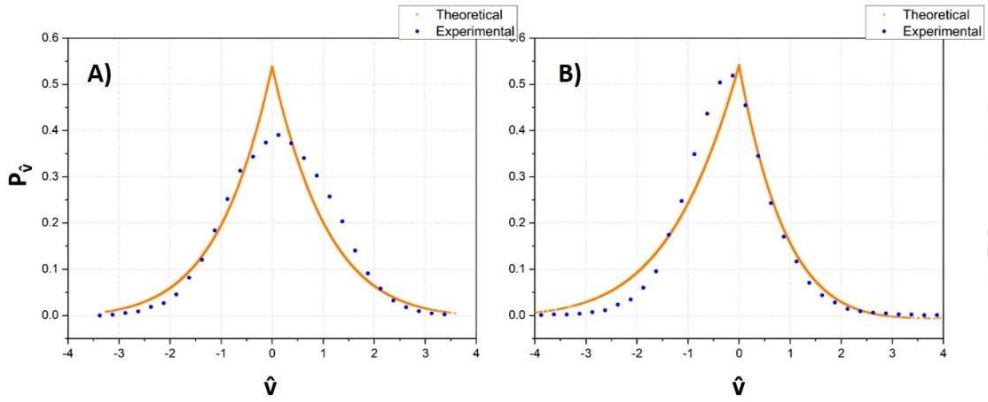

Figure 0.9: PDF of Transverse velocity fluctuations A) Partly vegetated vs. B) Wholly Vegetated at z = 0.17H at the center of the test section with the discharge of 0.0326 m^3/s

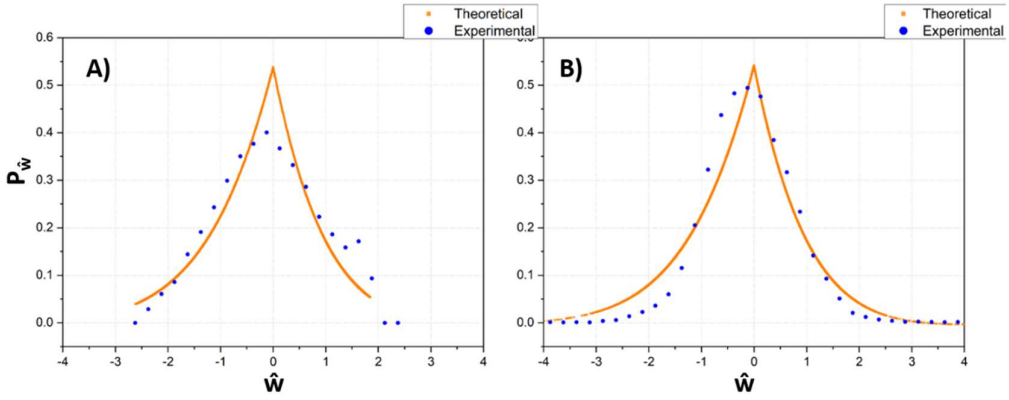

Figure 0.10: PDF of vertical velocity fluctuations A) Partly vegetated vs. B) Wholly Vegetated at z = 0.17H at the center of the test section with the discharge of 0.0326 m^3/s

The annotated peaks and widened curve at the center of the PDF of both û and v̂ in Figure 0.8(a) and Figure 0.8(a) as compared to Figure 0.8(b) and Figure 0.9(b), respectively, and the Maximum values of PDF presented in Table 8 suggest that a partly vegetated section observes lower probability of low streamwise, depthwise, and lateral velocity fluctuations but higher probability of more significant velocity fluctuations than that of the wholly vegetated test section. Similarly, for vertical velocity fluctuations, PDF has been shown in Figure 0.10. It suggests that more substantial fluctuations shall be present for the partly vegetated case, but their chances of occurrence will be less, whereas more fluctuations in velocity components shall be present for the wholly vegetated case but of lower magnitude, suggesting more but weaker events as compared to interface of the partly vegetated.

Table 8: Probability Density Function (Partly vs. Wholly Vegetated)

	Partly Covered	**Wholly Covered**
$P_{\hat{u}}$ max	0.398	0.474
$P_{\hat{v}}$ max	0.390	0.519
$P_{\hat{w}}$ max	0.400	0.494

Anisotropy

Reynolds stress anisotropy tensor ($b_{ik} = \frac{u'_i u'_k}{2k} - \frac{\delta_{ik}}{3}$) helps understand the nature of turbulence when parameters -*II* ($= \frac{b_{ik}b_{ik}}{2}$) and *III* ($= \frac{b_{ij}b_{jk}b_{ki}}{3}$) are plotted against each other (Banerjee et al., 2007, 2008; J. Barman & Kumar, 2022b; Kurien & Sreenivasan, 2007; Lumley, 1979; Mera et al., 2015; A. Sharma & Kumar, 2021; Tennekes & Lumley, 2020) where δ is the Kronecker delta function. The domain of Anisotropy Invariant Map (AIM) is bordered at the bottom by $II = \frac{3}{2}(\frac{4}{3}III)^{\frac{2}{3}}$ and at the top by $II = 2III + \frac{2}{9}$. The concentrated points of the partly vegetated

section suggest that one-dimensional turbulence is dominant instead of two-dimensional turbulence dominance in the wholly vegetated test section, which is close to the left boundary of the Lumley triangle or AIM in Figure 0.10. The presence of a few but strongest 1-D events (at the top right boundary of AIM) of wholly vegetated flow and the presence of a more significant number of points of partly vegetated flow below the strongest supports the results obtained from the PDF analysis studied in Table 8.

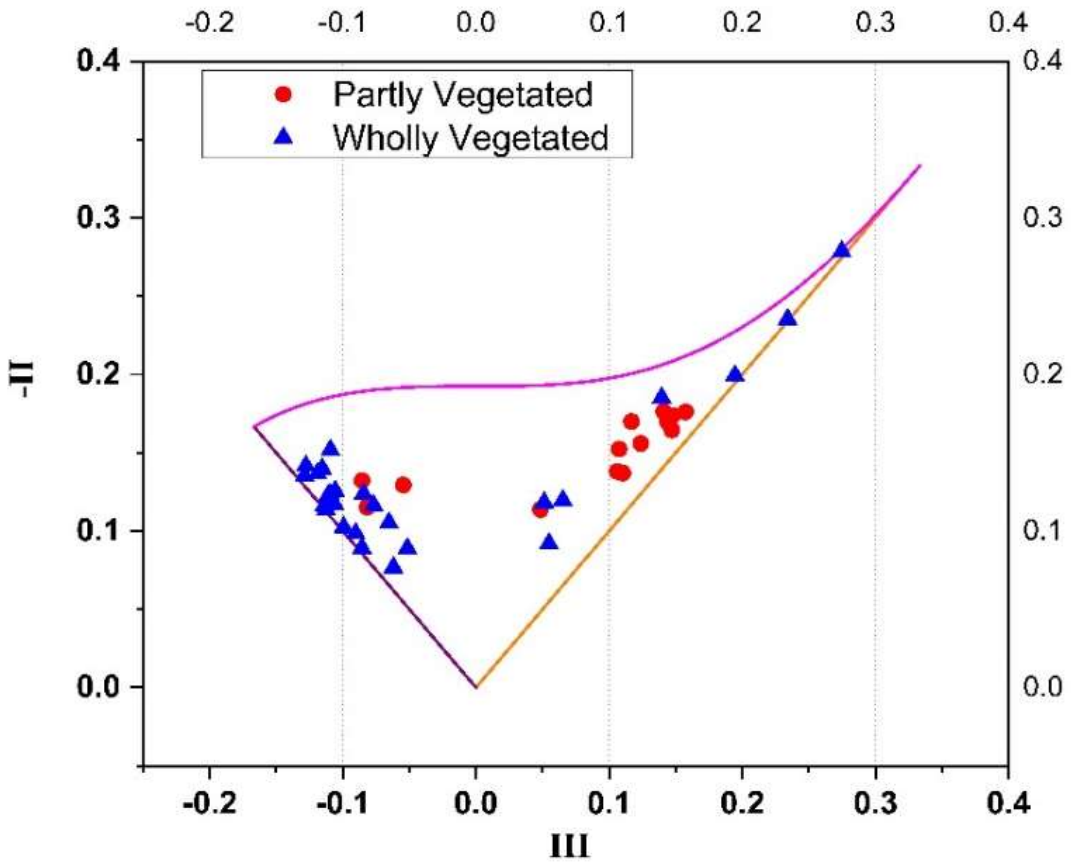

Figure 0.101: Anisotropy Invariant Map (AIM) of Partly and Wholly Vegetated section

Conclusions

The study of flow structure in a partly vegetated as compared to that in a wholly vegetated test section revealed the following observations: The study shows the accelerating flow at the interface of the partly vegetated moving away from the vegetated test segment to the unvegetated test segment to reach the flow area with less resistance to the flow.

1. The interface of the vegetated/unvegetated sections has higher turbulence than the wholly unvegetated test section, as per the literature, but is found to be having lower streamwise and transverse shear stresses than the same point with a wholly vegetated section.
2. The occurrence of the helical flow in the case of a partly vegetated test section contributes to deciding the suitability of the extent of vegetation near a structure of interest. (A structure that is sensitive to such a flow should have extended vegetation beyond its vicinity).
3. The transverse flux at the interface of partly vegetated verifies the lateral movement of the flow towards the unvegetated test section. Highly fluctuating transverse flux was observed in the case of wholly vegetated, which shows higher intermixing rather than unidirectional movement.
4. The turbulent kinetic energy is observed to be larger in the case of the wholly vegetated test section due to the three-directional movement of the flow instead of the unidirectional movement in the case of partly vegetated flow.
5. The PDF distribution of the observed streamwise, transverse velocity fluctuations has shown good agreement with the Gram-Charlier series. The attenuated peak of the observed data may have occurred due to the broad bandwidth selection of observed data.
6. The dampened and widened curve of PDF of partly vegetated flow suggests a lower possibility of small-scale fluctuations but a higher probability for large-scale fluctuations as compared to the wholly vegetated tests section. Reynolds stress anisotropy tensor supports the higher presence of a large-scale one-dimensional component of stress as

compared to two-dimensional components of the stress tensor in the case of the wholly vegetated test section.

The turbulence from a vegetation patch close to the structure of interest affects its stability and life span. The research proposes to have a wholly vegetated cover instead of partly vegetated cover at the riverbanks or near the structures such as bridge piers, river training structures that are affected by lateral flow or laterally accelerating flow. Differential roughness in such a case gives rise to vorticity at the interface. Vorticity measurement shall give further insight into the turbulence characteristics at the interface zone of the partly vegetated section, which will require a fine grid of the observation points and shall be taken for future work.